NUMERICAL AND EXPERIMENTAL INVESTIGATIONS ON FREE SURFACE CHARACTERISTICS OF SLOSHING WAVES IN EXTERNALLY INDUCED TANKS

A Thesis

Submitted in Partial Fulfilment of the Requirements

for the Degree of

DOCTOR OF PHILOSOPHY

By

M. ESWARAN

DEPARTMENT OF MECHANICAL ENGINEERING
INDIAN INSTITUTE OF TECHNOLOGY GUWAHATI
GUWAHATI, INDIA

October, 2011

DECLARATION

I hereby certify that the work contained in the thesis entitled '**Numerical and Experimental Investigations on Free Surface Characteristics of Sloshing Waves in Externally Induced Tanks**' has been done by me, a student in the Department of Mechanical Engineering, Indian Institute of Technology Guwahati under the guidance of Prof. Ujjwal K Saha for the award of Doctor of Philosophy and that this work has not been submitted elsewhere for a degree.

Date:

M.Eswaran
Research Scholar
Registration No. 06610309
Department of Mechanical Engineering
Indian Institute of Technology Guwahati

Indian Institute of Technology Guwahati
Department of Mechanical Engineering

CERTIFICATE

It is certified that the work contained in the thesis entitled '**Numerical and Experimental Investigations on Free Surface Characteristics of Sloshing Waves in Externally Induced Tanks**' by **M. Eswaran** (Registration No. 06610309), a student of the Department of Mechanical Engineering, India Institute of Technology Guwahati, for the award of the degree of Doctor of Philosophy has been carried out under my supervision and that this work has not been submitted elsewhere for a degree.

Date:

Dr. Ujjwal K. Saha
Associate Professor

To my parents

Acknowledgements

It is an honor for me to thank this institute for giving me such an excellent opportunity for undergoing my research. This thesis would not have been possible without support and encouragement from my supervisor Dr. Ujjwal K Saha who has made his help available at all time in so many ways. He made me to put my best efforts in writing this thesis. His inspiring guidance, motivation and sincere advice had enabled me to overcome all the difficulties during my research work. I am extremely fortunate to work under him.

I owe my deepest gratitude to my doctoral committee members to Dr. Anugrah Singh, Prof. Pinakeswar Mahanta and Dr. Subashisa Dutta for giving their valuable suggestions which helped me to shape myself to meet the requirement of a successful researcher. I also like to extend my sincere and heartfelt thanks to Dr. Ravi Mokashi Punekar from whom I used to get the required instruments in time for my laboratory work. Also I thank Mr. Shyam Anand for discussing subjects during the final phase of my research work. I specially acknowledge Dr. Damodar Maity and Dr. Arup Kumar Das for their expert advice and ideas on my research topic. It is my pleasure to thank Dr. Arnab K. De, Prof. Anoop K. Dass, Prof. Uday S. Dixit and Dr. P. Muthukumar for their teachings during the course work.

I would like to show my gratitude to Prof. D. Chakraborty (H.O.D, Mechanical Engineering Department) for providing all the facilities needed during my research work and financial support extended by the Mechanical Engineering Department. I like to mention my vote of thanks to all the faculty members for their cooperation. My special thanks to Mr. Amal Kalita for providing good facilities in CAD lab and Mr. Pankaj Kalita for providing me a separate computer for my research work. I extend my thanks to the technicians and machinists in Mechanical Engineering department for their assistance in the test set-up development.

I would like to place on record the financial grant offered by DST, New Delhi, which enabled me to attend and present a technical paper in ASME International Mechanical Engineering Congress and Exposition 2010 at Vancouver, Canada during November 12-18, 2010.

I am thankful to Dr. D. Santhosh Kumar, Dr. D. Arumuga Perumal, Mr. A. Ashok Kumar, Dr. D. Satheesh, Mr. C. Subramanian, Dr. Pandithevan, Mr. Yadav, Mr. Monash, Mr. Debnath, Mr. Anbarasu, Mr. Ravi, Mr. Sahoo, Mr. Pranjal and Mr. Satheesh with whom I had healthy discussions and they made my stay a pleasant one at IIT Guwahati Many thanks to my teammates in sports field for their friendship and company.

I am very grateful to my beloved parents for their immeasurable love, understanding and unwavering support, which made this feet possible. They gave me all the opportunities in the world, the freedom to pursue the ones I desired and the encouragement to follow through. I am blessed to have Mr. M.T.V. Krishnan, Mr. M. Shenbagaraj, Mr. L. Sankaranarayanan and Mr. Selvam as brothers; Mr. E.Velmurugan as uncle; and my mother-in-law Dr. C. Aruna for their encouragement. I am indebted to them for all the sacrifices they made for this effort. Last but not least, my love to my wife E. Vigneshwari and my son Master E. Rishi Gohul, as they never agree with any gesture of thanks from me.

M. Eswaran

Abstract

A moving tank partially filled with liquid that undergoes periodic motions is known to exhibit sloshing. Fluid motion in partially filled tanks may cause large structural loads if the period of tank motion is close to the natural period of fluid inside the tank. The free surface flow phenomenon is an important consideration in several engineering fields like safety assessment of power generation plants and for many other industrial purposes. Since early 1960s, the problem of liquid sloshing dynamics has been of major concern to aerospace, ocean and mechanical engineers. Civil engineers and seismologists have been studying liquid sloshing effects on large dams, oil tanks and elevated water towers under ground motion.

The capture of liquid free surface flow properties such as displacement, velocity and pressure has always been a challenging work. Many experimental and numerical techniques are available to capture these properties. However, some of the techniques yield the best results. This thesis is concerned with capturing the dynamic properties of the liquid free surface in partially filled tanks. The liquid free surface elevation, free surface velocity and pressure distributions are captured by numerical and experimental investigations.

The present investigation focuses on 2-D and 3-D rectangular domain with finite difference based Sigma-transformation (σ-transformation) for regular and random excitations, and the results obtained are compared with benchmark data. Techniques such as SURF, Marker and Cell (MAC), Volume of Fluid (VOF) require complex computer programming to treat the time varying free surface boundary and the computational mesh needs to be updated at every time step. The σ-transformation for treating the liquid free surface has gained wide spread popularity in recent years because of its simplicity and ease of implementation. This transformation is used to map the liquid domain onto a rectangle, such that the moving free surface in the physical plane becomes a fixed horizontal line in the computational mapped domain.

Further, investigations of free surface velocity with the aid of flow visualisation technique in an externally induced sloshed tank subjected to surge motion is scarce. In the present investigation, the interface location method has been used for capturing the liquid free surface experimentally, during the external excitation of the tank under low frequency. The 2-D planar Particle Image Velocimetry (PIV) technique is used to calculate the *U* and *V* velocity of the free surface, while the interface location technique is used for vertical velocity of the interface (*W*). In the interface location method, the videos captured by the movie camera are then transferred to the computer and further image analysis is carried out. Intensity gradient at each point is calculated, where the location of maximum gradient is considered as the interface. The luminance contrast between the liquid and the air which indicates the location of the interface is determined by maximum intensity gradient method.

The free surface velocity has been calculated by using the 2-D planar PIV technique. In this technique, the two images of each particle in the sheet are recorded in a short time interval. The images of marker particles in a fluid flow are used to measure instantaneous velocity fields. It is a technique which enables instantaneous measurement of the flow velocity at several positions in a plane. To extract the velocity vector, the mathematical correlation analysis is performed between two consecutive frames on each interrogation region**.** The PIV interrogation process is repeated until all the required velocity information is extracted from the captured record.

Finally, the dynamic response of liquid pressure in baffled liquid storage tank has been studied. The slosh arresting power of baffles is investigated through pressure measurement at various locations of the tank through experiments and numerical simulations. The pressure distributions are calculated experimentally by means of piezo-resistive type pressure sensors. In the numerical simulation, the fluid and solid are modeled in ADINA (Automatic Dynamic Incremental Nonlinear Analysis), and the results are compared with the present experimental data. The effects of a few parameters of the system, such as the liquid filling level, presence of passive sloshing damper at various frequencies have been examined.

Contents

Nomenclature

Symbol	**Description**
A	Wave amplitude, *m*
$\|\|a\|\|$	Root mean square of *a*
A_v	Vertical forcing amplitude, *m*
A_x	Horizontal forcing amplitude, *m*
b	Length of the tank, *m*
DT''	Transverse acceleration of the tank, m/s^2
E	Wave steepness
E_V	Volume error (%)
H_s	Significant wave height, *m*
h_s	Still water depth, *m*
h	Instant water height from tank bottom, *m*
K_n	Wave number
K_v, K_y	Nonlinearity forcing parameter in vertical direction
K_h, K_x	Nonlinearity forcing parameter in horizontal direction
L	Distance from free surface and tank center, *m*
N_w	Number of the linear monochromatic waves
n	Mode number
R	Radius of the tank , *m*
S_ζ	Spectrum
t	Time, *sec*
t^*	Non-dimensional time
Y_D''	Vertical acceleration of the tank, m/s^2
X_D''	Horizontal acceleration of the tank, m/s^2
$X(K)$	Spectra of wave elevation

Greek Symbols

ω_n	Natural sloshing frequency, *rad/s*
ω	Angular frequency, *rad/s*
ω_v	Frequency of vertical motion, *rad/s*
ω_h	Frequency of horizontal motion, *rad/s*
ω_p	Peak frequency, *rad/s*
ζ	Free-surface elevation, *m*
ζ_0	Initial free-surface elevation, *m*
ψ	Phase angle, *rad*
σ	Stretching factor
ϕ	Velocity potential function at physical domain (x, y, t)
Φ	Velocity potential function at transformed domain (X, σ, T)
φ	Velocity potential function at Computational domain (ξ, η, τ)
Ω_v	Frequency ratio in vertical direction $(= \omega_n / \omega_v)$
Ω_x	Frequency ratio in vertical direction $(= \omega_h / \omega_n)$
λ	Largest eigen value
δ^n	Residual at n^{th} iteration
δ, δ^2	First and second order central difference operators
$\delta_\xi \delta_\eta$	Mixed second order central difference operator.

Abbreviations

ALE	Arbitrary-Lagrangian-Eulerian
ADINA	Automatic Dynamic Incremental Nonlinear Analysis
BB	Back Boundary
BEM	Boundary Element Method
BET	Boundary Element Technique
BIT	Boundary Integral Technique
BMB	Bottom Boundary
CCD	Charged Coupled Device
CFD	Computational Fluid Dynamics
CV	Control Volume
EA	Excitation Amplitude
ER	Electro-Rheological
ER-TSD	Electro-Rheological Tuned Slosh Damper
EW	East-West
FB	Front Boundary
FDM	Finite Difference Method
FEM	Finite Element Method
FFT	Fast Fourier Transformation
FL	Fill-Level
FR	Frequency Ratio
FSI	Fluid Structure Interaction
FVM	Finite Volume Method
LB	Left Boundary
LBM	Lattice Boltzmann Method
LDV	Laser Doppler Velocimetry
LNG	Liquefied Natural Gas
MAC	Marker and Cell
MR	Magneto-Rhelogical
MRF	Medium Range Forecast
MT	Meshless Technique
MTMD	Multiple Tuned Mass Damper
NGM	Nested Grid Model
NS	North-South
ODE	Ordinary Differential Equation
PDE	Partial Differential Equation
PGF	Pressure Gradient Force
PIV	Particle Image Velocimetry
RB	Right Boundary
SOR	Successive Over Relaxation
TLCD	Tuned Liquid Column Damper
TLD	Tuned Liquid Damper
TSD	Tuned Sloshing Damper
VOF	Volume of Fluid
2-D	Two-Dimensional
3-D	Three-Dimensional

List of Figures

List of Tables

Chapter 1

INTRODUCTION

This chapter gives a general background on the importance of sloshing and highlights the motivation behind the present investigation. It also summarizes various numerical and experimental techniques used for capturing liquid free surface properties in a sloshed tank. The objectives of the present investigation have been addressed. At the end, the organization of thesis is described.

CONTENTS

1.1 General Background

Sloshing can generally be described as back and forth motions of the liquid in a partially filled tank. It is a phenomenon where liquid in the tank move irregularly with a splashing sound. Elevated water towers and industrial storage tanks under excited ground motion and sloshing effects on large dams, liquefied natural gas (LNG) ship tanks and moving oil tanks are studied by civil engineers and seismologists. Moreover, aerospace and nuclear engineers, designers of road, ship tank builders, applied mathematicians and physicists are having the great concern on liquid free surface problem like liquid sloshing. The large liquid movement creates highly localized impact pressure on tank walls which may in turn cause structural damage and may even create sufficient moment to affect the stability of the vehicle which carries the container.

The linear theory of liquid sloshing is adequate for determining the natural frequencies and wave height of the free surface. This theory is also useful for finding the liquid velocity, hydrodynamic pressure, forces and moments as long as the free surface maintains a planar shape with a nodal displacement that remains perpendicular to the line of excitation. Although the linear theory has been used widely as a practical technique, the non-linear analysis is to be performed when the excitation frequency is very close to the fundamental frequency of sloshing liquid or large amplitude of excitation. The analytical techniques for predicting large amplitude sloshing are still not fully explored. The numerical techniques such as the finite difference method (FDM), finite element method (FEM), finite volume method (FVM), meshless technique (MT), the boundary integral technique (BIT) and the boundary element method (BEM) have been used for the solution of the sloshing problems.

The sloshing in a moving liquid tank causes safety and comfort issues such as undesirable forces on brake systems (Figure 1.1) in liquid carrying tankers like LNG (Figure 1.2), high impact loads upon the containment system and structural parts (Graczyk *et al*., 2003; Lee, 2007). Further, under earthquake conditions, it creates fatigue, safety problems in nuclear reactors and power generating plants (Kimura *et al*., 1995). Sloshing also produces unnecessary noises referred to as “clinking noises” in automobile fuel tanks (Wiesche, 2006)

and safety issues in propellant tanks in the spacecraft under micro-gravity conditions (Snyder, 1999).

Figure 1.1: A typical road vehicle carrying liquid container.

As compared to rigid loads, the number of road accidents related to liquid loads is significantly higher. This is due to the fact that the dynamic behavior of a liquid in a transporting container considerably affects the stability and controllability of the vehicle (Popov *et al.*, 1992). Liquid sloshing occurs in several marine engineering applications including green water on ship decks and in vessels transporting liquids in hold tanks (Veldman, 2007). Hence, the problem of sloshing gains more attention and practical importance in the engineering community (Valentine, 2005).

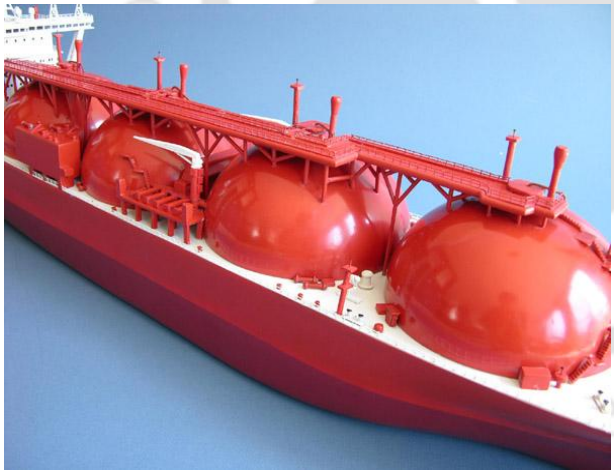

Figure 1.2: A typical ships carrying Liquified Natural Gas vessel.

(Photo credit : EERI)

Figure 1.3: Seismic effect to industrial liquid storage tanks.

The liquid in a tank subjected to forced oscillation at a frequency close to a natural frequency of oscillation exhibits resonance or system natural frequency. This may occur in the fuel tanks of rocket engines, in the holds of crude-oil carrying tankers and in large liquid reservoirs excited into motion by seismic activity (Figure 1.3). This resonance may lead to

the structural damages in tanks as shown in Figure 1.4. Depending on the type of disturbance and tank shape, the free liquid surface can experience different types of motion including simple planar, non-planar, rotational, irregular beating, symmetric, asymmetric, quasi-periodic and chaotic. The amplitude of slosh, in general, depends upon the amplitude of excitation and frequency of the tank motion, liquid-fill depth, liquid properties and tank geometry.

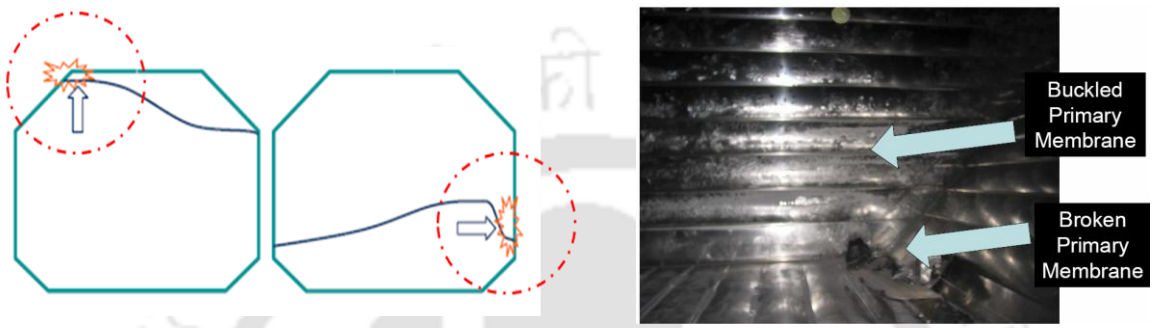

Figure 1.4: Structural damages in LNG ship container.

Many theoretical and experimental studies have been carried out in the area of liquid sloshing in fixed and moving tanks. Faltinsen (1974), Faltinsen and Timokha (2002), and Frandsen and Borthwick (2003) presented approximate theoretical forms for inviscid sloshing motion in fixed and moving tanks. Numerical simulations are used to verify the validity of analytical results if in case experimental results are not available. Extensive numerical analyses of liquid slosh dynamics have been undertaken by using numerical methods such as the FDM, FVM and BEM techniques, such as SURF, marker and cell (MAC), volume of fluid (VOF) are available to handle the free surface of the moving fluid (Hirt and Nichols, 1981; Popov *et al*., 1993; Cho *et al*., 2005; Akyildiz and Unal, 2006, Arafa, 2007). The σ -transformation is also frequently used in treating time varying free surface flows. The vast majority of the sloshing numerical works so far deals with 2-D liquid domain. Frandsen (2004) has also used σ -transformation technique for 2-D rectangular domain. The time-varying liquid free surface can be mapped onto a fixed plane surface by the proper coordinate transformations, called the σ -transformation, which prevents the need for free surface smoothing for the cases considered herein.

Various aspects of the 2-D and 3-D nonlinear liquid sloshing problems of excited tanks have been studied numerically with the help of coordinate transformations, where the fluid is assumed to be inviscid and irrotational. Hence, the governing equations and boundary

conditions of liquid dynamics in the tank are based on the potential flow theory. A numerical study on regularly and randomly excited tank in horizontal and vertical direction is carried out. The results are validated with benchmark results. The wave elevation time history, phase plane diagram and surface plots represent the wave nonlinearity during its motion.

A host of researchers, on the other hand, have carried out experimental investigations on the self-induced sloshing in a rectangular tank with circulating flow. Most of these studies carried out in the past two decades have been limited to self induced excitations (Okamoto *et al.*, 1991; Hu *et al.*, 1999). Further, the work in the area of flow visualisation techniques on externally induced sloshing with surge motion of tank is scarce. The unsteady free surface velocities during the surge motion of a liquid tank are determined through experimental investigation. Liquid height is observed by the intensity variation of the interface between the air and liquid (Law *et al.*,1999). The intensity gradient at each point has been calculated. The location of maximum gradient has been considered as interface. The movement of interface can be analyzing by cross-correlation between these matrices. The free surface oscillations are plotted for different excitation frequencies. The planar 2-D PIV technique (Adrian, 2004) is used to calculate the U and V velocity of the free surface, while the interface location technique is used for vertical velocity of the interface (W). The velocities are measured for various liquid fill levels and excitation frequencies. Finally, the pressure distribution at various locations of the excited tank is studied experimentally.

The interface location method (Law *et al.*, 1999) has also been used for capturing the liquid free surface during the external excitation of the tank under low frequency. In this method, the videos captured by the movie camera are usually transferred to a computer where image analysis is carried out. In this analysis, the location of maximum gradient was considered as interface. The luminance contrast between the liquid and the air which indicates the location of the interface is determined by maximum intensity gradient method. The 2-D planar PIV technique uses images of marker particles in a fluid flow to measure instantaneous velocity fields. Two images of each particle in the sheet are recorded in a short time interval. This technique that relies on the imaging of tracer particles embedded within a flow at two distinct times, t_1 and t_2, to estimate the velocity of the fluid. The distance separating the two images gives a local velocity vector. Correlation analysis is used to extract the particle displacements and for the cross correlation, the PIV-sleuth is used.

The effects of a few parameters of the system, such as the liquid filling level, presence of passive sloshing damper at various frequencies have been examined. The numerical results attained using ADINA-FSI are compared with experimental results. The response of the coupled system (fluid and solid domains) is obtained by using the well-known software ADINA (Automatic Dynamic Incremental Nonlinear Analysis), which offers efficient fully coupled fluid–structure interaction (Bathe, 1996; Rugonyi and Bathe, 2001; Bathe and Zhang, 2004). In order to study the influence of location and shapes of baffles under sinusoidal excitation, the fluid and solid domains are modeled and the dynamic response of baffled liquid storage tank has been analyzed extensively.

1.2 Present Objectives

The objective of the present investigation is to study the free surface characteristics through numerical and experimental investigation in partially filled moving tanks such as free surface displacement, velocity and pressure near the wall. In order to achieve this, the following specific goals have been addressed:

- To capture the free surface elevation during the motion of the tank experimentally by using interface location method, and numerically by finite difference based sigma transformation technique.

- To find free surface velocity and streamline profiles of liquid in the externally induced partially filled tank. To measure the liquid free surface velocities for various liquid fill levels and excitation frequencies.

- To calculate the liquid pressure at the tank walls by using piezo-resistive transducer and to compare with the fluid-structure coupled numerical analysis. To analyze effect of baffles through experimental and numerical investigations.

- To make a comparative analysis of the above numerical and experimental results.

1.3 Organization of the Thesis

The thesis is arranged in nine chapters as follows. Chapter-2 deals with a review of the existing literature encompassing the numerical simulation and experimental techniques. The detailed information about σ-transformation with advantages and limitations with overcoming procedures are reported in Chapter-3. Chapter-4 is devoted to the mathematical equations for 2-D and 3-D liquid domains and its boundary conditions. The mapping techniques are discussed elaborately in a step by step procedure. The time varying liquid free surface is mapped into a fixed domain using σ-transformation technique and the finite difference method is applied on the transformed governing and boundary conditions. Chapter-5 focuses on the results of liquid free surface elevation, wave phase plane, power spectral density, streamline and velocity vector diagrams from the numerical simulation of 2-D and 3-D liquid domains. The grid independence study, error study and validation tests are also reported in this chapter. The experimental procedures and the results for capturing the free surface elevation of liquid during the tank motion are discussed in Chapter-6. The behavior of free surface velocity using 2-D planar PIV technique is discussed in Chapter-7. Flow behavior in terms of streamline plots and vector plots are described in this chapter. Liquid pressure near tank wall is captured numerical and experimental techniques and results are compared in Chapter-8. The conclusions and future scope are presented in Chapter-9.

To clarify certain points a few appendices are also included in the thesis. Appendix-A consists of the pseudocode of the 3-D rectangular tank. The detailed error analysis for experimental measurements is showed in Appendix-B. The relevant details of the instruments used in the experiments and the error analysis are given in Appendix-C.

Chapter 2

REVIEW OF LITERATURE

In this chapter, a comprehensive review of literature has been carried out. Stating some notable facts in the area of liquid sloshing, the chapter identifies and discusses the various important terms and parameters associated with liquid sloshing. This is followed by a thorough review of both numerical and experimental investigations reported in open literature. In either case, the key issues and findings have been discussed, compared and summarized.

CONTENTS

2.1 Introductory Remark

As mentioned earlier, liquid sloshing in a moving tank constitutes a broad class of problems of great practical importance. Many researchers have been working on sloshing since last fifty years. Their research work deals with both experimental studies as well as numerical simulation.

2.2 Notable Facts in Sloshing

To begin with, a host of researchers have studied this phenomenon in moving vehicles. The earlier study relevant to this topic was performed by Jacobson and Ayre (1951), and Graham and Rodriguez (1952). In 1957, the flight of Jupiter IRBM AM-1B vehicle terminated at 93 seconds because of propellant slosh when the missile achieved an altitude of 60,000 feet. Housner (1957, 1963) developed an analytical method for the determination of hydrodynamic wall pressures under the assumption that the tank is a rigid structure fixed at the base and only the fundamental sloshing mode is important. Again in 1964, when the test vehicle F1 was launched, a catastrophic instability occurred, resulting in premature engine cut and an oscillation in both pitch and yaw plane. Loss of control of the vehicle near the end of the flight occurred due to fuel sloshing. Thereafter, sloshing had been extensively studied and used in many engineering applications by scientists, especially by the NASA people.

The early interest on the dynamic characteristics of a liquid free surface dates back to the beginning of the previous century. The 1964 Alaska earthquake and the extensive damage inflicted on various kinds of liquid storage tanks seems to have initiated an intense and uninterrupted interest on the seismic behavior of modern structures used for the storage of liquids or liquid like materials, e.g., water, fuel, oil products, chemicals, wastes, and LNG (Lamb, 1932, Drosos *et al*., 2008). As cited by Matsui (2007), many tanks during earthquakes have been subjected to serious damages, due to liquid sloshing. Especially, during the 2003 Tokachi-oki earthquake, seven oil-storage tanks of floating roof type located at Tomakomai, Hokkaido, Japan were seriously damaged (Hatayama *et al*., 2005). In addition, the failure of the floating roof and the fire of oil-storage tanks have been observed frequently, e.g., during the 1964 Niigata and the 1983 Nihonkai-chubu earthquakes. The sinking of the floating roof caused by sloshing has never been experienced so far in Japan (Matsui, 2009).

Applications in the aerospace industry has been reviewed and discussed by Abramson (1966) both analytically and experimentally. In the 1970s and early 1980s, sloshing flows in liquid oil carrier vehicles have been extensively studied, since slosh-induced loads can cause serious damage to cargo structure in marine engineering. Feng (1973) used a three-dimensional version of the Marker and Cell method (MAC) in a rectangular tank. This method consumes large amount of computer memory and CPU time and the results reported indicate the presence of instability. A nonlinear analytic method for simulating sloshing, which satisfies the nonlinear boundary condition at the free surface was suggested by Faltinsen (1974). The coupling effect between liquid sloshing and structural vibration is usually neglected in practice. The preliminary study of these coupling effects in cylindrical tanks was carried out by Haroun (1980, 1983). Partom (1987) presented the most popular Volume of Fluid (VOF) method developed by Hirt and Nichols (1981) for tracking the free surface boundary for cylindrical tank. From 1980, much attention has been paid to model the transient free-surface potential flows by means of the Boundary-Element Technique (BET), Finite Volume Method (FVM), Finite Difference Method (FDM) and Finite Element Method (FEM) after the booming of new numerical techniques and invention of high speed computers.

Recently, Space Exploration Technologies (SpaceX) launched Demo Flight 2, Falcon 1 launch vehicle on March 20, 2007. Initially, instability grew in pitch and yaw axes, and after about 30 seconds a noticeable roll torque was also induced. This roll torque eventually overcame the 2nd stage's roll control thrusters and centrifuged the propellants, causing flame-out of the Kestrel engine. There is high confidence that LOX slosh was the primary contributor to this instability (http://sloshcentral.bbbeard.org/Refs/F1-DemoFlight2-Flight-Review.pdf).

2.3 Description of Sloshing Parameters

This section deals with the description of the sloshing parameters, such as tank shape, excitation, flow impediment objects, fluids used, tank wall, and the field in which the experiments are conducted. Fifteen research articles (Cole, 1966; Dodge, 1966; Bugg, 1970; Sudo *et al.,* 1987; Chiba, 1992; Warnitchai and Pinkaew, 1998; Modi and Munshi, 1998; Grundelius and Bernhardsson, 1999; Pal *et al.,* 2001, Sakamoto *et al.,* 2001; Sawada *et al.,* 2002; Akyildiz and Unal, 2005; Yano and Terashima, 2005; Nasar *et al.,* 2008; and

Panigrahy *et al.*, 2009) have been chosen to find and analyze the effect of these parameters on sloshing. The work reported in these investigations has been compared and summarized in Table-2.1 (refer page 20).

2.3.1 Tank Shape

The first parameter concerns with the shape of the tank which can be either symmetric or asymmetric as shown in Figure 2.1. From Table-2.1, it is clear that both the rectangular and cylindrical shaped tanks seem to have equal importance. It is noticeable that no one used asymmetric tank in their experiments. This is probably due to the fact that in real time applications, liquid tanks are often built symmetrically.

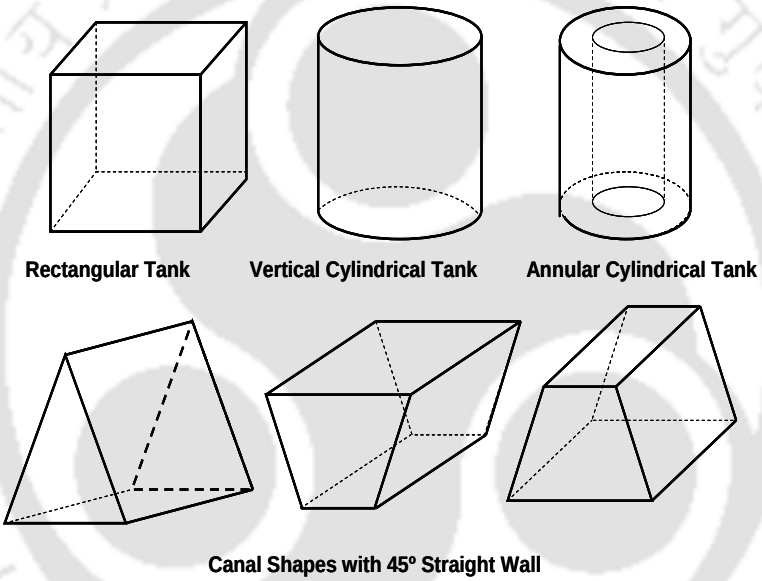

Figure 2.1: Various types of tank shape (symmetric and asymmetric geometries).

The recent increase in demand for midsize tankers and LNG carriers entails more attention on the accurate prediction of sloshing fluid behavior inside tanks, whereby ship motions are more reactive to the external disturbances and the natural periods of sloshing are longer due to growing individual tank sizes and its shapes (Rhee, 2005). In general, many researchers used basic tank shapes like rectangular and cylindrical tanks for their analytical and numerical studies because of its simplicity. Other tank geometries such as annular cylinder, horizontal cylinder, spherical, triangle, oblate spherical, canal shape, elliptic tanks etc. have also been used in rare cases. Over the years, the study of LNG tank shapes continues to be an interesting topic. During the filling process, the LNG exercises unsteady forces on the tank walls and makes the vessel react to these forces by ship motion. Baeten (2009) predicted the

hydrodynamic wall pressure from LNG sloshing on different tank shapes and specific test cases have been validated against experimental data.

The sloshing frequencies of a horizontally resting cylindrical tank are difficult to obtain, even for an ideal frictionless liquid (Wiesche, 2008). Calculating the natural frequency is quite easy for simple geometric shapes, but for complex nonlinear designs, it becomes significantly more complex. While solving natural frequency for complicated tank shapes numerically, the set of nonlinear equations needs to be solved in asymmetric and non-uniform cells. Problems arise not only in grid generation but also in the computation part. It is difficult to analyze and determine the free liquid natural frequencies and mode shapes of horizontal cylinders and spherical tanks that are partially filled with liquid. The difficulties arise due to the fact that the walls are not straight and parallel to the axis of symmetry (Ibrahim, 2005).

Romero *et al.* (2005) conducted experiments to determine the magnitudes of lateral sloshing forces within tanks of three tank shapes like oval, circular and modified oval (that are commonly used in commercial applications) under high fill volumes (about 90 % to 98 %). The results showed that the sloshing forces depends on the angle between the fluid free surface and the tank wall, the outage's length and average height of the tanks. For the 90 % of fill level, highest sloshing forces first occurred on the circular tank followed by the oval and the modified oval shapes. However, for 98% of fill level, this order just got reversed. Moreover, the sloshing pressure was investigated for two different sized tanks by Hwang *et al.* (2008). The tank shape mainly defines the liquid free surface profile.

2.3.1.1 Effect of Inclination of Tank in Sloshing

Bugg (1970) performed experiments to determine the effect on liquid oscillation frequency of changes in the angle (Figure 2.2) between the tank axis and force body vector. Tank was tilted from 0° to 60° to the local vertical, and the liquid depth to tank radius (d/r) was also varied. Two modes of oscillation were studied, one with its nodal line along the minor axis of the liquid free surface, and the other with its nodal line along the major axis of the surface. The frequency of each of these modes was decreased by increasing the tank tilt, with the frequency of the former being decreased much more than the frequency of the latter. He concluded that the tank angle made only a small effect on shuttle propellant dynamics during launch for the expected 10° or less angle between thrust vector and tank axis. Very few reports dealt with sloshing in an inclined tank or inclined wall. These types of investigation

were recently reported by Behr and Abraham (2002), Taniguchi (2004), Moaleji and Greig (2007), Liu and Lin (2008), and Sweedan (2009).

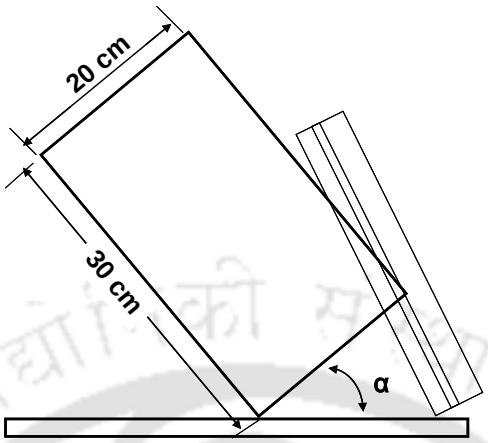

Figure 2.2: Schematic diagram of test set-up of Bugg (1970).

2.3.2 Excitation

The second important parameter concerns with the types of excitation that produces a free oscillation or a forced oscillation. A majority of investigators made use of simple harmonic excitation which comes under forced oscillation. A few of them used linear forced oscillation and random forced oscillation. The knowledge of natural frequencies for liquid free surface is important in the design of liquid tanks subjected to different types of excitation. The dynamic behavior of a free liquid surface depends on the type of excitation and its frequency content. The excitation can be linear, sinusoidal, ramp or random. Its orientation with respect to the tank can be surge, sway, heave or pitch, yaw, roll or a combination of these.

Hashimoto and Sudo (1988) concluded from the vertical vibration of cylindrical liquid tank experiments that the first resonant frequency of the axial vibration of the liquid column depends on the excitation acceleration. The first resonant frequency decreases as the excitation acceleration of the tank containing liquid increases. The first resonant frequency of the axial vibration of the liquid column decreases as the liquid height in the cylindrical tank increases. Colagrossi *et al.* (2004) observed an asymmetric behavior of the wave elevation along the tank, as well as alternation of the breaking phenomenon at the two tank sides. By varying the excitation period of the sinusoidal horizontal motion of the tank and by increasing its amplitude of oscillation, some peculiar phenomena were observed for excitation period near the linear sloshing natural period. Such phenomena are connected with important water-

wall interactions and with the vortex generation consequent to the post breaking phenomena. Because of their complex features, they cannot be predicted by potential flow models.

Rotation motions can be considered for space vehicles and ocean going vehicles. The ship motions excite sloshing, which in turn affects the ship motions. The sloshing induced roll movement on the vessel will cause roll damping by properly choosing the highest natural sloshing period close to the roll natural period. Under the roll excitation, the fluid in the horizontal cylindrical tank does not participate in the tank motion since it is assumed to be inviscid. If the fluid viscosity is considered, then one has to solve the full Navier-strokes equations to estimate the thickness of the fluid participating in the tank motion. Researchers generally applied the simple harmonic motion or linear motion to the sloshing tank. In many practical situations, a system may undergo sudden changes such as mechanical impact, water hammer, etc. These can be represented and analyzed using an impulse input. In nature, very few motions are periodic, even sinusoidal. Sinusoidal make up the particular class of periodic functions. It can be expressed in terms of cosine functions. Therefore, one should know necessarily how a measurement device responds to the sinusoidal input.

2.3.2.1 Excitation direction

The types of tank motions are depicted in Figure 2.3. There is no necessity to apply all the motions at the same time. It is just adequate that any one or two motions can be merely applied to a tank in regard to the application. Type of tank motions is usually preferred based on the applications. For example, vertically excited motion is considered as an ideal type for earthquake condition. Most of the works reported are under earthquake condition where the tank is given a vertical motion or a combined excited tank motion (Frandsen and Borthwick, 2003, Hashimoto and Sudo, 1988).

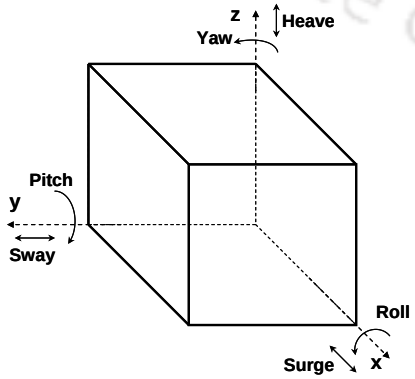

Figure 2.3: Illustration of tank motions.

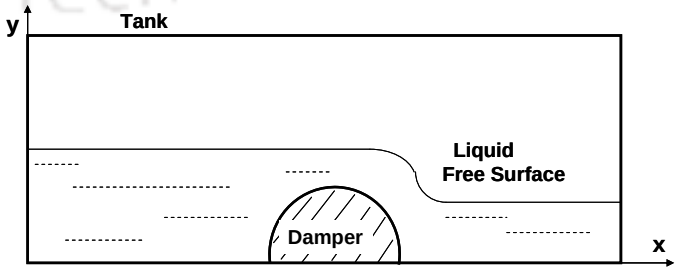

Figure 2.4: Tank with liquid semi-circular damper.

2.3.3 Flow Impediment Objects

The third parameter deals with the kind of damping devices used for conducting experiments. Investigations have been carried out without and with baffles (horizontal and vertical). Modi and Munshi (1998) used a semi-circular solid damping device with a tuning arrangement (Figure 2.4). A liquid sloshing damper, also known as nutation damper or tuned liquid damper, operates on the principle of energy dissipation through liquid sloshing and wave breaking of the free surface. The device consists of a suitably shaped tank partially filled with a liquid (e.g., water). When such a system is subjected to acceleration, the liquid is set into sloshing motion, accompanied by waves at the free surface. Such a device, in a sense, is similar to a multiple tuned mass damper (MTMD) because of its effectiveness over a range of frequencies (Modi and Munshi, 1998). With a proper design, a tank partially filled with liquid can be used as an effective damper for suppressing horizontal vibration of structures. This type of damper has gained popularity in practical use due to its low cost and simplicity (Fujino *et al.*, 1992; Ueda *et al.*, 1992). A tuned liquid damper (TLD) had been used to utilize the dynamic effect of liquid sloshing (Warnitchai and Pinkaew, 1998). TLD is used to adjust the natural frequency of the system by adding or removing weights.

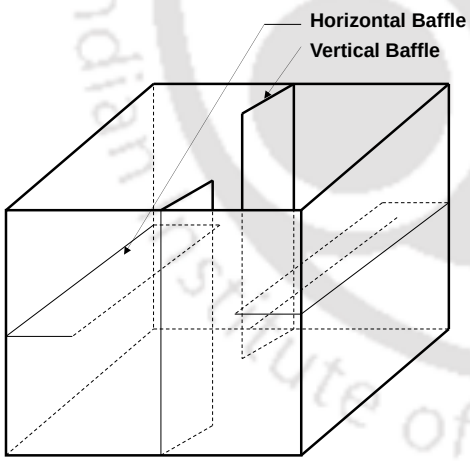

Figure 2.5: Tank with vertical and horizontal baffle.

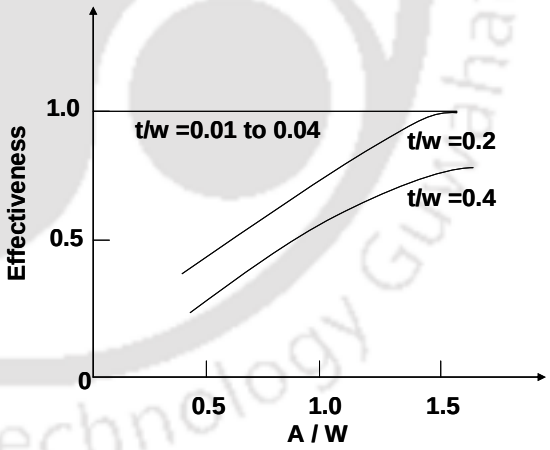

Figure 2.6: Variation of the baffle thickness with amplitude to width ratio (Cole, 1966).

2.3.3.1 Effect of baffles on sloshing

Baffles are generally used as passive slosh damping devices in the liquid storage tanks to obstruct the vertical velocity of the sloshing fluid. The basic concept of passive sloshing damper is to dissipate the sloshing motion energy by breaking a main sloshing flow into several weaker sub-streams. Different types of baffles viz., horizontal, vertical, and annular

or ring baffles have been used in the past (Pal *et al*., 2001; Akyildiz and Unal, 2005; Panigrahy *et al*., 2009). They can be either flat or curved structures fixed to the walls of the tank as shown in Figure 2.5. These structures lie on the liquid-flow path, and hence act as a barrier for the smooth flow of the fluid, and have varied functions depending on the circumstances. They are used for dissipating the kinetic energy of fluid in motion, enhancing the mixing process in a mixing tank and yet sometimes for aggravating convection in heat generating regions. The flow impediment objects drastically reduce the free surface elevation, and also the hydrodynamic pressure.

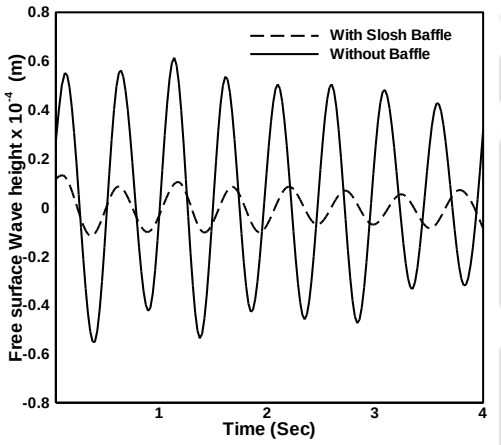

Figure 2.7: Experimental observation (Pal *et al*., 2001).

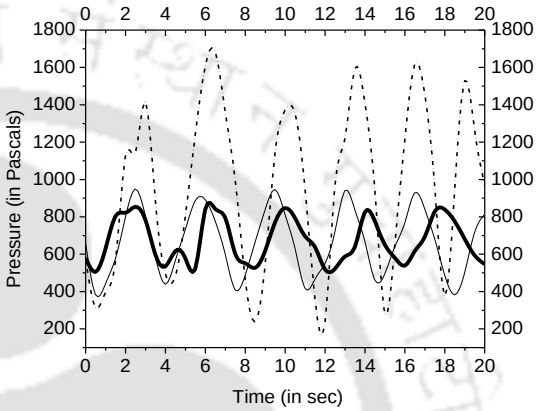

Figure 2.8: Experimental observation (Panigrahy, 2006).

Cole (1966) conducted ink-trace experiments in a cylindrical tank to study the baffle thickness effects in fuel sloshing. His work on the effectiveness of baffle with respect to amplitude to width ratio (*A/W*) showed that baffle thickness decreases baffle effectiveness by as much as 50 percent at moderate amplitudes of oscillation (Figure 2.6). Pal *et al*., (2001) studied the free surface displacement of the liquid with respect to time (Figure 2.7) in a tank equipped with ring baffles. Akyildiz and Unal (2005) investigated liquid sloshing in a rectangular tank at a model scale with various fill levels and baffles. In an experimental study, Panigrahy (2006) investigated the effect of baffles on sloshing behavior of liquids in a rectangular tank by studying pressure variation with respect to time (Figure 2.8). The observation shows that the ring baffles are the best choice as they reduce the pressure to the maximum extent. This happens because the ring baffle not only suppresses the velocity of impact of the fluid at the walls, but also retards the vertical motion of the liquid near the other two adjacent walls, thereby suppressing the wave amplitude. The introduction of baffles in the tank decreases the sloshing effect by a considerable amount. This is because the baffles

create turbulence in the flow field thereby dissipating the excess kinetic energy to the walls. Baffles can significantly reduce fluid motions and more investigations are needed to study the effect of the fluid viscosity on impact pressures.

2.3.3.2 Effect of tuned liquid dampers on sloshing

When the fluid imparts forces to its tank which in turn are transmitted to the vibrating structure influencing its motion, the imparted forces during sloshing are inertial, gravitational, and dissipative in nature (Sayar and Baumgarten, 1982). Use can be made of the inertial forces for vibration absorption and of the dissipative forces for damping. Tuned Liquid Dampers encompassing both Tuned Sloshing Dampers (TSDs) and Tuned Liquid Column Dampers (TLCDs) have become the popular form of initial damping device. A tuned sloshing damper (also known as nutation damper) is extremely practical and operates on the principle of energy dissipation through liquid sloshing and wave breaking of the free surface. Fundamental mode frequency of liquid sloshing is tuned to the natural frequency of structure and the damping ratio of the sloshing mode is set to an optimal value (Vandiver and Mitome, 1982; Guzel *et al*., 2004).

2.3.4 Fluids Used

The fourth parameter associated with sloshing concerns with the type of fluids used in the experiments. Most of the researchers preferred water as a fluid in their studies not only because it is easily available, but also it satisfies their practical needs effectively. For example, even if the real plants like casting industries are considered, it is possible to use water in the study. This is because the Reynolds number of water at normal temperatures is almost the same as that of molten iron or molten aluminum at high temperatures considering the similarity law in fluid dynamics. For example, the kinematic viscosities of molten iron metal at 1350 K and 1400 K are 1.365 x 10^{-6} *mPa.S* and 1.237 x 10^{-6} *mPa.S*, respectively, while that of water at 293 K is 1.0 x 10^{-6} *mPa.S* (Yano and Terashima, 2005; Terashima and Yano, 2001).

2.3.4.1 Effect of compressibility of fluid

Topliss *et al.* (1992) studied the water impact on a wall with air bubble formation and developed a potential flow model to determine the frequency of oscillation of the bubble pressure. As reported by Godderidge *et al*. (2009), the potential flow model developed by

Topliss *et al.* (1992) overestimates the experimentally observed pressure oscillation frequency. Godderidge *et al*. (2009) studied the effect of compressibility, various combinations of compressibility models for air and water and found that the inclusion of fluid compressibility can have a significant effect on the pressure evolution of a sloshing flow. When fluid impact is not a significant feature of sloshing, then an incompressible fluid model can be used for both fluids. When modeling the sloshing with significant air entrapment, compressibility of both air and water should be included. An isothermal compressibility model for air may still be preferable. The non-dimensional pressure impact parameter is based on the tank size. Rise of pressure during impact, can be used to determine whether air and water should be modeled as compressible fluids. Hashimoto and Sudo (1988) investigated the bubble cluster formation in the liquid and tank wall responses during the vibration. Bubble formation was observed in cylindrical tanks. It was found that the resonant frequency of the liquid-tank vibration system depended on the excitation acceleration. The response of the liquid pressure and the tank wall acceleration was suddenly changed by the formation of a bubble cluster in the oscillating liquid column.

A few articles as shown in Table-2.1 were concerned with Magnetic Rhelogical (MR) and Electro-Rhelogical (ER) fluids. ER fluids are same as the magnetic fluids, but it needs electric field instead of magnetic field. From Table-2.1, it can be seen that only in three cases, investigators used fluids like methanol, carbon tetrachloride (CCl_4) etc., other than water, MR and ER fluids.

2.3.4.2 Effect of magnetic field in sloshing

Magnetic fluids were developed as a way to control the position of the liquid fuel in space (Papell, 1965). In particular, when a magnetic field is applied to a magnetic fluid, several interesting characteristics have been observed because of the combination of the strong magnetism and liquidity. When the non-uniform magnetic field was applied to the tank, the resonant frequency of the system moved toward the high frequency region with the magnetic field intensity.

2.3.4.3 Effect of electric field in sloshing

Electro-Rheological (ER) fluids change their physical properties in the presence of an electric field. The effect is sometimes called the Winslow effect, after its discoverer, who obtained a US patent on the effect in 1947 and published an article in 1949 (Winslow, 1949). Sakamoto

et al. (2001) proposed the Tuned Sloshing Damper (TSD) utilizing an electro-rheological (ER) fluid as a sloshing liquid (ER-TSD) and carried out the experiments for the forced and free vibration tests with and without ER-TSD. In course of the experiments, the electric field between the electrodes and fill levels were varied to find the maximum displacement.

2.3.5 Tank Wall

The fifth item concerns with the type of tank wall which can be either rigid or flexible. A majority of the investigators used rigid wall tank. The forced excitation of liquid tanks of different geometries has been treated based on the linear theory of small oscillations. Under forced excitation, it is important to determine the hydrodynamic loads acting on a tank and their phase with respect to the excitation. One should determine the wave height of liquid free surface, which affects the location of the center of mass in tank and the hydrodynamic forces, which are estimated by integrating the pressure distribution over the wetted area. Distribution of hydrodynamic pressure due to excitation gets influenced by wall flexibility. For tanks with rigid wall, it is linearly distributed i.e., hydrodynamic pressure is distributed same as hydrostatic pressure. Chiba (1992) conducted experiments for studying the effect of wall flexibility in the nonlinear hydro-elastic vibration of a cylindrical tank with elastic bottom containing liquid. However, in most of the researches, the tank was made up of plastic like perspex, acrylic or glass material. Usually, these materials are considered as rigid walls. The rigid and flexible walls are also one of the factors affecting the sloshing forces, moments and pressure at the tank wall.

2.3.6 Field

The last item under consideration deals with the field where most of the experiments have been conducted in gravity fields. Dodge (1966) conducted experiments with high bond number by varying the radius of the tank as applicable in space. The problems of liquid slosh dynamics under microgravity are different from those encountered in a regular gravitational field. These problems include liquid reorientation and the difficulty of moving and handling, since body force is almost negligible. Under microgravity, surface tension forces become predominant. The bond number, given by the ratio of the gravitational to capillarity forces, plays a major role in the free surface liquid characteristics.

Table 2.1: Comparative data of major sloshing parameters.

Sl. No	1	2	3	4	5	6	7	8	9	10	11	12	13	14	15
Research articles [See Footnote]	**[1]**	**[2]**	**[3]**	**[4]**	**[5]**	**[6]**	**[7]**	**[8]**	**[8]**	**[10]**	**[11]**	**[12]**	**[13]**	**[14]**	**[15]**
(a) Tank Shape								-							
Symmetric															
Rectangular	**x**			**x**		**x**	**x**			**x**		**x**		**x**	**x**
Cylindrical	**x**	**x**	**x**	**x**	**x**				**x**		**x**		**x**		
Asymmetric															
(b) Excitation															
Free Oscillation			**x**												
Forced Translation															
Linear								**x**							
Harmonic	**x**	**x**	**x**	**x**	**x**	**x**	**x**		**x**	**x**		**x**		**x**	**x**
Forced Rotation															
Random / Combination											**x**		**x**		
(c) Damping Devices															
No baffles		**x**	**x**	**x**	**x**			**x**	**x**	**x**	**x**	**x**	**x**	**x**	**x**
Horizontal Baffle	**x**											**x**			**x**
Vertical Baffle												**x**			**x**
Ring baffle	**x**								**x**						**x**
Semi-circular solid							**x**								
Others															
TSD/TLD						**x**	**x**								
(d) Fluids Used															
Inviscid fluid															
Water	**x**	**x**			**x**	**x**	**x**		**x**			**x**	**x**	**x**	**x**
Viscous fluid															
ER/MR Fluid				**x**						**x**	**x**				
Others		**x**	**x**					**x**							
(e) Tank Wall															
Rigid wall	**x**	**x**	**x**	**x**		**x**	**x**		**x**	**x**	**x**	**x**	**x**	**x**	**x**
Flexible Wall					**x**			**x**							
(f) Field															
Gravity Field	**x**		**x**	**x**	**x**	**x**	**x**	**x**	**x**	**x**	**x**	**x**	**x**	**x**	**x**
High bond number (Low / Micro gravity		**x**													

x - the possibility was mentioned to exist; blank - the possibility was mentioned not to exist or was not mentioned.

[1] Cole (1966); [2] Dodge (1966); [3] Bugg (1970); [4] sudo *et al*. (1987); [5] Chiba (1992); [6] Warnitchai and Pinkaew (1998); [7] Modi and Munshi (1998); [8] Grundelius and Bernhardsson (1999); [9] Pal *et al*., (2001); [10] Sakamoto *et al*. (2001); [11] Sawada *et al*. (2002) , [12] Akyildiz and Unal (2005), [13] Yano and Terashima (2001), [14] Nasar *et al*. (2008), and [15] Panigrahy *et al*. (2009)

2.4 Review of Numerical Work

A lot of researchers have done numerical simulation either by using self-made program or by using commercial CFD packages (Modi and Seto, 1997, Frandsen and Borthwick, 2003, Kim *et al.*, 2001). Various models and techniques have been used to solve the problem. Following is the review of the literature which briefly cites the study done till now.

2.4.1 Numerical Methods

Numerical analyses are popular in studying liquid sloshing in moving tanks. Numerical investigations on sloshing in two-dimensional and three dimensional problems were carried out by several studies using different approaches. Among these, most of the researchers preferred the finite element method, finite volume method and finite difference method to predict the free surface displacements and hydrodynamic pressures during sloshing.

2.4.1.1 Finite volume method (FVM)

It was first employed by McDonald for the simulation of 2-D inviscid flows (Blazek, 2001). The FVM utilizes the integral form of the conservation equations. Governing equations converted into integral form and the solution domain is subdivided into a finite number of arbitrary polyhedral and non-overlapping control volumes. The conservation equation was applied to each control volume (CV). Interpolation is used to express variable values at the control volume surface in terms of nodal center values. The FVM is suitable for any type of grid especially for complex geometries (Versteeg and Malalasekera, 1995). Few researchers reported the finite volume techniques for sloshing problems (Zhu *et al*., 2001; Bucchignani *et al*., 2004; Siva Prasad, 2006; Djavareshkian and Khalili, 2006). Recently, Djavareshkian and Khalili (2006) solved the sloshing using FVM for a half empty cylinder and tracked the free surface using VOF techniques. They validated their code with analytical results. The collocated pressure based formulations are used for predicting the pressure on walls of tank.

2.4.1.2 Finite element method (FEM)

The discovery of FEM is often attributed to Courant (1943). The use of this method in aircraft structural analysis was first reported by Turner *et al.* (1956). It is similar to the FVM in many ways. In FEM, region of interest is divided into a number of elements. Differential

equations are reduced to algebraic equations by using appropriate approximations for the variables over the elements. Equations are multiplied by a weight function before integrated over the entire domain. An important advantage of finite element methods is the ability to deal with arbitrary geometries. The principal drawback is that the unstructured grid matrix of the linearized equations is not as well structured as those for regular grids making it more difficult to find efficient solution methods. Many researchers developed FEM soft code or FEM procedures for solving the sloshing problems (Liu and Uras, 1988; Bo and Jia-xiang, 1994; Uras and Tang, 1994; Guptha, 1995; Wu *et al*., 1998; Pal *et al*., 1999; Biswal, 2003; Cho and Lee, 2004; Yang and Löhner, 2005; Wang, 2005; Arafa, 2007; Guilot, 2006; Kwon, 2008).

Arafa (2006) developed a finite element formulation to investigate the sloshing of liquids in partially filled rigid rectangular tanks. The liquid domain is discretized into two-dimensional four-node rectangular elements with the liquid velocity potential representing the nodal degrees of freedom. Liquid sloshing effects induced by both steady-state harmonic and arbitrary horizontal base excitation are investigated in terms of the slosh frequencies, liquid velocity field, free surface displacement and hydrodynamic forces acting on the tank walls.

2.4.1.3 Finite difference method (FDM)

FDM was introduced by Euler in the 18^{th} century. It is the easiest method for solving simple geometries. Governing equations are in differential form in which the partial derivatives are replaced by approximations in terms of node values of the functions. The domain of interest is divided into a number of grid points and one algebraic equation is solved per grid node. FDM can be applied to structured grids. The disadvantage of FDM is that the conservation is not enforced unless special care is taken. Also complex flows are intricate to solve. Many people used FDM as their tool for solving the sloshing problems (Chen, 1999; Kim, 2001; Wiesche, 2003; Frandsen, 2004; Dai and Xu, 2006; Sriram, 2006; Binghom, 2007; Lee *et al*., 2007, etc.). Kim (2001) simulated the violent sloshing flows based on finite difference method in the two and three dimensional liquid tanks. The free surface profile was assumed to be a single valued function and solved using the SOLA scheme. His computational results show a favorable agreement of impact pressure as well as global fluid motion with experimental results.

2.4.2 Approach for Free Surface Wave Problem

The motion induced by the surface waves may be irrotational in most instances when a quiescent body of liquid experiences gravity waves on its free surface. The flows associated with surface waves are assumed to be potential, which is the valid approximation for many free surface phenomena. Then the velocity vector may be expressed as the gradient of a velocity potential, which in turn, must satisfy the Laplace's equation.

Figure 2.9 shows a body of liquid on a flat surface in which waves exist on the free surface of the liquid. The *x* axis of the coordinate system is located at the mean level of the free surface, which is defined by the equation $y = \zeta(x, z, t)$ and the mean depth of the liquid is h_s. Two boundary conditions must be imposed on the free surface $y = \zeta$. The first condition is called the kinematic condition, and it states that a particle of fluid that is at some time on the free surface will always remain on the free surface. Then, since the equation of the free surface is $y - \zeta = 0$, it follows that

$$\frac{D}{Dt}(y - \zeta) = 0 . \tag{2.9}$$

In terms of Eulerian coordinates this boundary conditions becomes

$$\frac{\partial}{\partial t}(y - \zeta) + \underset{\sim}{q}.\underset{\sim}{\nabla}(y - \zeta) = 0 \tag{2.10}$$

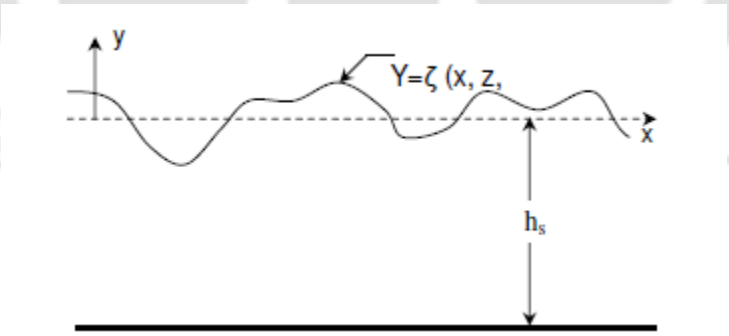

Figure 2.9: Sketch of free surface.

However, in the Eulerian frame of the reference, the coordinates *x*, *y*, *z* and *t* are independent. Also, the function ζ depends on *x*, *z* and *t* only. Hence, the above equation may be expanded to give,

$$-\frac{\partial \zeta}{\partial t} - u\frac{\partial \zeta}{\partial x} + v - w\frac{\partial \zeta}{\partial z} = 0 \tag{2.11}$$

where it has been noted that $\partial x_i / \partial x_j = \delta_{ij}$. Finally, expressing the velocity components in terms of the velocity potential ϕ, the kinetic surface condition becomes

$$\frac{\partial \zeta}{\partial t} + \frac{\partial \phi}{\partial x}\frac{\partial \zeta}{\partial x} + \frac{\partial \phi}{\partial z}\frac{\partial \zeta}{\partial z} = \frac{\partial \phi}{\partial y}. \tag{2.12}$$

The other boundary condition that must be imposed on the free surface is a dynamic one. This condition is implemented through the Bernoulli equation. The appropriate form of the Bernoulli equation is for unsteady, irrotational motion. Since gravitational forces are intrinsically important in free surface waves, gravity must be included in the body force term.

$$\frac{\partial \phi}{\partial t} + \frac{P}{\rho} + \frac{1}{2}\nabla\phi \cdot \nabla\phi + g\zeta = F(t). \tag{2.13}$$

Finally, the boundary condition at the bed must be imposed. For the case of an inviscid fluid, one can assume as the velocity component normal to the boundary is zero. For a flat bed, this simply amounts to specifying that $\partial\phi / \partial y = 0$ on $y = - h_s$.

In summary, the conditions to be satisfied for surface wave motions in terms of the velocity potential ϕ are the following:

$$\nabla^2\phi = 0 \tag{2.14}$$

$$\frac{\partial \zeta}{\partial t} + \frac{\partial \phi}{\partial x}\frac{\partial \zeta}{\partial x} + \frac{\partial \phi}{\partial z}\frac{\partial \zeta}{\partial z} = \frac{\partial \phi}{\partial y} \qquad \text{on } y = \zeta \tag{2.15}$$

$$\frac{\partial \phi}{\partial t} + \frac{P}{\rho} + \frac{1}{2}\nabla\phi \cdot \nabla\phi + g\zeta = F(t) \qquad \text{on } y = \zeta \tag{2.16}$$

$$\partial\phi / \partial y = 0 \qquad \text{on } y = - h_s. \tag{2.17}$$

The difficulty in solving surface wave problems may be seen to be in the boundary conditions rather than the differential equation. Nonlinear boundary conditions (Equation 2.15 and 2.16) are to be imposed on the free surface $y = \zeta$. In real situations, this surface may not be known a priori and may be one of the quantities that come out of the solution itself. However, many interesting features of free surface wave flows do not depend upon these complex features of the problem. That is, by linearizing the problem, the difficulties discussed above may be avoided while the basic features of the flow are not destroyed.

2.4.2.1 Modeling of free surface

When free surface flows are modeled, a number of techniques are available to compute the interface. Most numerical models treat the moving free surface boundary in one of the two

ways: either by using Lagrangian tracking of free surface nodes with regridding or by mappings (Frandsen and Borthwick 2003). In general, the existing methods for handling free surfaces and fluid interfaces in CFD can be divided into two groups, which are surface tracking and surface capturing (Ferziger and Peric, 2002).

The surface tracking methods are characterized by an explicit representation of the surface. The free surface is modeled using a free-surface tracking algorithm where a two-dimensional kinematic free-surface boundary condition is solved for the wave elevation and the computational grid is dynamically conformed to the hull and predicted free surface at each time step. The surface-tracking approach becomes problematic for free-surface flows with large wave steepness and/or large differences between the non-conformed and conformed grid (Kim 2002). This is normally done by adapting the grid to the free surface and updating the grid at each time step to track the new location of the free surface by using a height function to describe the vertical height of the free surface location. The drawback of the surface tracking methods is the inability to handle complex surface geometries and overturning waves. Moreover, surface velocities are difficult to predict correctly, and so free surface smoothing is required. This makes the surface tracking methods unable to model the wave pattern of for instance high-speed crafts, in which case overturning waves or breaking waves are expected in general. Surface tracking is still widely used when effects of overturning or breaking waves are considered negligible.

The surface capturing method is quite different. A number of schemes are available and all use an implicit representation of the interface which is then captured as part of the solution algorithm. This requires that the computational grid extends above the region contained fluid in order to be able to capture the surface throughout the computation. In cases of the moving structures or boundaries, the surface capturing methods can also be coupled with lagrangian grids, forming a type of ALE method, by which a structure is tracked by the grid in the remaining domain, is moving along.

The most well known schemes are SURF, MAC and VOF techniques to solve the free surface profile of sloshing tanks. The SURF scheme assumes a single-valued profile and is potentially able to deal with the uniform representation of large free surface waves and even for the inception of overturning. The MAC method is based on Lagrangian concepts and can treat overturning waves and reentry inception with simple logic. A simple, but powerful

method is the VOF (Akyildiz and Unal, 2006; Hirt and Nichols, 1981). This method seems to be more flexible and efficient than other methods for treating complicated free surface. It was designed for two or more immiscible fluids where the position of the interface between the fluids is of interest. The VOF method has been used for many years in sloshing applications including free surface flows, marine tank, etc. The main advantage of the VOF method is their ability to capture the complex surface geometries with overturning or breaking waves and splashing (Nielsen, 2003).

2.4.3 σ - Transformation

The σ-transformation technique has also been used for capturing the liquid free surface elevation. One can avoid this difficulty by transforming the physical domain onto a rectangular region bounded by horizontal and vertical sides. The approach is to use the so-called σ- transformation. Table 2.2 gives the summary of mapping and σ-transformation works. The detailed discussion about σ-transformation procedure, limitation and advantages are discussed in Chapter 3.

2.4.4 Summary of Numerical Work

This survey of literature focuses on various numerical works by several researchers for the study of liquid sloshing and its control techniques. The following conclusions can be drawn from the above survey of numerical works

i. Many 2-D sloshing works are reported. Effect of 3-D sloshing waves can be studied by the free surface elevation of the liquid and its wave profiles.
ii. One can expect good results from the σ-transformation technique where the time dependent domain is transformed to a fixed unit square by proper mapping functions. In this method, free surface smoothing is not required and also re-meshing is avoided due to the wavy free surface. Frandsen (2004) results show that the mapping techniques coincide well with the second order potential theory solutions.
iii. The potential flow theory is enough to study the gravity waves. However, the sloshing amplitude of the free surface at the wall depends on fluid viscosity and its Reynolds number.
iv. The flow visualization can be performed to find the free surface velocity during the externally induced sloshing.

Table 2.2: Mapping and σ - transformation works on sloshing.

Author Details	Aim	Details	Observation/ Remark
Chern *et al*. (1999)	Simulations of non-overturning transient waves in fixed and base-excited tanks	2-D tank , periodic horizontal base displacement $X = a \sin(\omega t)$	▪ Simulations have been obtained for standing waves in a fixed rectangular tank and for sloshing free-surface motions in a base-excited tank ▪ Results for base-excited sloshing waves are very similar to linear analytical solutions derived by Wu *et al*., (1998)
Dai and Xu (2006)	Analysis of liquids sloshing in horizontal cylindrical rigid container using FDM under normal highway operating conditions	2-D and 3-D horizontal cylindrical containers, with lateral accelerations	▪ 2-D circular containers under harmonic acceleration with small amplitude are simulated ▪ Transient responses of the liquid in the road containers have been studied in detail under turning, lane-change
Frandsen and Borthwick (2003)	Study the effects sloshing wave motion in a tank moved under both horizontal and vertical excitation	2-D container, with horizontal and vertical oscillation induced by harmonic motion	▪ Excellent agreement has been obtained between second-order potential theory solutions and the numerical model predictions for small amplitude wave cases ▪ When the wave number increases, the fluid behavior is no longer perfectly periodic, and irregular amplitudes occur, even for small amplitude waves
Chen and Nokes (2005)	Numerical simulation of sloshing flow under tank motion which matches with real earthquake motions (surge and pitch) considering the viscous effects	2-D tank, surge and pitch motions	▪ The coupled effect of surge and pitch motion is significant and should be considered in a real earthquake analysis ▪ Combination of free-surface velocity, the gradient of surface displacement, and the surface curvature effect are important in the generation, propagation, and stability of the surface vorticity that in turn affects the free-surface elevation

2.5 Review of Experimental Work

Nonlinear nature of the sloshing is the greatest hindrance in solving such a problem analytically and even numerically. Further a number of assumptions are to be made, in which the solutions may deviate from the actual values. Experimental studies have been the most popular approach for liquid sloshing and have provided valuable insights into the physics (Rhee, 2005). Hence, an experimental approach may be considered to be the best method to study the sloshing effect.

2.5.1 General Experimental Procedure

In most of the experimental studies, as shown in Figure 2.10, the tank attached to a shaking table can be moved to and fro by a hydraulic actuator (Popov *et al.*, 1992) or mechanical arrangement driven by a motor (Akyildiz and Unal, 2005; Panigrahy, 2006) or by a lathe machine (Pal *et al.*, 2001).

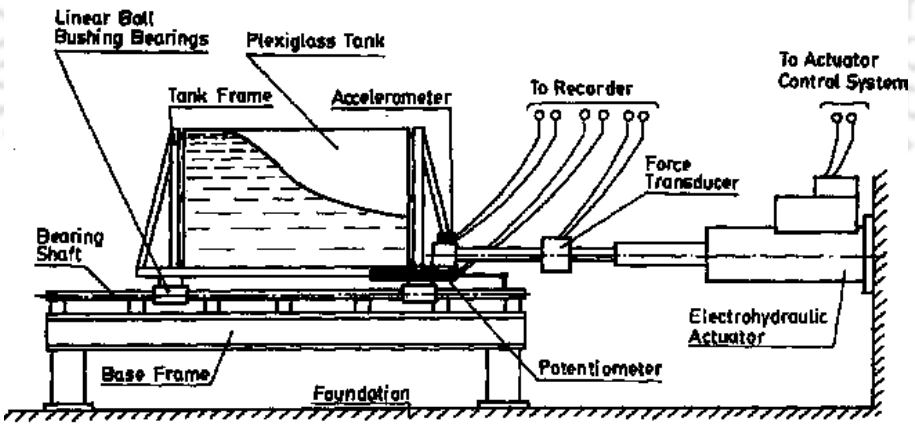

Figure 2.10: Set-up with a rectangular tank by Popov *et al.* (1992).

For the pressure measurement, pressure sensors are fixed on the walls of the tank. The output of the pressure gauges was fed to the channels of the data acquisition system or a data logger that was coupled to a PC. The data were decrypted using any commercial data acquisition software that displayed the output in millivolts. The free surface displacement was captured using a

motion movie camera or a laser sensor or some other capturing device. Popov *et al.* (1993) developed the sloshing set-up for measuring liquid height to validate his numerical values. An electro hydraulic actuator fixed horizontally was used to generate translational motion of the tank in the horizontal plane. The displacement and acceleration of the tank as well as the force developed in the link between the tank and actuator were recorded. The liquid free-surface oscillations were also recorded with a video camera in order to compare them with those computed numerically at similar conditions.

Sloshing can be broadly classified into two types namely self-induced sloshing and externally induced sloshing based on how sloshing is generated inside its tank. The main difference is that in self-induced sloshing, the tank is immobile, whereas in externally induced sloshing, the tank will move due to external disturbances. The fluctuation of the inlet plane jet and the periodically shedding of the unsteady vortices were conjectured to be the excitation source of the self-induced sloshing (Saga *et al*., 2000(a)). In case of externally induced sloshing, external forces like earthquake, sudden brake on a moving tank vehicle etc acts as the excitation source for sloshing. And this type of sloshing can be found in real time applications like liquid oil carrier vehicles, space vehicles, LNG vessels in cargo ships, etc. The fluid dynamic mechanism of the externally or self-induced sloshing phenomena should be understood clearly in order to have an optimum safety design of the reactor vessels to prevent the occurring of sloshing (Saga *et al*., 2000b). For example, in the Liquid Metal Fast Breeder Reactor, the self-induced or externally induced sloshing of the high temperature sodium coolant may occur in reactor vessels. Such kind of sloshing will result in very high thermal stresses on the vessel walls, which may cause severe damage to the vessel structures (Okamoto and Madarame, 1998).

2.5.2 Review on Flow Visualization

The basic theory for particle image velocimetry was first presented nearly 25 years ago and the technique has undergone tremendous developments in the last ten to fifteen years (Adrian, 1991). PIV is a non-intrusive measurement technique for studying the velocity profiles. It uses images of marker particles in a fluid flow to measure instantaneous velocity fields. It is a technique

which enables instantaneous measurement of the flow velocity at several positions in a plane. Two images of each particle in the sheet are recorded in a short time interval. This technique relies on the imaging of tracer particles embedded within a flow at two distinct times, t_1 and t_2, to estimate the velocity of the fluid. The distance separating the two images gives a local velocity vector. The images are generally recorded onto either film (photographic or holographic) or a Charge Coupled Device (i.e., CCD) array. Correlation analysis is used to extract the particle displacements, ΔX and the first-order velocity estimate,

$$U = \frac{\Delta X}{\Delta t}, \tag{1}$$

where Δx is the average displacement of the particles in the fluid over the time interval $\Delta t = t_1 - t_2$ (Adrian, 1991). The t_1 and t_2 images can either be made on the same frame or on to separate frames (referred to as one-frame and two-frame PIV, respectively).

In case of self-induced sloshing, the tank is stationary so that the images can be easily taken for PIV analysis. If the tank moves, the camera probably cannot focus the liquid portion alone. This means, it is possible that the tank can slide away from the camera's focus area. For the above reason, image processing cannot be performed easily in such type of distorted images with accuracy. Hu *et al.* (1999) investigated the self-induced sloshing phenomena using Particle Imaging Velocimetry technique experimentally and found three different flow patterns in the test tank for the same system parameter setting, which are reverse vortex flow pattern, first sloshing mode and second sloshing mode flow patterns. As reported by Hu *et al.* (1999), the self-induced sloshing in a rectangular tank was first systemically studied by Okamoto *et al.* (1991). Particle Imaging Velocimetry and also Laser Doppler Velocimetry (LDV) measurements on a self-induced sloshing flow in a rectangular tank had been conducted by Saga *et al.* (2000b) and PIV measurements were compared with LDV measurements quantitatively in order to evaluate the accuracy level of the PIV measurement. Singh *et al*. (2006) measured the magnitude of fluid velocity fluctuations from PIV analysis for concentrated suspension in free surface flow in a channel. Khezzar *et al*. (2009) performed the experimental flow visualization and CFD modeling based on a two-dimensional geometry using a commercial CFD package for a rectangular tank subjected to sudden (impulsive) impact. A comprehensive experimental program had been

conducted by Nasar *et al.* (2009) to find the liquid sloshing pressure in a rectangular tank equipped inside the barge and the barge responses. Several experimental and numerical investigations on the self-induced sloshing in a rectangular tank with circulating flow had been conducted in the past twenty years (Takizawa *et al*., 1992; Okamoto *et al*., 1993; Fukaya *et al*., 1996). Most of the studies on sloshing were limited to self-induced excitations. However, work in the area of flow visualisation techniques on externally induced sloshing with surge motion of tank is scarce.

2.5.3 Comparative Analysis

Table –2.3 gives a vivid picture of the complete summary of investigations highlighting details of experimentation such as type of oscillations, tank dimensions, fluids used, type of baffles, and the their key findings. Table-2.3 shows all the studies carried out in gravity field.

2.5.4 Summary of Experimental Work

Experimental studies endorse researchers to check the validity of assumptions of the mathematical model, numerical simulations and to employ the model effectively for design applications. Adequate understanding of any complex physical phenomenon such as sloshing is enhanced to a great extent by the use of experimental techniques. A survey of literature has indicated various experimental investigations by several researchers on study of liquid sloshing and its control techniques. The overall observation from these experimental results gives an idea that sloshing in a tank is a function of the liquid depth, the dimensions of the tank, amplitude, frequency of excitation and density of the liquid. As the amplitude of excitation is increased, the liquid responds violently such as occurrence of turbulence, hydraulic jump, wave breaking and three-dimensional effects. Therefore, the rolling amplitude and frequency of the tank directly affects the degrees of non-linearity of the sloshing.

Table 2.3: Comparative analysis of experimental investigations in gravity field.

Author Details	***Aim***	***Force Applied, Details of Tank and Baffles***	***Instruments, Materials and Varying Parameters***	***Remarks***
Cole (1966)	To study the effect of baffle thickness from forced oscillations in a 2-D tank (Analytical) Free oscillation-cylindrical tank (Analytical & Experimental)	Sinusoidal motion. **Tank:** 1) A plate 1/16 inch thick. 2) 3-foot-diameter cylindrical tank. **Fluid:** Water **Baffle:** (Refer Appendix-A, A1) 2-D tank -spanning the width of the tank. Cylindrical-ring baffles.	India ink was introduced. **Motion** -16 mm movie camera. **Variables**: Amplitude (A) / width (W) ratios - 0.33 to 2.5. Reynolds no. $5x10^3$ to 40 x 10^3.	• Moderate baffle thickness reduces the baffle effectiveness by as much as 50% • The effectiveness of baffles depends on the thickness of the baffle and the amplitude of oscillation • In comparison of theory and experiment in small-scale tests, results are not reliable unless actual similarity of flow is established
Bugg (1970)	To determine the effect on liquid oscillation frequency of changes in the angle between the tank axis and the body force vector	Longitudinal excitation. **Tank**: Plexiglass right circular cylindrical. 20 cm inner dia 38 cm tall. **Fluid:** Distilled water with two parts per thousand Aerosol MA. **Baffle:** No.	**Viscosity**: Oswalt-type viscometer. Period of oscillation: Stop watch. **Inclination** of the tank = 0^o, 30^o,45^o and 60^o.	▪ The longitudinal mode, the frequency parameter (w^2) was reduced, by inclining the tank at 60°, to 27° % of its value with the tank upright ▪ Tank tilt should have only a small effect on Shuttle propellant dynamics during launch for the expected 10^o or less angle between thrust vector and tank axis
Chiba (1992)	To find the influence of elastic bottom wall in a tank by varying sheet thickness	Harmonic vibration **Tank:** Cylindrical container inner R = 144 mm L=520 mm, sidewall thick 6 mm. Flexible bottom wall Polyester sheet of thick (i) 0.254 (ii) 0.357. **Fluid:** Water	**Displacement:** Optical Displacement sensor Oscilloscope. **Variables:** (i) Bottom wall thickness (ii) Height of the bottom wall. (iii) Water height (iv) Frequency	▪ Center of the bottom plate is excited with constant frequency, then the amplitude is increased the free surface loses its stability and sways in a horizontal direction, its peak vibrating in the radial direction of the free surface ▪ The nonlinear characteristics of liquid exhibits a softening behavior for large liquid heights, while for decreased liquid heights it changes to a hardening type

Warnitchai and Pinkaew (1998)	1. To develop a new mathematical model of liquid sloshing in rectangular tanks for TLD applications. 2. To check the effects of flow-dampening devices experimentally and analytically.	Sinusoidal motion **Tank:** Rectangular acrylic tank with 40 x 20cm. **Fluid:** Plain water. Damping ratios obtained from: (a) A plain tank. (b) A tank with two circular section poles of d = 22 mm. (c) A tank with a flat plate of d= 50 mm and thickness = 3 mm. (d) A tank with a wire-mesh screen with wire diameter = 0.26 mm and solidity ratio = 0.29.	**Feedback**-control hydraulic actuator – drive the shaking table (one-dimensional type). **Displacement** transducer - the motion of tank. The force transducer-(steel pipe attached with two semiconductor strain gauges). **Variables:** Water depth ratio was set to 0.3. (All cases).	Damper application, a new mathematical model of liquid sloshing in rectangular tanks has been developed ▪ Model can accurately represent the complex behavior of liquid sloshing ▪ The non-linear characteristics of the damping increases and a slight reduction in sloshing frequency occurs
Modi and Munshi (1998)	1. Study the performance characteristics of a rectangular liquid sloshing damper, without any obstacle. 2. Experiments with a family of semicircular cross-section obstacles, their effectiveness in increasing the damping. 3. To evaluate the effectiveness of the improved liquid sloshing damper.	Angular vibration. **Tank:** Rectangular L=370 mm, W=166 mm, and H=125 mm. **Obstacles:** Family of obstacles (r = 6-22 mm). **Fluid:** Plain water.	**Displacement** of the rod - strain-gauged beam -output is processed by - signal conditioning – **amplification**- spectrum analyzer- computer. **Variables:** Height of the liquid = 0–60 mm. **Angular displacement** = 1°-2.5°.	▪ Increased up to 60%, in the energy dissipation capacity of the liquid sloshing damper by introduction of an optimum obstacle ▪ The presence of an obstacle leads to a wider peak, i.e., to higher damping over an extended range of liquid frequencies ▪ The performance of the damper depends on both the frequency ratio (f_n/f_1) and initial displacement (h_o). ▪ Optimum size and location of the obstacle as r/L = 0.016 and d/L = 0 (i.e., one obstacle)

Grundelius and Bernhardsson (1999)	1. To capture the free surface elevation using techniques from optimal control both numerically and analytically. 2. To calculate the acceleration profile for the container using optimal control techniques.	**Tank:** Rectangular container. Height of fluid = 0.2 m and Width of the tank = 0.07 m. (Refer Appendix-A, A2)	**Surface elevation**: Infrared laser displacement sensor. Small video camera. Carriage is mounted on a belt driven servo system. **Variables:** 1. Max. Acceleration = 9.81m. 2. Max. Slosh = 0.035 m. 3. Initial State= [0 0 0 0] m Final state-[0 0 0 L] m. Movement distance L= 0.2 m. $a(t) = \begin{cases} 6 & 0 \geq t < 0.05 \\ -6 & 0.05 \geq t < 0.1 \\ 0 & 0.1 \geq t \end{cases}$	▪ Open container with liquid should be moved quickly without excessive slosh ▪ The calculated controllers have been implemented and verified in an industrial test bed that gave a better performance than previous controllers
Pal *et al*. (2001).	To conduct experiments for measuring some of the basic parameters of sloshing, and to verify certain parametric relationships with numerical computations.	(Horizontal) excitation and sinusoidal motion. Tank: Perspex cylindrical tank. (R=96 mm) Fluid: Water. Baffle: Ring baffle of 25 mm width and 6 mm thickness.	Shaking- a lathe machine Cam mechanism- Circular to a linear movement of the platform. **Platform**- Linear variable differential transducer. DAS-32-channel dynamic data acquisition system. **Displacement**- Wave height sensors. **Varying Parameters:** Fill level =30-30-150.	▪ Experimental studies allow researchers to check the validity of assumptions of the mathematical model and to employ the model effectively for design applications ▪ Measurement of free-surface liquid response in absence of any excitation source is done to assess possible slosh suppression techniques from the rate of decay of the slosh amplitude
Sakamoto *et al*. (2001)	To design and fabricate a TSD both experimentally and analytically.	**Tank:** Rectangular tank. Length=120 mm. Depth of fluid = 30 mm **Fluid**: Electro-rheological (TX-2128 ER fluid).	**Displacement:** Non-contacting Laser displacement pick-up. **Variables:** Frequency: 0.1 - 0.05 - 3.0 Hz. Electric field between the electrodes: 0, 200, 400 and 600 V mm−1. Four liquid levels: 20, 30, 40 and 50 mm. (*a*) Without the ER-TSD. (*b*) With the ER-TSD and no electric field. (*c*) With the ER-TSD and an electric field of 600Vmm−1.	▪ Sloshing frequency of the ER-TSD can be controlled by applying the electric field to the ER-TSD ▪ ER-TSD can suppress the vibrations of the structure even when the natural frequency of the structure changes ▪ The effects of the ER-TSD on the structural responses are qualitatively explained in terms of the simplified TMD model

Celebi and Akyildiz (2002)	Experimental investigations on the pressure distribution around a large vertical cylinder fixed on a wave channel, piercing the free surface.	**Tank:** Vertical cylinder: 4.9 m wide and 28.1 m long wave channel with a constant water depth of 0.45 m. **Fluid :** Water depth 45 cm. d/a = 1.2328. a=radius of tank.	**Pressure:** 0.1 bar pressure transducers. **Data logger:** Agilant 34970 automatic DAS. **Variables:** A direct current motor; a 1/15.7 reducter of AT32 type with a 4 kW power.	▪ The experimental results near the free surface do not agree well with the diffraction theory of Akyildiz (1999). ▪ Experimental results correlate better with the second-order solution. ▪ Linear and the second-order theory give different results for the front and back sides of the cylinder.
Akyildiz and Unal (2005)	To develop an experimental system accounting for the effects of large tank motions, large amplitude wave motions, fluid viscosity and baffle arrangements.	Harmonic excitation. **Tank:** Rectangular tank. 92X62X46 cm model tank. **Baffle:** Bottom transverse - larger baffle - (15.4 cm high) made of 1.5 cm Plexiglas plate. Right side- A smaller baffle (7.6 cm high) 1.5 cm Plexiglas plate. **Fluid:** Water.	**Pressure:** Nine pressure transducers (PT), sensitivity 0 to 1 bar. **Data logger:** Agilant 34970 automatic DAS. **Platform:** Base frame was driven by DC motor (15 kW). **Variables:** Fill level : (d/H) = 0.25, 0.5, 0.75 Pitch angle: 4º, 8º. Frequency: 0.5 - 3.785.	▪ Baffles significantly reduce fluid motion, however, more experimental investigations are needed considering the effects of fluid viscosity on impact pressures. ▪ Model studies for sloshing under multi-component random excitations with phase difference should be carried out to investigate sloshing load.
Yano and Terashima (2005)	To develop a liquid container transfer system with a 3-D transfer path that suppresses sloshing without vibration feedback.	Linear motion. **Tank:** 3-D cylindrical container. 0.12 m and its height is 0.3 m. **Fluid:** Water. The static liquid level is 0.16 m.	**Displacement:** Two-level sensors **Variables:** Proposed gain 34.0, 55.5, and 61.5. Start point [0,0,0] Endpoint [0.3, 0.3, 0].	▪ Hybrid shape approach was applied for trajectory control with vibration damping on transfer systems with vibration mechanisms. ▪ With restriction control specifications in both the time and frequency domains, using only feedback on the container's position.

The suppression of sloshing behavior using baffles is also a subject of interest in the recent years. The effectiveness of fuel-sloshing baffles depends on the thickness of the baffle and the amplitude of oscillation, and these effects should be taken into account in applying model results to full-scale designs and in comparing results of experiments. The baffle has significant effect on the non-linear slosh amplitude of liquid when placed close to the free surface of liquid. The effect is almost negligible when the baffle is moved very close to the bottom of the tank. Modi and Munshi (1998) suggested a significant increase, up to 60%, in the energy dissipation capacity of the liquid sloshing damper by introduction of an optimum obstacle in the path of the moving liquid.

The sloshing frequency of the ER-TSD system can be controlled by applying the electric field to the ER fluid and one can tune the natural frequency of the system. The ER-TSD can suppress the vibrations of the structure even when the natural frequency of the structure changes. The experimental results concerning the effects of the ER-TSD on the structural responses are qualitatively explained in terms of the simplified TMD model, including the ER-TSD. Magnetic field has been used as slosh damping devices in the liquid storage tanks to reduce the impact load on walls of the tank and to reduce the surface displacement. Instruments like Doppler anemometry or PIV have been used to measure the velocity profiles during sloshing. In the view of the microgravity fluid physics, several forces determine the nature of surface waves. When the fluid is not rotating, the relevant forces are surface tension and gravity. With rotation, the centrifugal and coriolis forces are also present. In the space sloshing study, the motion of the tank can be specified by three translations and three rotations about the center of mass of the liquid.

2.6 Overall Summary

Having given a brief historical note, the chapter gives a description of various parameters associated with liquid sloshing. Thereafter, it reviews the numerical and experimental investigations reported in literature. Important issues and milestone results are discussed, tabulated and summarized.

Chapter 3

SIGMA–TRANSFORMATION TECHNIQUE

This chapter elucidates the sigma transformation (or σ- transformation) technique together with its advantages and limitations in detail. The history of this technique is also briefly outlined. The use of sigma transformation process for a 2-D domain is discussed.

CONTENTS

3.1 Introductory Remark

As reported in literature, Marker and Cell (MAC), Volume of Fluid (VOF), level set methods are available to handle the free surface of the moving fluid (Popov *et al.*, 1993, Akyildiz and Unal, 2006; Cho *et al.*, 2005; Arafa, 2007; Hirt and Nichols, 1981). Since these methods require complex computer programming to treat the time varying free surface boundary and as computational mesh needs to be updated at every time step, use of σ - transformation for treating the liquid free surface has gained widespread popularity in recent years. σ -transformation technique is simple, easy to implement and eliminates the need for re-meshing the computational domain at each time step. This technique was applied and found to produce good quality results for sloshing problems by Chern *et al*. (1999), Turnbull *et al*. (2003), Chen and Nokes (2005), Dai and Xu (2006).

Previous numerical models generally treat the moving free surface boundary in one of two ways: either by using Lagrangian tracking of free surface nodes with re-gridding, or by mappings. The former one has the disadvantage of predicting the surface velocities correctly and so free surface smoothing is often required. Although mappings inherently overcome this problem, they are less flexible to apply in irregular geometries or in cases where submerged bodies are present in the flow domain. Moreover, schemes of mapping types cannot predict run-up/overturning due to the single value formulation (Abramson *et al*., 1974).

3.1.1 What is Sigma-Transformation?

The time-varying fluid surface can be mapped onto a rectangular domain by the σ - transformation. This method is a simple way to simulate non-breaking waves quickly and accurately especially that has a low steepness. The σ - coordinate system defines the base at the model's ground level. The surfaces in the σ - coordinate system follow the model terrain and are steeply sloped in the regions where terrain itself is steeply sloped. Assume the field variable is velocity in the fluid domain and the sigma coordinate system defines the vertical position of a point in the fluid domain as a ratio of the velocity difference between that point and the top of the domain to that of the velocity difference between a fundamental base below the point and the top of the

domain. Because it is velocity based and normalized, it is easy to cast governing equations of the fluid domain mathematically into a relatively simple form. Medium Range Forecast (MRF) model, Nested Grid Model (NGM) and European Center Medium Range Weather Forecasting Model (ECMWF) are the popularly used examples of σ - models or Variants for weather forecasting.

3.1.2 Advantages of Sigma-Transformation Technique

- The accurate assimilation of the bottom and surface boundaries and the possibility of easily incorporating boundary layers.

- The σ - coordinate system conforms to natural terrain. Hence, it permits the good depiction of continuous fields, such as temperature advection and winds, in areas where terrain varies widely but smoothly.

- It lends itself to increasing vertical resolution near the ground. This let the model to define boundary-layer processes, such as diurnal heating, low-level winds, turbulence, low-level moisture, and static stability in a better manner (Decoene and Gerbeau, 2009).

- It eliminates the problem of vertical coordinate systems intersecting the ground, unlike height or isentropic coordinates.

3.1.3 Limitations of Sigma-Transformation

However, the above benefits do not come without penalties. It limits the possibility of vertical discretization, and therefore, prevents the adaptation of the mesh to the particular needs of the simulation. On the other hand, the classical σ - transformation can induce an important error in the computation of the horizontal pressure gradient in the presence of surface or bottom gradients (Haney, 1991). In particular, this error leads to an inaccurate representation of possible density stratifications. The pressure gradient force (PGF) is easily calculated in pressure coordinates when the height is known. Yet, when σ surfaces slopes, the PGF must be expanded to include the effects of the slope. This introduces errors because the lapse rate must be

approximated at points that lie in between the pressure surfaces where height is observed (Decoene and Gerbeau, 2009).

3.1.3.1 Transformation of High Steep Waves

While transforming the high steep waves, some of the limitations arise during the σ - transformation procedures. This section explains those limitations and also its overcome procedures.

Pressure gradient terms

While all numerical models experience difficulties in handling high steep waves from one grid point to the next, the σ - coordinate models appear to suffer proportionately more. The problem lies in the calculation of the pressure gradient terms in the momentum equations. In σ - coordinates, high steep waves from one grid point to the next means that the calculation of the pressure gradient involves taking the difference between two large terms (Haney, 1991) and therefore large round off errors. While this problem can be alleviated by increasing the horizontal resolution, it can also be mitigated by subtraction of horizontal averages of density from the density terms before computing the density-gradient induced pressure differences from one grid point to the next.

Hydrostatic inconsistency

The other problem associated with high steep waves, namely the hydrostatic inconsistency, can be reduced in severity only by smoothing the horizontal gradients of field variables. It is generally wise to process the variables at bottom with a filter that caps the ratio of bottom depths of adjacent grid points before using it in the model. However, care must be taken to ensure that the variables are not severely corrupted by this processing, especially over the shallow coastal regions.

3.2 History of Sigma-Transformation

Originally, σ - transformation was proposed for meteorological forecasting by Phillips (1957), however, later, Blumberg and Mellor (1980) and Mellor and

Blumberg (1985) applied in the context of oceanic and coastal flows. σ-transformation was applied to non-linear steep waves in fixed and base excited tanks by Chern *et al*. (1999) and the waves simulated in relatively deep water by Turnbull *et al*. (2003). Frandsen (2003, 2004) investigated numerically the steep free surface sloshing in fixed and base-excited rectangular tanks with a focus on moving liquid tank by horizontal and vertical excitations. Frandsen (2004) investigated 2-D fixed and base-excited rectangular tanks, using σ-transformation and compared the results with third-order single modal solutions and theoretical results (multidimensional modal analysis) of Faltinsen *et al.* (2000). Chen and Nokes (2005), and Dai and Xu (2006) applied σ- transformation to predict the sloshing effects on horizontal cylindrical tank and 2-D rectangular tank respectively.

3.3 Use of the Sigma-Transformation

A major difficulty in obtaining a numerical solution of the above initial value problem is that at $t \succ 0$, the coupled non-linear free surface conditions are applied on an unknown line $\zeta(x,t)$. One can avoid this difficulty by transforming the physical domain onto a rectangular region bounded by horizontal and vertical sides. The approach is to use the so-called σ- transformation. As discussed earlier, the σ-transformation was first used by Phillips (1957) for weather prediction. However, it has been applied recently in the research of hydrodynamics and sloshing in combination with different numerical methods.

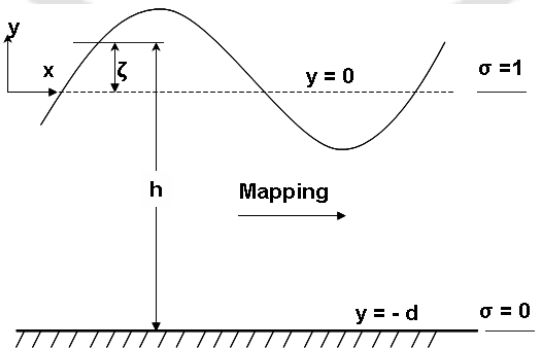

Figure 3.1: A sketch of the σ - transformation.

σ- transformation is used to map the liquid domain onto a rectangle, such that the moving free surface in the physical plane becomes a fixed horizontal line in the

computational mapped domain. Figure 3.1 is a sketch illustrating the σ-transformation. The mapping function $\sigma(x,t)$ is defined as

$$\sigma = \frac{y+d}{h}, \tag{3.1}$$

where

$$h(x,t) = \zeta(x,t) + d. \tag{3.2}$$

Consider a potential function ϕ(x, y, t) which is needed to transform derivatives of the potential function $\Phi(x,\sigma,t)$. Using the chain rule, we have

$$\frac{\partial \phi}{\partial t} = \frac{\partial \Phi}{\partial t} + \frac{\partial \Phi}{\partial \sigma}\frac{\partial \sigma}{\partial t}, \tag{3.3}$$

and

$$\frac{\partial \phi}{\partial x} = \frac{\partial \Phi}{\partial x} + \frac{\partial \Phi}{\partial \sigma}\frac{\partial \sigma}{\partial x}, \tag{2.23}$$

where

$$\frac{\partial \sigma}{\partial t} = \frac{\partial}{\partial t}\left(\frac{y+d}{h}\right) = -\frac{\sigma}{h}\frac{\partial \zeta}{\partial t} \quad \text{and} \quad \frac{\partial \sigma}{\partial x} = -\frac{\sigma}{h}\frac{\partial \zeta}{\partial x}. \tag{3.4}$$

Therefore, the first derivatives of ϕ with respect to x, t can be rewritten as

$$\frac{\partial \phi}{\partial x} = \frac{\partial \Phi}{\partial x} - \frac{\sigma}{h}\frac{\partial \zeta}{\partial x}\frac{\partial \Phi}{\partial \sigma} \tag{3.5}$$

and

$$\frac{\partial \phi}{\partial t} = \frac{\partial \Phi}{\partial t} - \frac{\sigma}{h}\frac{\partial \zeta}{\partial t}\frac{\partial \Phi}{\partial \sigma}. \tag{3.6}$$

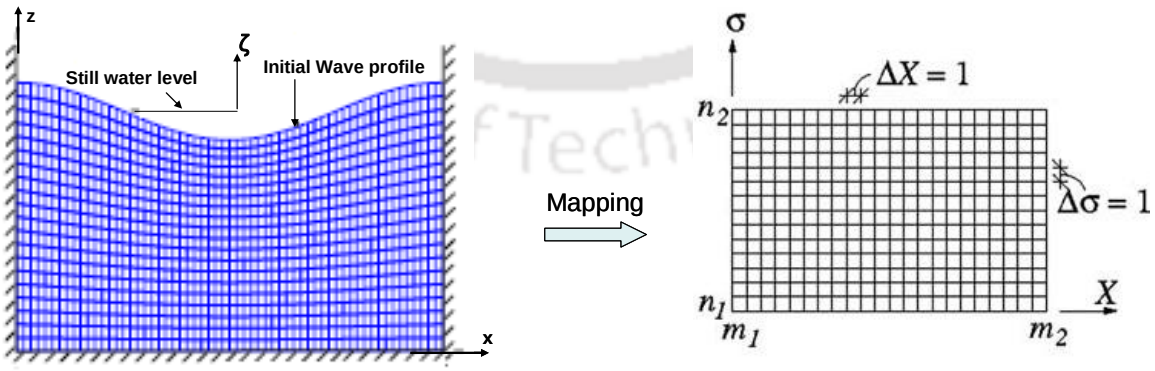

(a) (b)

Figure 3.2: The σ-transformation process of 2-D domain by Frandsen (2004); (a) physical domain (b) computational domain.

The second derivative of ϕ with respect to *x*, *z*, *t* can be derived using the same chain rule.

$$\frac{\partial^2 \phi}{\partial x^2} = \frac{\partial^2 \Phi}{\partial x^2} + \left[2\frac{\sigma}{h^2}\left(\frac{\partial \zeta}{\partial x}\right)^2 - \frac{\sigma}{h}\left(\frac{\partial^2 \zeta}{\partial x^2}\right)\frac{\partial \Phi}{\partial \sigma} \right] - 2\frac{\sigma}{h}\frac{\partial \zeta}{\partial x}\frac{\partial^2 \Phi}{\partial x \partial \sigma} + \left(\frac{\sigma}{h}\frac{\partial \zeta}{\partial x}\right)^2 \frac{\partial^2 \Phi}{\partial \sigma^2} \tag{3.7}$$

Using these relations one can get the modified governing equation and corresponding boundary conditions. Figure 3.2 shows the conversion of physical domain to computational domain by using the σ-transformation process of 2-D geometry (Frandsen, 2004). Any numerical scheme can be applied to solve the computational domain equations.

3.4 Summary

Some of the most challenging problems in engineering analysis are the modeling and analysis of the free surface flow problems. Many techniques have been used to track the liquid free surface properties. The σ - transformation is among one of the techniques to capture the liquid free surface. Recently, this technique is also being used for tank sloshing problems. This chapter narrated the σ - transformation technique sufficiently. After this σ - transformation, one can solve the computational domain equations by any of the numerical methods like finite difference, finite volume, meshless technique etc.

The σ-transformation technique is simple, quick and accurate computationally. For the technique presented herein, there is no need for free surface smoothing. The potential flow model provides a simple way of simulating steep non-breaking waves that may be readily extended to the prediction of 3-D wave motion and can be applied to polar coordinate as well.

Chapter 4

MATHEMATICAL FORMULATION AND MAPPING PROCEDURES

The governing equations along with the detailed theoretical formulations based on σ-transformation technique and the solution procedures are presented for a 2-D rectangular tank and a 3-D rectangular tank in this chapter. In order to ensure that σ-transformation technique can be applied to polar co-ordinate, a 2-D cylindrical problem has also been solved. In the final part of this chapter, the governing equation and boundary conditions in the computational domain are discretized using finite difference method. Adams-Bashforth scheme is utilized for temporal discretization to compute the non-linear solutions.

CONTENTS

4.1 Introductory Remark

A host of researchers used the potential flow theory to solve the tank sloshing problems (Babu and Bhattacharyya, 1996; Wu *et al*., 1998; Biswal 2003; Cho and Lee, 2004; Arafa 2006; Pal, 2008). However, they used different numerical schemes to approximate the equations and different algorithms for treating the free surface like MAC, VOF, SURF etc., but finite difference based σ -transformation technique is used in this investigation.

4.1.1 Why Potential Flow Theory?

Tank sloshing problems can be solved using full Navier-Stokes equations, however, these equations are unnecessary for wave simulation problem. In the gravity region, the gravity forces are predominant than the other forces like surface tension, viscous effects etc. Here, some major reasons are pointed out for choosing the potential theory.

i. If the tank size is large enough, the effects of viscosity and surface tension can be neglected and the energy dissipation is caused by wave breaking only. The fluid model herein is applicable from small to steep waves, which is desirable for many structural systems in which fatigue loading is of a concern. The solver is valid at any water depth, except for smaller depths where shallow water waves, surface tension and viscous effects would become important.

ii. The fluid used for the experimental work is water. According to one of the objectives of this work i.e. to compare the experimental results with numerical results, the above assumption is valid and essential for this work.

4.2 Mathematical Formulation

A rectangular cartesian co-ordinate system is initially employed with an origin on the mean free-surface at the left wall of the tank. Primarily, a 2-D non-linear wave problem is considered, as depicted in Figure 4.1, where ζ is the free-surface elevation above still water level, b is the length of the tank, and h_s is the still water depth. The fluid in the tank is assumed to be inviscid and irrotational.

4.3 Mathematical Formulations for a 2-D Rectangular Tank

Taking the assumption that the fluid is governed by potential flow theory, the velocity potential ϕ satisfies the Laplace equation. The velocity components normal to the fixed boundaries are zero by definition.

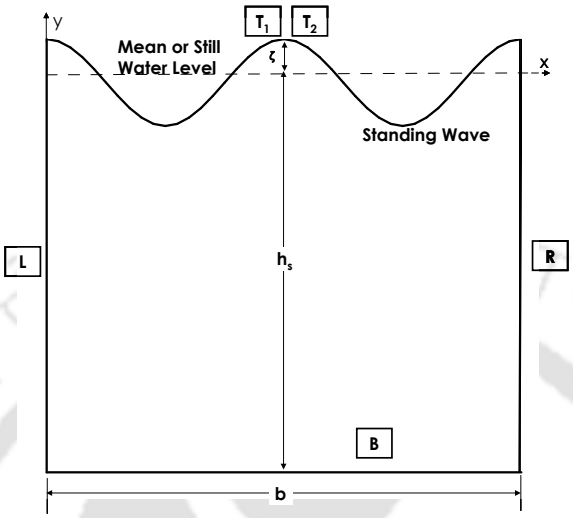

Figure 4.1: Sketch of a standing wave in 2-D tank.

As shown in Figure 4.1, the tank boundaries are indicated by L, R, and B. The free surface occurs at the interface between two fluids. Such an interface requires two boundary conditions to be applied**,** viz., (i) a kinematic condition that relates the motion of the free interface to the fluid velocities at the free surface (i.e., T1) and (ii) a dynamic condition which is concerned with the force balance at the free surface (i.e., T2). Liquid velocity components normal to the walls and bottom of the tank are zero. Zero pressure at the free surface of the fluid is also assumed for the analysis. In view of the fact mentioned above, kinematic and dynamic conditions must be satisfied on the free surface. Therefore, the governing equations in the physical domain are given as,

$$\frac{\partial^2\phi}{\partial x^2}+\frac{\partial^2\phi}{\partial y^2}=0 \qquad \text{in the fluid domain} \qquad (4.1)$$

$$\frac{\partial\phi}{\partial n}=0 \qquad \text{on the side walls} \qquad (4.2)$$

$$\frac{\partial\zeta}{\partial t}+\frac{\partial\phi}{\partial x}\frac{\partial\zeta}{\partial x}=\frac{\partial\phi}{\partial y} \qquad \text{on the free surface} \qquad (4.3)$$

$$\frac{\partial\phi}{\partial t}+\frac{1}{2}\nabla\phi.\nabla\phi+(g+\ddot{Y}_t)\zeta=0 \qquad \text{on the free surface} \qquad (4.4)$$

Here, $\ddot{Y}_t$ is the acceleration of the tank in the vertical direction which can be neglected from the free surface dynamic boundary condition for fixed tank analysis.

The following quantities are introduced for generating dimensionless governing equations for the present study,

$$x' = \frac{x}{b}; \quad y' = \frac{y}{b}; \quad \zeta' = \frac{\zeta}{A}; \quad \ddot{Y}_t' = \frac{\ddot{Y}_t}{g}; \quad t' = \sqrt{\frac{g}{b}}t; \quad \phi' = \frac{1}{A\sqrt{bg}}\phi \tag{4.5}$$

where, g is the acceleration due to gravity, A is the wave amplitude, $\ddot{Y}_t$ is the acceleration of the tank and t is the time. Here $x', y', \zeta', \ddot{Y}_t', t'$ and ϕ' represent the dimensionless quantities. Using Eq. (4.5) (hereafter, primes are omitted for simplification), the non-dimensional governing equation and boundary conditions can be written as follows,

$$\frac{\partial^2\phi}{\partial x^2} + \frac{\partial^2\phi}{\partial y^2} = 0 \tag{4.6}$$

L: $$\frac{\partial\phi}{\partial x} = 0 \quad \text{on} \quad x = 0 \tag{4.7}$$

R: $$\frac{\partial\phi}{\partial x} = 0 \quad \text{on} \quad x = b \tag{4.8}$$

B: $$\frac{\partial\phi}{\partial y} = 0 \quad \text{on} \quad y = -h_s \tag{4.9}$$

T1: $$\frac{\partial\zeta}{\partial t} + E_b\frac{\partial\phi}{\partial x}\frac{\partial\zeta}{\partial x} = \frac{\partial\phi}{\partial y} \quad \text{on} \quad y=\zeta \tag{4.10}$$

T2: $$\frac{\partial\phi}{\partial t} + E_b\frac{1}{2}\nabla\phi.\nabla\phi + (1+\ddot{Y}_t)\zeta = 0 \quad \text{on} \quad y=\zeta \tag{4.11}$$

where E_b is the amplitude-length ratio (=A/b). The Eqns. (4.6) through (4.11) form an initial boundary value problem which is the Laplace equation with non-linear boundary conditions imposed on the free surface. Here, the non-linearity is significant for two reasons. Primarily, the elevation of the moving free surface is not known a priori at any given time instant and secondly, the boundary conditions on the free surface (i.e., Eqns. 4.10 and 4.11) contain second order differential terms.

4.3.1 Mapping Procedure for a 2-D Rectangular Tank

The time-varying liquid free surface can be mapped onto a fixed plane surface by the σ-transformation, which prevents the need for free surface smoothing for the cases considered

herein. In this thesis work, σ - transformation is applied in the horizontal direction which stretches between the left and the right wall and in the vertical direction which stretches between the moving liquid free surface and the bottom of the liquid tank to convert the moving free-surface physical domain onto a fixed square computational domain. The following section discusses the transformation technique in 2-D and 3-D tanks elaborately. During the transformation, the governing equation and boundary conditions will change appropriately.

4.3.2 Transformation of 2-D Rectangular Tank

Initially, formulations are developed for the fixed tank condition, so the horizontal and vertical excitation terms are neglected from the Eq. 4.4 in the following formulation part.

4.3.2.1 Step 1: First Coordinate Transformation:

The first transformation adopts the σ -transformation technique to map the liquid domain onto a rectangle, such that the moving free surface in the physical plane (Figure 4.2) becomes a fixed horizontal line in the σ -transformed domain (Figure 4.3).

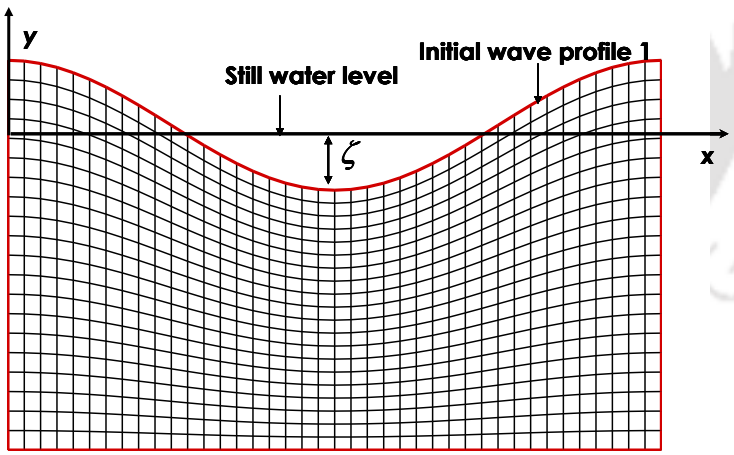

Figure 4.2: The 2-D physical domain.

The mapping function $\sigma(x,t)$ is defined as

$$\sigma = \frac{y + h_s}{h}, \tag{4.12}$$

where

$$h(x,t) = E_b \zeta(x,t) + h_s, \tag{4.13}$$

Here, $\sigma(x,t)$ is the stretching factor, which varies from 0 to 1. The value of σ at the bottom of the tank is *0*, while at the free surface is *1*. The first-order derivatives of σ can be calculated as follows:

$$\frac{\partial \sigma}{\partial t} = \frac{\partial}{\partial t}\left(\frac{y+h_s}{h}\right) = -E_b \frac{\sigma}{h}\frac{\partial \zeta}{\partial t} \qquad \text{and} \qquad \frac{\partial \sigma}{\partial x} = -E_b \frac{\sigma}{h}\frac{\partial \zeta}{\partial x}. \tag{4.14}$$

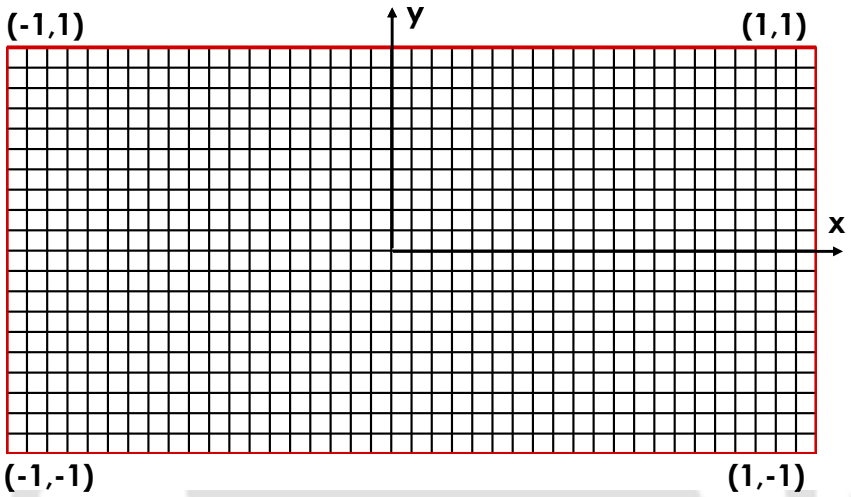

Figure 4.3: The 2-D intermediate domain after first transformation.

The potential function $\phi(x,y,t)$ in the physical domain is transformed to the potential function $\Phi(X,\sigma,T)$ in the σ -transformed domain.

$$x \leftrightarrow X,\ X = 2x-1;\ y \leftrightarrow Y,\ Y = 2\sigma - 1;\ \text{and}\ t \leftrightarrow T,\ T=t; \tag{4.15}$$

Using the chain rule, the first set of derivatives of ϕ with respect to *x*, *y* and *t* gets transformed as

$$\frac{\partial \phi}{\partial x} = 2\frac{\partial \Phi}{\partial X} - E_b \frac{4\sigma}{h}\frac{\partial \zeta}{\partial X}\frac{\partial \Phi}{\partial Y} \tag{4.16}$$

$$\frac{\partial \phi}{\partial y} = \frac{2}{h}\frac{\partial \Phi}{\partial Y} \tag{4.17}$$

and

$$\frac{\partial \phi}{\partial t} = \frac{\partial \Phi}{\partial T} - E_b \frac{\sigma}{h}\frac{\partial \zeta}{\partial T}\frac{\partial \Phi}{\partial \sigma} \tag{4.18}$$

The second set of derivatives of ϕ with respect to *x* and *y* gets transformed as,

$$\frac{\partial^2 \phi}{\partial x^2} = 4\frac{\partial^2 \Phi}{\partial X^2} + l_1 \frac{\partial^2 \Phi}{\partial Y^2} - l_2 \frac{\partial^2 \Phi}{\partial X \partial Y} + l_3 \frac{\partial \Phi}{\partial Y} \tag{4.19}$$

$$\frac{\partial^2 \phi}{\partial y^2} = \frac{4}{h^2}\frac{\partial^2 \Phi}{\partial Y^2} \tag{4.20}$$

where, $l_1 = \left(\frac{4\sigma}{h}\frac{\partial h}{\partial X}\right)^2$; $l_2 = \left[\frac{8\sigma}{h}\frac{\partial h}{\partial X}\right]$; $l_3 = \left[\sigma\left(\frac{4}{h}\frac{\partial h}{\partial X}\right)^2 - \frac{8\sigma}{h}\frac{\partial^2 h}{\partial X^2}\right]$.

Hence, by using the σ transformation, we can derive the new governing equation and boundary conditions specified on the rectangular σ-transformed domain. The governing equation after the first coordinate transformation is given as:

$$\frac{\partial^2 \Phi}{\partial X^2} + L_1\frac{\partial \Phi}{\partial Y} - L_2\frac{\partial^2 \Phi}{\partial X \partial Y} + L_3\frac{\partial^2 \Phi}{\partial Y^2} = 0 \tag{4.21}$$

$$\text{where, } L_1 = \left[\frac{4\sigma}{h^2}\left(\frac{\partial h}{\partial X}\right)^2 - \frac{2\sigma}{h}\frac{\partial^2 h}{\partial X^2}\right];\ L_2 = 2\frac{\sigma}{h}\frac{\partial h}{\partial X};\ L_3 = \left[\frac{1}{h^2} + \left(\frac{2\sigma}{h}\frac{\partial h}{\partial X}\right)^2\right] \tag{4.22}$$

Boundary conditions after the first coordinate transformation are given as:

$$\text{L:} \quad \frac{\partial \Phi}{\partial X} - \frac{2\sigma}{h}\frac{\partial h}{\partial X}\frac{\partial \Phi}{\partial Y} = 0 \qquad \text{on} \quad X = -1 \tag{4.23}$$

$$\text{R:} \quad \frac{\partial \Phi}{\partial X} - \frac{2\sigma}{h}\frac{\partial h}{\partial X}\frac{\partial \Phi}{\partial Y} = 0 \qquad \text{on} \quad X = +1 \tag{4.24}$$

$$\text{B:} \quad \frac{\partial \Phi}{\partial Y} = 0, \qquad \text{on} \quad Y = -1 \tag{4.25}$$

$$\text{T1:} \quad \frac{\partial \zeta}{\partial T} = \left[\frac{2}{h} + \frac{8E_b\sigma}{h}\left(\frac{\partial \zeta}{\partial x}\right)^2\right]\frac{\partial \Phi}{\partial Y} - 4E_b\frac{\partial \Phi}{\partial X}\frac{\partial \zeta}{\partial X}, \qquad \text{on} \quad Y = +1 \tag{4.26}$$

$$\text{T2:} \quad \frac{\partial \Phi}{\partial T} = M_1\frac{\partial \Phi}{\partial Y} - 2E_b\left[\left(\frac{\partial \Phi}{\partial X} - M_2\frac{\partial \Phi}{\partial Y}\right)^2 + \left(\frac{1}{h}\frac{\partial \Phi}{\partial Y}\right)^2\right] - (1 + \ddot{Y}_t)\zeta, \text{ on } Y = +1 \tag{4.27}$$

$$\text{where,} \qquad M_1 = \frac{2\sigma}{h}\frac{\partial h}{\partial T}; \qquad M_2 = \frac{2\sigma}{h}\frac{\partial h}{\partial X}. \tag{4.28}$$

4.3.2.2 Step 2: Second Coordinate Transformation:

After the first coordinate transformation, the liquid domain becomes a rectangle defined by $-1 \le X \le +1, -1 \le Y \le +1$. The time-varying curved free surface hence, is replaced by the fixed straight line. Any numerical method can be employed to solve the governing equations in the computational domain. Now the second transformation is performed for the clustering of grid points near liquid free surface. The second coordinate transformation is applied by the following equations

$$X \leftrightarrow \xi, \xi = X; \quad Y \leftrightarrow \eta, \eta = \alpha + (1-\alpha)\frac{\ln\left[\left(\beta + \left[\frac{Y+1}{h_{cd}}\right]\right)\Big/\left(\beta - \left[\frac{Y+1}{h_{cd}}\right]\right)\right]}{\ln\left(\beta + 1/\beta - 1\right)};$$

and $\quad T \leftrightarrow \tau, \quad \tau = T;$ (4.29)

where β is the grid vertical stretching factor and α is a parameter that controls the range of η. The above transformation produces clustering of the grids near the free surface depending on the value of β chosen. The clustering of grids near the free surface improves accuracy and eases convergence of the computational algorithm. As β approaches unity, the mesh gets refined more along the free surface of the liquid. Another parameter in the transformation, α adjusts the position of the bottom in the transformed coordinates. Here the value of α has been taken as -1 so that the computational domain after the second transformation is a rectangle defined by $-1 \le \xi \le 1$ and $-1 \le \eta \le 1$ with grid stretching near free surface as shown in Figure 4.4. The mapping is performed from the σ-transformed $\Phi(X,Y,T)$ domain to the computational domain $\varphi(\xi,\eta,\tau)$. The height of the liquid surface $h(X,T)$ is transformed to the height of the liquid surface in the transformed computational domain $h_*(\xi,\tau)$, where h_{cd} is the difference between the nodal indices along Y axis of the grid after the first coordinate transformation.

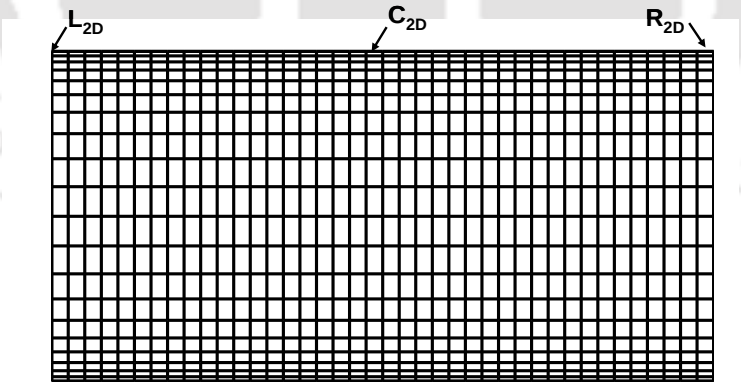

Figure 4.4: The 2-D computational domain after second transformation.

The derivatives of the function $\Phi(X,Y,T)$ with respect to *X*, *Y* and *T* are transformed into derivatives of $\varphi(\xi,\eta,\tau)$ with respect to ξ, η and τ. The first set of derivatives of $\Phi(X,Y,T)$ gets transformed as:

$$\frac{\partial \Phi}{\partial X} = \frac{\partial \varphi}{\partial \xi}, \quad \frac{\partial \Phi}{\partial Y} = \frac{\partial \varphi}{\partial \eta} \times \frac{\partial \eta}{\partial Y} \quad \text{and} \quad \frac{\partial \Phi}{\partial T} = \frac{\partial \varphi}{\partial \tau} \tag{4.30}$$

$$\text{where, } \frac{\partial \eta}{\partial Y} = \frac{(1-\alpha)}{\ln(\beta+1/\beta-1)} \times \frac{2\beta}{h_{cd} \times (\beta^2 - \sigma^{*2})} \tag{4.31}$$

The second set of derivatives gets transformed as follows:

$$\frac{\partial^2 \Phi}{\partial X^2} = \frac{\partial^2 \varphi}{\partial \xi^2} \quad , \quad \frac{\partial^2 \Phi}{\partial X \partial Y} = \frac{\partial^2 \varphi}{\partial \xi \partial \eta} \times \frac{\partial \eta}{\partial Y} \text{ and } \quad \frac{\partial^2 \Phi}{\partial Y^2} = \frac{\partial^2 \varphi}{\partial \eta^2} \times \left(\frac{\partial \eta}{\partial Y}\right)^2 + \frac{\partial \varphi}{\partial \eta} \times C_1 \tag{4.32}$$

After the second coordinate transformation the governing equation (Eq. 4.21) becomes,

$$\frac{\partial^2 \varphi}{\partial \xi^2} + L_1 \frac{\partial \varphi}{\partial \eta} - C_3 L_2 \frac{\partial^2 \varphi}{\partial \xi \partial \eta} + C_3^{\,2} L_3 \frac{\partial^2 \varphi}{\partial \eta^2} = 0 \tag{4.33}$$

$$\text{where } L_1 = \left(\frac{4\sigma^*}{h_*^2} \left[\frac{\partial h_*}{\partial \xi} \right]^2 - \frac{2\sigma^*}{h_*} \frac{\partial^2 h_*}{\partial \xi^2} + C_1 \times L_3 \right); \; L_2 = \left[\frac{2\sigma^*}{h_*} \frac{\partial h_*}{\partial \xi} \right]; \; L_3 = \left[\frac{1}{h_*^2} + L_2^{\,2} \right];$$

$$C_1 = \frac{(1-\alpha)}{\ln(\beta+1)/(\beta-1)} \times \frac{4 \times \beta \times \sigma^* \times C_2}{\left(h_{cd} \times \left(\beta^2 - \sigma^{*2} \right)^2 \right)}$$

$$C_2 = \frac{\beta \times C_4}{(\beta+1)^{\frac{\eta-\alpha}{1-\alpha}} + (\beta-1)^{\frac{\eta-\alpha}{1-\alpha}}} + \frac{\beta \times \left[(\beta-1)^{\frac{\eta-\alpha}{1-\alpha}} - (\beta+1)^{\frac{\eta-\alpha}{1-\alpha}} \right] \times C_5}{\left[(\beta+1)^{\frac{\eta-\alpha}{1-\alpha}} + (\beta-1)^{\frac{\eta-\alpha}{1-\alpha}} \right]^2}; \; C_3 = \frac{\partial \eta}{\partial Y};$$

$$C_4 = \left(\frac{\log(\beta-1)(\beta-1)^{\frac{\eta-\alpha}{1-\alpha}}}{(\alpha-1)} - \frac{\log(\beta+1)(\beta+1)^{\frac{\eta-\alpha}{1-\alpha}}}{(\alpha-1)} \right)$$

$$C_5 = \left(\frac{\log(\beta-1)(\beta-1)^{\frac{\eta-\alpha}{1-\alpha}}}{(\alpha-1)} + \frac{\log(\beta+1)(\beta+1)^{\frac{\eta-\alpha}{1-\alpha}}}{(\alpha-1)} \right);$$

$$\sigma^* = \left(\beta \times \left[\frac{(\beta+1)^{\frac{\eta-\alpha}{1-\alpha}} - (\beta-1)^{\frac{\eta-\alpha}{1-\alpha}}}{(\beta+1)^{\frac{\eta-\alpha}{1-\alpha}} + (\beta-1)^{\frac{\eta-\alpha}{1-\alpha}}} \right] \right) \tag{4.34}$$

Boundary conditions after the second transformation are given as:-

$$\text{L:} \quad \frac{\partial \varphi}{\partial \xi} - \frac{2\sigma^*}{h_*} C_3 \frac{\partial h_*}{\partial \xi} \frac{\partial \varphi}{\partial \eta} = 0 \qquad \text{on } \; \xi = -1 \tag{4.35}$$

$$\text{R:} \quad \frac{\partial \varphi}{\partial \xi} - \frac{2\sigma^*}{h_*} C_3 \frac{\partial h_*}{\partial \xi} \frac{\partial \varphi}{\partial \eta} = 0 \qquad \text{on } \; \xi = 1 \tag{4.36}$$

$$\text{B:} \quad \frac{\partial \varphi}{\partial \eta} = 0 \qquad \text{on } \; \eta = -1 \tag{4.37}$$

$$\text{T1:} \quad \frac{\partial \zeta^*}{\partial \tau} = L_4 C_3 \frac{\partial \varphi}{\partial \eta} - 4E_b \frac{\partial \varphi}{\partial \xi} \frac{\partial \zeta}{\partial \xi} \qquad \text{on } \; \eta = 1 \tag{4.38}$$

$$\text{T2:}\quad \frac{\partial \varphi}{\partial \tau} = C_3 L_5 \frac{\partial \varphi}{\partial \eta} - 2E_b \left[\left(\frac{\partial \varphi}{\partial \xi} - C_3 L_6 \frac{\partial \varphi}{\partial \eta} \right)^2 + \left(\frac{C_3}{h_*} \frac{\partial \varphi}{\partial \eta} \right)^2 \right] - \left(1 + Y_\tau^*\right) \zeta^* \quad \text{on} \quad \eta = 1 \qquad (4.39)$$

$$\text{where}\quad L_4 = \left[\frac{2}{h_*} + 4E_b L_2 \left(\frac{\partial h_*}{\partial \xi} \right) \right];\quad L_5 = \frac{2\sigma^*}{h_*} \frac{\partial h_*}{\partial \tau};\quad L_6 = \left[\frac{2\sigma^*}{h_*} \frac{\partial h_*}{\partial \xi} \right] \qquad (4.40)$$

The governing equation and the boundary conditions in the computational domain are given by Eqns. 4.33 – 4.40 and any numerical method can be used to solve them. One more feature of this σ-transformation technique is that it can be easily extended to 3-Dimensional coordinates in a similar way.

4.4 Transformation for a 3-D Rectangular Tank

The 3-D rectangular domain is bounded by 5 regular surfaces and 1 free surface. The velocity components normal to the fixed surfaces are zero. The left, right, front and back and the bottom surfaces boundary conditions are indicated by LB, RB, FB, BB and BMB, respectively in Eqns. 4.42 – 4.44. As usual, the top surface has two boundary conditions, viz., the kinematic condition (TB1) and the dynamic condition (TB2). When the tank is subjected to vertical acceleration, the non-dimensional governing equations based on the potential flow theory are as follows:

$$\frac{\partial^2 \phi}{\partial x^2} + \frac{\partial^2 \phi}{\partial y^2} + \frac{\partial^2 \phi}{\partial z^2} = 0 \qquad (4.41)$$

$$\text{LB and RB:}\quad \frac{\partial \phi}{\partial x} = 0 \qquad \text{on} \quad x = 0, b \qquad (4.42)$$

$$\text{FB and BB:}\quad \frac{\partial \phi}{\partial z} = 0 \qquad \text{on} \quad z = 0, w \qquad (4.43)$$

$$\text{BMB:}\quad \frac{\partial \phi}{\partial y} = 0 \qquad \text{on} \quad y = -h_s \qquad (4.44)$$

$$\text{TB1:}\quad \frac{\partial \zeta}{\partial t} + E_b \frac{\partial \phi}{\partial x} \frac{\partial \zeta}{\partial x} + E_b \frac{\partial \phi}{\partial z} \frac{\partial \zeta}{\partial z} = \frac{\partial \phi}{\partial y} \qquad \text{on} \quad y = \zeta \qquad (4.45)$$

$$\text{TB2:}\quad \frac{\partial \phi}{\partial t} + E_b \frac{1}{2} \nabla \phi . \nabla \phi + (1 + \ddot{Y}_t) \zeta = 0 \qquad \text{on} \quad y = \zeta \qquad (4.46)$$

where, w is width of the rectangular tank. The derivation of the governing equations can be performed in the same way as the two-dimensional case by the following two transformations. The first transformation is performed for conversion from physical domains

(Figures 4.5 and 4.6) to σ -transformed domain (Figure 4.7) and the second transformation is for σ -transformed domain to computational domain (Figure 4.8).

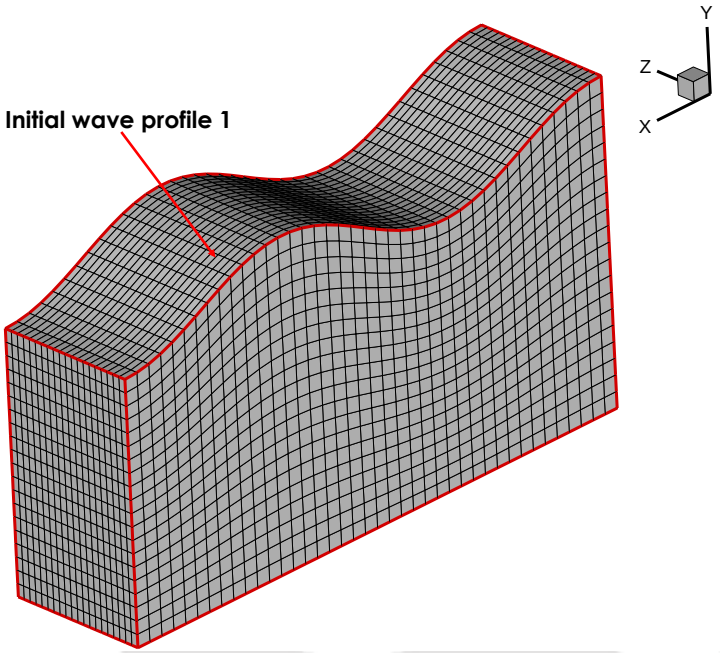

Figure 4.5: The 3-D physical domain with initial wave profile 1.

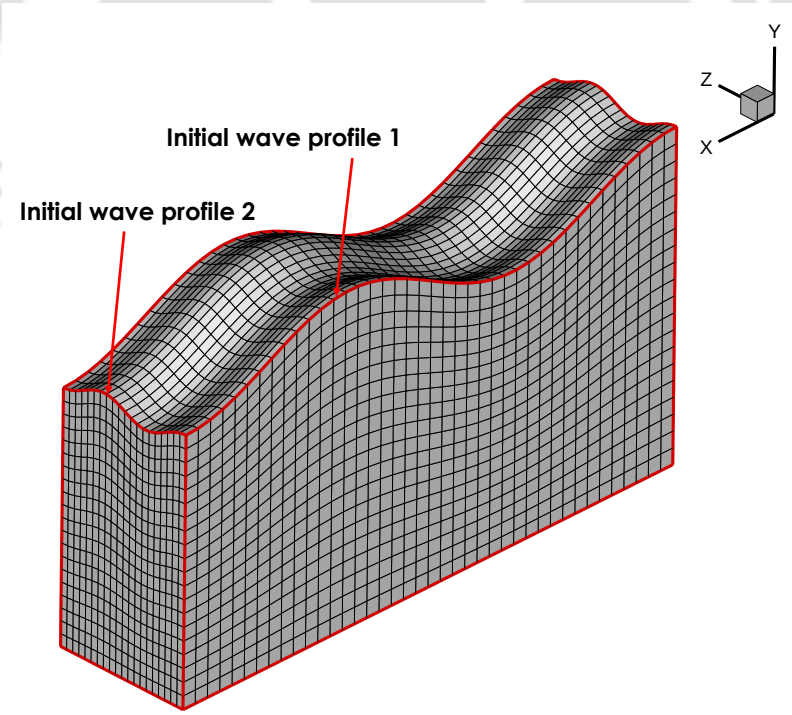

Figure 4.6: The 3-D physical domain with initial wave profiles 1 and 2.

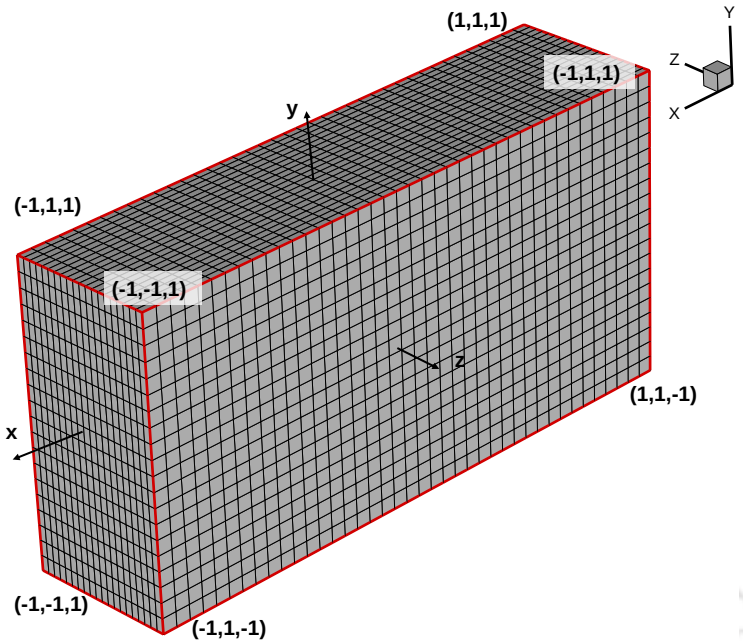

Figure 4.7: The 3-D intermediate domain after first transformation.

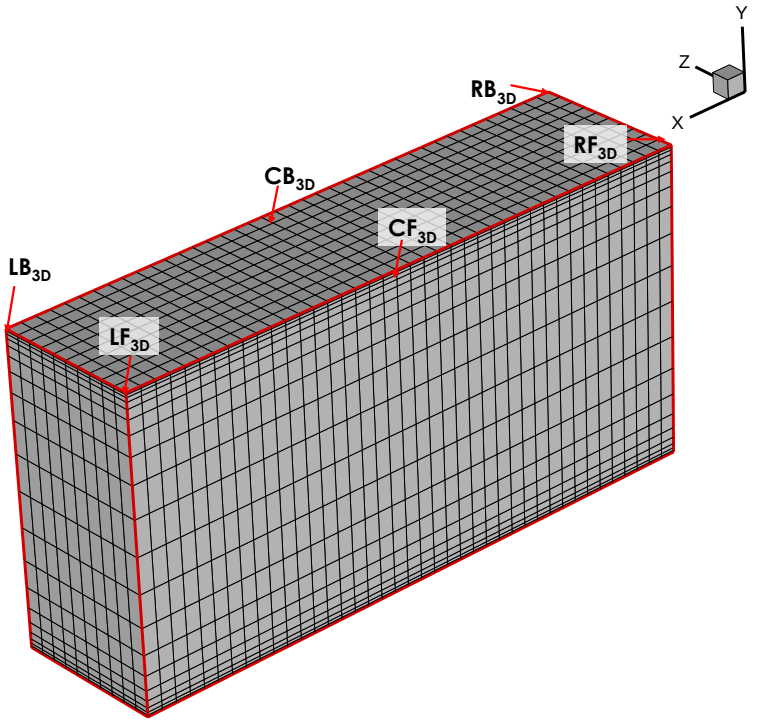

Figure 4.8: The 3-D computational domain after second transformation.

4.4.1 First and Second Transformation for 3-D Rectangular Tank

The mapping relations for first transformation are given as,

$$X = 2x - 1; \quad Y = 2\sigma - 1; \quad Z = 2z - 1 \text{ and } T = t. \tag{4.47}$$

Hence the transformed governing equation becomes:

$$\frac{\partial^2\Phi}{\partial X^2}+K_1\frac{\partial\Phi}{\partial Y}-K_2\frac{\partial^2\Phi}{\partial X\partial Y}-K_3\frac{\partial^2\Phi}{\partial Z\partial Y}+K_4\frac{\partial^2\Phi}{\partial Y^2}+\frac{\partial^2\Phi}{\partial Z^2}=0 \tag{4.48}$$

where, $K_1=\left[\frac{4\sigma}{h^2}\left(\frac{\partial h}{\partial X}\right)^2-\frac{2\sigma}{h}\frac{\partial^2 h}{\partial X^2}+\frac{4\sigma}{h^2}\left(\frac{\partial h}{\partial Z}\right)^2-\frac{2\sigma}{h}\frac{\partial^2 h}{\partial Z^2}\right]$; $K_2=\frac{2\sigma}{h}\frac{\partial h}{\partial X}$;

$$K_3=\frac{2\sigma}{h}\frac{\partial h}{\partial Z};\ K_4=\left[\frac{1}{h^2}+K_2{}^2+K_3{}^2\right] \tag{4.49}$$

The boundary conditions are given as:

$$\text{LB and RB: } \frac{\partial\Phi}{\partial X}-\frac{2\sigma}{h}\frac{\partial h}{\partial X}\frac{\partial\Phi}{\partial Y}=0 \text{ on } X = -1, +1 \tag{4.50}$$

$$\text{FB and BB: } \frac{\partial\Phi}{\partial Z}-\frac{2\sigma}{h}\frac{\partial h}{\partial Z}\frac{\partial\Phi}{\partial Y}=0 \text{ on Z = } -1, +1 \tag{4.51}$$

$$\text{BMB : } \quad \frac{\partial\Phi}{\partial Y}=0, \quad \text{on} \quad Y=-1 \tag{4.52}$$

On the free surface,

$$TB1:\ \frac{\partial\zeta}{\partial T}=K_5\frac{\partial\Phi}{\partial Y}-4E_b\frac{\partial\Phi}{\partial X}\frac{\partial\zeta}{\partial X}-4E_b\frac{\partial\Phi}{\partial Z}\frac{\partial\zeta}{\partial Z} \quad \text{on} \quad Y=+1 \tag{4.53}$$

$$TB2:\ \frac{\partial\Phi}{\partial T}=K_6\frac{\partial\Phi}{\partial Y}-2E_b\left[\left(\frac{\partial\Phi}{\partial X}-K_7\frac{\partial\Phi}{\partial Y}\right)^2+\left(\frac{1}{h}\frac{\partial\Phi}{\partial Y}\right)^2+\left(\frac{\partial\Phi}{\partial Z}-K_8\frac{\partial\Phi}{\partial Y}\right)^2\right]-(1+\ddot{Y}_t)\zeta \text{ on } Y=+1 \tag{4.54}$$

where, $K_5=\left[\frac{2}{h}+\frac{8E_b\sigma}{h}\left(\frac{\partial\zeta}{\partial X}\right)^2+\frac{8E_b\sigma}{h}\left(\frac{\partial\zeta}{\partial Z}\right)^2\right]$; $K_6=\frac{2\sigma}{h}\frac{\partial h}{\partial T}$; $K_7=\frac{2\sigma}{h}\frac{\partial h}{\partial X}$;

$$K_8=\frac{2\sigma}{h}\frac{\partial h}{\partial Z}. \tag{4.55}$$

The mapping relations for second transformation are given as,

$$X\leftrightarrow\xi,\xi=X;\quad Y\leftrightarrow\eta,\eta=\alpha+(1-\alpha)\frac{\ln\left(\left(\beta+\left[\frac{Y+1}{h_{cd}}\right]\right)\Big/\left(\beta-\left[\frac{Y+1}{h_{cd}}\right]\right)\right)}{\ln\left[(\beta+1)/(\beta-1)\right]};\ Z\leftrightarrow\kappa,$$

$$\kappa=Z \quad \text{and} \quad T\leftrightarrow\tau,\ \tau=T. \tag{4.56}$$

The mapping is performed from the σ-transformed $\Phi(X,Y,Z,T)$ domain to the computational domain $\varphi(\xi,\eta,\kappa,\tau)$. The height of the liquid, $h(X,Z,T)$ surface is transformed to the height of the liquid in the transformed computational domain, $h_*(\xi,\kappa,\tau)$.

The h_{cd} is the difference between the nodal indices along Y axis of the grid after the first coordinate transformation. The derivatives of the function $\Phi(X,Y,Z,T)$ with respect to *X*, *Y*, *Z* and *T* are transformed into derivatives of $\varphi(\xi,\eta,\kappa,\tau)$ with respect to ξ,η,κ and τ. After the second coordinate transformation, the governing equation in the fluid domain becomes,

$$\frac{\partial^2\varphi}{\partial\xi^2}+C_4\frac{\partial\varphi}{\partial\eta}-C_3U_1\frac{\partial^2\varphi}{\partial\xi\partial\eta}-C_3U_2\frac{\partial^2\varphi}{\partial\kappa\partial\eta}+C_5\frac{\partial^2\varphi}{\partial\eta^2}=0 \tag{4.57}$$

where $U_1=\left[\frac{2\sigma^*}{h_*}\frac{\partial h_*}{\partial\xi}\right]$; $U_2=\left[\frac{2\sigma^*}{h^*}\frac{\partial h_*}{\partial\kappa}\right]$;

$$U_3=\left(\frac{\log(\beta-1)(\beta-1)^{\frac{\eta-\alpha}{1-\alpha}}}{(\alpha-1)}-\frac{\log(\beta+1)(\beta+1)^{\frac{\eta-\alpha}{1-\alpha}}}{(\alpha-1)}\right);$$

$$U_4=\left(\frac{\log(\beta-1)(\beta-1)^{\frac{\eta-\alpha}{1-\alpha}}}{(\alpha-1)}+\frac{\log(\beta+1)(\beta+1)^{\frac{\eta-\alpha}{1-\alpha}}}{(\alpha-1)}\right);$$

$$C_1=\frac{(1-\alpha)}{\ln\left(\frac{\beta+1}{\beta-1}\right)}\times\frac{4\beta\times\sigma^*\times C_2}{\left(h_{cd}\times\left[\beta^2-\sigma^{*2}\right]^2\right)};$$

$$C_2=\frac{\beta\times U_3}{(\beta+1)^{\frac{\eta-\alpha}{1-\alpha}}+(\beta-1)^{\frac{\eta-\alpha}{1-\alpha}}}+\frac{\beta\times\left[(\beta-1)^{\frac{\eta-\alpha}{1-\alpha}}-(\beta+1)^{\frac{\eta-\alpha}{1-\alpha}}\right]\times U_4}{\left[(\beta+1)^{\frac{\eta-\alpha}{1-\alpha}}+(\beta-1)^{\frac{\eta-\alpha}{1-\alpha}}\right]^2};$$

$$C_3=\frac{\partial\eta}{\partial Y};\ C_4=\left(\frac{4\sigma^*}{h_*^2}\left(\left[\frac{\partial h_*}{\partial\xi}\right]^2+\left[\frac{\partial h_*}{\partial\kappa}\right]^2\right)-\frac{2\sigma^*}{h_*}\left(\frac{\partial^2 h_*}{\partial\xi^2}+\frac{\partial^2 h_*}{\partial\kappa^2}\right)+C_1\times U_5\right);$$

$$U_5=\left[\frac{1}{h_*^2}+\left(\frac{2\sigma^*}{h_*}\frac{\partial h_*}{\partial\xi}\right)^2+\left(\frac{2\sigma^*}{h_*}\frac{\partial h_*}{\partial\kappa}\right)^2\right];$$

$$C_5=C_3^{\,2}\times\left[\frac{1}{h_*^{\,2}}+\left(\frac{2\sigma^*}{h_*^2}\frac{\partial h_*}{\partial\xi}\right)^2+\left(\frac{2\sigma^*}{h_*}\frac{\partial h_*}{\partial\kappa}\right)^2\right];\ \sigma^*=\left(\beta\left[\frac{(\beta+1)^{\frac{\eta-\alpha}{1-\alpha}}-(\beta-1)^{\frac{\eta-\alpha}{1-\alpha}}}{(\beta+1)^{\frac{\eta-\alpha}{1-\alpha}}+(\beta-1)^{\frac{\eta-\alpha}{1-\alpha}}}\right]\right). \tag{4.58}$$

Boundary conditions after the second transformation are given as:-

LB and RB: $\frac{\partial\varphi}{\partial\xi}-\frac{2\sigma^*}{h_*}C_3\frac{\partial h_*}{\partial\xi}\frac{\partial\varphi}{\partial\eta}=0$ on ξ = *-1, 1* (4.59)

FB and BB: $\frac{\partial\varphi}{\partial\kappa}-\frac{2\sigma^*}{h_*}C_3\frac{\partial h_*}{\partial\kappa}\frac{\partial\varphi}{\partial\eta}=0$ on κ = *-1, 1* (4.60)

$$\text{BMB}: \qquad \frac{\partial \varphi}{\partial \eta} = 0 \qquad \text{on} \quad \eta = -1 \tag{4.61}$$

On the free surface,

$$\text{T1}: \quad \frac{\partial \zeta^*}{\partial \tau} = C_3 \left[\frac{2}{h_*} + U_9 \right] \frac{\partial \varphi}{\partial \eta} - 4E_b \left(\frac{\partial \varphi}{\partial \xi} \frac{\partial \zeta}{\partial \xi} + \frac{\partial \varphi}{\partial \kappa} \frac{\partial \zeta}{\partial \kappa} \right) \quad \text{on} \quad \eta = 1 \tag{4.62}$$

$$\text{T2}: \quad \frac{\partial \varphi}{\partial \tau} = U_6 \frac{\partial \varphi}{\partial \eta} - 2E_b \left[\left(\frac{\partial \varphi}{\partial \xi} - U_7 \frac{\partial \varphi}{\partial \eta} \right)^2 + \left(\frac{C_3}{h_*} \frac{\partial \varphi}{\partial \eta} \right)^2 + \left(\frac{\partial \varphi}{\partial \kappa} - U_8 \frac{\partial \varphi}{\partial \eta} \right)^2 \right] - \left(1 + Y_\tau^* \right) \zeta^* \quad \text{on} \quad \eta = 1 \tag{4.63}$$

where,

$$U_9 = \frac{8E_b \sigma^*}{h_*} \left(\left(\frac{\partial h_*}{\partial \xi} \right)^2 + \left(\frac{\partial h_*}{\partial \kappa} \right)^2 \right); \qquad U_7 = C_3 \frac{2\sigma^*}{h_*} \frac{\partial h_*}{\partial \xi}; \qquad U_8 = C_3 \frac{2\sigma^*}{h_*} \frac{\partial h_*}{\partial \kappa};$$

$$U_6 = C_3 \frac{2\sigma^*}{h_*} \frac{\partial h_*}{\partial \tau}. \tag{4.64}$$

Since sloshing is a highly non-linear phenomenon, the amplitude of excitation, frequency of excitation and tank dimensions play a vital role in determining the shape of the non-linear free surface. An amplitude–frequency relationship for the fluid response in a two-dimensional rectangular tank is presented by Faltinsen *et al.* (2000). Obviously, the stretched grid system exactly matches the time-dependent free-surface wave profile due to the σ-transformation.

4.5 Transformation for a 2-D Horizontal Cylindrical Tank

In this section, a simple mapping function is used to remove the time-dependence of the free surface in the fluid domain. The non-linear wave in the fluid domain is transformed into a straight line by using linear equations. The fluid motion is solved in a unit square mesh in the transformed flow domain (i.e., computational domain). The fourth order central difference scheme and the Gauss–Seidel point successive over-relaxation iterative procedure are used to capture the free surface wave profiles and free surface elevation plots of the fluid domain. The sloshing characteristics of the liquid in a horizontal cylinder, subjected to the EW and NS components of the EL-Centro earthquake, California is also studied.

4.5.1 Mathematical Formulation for 2-D Horizontal Cylinder

A cylindrical coordinate system is first employed, with origin at the mean free-surface, and at the left-hand side of the tank. An irrotational motion of an inviscid and incompressible fluid in a 2-D tank is considered. The coordinate system is chosen such that the y-axis directs against the gravity. A 2-D nonlinear wave problem is considered in this case, as depicted in Figure 4.9, where ζ is the free-surface elevation above still water level, b is the length of the tank, and h_s is the still water depth.

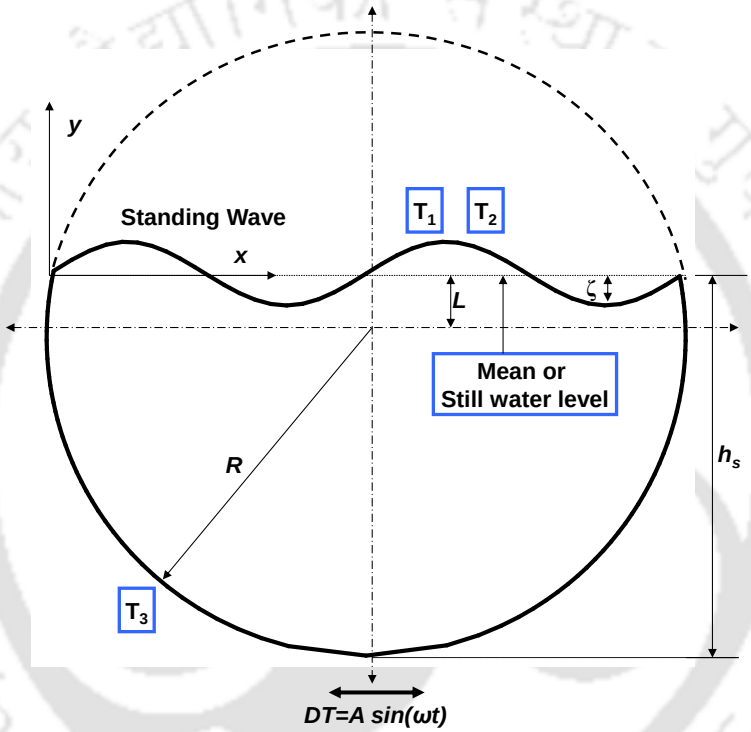

Figure 4.9: Sketch of a standing wave in 2-D horizontal cylindrical tank.

The fluid in the tank is assumed to be inviscid and irrotational. Therefore, the governing equation of fluid motion is given by the Laplace's equation.

$$\frac{\partial^2 \phi}{\partial x^2} + \frac{\partial^2 \phi}{\partial y^2} = 0 \tag{4.65}$$

where, ϕ is the velocity potential function. The velocity components normal to the fixed boundaries are zero by definition. On the rigid wall, the free-slip boundary condition is applied for the tangential velocity component.

The free surfaces occur at the interface between two fluids. Such interfaces require two boundary conditions to be applied: viz., (i) a kinematic condition that relates the motion of the free interface to the fluid velocities at the free surface (i.e., T_1) and (ii) a dynamic condition which is concerned with the force balance at the free surface (i.e., T_2). The tank is studied satisfying the condition that velocity at the wetted surface is zero (i.e., T_3). Zero pressure at the free surface of the fluid is also considered in the analysis. In view of mentioned above, kinematic and dynamic conditions must be satisfied on the free surface. Therefore, the boundary conditions for the physical domain are given by

$$T_1: \quad \frac{\partial \phi}{\partial t} + \frac{1}{2}\nabla\phi \cdot \nabla\phi + g\zeta = -DT''x \qquad \text{on } y = \zeta \tag{4.66}$$

$$T_2: \quad \frac{\partial \zeta}{\partial t} + \frac{\partial \phi}{\partial x}\frac{\partial \zeta}{\partial x} = \frac{\partial \phi}{\partial y} \qquad \text{on } y = \zeta \tag{4.67}$$

$$T_3: \quad \frac{\partial \phi}{\partial n} = 0 \qquad \text{on} \quad \text{wetted surface} \tag{4.68}$$

where n is the normal vector and t is the time. DT'' is the horizontal acceleration of the tank and g is the acceleration due to gravity.

4.5.2 Mapping Procedures

In this section, the mapping procedure is discussed to convert from semi-circular domain to a square domain. The time varying non-linear free surface is converted into a straight line by appropriate linear transformations. A horizontal linear mapping is also applied, so that the resulting computational domain is rectangular. Finite difference (FDM) and volume methods (FVM) can be applied to Eq. 4.65 through 4.68 for solving the free surface profile of the sloshed tank. Here, the simple mapping procedure is adopted to convert the semi-circular domain to square domain and subsequently the σ-transformation is applied to capture the free surface of the liquid.

4.5.3 Coordinate Transformation

Generally, the derivation of governing equations and implementation of calculation would be intricate in the polar coordinate system. Moreover, additional work is to be done to retreat the liquid free surface in the time varying integration domain. To trounce above difficulties caused by the curved boundary, the coordinate transformation is performed by using the linear relations

$$x \leftrightarrow X\,,\; X = \frac{x}{\sqrt{1-(y+L)^2}}\,;\; y \leftrightarrow \sigma\,,\; \sigma = \frac{y+d}{h}\,;\; t \leftrightarrow T\,,\; T = t\,. \qquad (4.69)$$

where $$h(x,t) = \zeta(x,t) + h_s \qquad (4.70)$$

The transformation along x axis ($x \leftrightarrow X$) converts the semicircular domain (Figure 4.10) into rectangular domain with moving non-linear free surface boundary. This will construct the intermediate domain (X, y, T) as shown in Figure 4.11. Again the transformation along y axis ($y \leftrightarrow \sigma$), makes the nonlinear free surface to get converted into a flat straight line. $\sigma(x,t)$ is a stretching variable introduced in the vertical direction, taking the value 0 at the bottom and 1 at the free surface. This σ-transformation, is used to map the liquid domain onto a rectangle, such that the moving free surface in the physical plane becomes a fixed horizontal line in the σ-transformed domain (Figure 4.12).

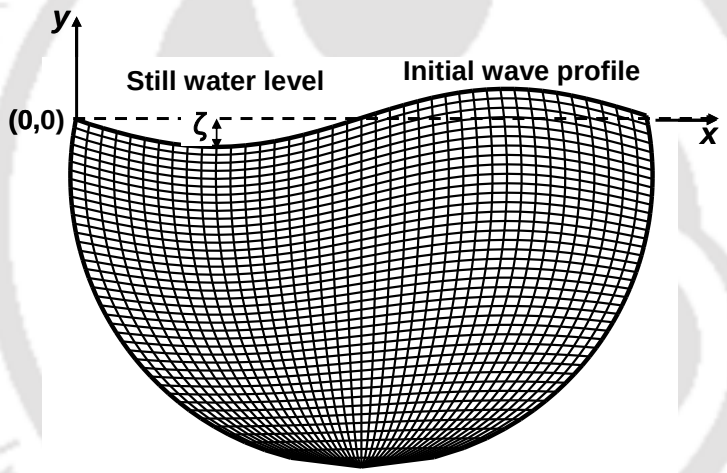

Figure 4.10: Physical domain of horizontal cylindrical tank (x, y, t).

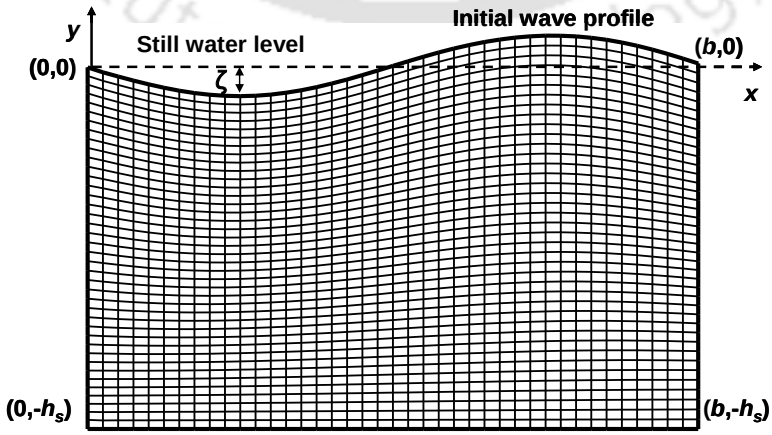

Figure 4.11: Intermediate domain of horizontal cylindrical tank (X, y, T).

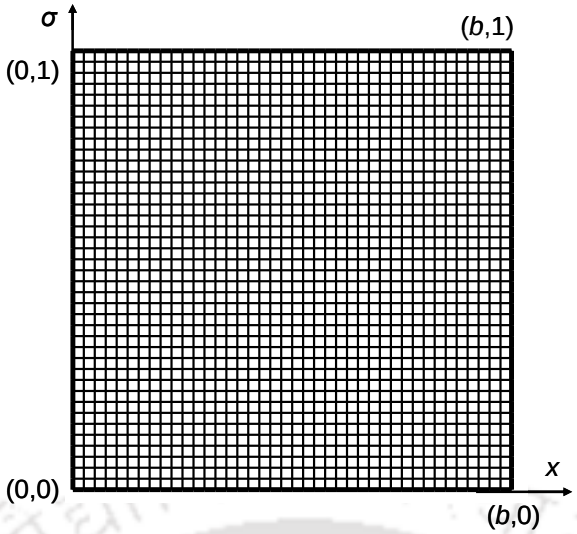

Figure 4.12: Computational (or σ -transformed) domain of horizontal cylindrical tank (X,σ,T).

Consider a potential function $\phi(x,y,t)$ which is needed to transform derivatives of the potential function $\varphi(X,\sigma,T)$.

$$\frac{\partial\sigma}{\partial t}=\frac{\partial}{\partial t}\left(\frac{y+hs}{h}\right)=-\frac{\sigma}{h}\frac{\partial\zeta}{\partial t}=-\frac{\sigma}{h}\frac{\partial\zeta}{\partial T} \tag{4.71}$$

$$\text{and } \frac{\partial\sigma}{\partial x}=-\frac{\sigma}{h}\frac{\partial\zeta}{\partial x}=-\frac{\sigma}{h}\frac{\partial\zeta}{\partial X}\left(\frac{1}{\sqrt{1-(y+L)^2}}\right) \tag{4.72}$$

Using the chain rule, the first derivatives of ϕ with respect to x, t can be written as

$$\frac{\partial\phi}{\partial x}=\left(\frac{1}{\sqrt{e}}\right)\left(\frac{\partial\varphi}{\partial X}-\frac{\sigma}{h}\frac{\partial\zeta}{\partial X}\frac{\partial\varphi}{\partial\sigma}\right) \tag{4.73}$$

$$\text{and } \frac{\partial\phi}{\partial t}=\left(\frac{\partial\varphi}{\partial T}-\frac{\sigma}{h}\frac{\partial\zeta}{\partial T}\frac{\partial\varphi}{\partial\sigma}\right) \tag{4.74}$$

where $e=1-(y+L)^2$. The second derivatives of ϕ with respect to x can be written as

$$\frac{\partial^2\phi}{\partial x^2}=\left[\frac{1}{e}\frac{2\sigma}{h^2}\left(\frac{\partial\zeta}{\partial X}\right)^2-\frac{1}{e}\frac{\sigma}{h}\left(\frac{\partial^2\zeta}{\partial X^2}\right)\right]\frac{\partial\varphi}{\partial\sigma}+\frac{1}{e}\frac{\partial^2\varphi}{\partial X^2}+\left[\frac{1}{e}\frac{\sigma^2}{h^2}\left(\frac{\partial\zeta}{\partial X}\right)^2\right]\frac{\partial^2\varphi}{\partial\sigma^2}-\left(\frac{2}{e}\frac{\sigma}{h}\frac{\partial\zeta}{\partial X}\right)\frac{\partial^2\varphi}{\partial x\partial\sigma}$$

Hence, by using the σ -transformation, one can derive a new governing equation and boundary conditions specified on a rectangular domain. Thus, the governing equation becomes,

$$S_1\frac{\partial\varphi}{\partial\sigma}+S_2\frac{\partial\varphi}{\partial X}+S_3\frac{\partial^2\varphi}{\partial X^2}+S_4\frac{\partial^2\varphi}{\partial\sigma^2}+S_5\frac{\partial^2\varphi}{\partial x\partial\sigma}=0 \tag{4.76}$$

New boundary conditions after the transformation are

$$\mathrm{T}_1\text{: } \frac{\partial \varphi}{\partial T} = -\frac{1}{2}\left[B1\left(\frac{\partial \varphi}{\partial X}\right)^2 + B2\left(\frac{\partial \varphi}{\partial \sigma}\right)^2 + B3\frac{\partial^2 \varphi}{\partial X \partial \sigma}\right] + B_4\frac{\partial \varphi}{\partial \sigma} - g\zeta - DT''X\sqrt{e} \text{ on } \sigma = 1 \tag{4.77}$$

$$\mathrm{T}_2\text{: } \frac{\partial \zeta}{\partial T} = B_5\frac{\partial \varphi}{\partial X} + B_6\frac{\partial \varphi}{\partial \sigma} \text{ on } \sigma = 1 \tag{4.78}$$

$$\mathrm{T}_3\text{: } B_7\frac{\partial \varphi}{\partial X} + B_8\frac{\partial \varphi}{\partial \sigma} = 0 \text{ on } \sigma = 0 \tag{4.79}$$

$$\text{and } B_9\frac{\partial \varphi}{\partial X} + B_{10}\frac{\partial \varphi}{\partial \sigma} = 0 \text{ on } X = 0, b \tag{4.80}$$

where, $S_1 = \left[\frac{1}{e}\frac{2\sigma}{h^2}\left(\frac{\partial \zeta}{\partial X}\right)^2 - \frac{1}{e}\frac{\sigma}{h}\left(\frac{\partial^2 \zeta}{\partial X^2}\right)\right]$; $S_2 = \left[\frac{X(1+2(y+L)^2)}{e^2}\right]$;

$S_3 = \left[\frac{1}{e} + \left(\frac{X(y+L)}{e}\right)^2\right]$; $S_4 = \left[\frac{1}{e}\frac{\sigma^2}{h^2}\left(\frac{\partial \zeta}{\partial X}\right)^2 + \frac{1}{h^2}\right]$; $S_5 = \left(\left(\frac{2}{h}\frac{X(y+L)}{e}\right) - \frac{2}{e}\frac{\sigma}{h}\frac{\partial \zeta}{\partial X}\right)$;

$B_1 = \left[\frac{1}{e^2}\right]$; $B_3 = \left[-\frac{2}{e^2}\frac{\sigma}{h}\frac{\partial \zeta}{\partial X}\right]$; $B_4 = \left[\frac{\sigma}{h}\frac{\partial \zeta}{\partial T}\right]$; $B_5 = \left[\frac{X(y+L)}{e} - \frac{1}{e}\frac{\partial \zeta}{\partial x}\right]$;

$B_6 = \left[\frac{1}{e}\frac{\sigma}{h}\left(\frac{\partial \zeta}{\partial X}\right)^2 + \frac{1}{h}\right]$; $B_7 = \left[\frac{X(y+L)}{e}\right]$; $B_8 = \left[\frac{1}{h}\right]$; $B_9 = \left[\frac{X(y+L)}{e}\right]$; $B_{10} = \left[\frac{(y+L)}{h}\right]$

4.6 Finite Difference Discretization in the Computational Plane

In the current study, a finite difference scheme is used for the numerical study of the liquid sloshing. The computational domain is rectangular in shape for 2-D numerical simulations and cuboidal for 3-D numerical simulations. The governing equation and boundary conditions in the computational domain (Eqns. 4.33 to 4.40) are discretized using finite difference method. Adams-Bashforth scheme is utilized for the computation of nonlinear solutions. As Adams-Bashforth scheme requires results from previous time steps to calculate the current time step result, the semi-implicit scheme is used to generate results for the initial time steps.

4.6.1 Semi-Implicit Scheme at Top Boundary (Free Surface)

The semi implicit scheme is applied at the top boundary of the computational domain. As discussed, the top boundary consists of two conditions viz. kinematic condition and dynamic

condition. In computational domain, the kinematic condition (Eq. 4.38) is discretized by a forward scheme at $\eta = 1$ as follows

$$\left.\frac{\partial \zeta^*}{\partial \tau}\right|^n = L_4 C_3 \left.\frac{\partial \varphi}{\partial \eta}\right|^n - 4E_b \left.\frac{\partial \zeta}{\partial \xi}\right|^n \left.\frac{\partial \varphi}{\partial \xi}\right|^n , \tag{4.82}$$

where $$\left[\frac{\partial \zeta}{\partial T}\right]^n = \frac{\zeta^{n+1} - \zeta^n}{\Delta T} \tag{4.83}$$

At $\sigma = 1$, the dynamic condition (Eq. 4.39) is discretized as:

$$\left.\frac{\partial \varphi}{\partial \tau}\right|^n = C_3 L_5 \left.\frac{\partial \varphi}{\partial \eta}\right|^n - 2E_b \left[\left(\left.\frac{\partial \varphi}{\partial \xi}\right|^n - C_3 L_6 \left.\frac{\partial \varphi}{\partial \eta}\right|^n\right)^2 + \left(\frac{C_3}{h_*^2}\left.\frac{\partial \varphi}{\partial \eta}\right|^n\right)^2\right] - \left(1 + Y_\tau^*\right)\left.\zeta^*\right|^{n+1} \tag{4.84}$$

where $$\left[\frac{\partial \varphi}{\partial T}\right]^n = \frac{\varphi^{n+1} - \varphi^n}{\Delta T} . \tag{4.85}$$

The value of ζ^{n+1} is computed using Eq. 4.83 and is substituted in Eq. 4.84. Then, the new φ^{n+1} is found at the top boundary of the computational domain using Eq. 4.85. The first and second order derivatives in above equations are discretized by means of second order central difference scheme within the liquid domain, and second order forward and backward differences are employed at the boundaries.

4.6.2 Adams-Bashforth Scheme

The semi-implicit scheme is used to provide information at the first and second time steps, since the Adams-Bashforth is a multistep method. Euler and Runge-Kutta methods are single step methods, because they use only the information from the previous step. Adams methods are known as explicit schemes because current and previous time step values are used to obtain the values for future time steps. Here, three point Adams-Bashforth scheme as mentioned in Eqns. 4.86 and 4.87 has been used.

$$(\Delta\varphi)^{n+1} = \frac{\Delta t}{12}\left(23\varphi^n - 16\varphi^{n-1} + 5\varphi^{n-2}\right) \tag{4.86}$$

and $$(\varphi)^{n+1} = \varphi^n + (\Delta\varphi)^{n+1} + O(\Delta t^3) \tag{4.87}$$

The governing equation (Eq. 4.33) is discretized by the standard fourth order central difference approximation and is given by

$$\delta_\xi{}^2 = \frac{-\varphi_{i-2,j} + 16\varphi_{i-1,j} - 30\varphi_{i.j} + 16\varphi_{i+1,j} - \varphi_{i+2,j}}{12(\Delta\xi^2)} + O(\xi^4) \tag{4.88}$$

$$\delta_\xi \delta_\eta = \frac{1}{2\Delta\xi}\left(\frac{\varphi_{i+1,j+1}-\varphi_{i+1,j-1}}{2(\Delta\eta)} - \frac{\varphi_{i-1,j+1}-\varphi_{i-1,j-1}}{2(\Delta\eta)}\right) + O(\xi^2, \eta^2) \qquad (4.89)$$

where $\varphi(i, j)$ denotes $\varphi(\xi_i, \eta_j)$; $\delta_\xi, \delta_\xi{}^2$ and $\delta_\eta, \delta_\eta{}^2$ are the first and second order central difference operators along ξ and η directions respectively and $\delta_\xi \delta_\eta$ is the mixed second order central difference operator.

4.7 Summary

The mathematical formulations and followed by corresponding mapping procedure that maps the physical domain onto the computational domain for 2-D and 3-D domains are summarized elaborately in this chapter. A fully non-linear numerical model for idealized 2-D and 3-D sloshing waves in rectangular and cylindrical tanks has been developed. The asymmetric physical domain has been mapped onto a square computational domain using σ-transformation. The finite difference scheme has been used to solve the discretized governing equations in the transformed computational domain to obtain the free surface elevation time histories, phase plane diagram, spectrum analysis and free surface profiles in the physical domain.

Chapter 5

NUMERICAL INVESTIGATION OF LIQUID FREE SURFACE ELEVATION

In this chapter, results of numerical simulation of 2-D and 3-D nonlinear liquid sloshing problems in moving tanks are discussed. A fully non-linear model for idealized 2-D waves in a numerical wave tank has been developed. Section 5.2 discusses the credibility of the code by performing the grid independence study and validation tests. Liquid behavior in a rectangular tank under different regular wave excitations (viz., horizontal, vertical and combined conditions) is studied in section 5.3 to 5.6. Spectrum analysis of horizontally excited tank and the stable, unstable conditions of vertically excited and combined motions are also discussed. Section 5.7 presents the numerical results on regularly and randomly excited tank in vertical direction which is carried out for four different cases viz., 2-D tank with regular excitations, regularly excited 3-D tank with two different initial conditions for the liquid free surface, and finally 3-D tank with random excitation in the vertical direction. The wave elevation time history, phase plane diagram and surface plots are presented and discussed.

CONTENTS

5.1 Introductory Remark

The σ-transformation technique is used to capture the liquid free surface that maps the asymmetric liquid domain onto a rectangle, such that the moving free surface in the physical plane becomes a fixed line in the computational mapped domain. The computational governing equations and boundary conditions of liquid dynamics in the tank are discussed and derived in Chapter-4. In this work, the fourth order central difference scheme and the Gauss–Seidel point successive over-relaxation iterative procedure are used to capture the free surface wave profiles and free surface elevation plots of the fluid domain. The results are validated with benchmark results. An error estimation method is used to stop the iterative solver (used for solving the discretized governing equations in the computational domain) upon reaching the steady state of results at each time step. In the present case, this method is found to produce quite accurate results and is more time efficient as compared to other conventional stopping procedures for iterative solvers.

5.2 Establishing the Credibility of the Code

In an iterative method, it is important to estimate the iteration error in order to decide when to stop iterating. An accurate error measurement helps to improve the performance of the numerical code. Moreover, the grid independent test, time independent test and validation test with benchmark results play a vital role to show the credibility of the code. The following sections discuss the above tests.

5.2.1 Convergence Criteria Used for the Iterative Solver

It can be seen that the numerical algorithm requires solving a linear equation $A\phi = B$ in the fluid domain at every time step. To solve this equation, various methods are available. However, the iterative methods have been chosen for this work to find the solution for the velocity potential ϕ at every time step since these are known to have the advantages of lesser discretization error and better speed of computation as compared to other direct methods. The successive over relaxation method has been chosen to solve the linear equation. Using an iterative solver, it is very important to stop the iterations at the right time i.e., when the

iteration error has decreased by an acceptable amount. Iteration errors (Ferziger and Peric, 2002) can be calculated as,

$$\delta^n = \phi^{n+1} - \phi^n \approx (\lambda_1 - 1)(\lambda)^n a_1 \psi_1 \tag{5.1}$$

where δ^n is the difference between solutions at iterations *n+1* and *n*, and λ_1 is the spectral radius or the largest eigen value of the iteration matrix. It can be estimated from Eq. 5.2.

$$\lambda_1 \approx \frac{\|\delta^n\|}{\|\delta^{n-1}\|}, \tag{5.2}$$

where $\|a\|$ represents the norm (here, chosen as root mean square) of *a*. After obtaining an estimate of the largest eigen value (λ_1), the iteration error can be approximated from the Eq. 5.3. Hence a good estimate of error is available.

$$\|\varepsilon^n\| = \phi - \phi^n \approx \frac{\|\delta^n\|}{\lambda_1 - 1}. \tag{5.3}$$

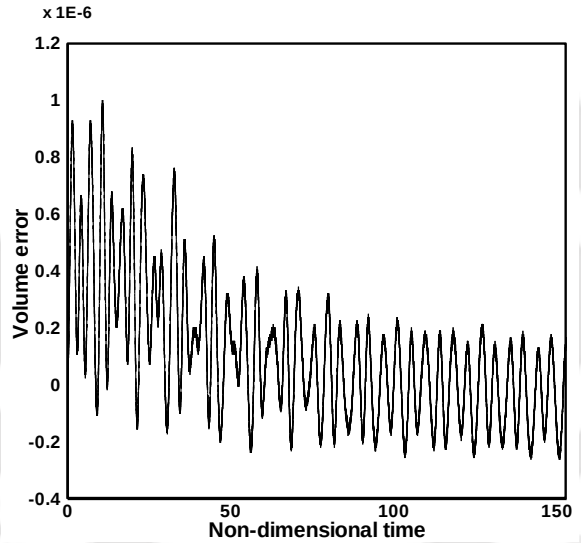

Figure 5.1: Volume error for the 2-D numerical simulation *(*for *n =1*; $\Omega_v = \frac{\omega_v}{\omega}$ =1.253; K_v =0.4; E_b = 0.0033 and K_x= 0.015*)* versus non-dimensional time ($t \times \omega$).

The above given procedure produces pretty accurate results. The volume errors for all the cases studied are found to be within the range of $\left[-10^{-6}, 10^{6}\right]$ as shown in Figure 5.1. This procedure is better than the difference procedure used to stop the iterative solver (where the iterations are stopped when the difference between two successive iterations falls below a predefined tolerance limit) since the difference between two successive iterations falling below a particular limit does not ensure that the error of the iteration has also fallen down by

the same order. Another widely used criterion for stopping is the residual stopping criterion, where the iterative solver is stopped when the residual norm falls below a preset fraction (tolerance limit) of its initial value. The residual and error are related as

$$A\varepsilon_n = \rho_n \tag{5.4}$$

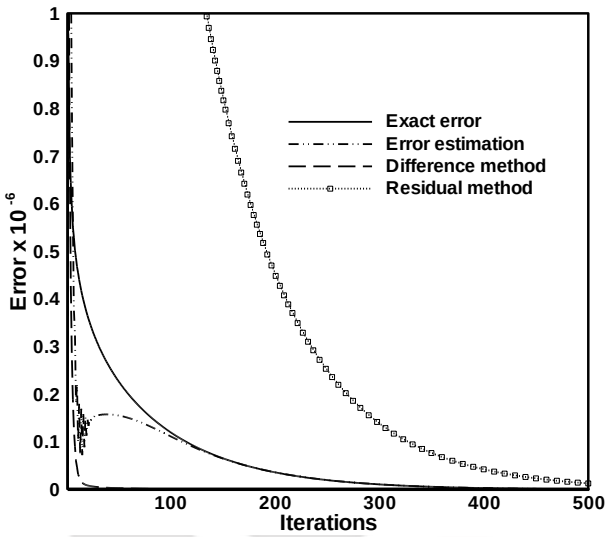

Figure 5.2: Variation of the norm of the exact, estimated, residual and difference methods error plot for 2-D tank with 41 × 81 grid.

where A represents the iteration matrix, ε_n represents the error norm and ρ_n represents the residual norm at any particular iteration n. As seen from Eq. (5.4), the residual is A times the error, and thus, the reduction of the residual norm below the tolerance limit does not ensure that the error norm had also fallen below the same tolerance limit. Hence, proper evaluation of error at each iteration is essential to ensure the accuracy of solution. For the case of 2-D vertical regular excitations in a rectangular tank, a comparison is done for the various iterative solver stopping criteria as shown in Figure 5.2. For iterations at the first time step, the variation of norm of the exact error, estimated error with the above procedure, residual and difference between two successive iterations is plotted against the iterations. It can be noted that the difference norm falls well below 0.1×10^{-5} by 50 iterations whereas the exact error is still above 0.2×10^{-5}. Hence this stopping criterion is not suited for the present case. Looking at the residual norm, it is seen that it has a quite higher value than the exact error for all iterations. Estimated error is noticed to be nearly the same as the exact error in this case (except for the initial iterations where it shows slight oscillations). Using residual stopping criterion ensures that the exact error has fallen well below the tolerance limit but it results in higher computational time for the solver without achieving higher accuracy than the estimated error stopping criterion. Comparisons made for later time steps also show a similar

behavior of the norms of the stopping criteria with iterations. Hence, the error estimation stopping criteria for the successive over relaxation (SOR) solver is most suited for the current problem.

5.3 Results and Discussion for 2-D Rectangular Domain

In this section, the initial wave profile is considered as $\zeta(x,t)\big|_{\tau=0} = A\cos(K_n x)$ and $\varphi(\xi,\eta)\big|_{\tau=0} = 0$, where A is the initial wave amplitude, K_n is the wave number $\left(=\frac{n\pi}{b}\right)$ for n^{th} mode number (n = 0, 1, 2, …..) and x is the distance in the horizontal direction. The initial wave steepness is defined for fixed tank studies as $E = A\omega_n^{\,2}/g$, where gravity field g is usually considered as 9.81 m/s^2. Here, the ratio of h_s to b is considered as 1:2. The linear natural sloshing frequencies in the 2-D rectangular tank are expressed by

$$\omega_n = \sqrt{K_n g \tanh(K_n h_s)}, \qquad n=1, 2, 3\ldots \tag{5.5}$$

Now X_D'' and Y_D'' are switched off for fixed tank condition in dynamic boundary condition. Two quantities are usually kept in mind in the sloshing studies: the amplitude of the wave and the excitation frequency. The amplitude is measured by the wave steepness. The relation between the acceleration and wave steepness is discussed above.

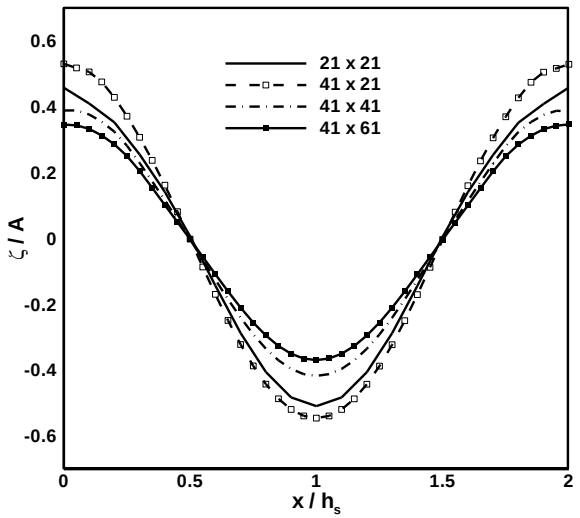

Figure 5.3: Grid independence study for E=0.033 at time 7.5 sec.

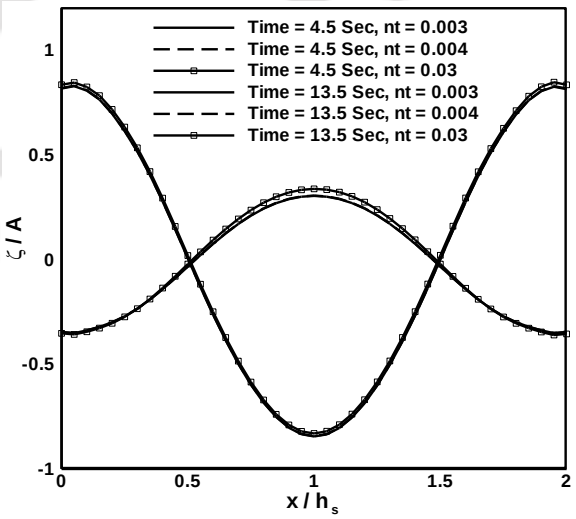

Figure 5.4: Time independence study for E=0.033 and grid size 41×61.

5.3.1 Independence Study

In order to display that the solution is grid and time independent, simulations have been performed using different number of grid nodes and different values of Δt as shown in Figures 5.3 and 5.4. The wave profiles along the tank at three different times for the first sloshing mode (n=2) are plotted. Results for different grid resolutions are shown related to moderate a wave amplitude (E=0.0338) for time steps of $\Delta t = 0.003$ sec. Figure 5.3 shows the free surface elevation of liquid at tank left wall for different grid size of 21×21, 41×21, 41×41 and 41×61. Initially, the grid size is increased in the horizontal direction from 21 to 41. As it is a fixed boundary, it is found that there is not much variation on horizontal direction and then the grid points are increased from 21 to 41 and 61 in vertical direction. Increasing the grid points in the vertical direction is found to be more effective in terms of improving the accuracy than increasing the grid points in the horizontal direction since it has the moving boundary at top. It has been found that grid size of 41×61 and 41×41 and time step of 0.003 sec and 0.004 sec provide sufficient accuracy to capture nonlinearities related to steep wave predictions (E > 0.02). There is not much variation in vertical direction above the grid size of 41×41 for moderate wave steepness, and therefore, the grid size of 41×41 is sufficient for this problem. The time independence study is performed (Figure 5.4) for three different time steps at E=0.033 and grid size 41×61.

5.3.2 Effect of Wave Steepness in Fixed Tank

The wave characteristics include a crest at the top and a trough at the bottom. The difference in elevation between the crests and trough is the wave height. The distance between the adjacent crests or the troughs of wave is termed the wavelength. The ratio of wave height to wavelength is the wave's steepness. While increasing the wave steepness the non-linearity increases. The free surface elevations at the left wall, in the middle and at the right wall of the tank are shown in Figures 5.5 (a) and 5.5 (c). When wave steepness increases, the considerable changes have been observed in the free surface wave profile. On the other hand, the wave phase plane diagrams are shown in Figures 5.5 (b) and (d). These profiles are a repeatable pattern which is observed at left wall of the tank. The wave phase plane diagram for low steepness is almost a perfect circle as seen from Figure 5.5 (b). But at the same time, increasing the steepness makes the phase plane diagram to become oval as depicted in 5.5 (d).

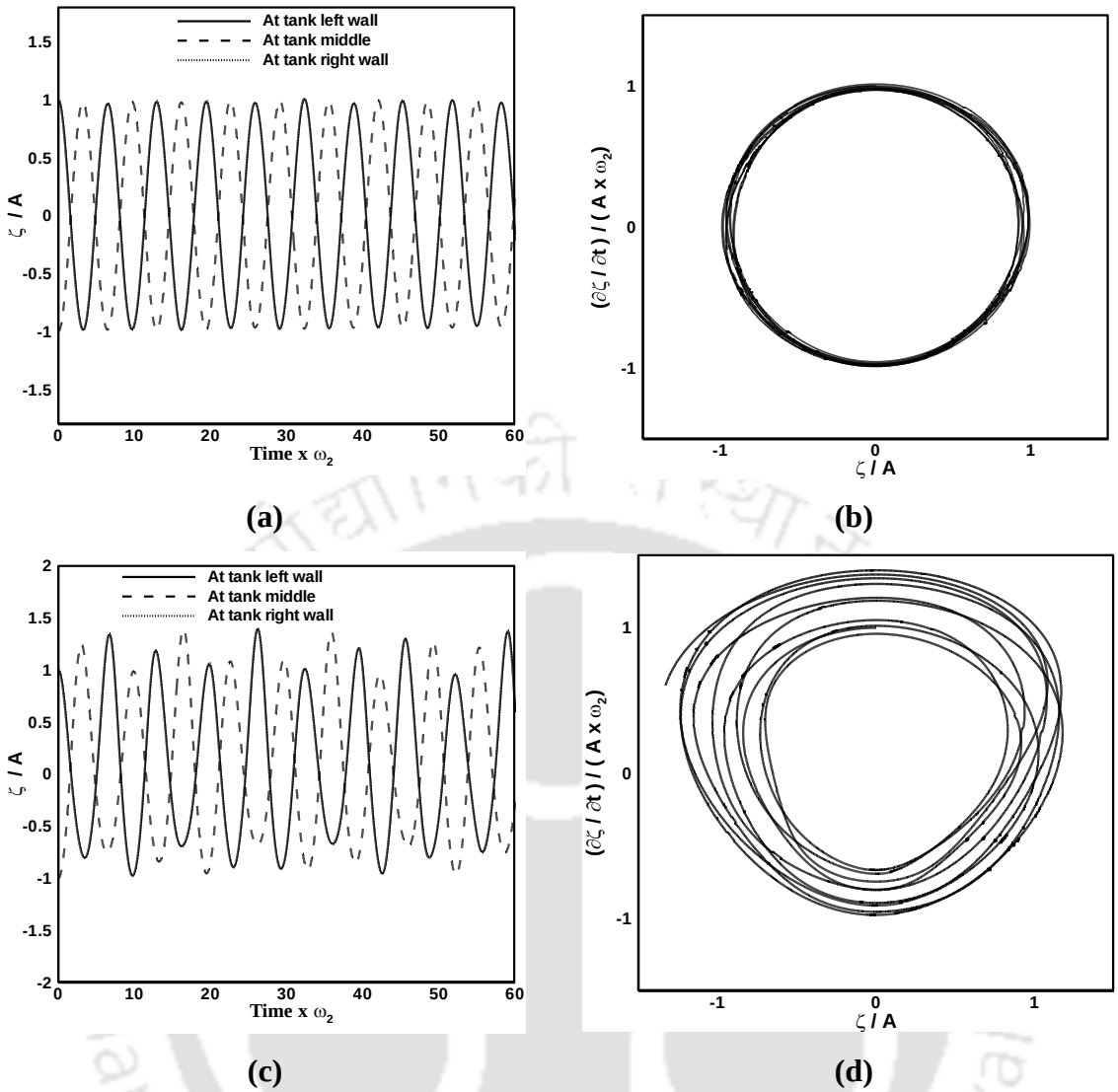

Figure 5.5: Fixed tank elevation and phase plane diagram for n=2 with grid size 41×41 and $\Delta t = 0.003$ sec (a) - (b) E = 0.0338; (c) - (d) E = 0.338.

5.3.3 Effect of Vertical Forcing Parameter K_v

In the vertically excited tank test cases, the parameter $K_v = a_v\omega_v^2/g$ is a measure of importance of the vertical forcing motion, where a_v is the vertical forcing amplitude and ω_v is the angular frequency of forced vertical motion. The effect of K_v on free surface elevation on left wall of the tank has been studied for combined excitation tank as shown in Figure 5.6. While increasing the K_v, the wave elevation decreases. But at the same time, the nonlinearity of the wave also changes drastically. Figures 5.7 and 5.8 show the nonlinearity of the waves for K_v = 0.2 and K_v = 0.9. In this thesis work, moderate K_v values are used to maintain the wave amplitude and nonlinearity of the liquid free surface. The effects of ω_v/ω will be examined later.

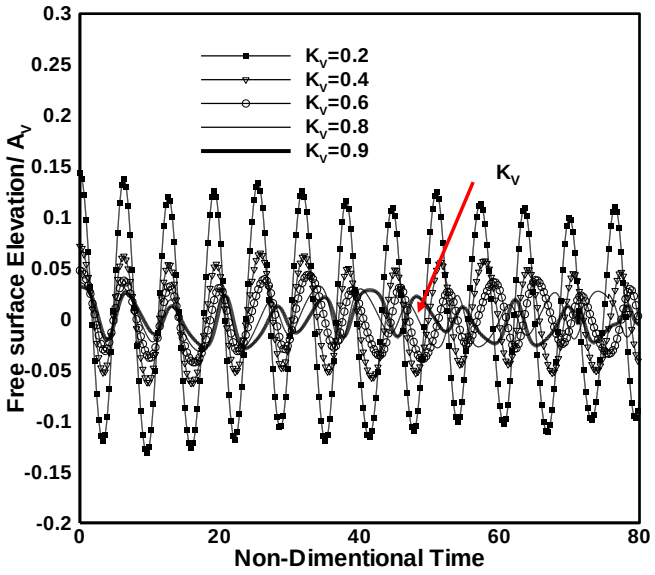

Figure 5.6 Effect of vertical forcing parameter K_v on free surface elevation.

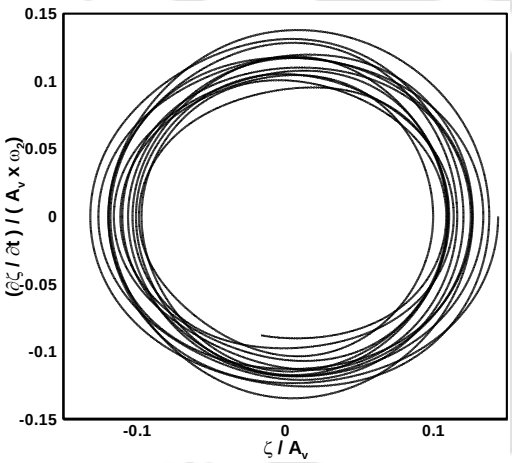

Figure 5.7: Phase-plane diagram for K_v = 0.2

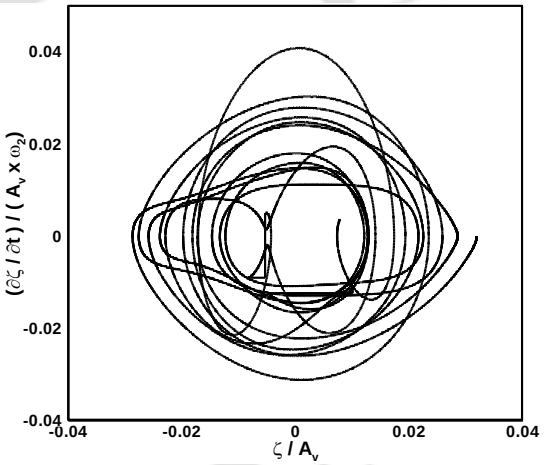

Figure 5.8: Phase-plane diagram for K_v= 0.9

5.3.4 Horizontally Excited Tanks

For the horizontally excited tank condition, Y_D'' is switched off from the dynamic boundary condition at top wall. The horizontal excited acceleration is fixed as $X_D'' = (-\omega_h A_h \cos(\omega_h t))$. When the external horizontal forcing frequency is equal to the natural sloshing frequency of the liquid, the resonance will occur. In this section, the free surface motions are numerically examined off and at resonance conditions. The initial wave profile is considered as $\varphi(\xi,\eta)\big|_{\tau=0} = 0$. The initial wave impulse is considered as $\zeta(x,t)\big|_{\tau=0} = A\cos(K_n x)$ and zero impulse condition is $\zeta(x,t)\big|_{\tau=0} = 0$. The measure of nonlinearity parameter, K_h is which is

calculated from $K_h = \frac{A_h \omega_h^2}{g}$, where A_h is the excitation amplitude. The sloshing motion is more violent at the natural frequency of the tank when the excitation frequency is equal to the first mode rather than at the third mode, which is a well-known resonance phenomenon.

5.3.4.1 Off and at Resonance of Horizontally Excited Tanks

The horizontal frequency ratio $\Omega_x \left(= \frac{\omega_h}{\omega_n} \right)$ is speckled as 0.7, 0.9 and 1.3 for off-resonance and 1 for at resonance conditions. In order to validate the developed model, the present data have been compared with the results of Frandsen (2004). The results have been found to be in good agreement as seen from Figure 5.9 (a). While increasing the excitation frequency, some interesting free surface elevation shapes are observed (Figures 5.9 (a), 5.9 (c), 5.10 (a) and 5.11 (a)). The elevation of standing waves is observed near the left wall of the tank for different frequency ratios. When the frequency ratio Ω_x is small, the elevation also tends to be small. While increasing the frequency ratio, the wave elevation also increases gradually as shown in Figure 5.9 (a) and when Ω_x value comes around 0.8 to 0.9, the elevation pattern differs completely which has cunning points at certain intervals.

After reaching the Ω_x=0.99, the free surface elevation are growing continuously with constant increments (Figure 5.10). It is because at this point, the excitation frequency matches very close to the system natural frequency. From Figure 5.10 (a), one can observe that the free surface elevation is 36 times greater as compared to the amplitude of excitation approximately at non-dimensional time 80. In Figure 5.10 (a), free surface elevation is shown with two initial conditions viz., zero impulse and initial impulse. After few seconds, both the results match very closely. It is observed that the initial impulse has not undergone much variation from the original behavior of the liquid wave profiles during sloshing. However, at low frequencies, one can expect very small deviations between the initial impulse and the zero impulse. Finally, the frequency ratio was increased to Ω_x = 1.3, whereby the free surface elevation drastically reduces to 3.4 times (from 36 times at resonance frequency) to the excitation amplitude approximately at non-dimensional time 80. Figures 5.9 (b), 5.9 (d), 5.10 (b) and 5.11 (b) show the phase plane diagram for their respective frequencies. In Figure 5.10 (b), the phase plane diagram is moving in a circular path and finally it attains the spiral shape, since it is drawn at the resonance condition.

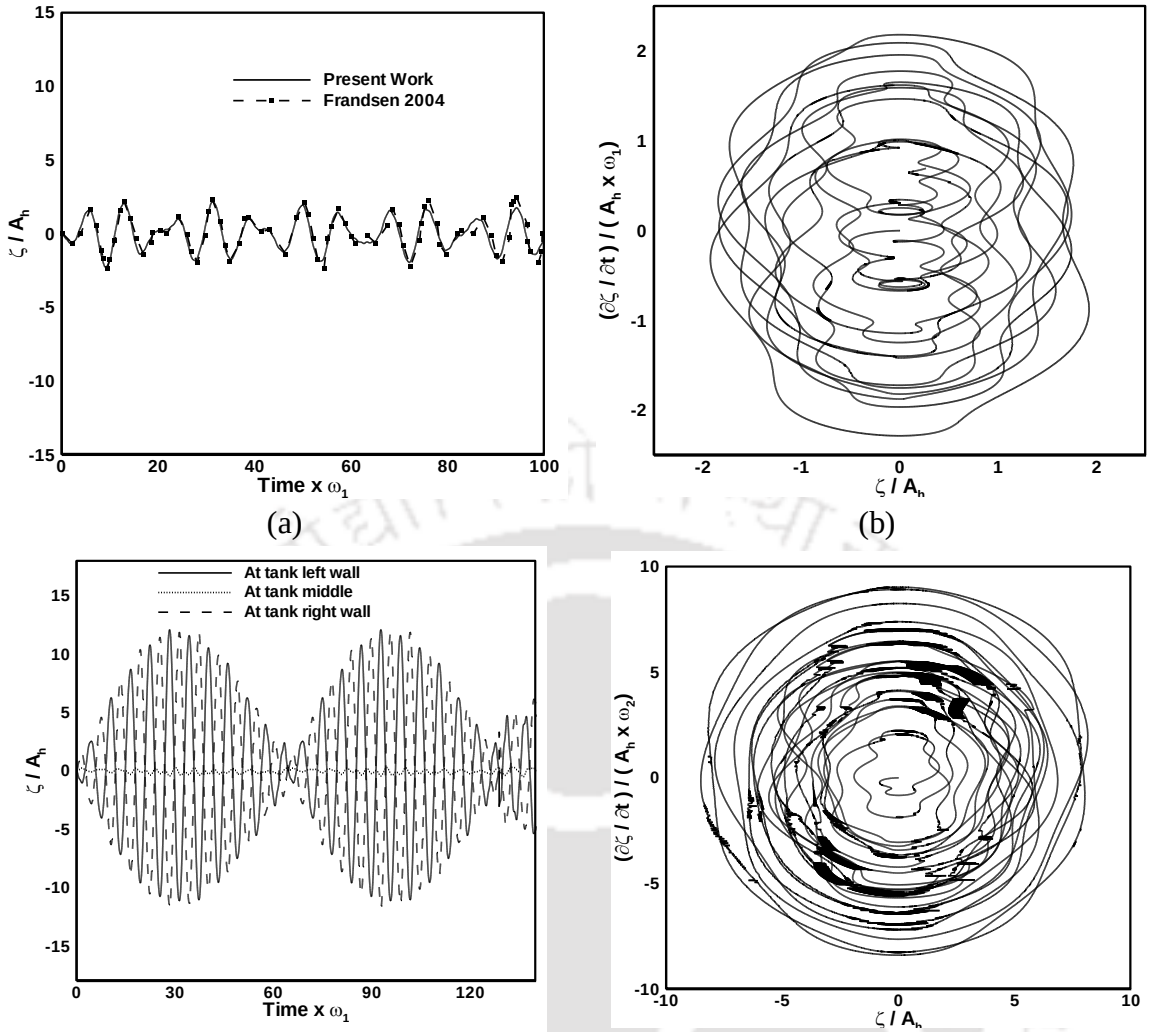

Figure 5.9: Off-resonance horizontal excited tank elevation and phase plane diagram for n=1 with grid size 41×61 K_h=0.0034 and $\Delta t = 0.003$ sec: (a) - (b) $\Omega_x = 0.7$ and (c) - (d) $\Omega_x = 0.9$.

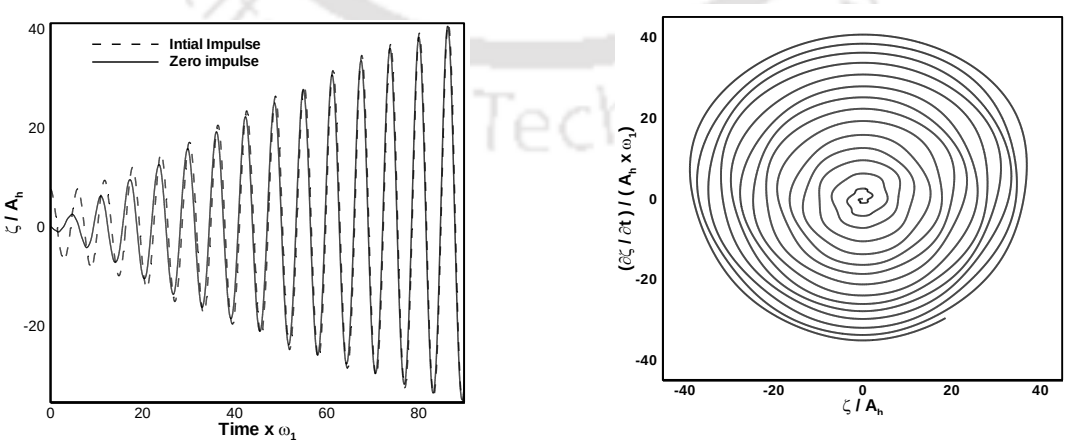

Figure 5.10: At resonance conditions horizontal excited tank elevation and phase plane diagram for n=1 with grid size 41×61 K_h=0.0034 and $\Delta t = 0.003$ sec.

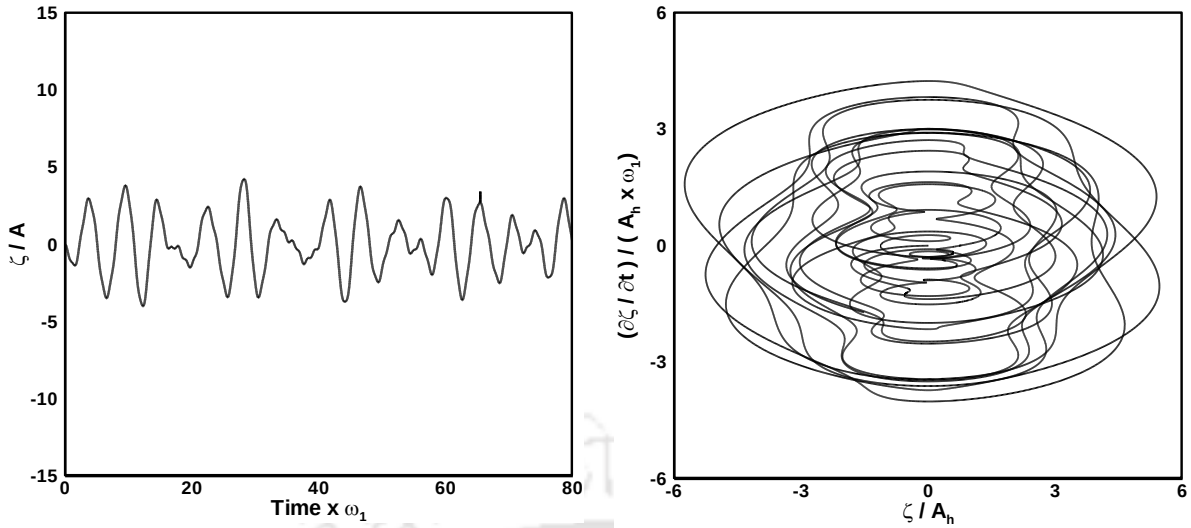

(a) (b)

Figure 5.11: Off-resonance horizontal excited tank elevation and phase plane diagram for n=1 with grid size 41×61, K_h=0.0034 and $\Delta t = 0.003$ sec $\Omega_x = 1.3$.

5.3.4.2 Spectrum Analysis for Horizontally Excited Tanks

The Fast Fourier Transform (FFT) is extremely important in the area of frequency (spectrum) analysis because it takes a discrete signal in the time domain and transforms that signal into its discrete frequency domain representation. The FFT does not directly give the spectrum of a signal. The shift is required for visualizing the Fourier transform with the zero-frequency component in the middle of the spectrum.

The spectra of a wave elevation is computed by the Fast Fourier Transform (FFT), which is given by

$$X(K) = \sum_{j=1}^{N} x(j)\omega_N^{(j-1)(k-1)}, \tag{5.6}$$

where $\omega_n = e^{(-2\pi i)} / N$ is the N^{th} root of unity. In order to avoid the effect of discontinuity at the boundary, the hamming window is given by

$$\omega(n) = 0.54 - 0.46\cos\left(2\pi\frac{n}{N}\right), 0 \le n \le N \tag{5.7}$$

Figure 5.12 shows the spectra of wave elevations at the tank left corner. It also caused peaks in the power spectra to become bigger and more peaks appear at different frequencies. Figure 5.12 (a) shows that the maximum spectral peak occurs at the excitation frequency when the

excitation frequency is less than the first natural frequency and a secondary peak occurs at the tank natural frequency. While frequency ratio Ω_x approaches 0.9, the partial merging of first mode frequency and the excitation frequency slightly increase the energy of the signal as shown in Figure 5.12 (b). In Figure 5.12 (c), a single peak of the dimensionless sloshing energy is observed at frequency ratio of 1, which is irrespective of the magnitude of the excitation frequency. At the first modal frequency, the response component is observed to increase as the frequency increases. When the excitation frequency is greater than ω_1, the domination of the first mode reduces with an increase in the frequency ratio. When the excitation frequency is greater than the first mode (Figure 5.12d), the sloshing dominates at the first modal frequency up to second mode ($\omega_2 = 1.5\omega_1$) and till this frequency, the secondary peak is observed at the excitation frequency as can be seen in Figure 5.12 (d).

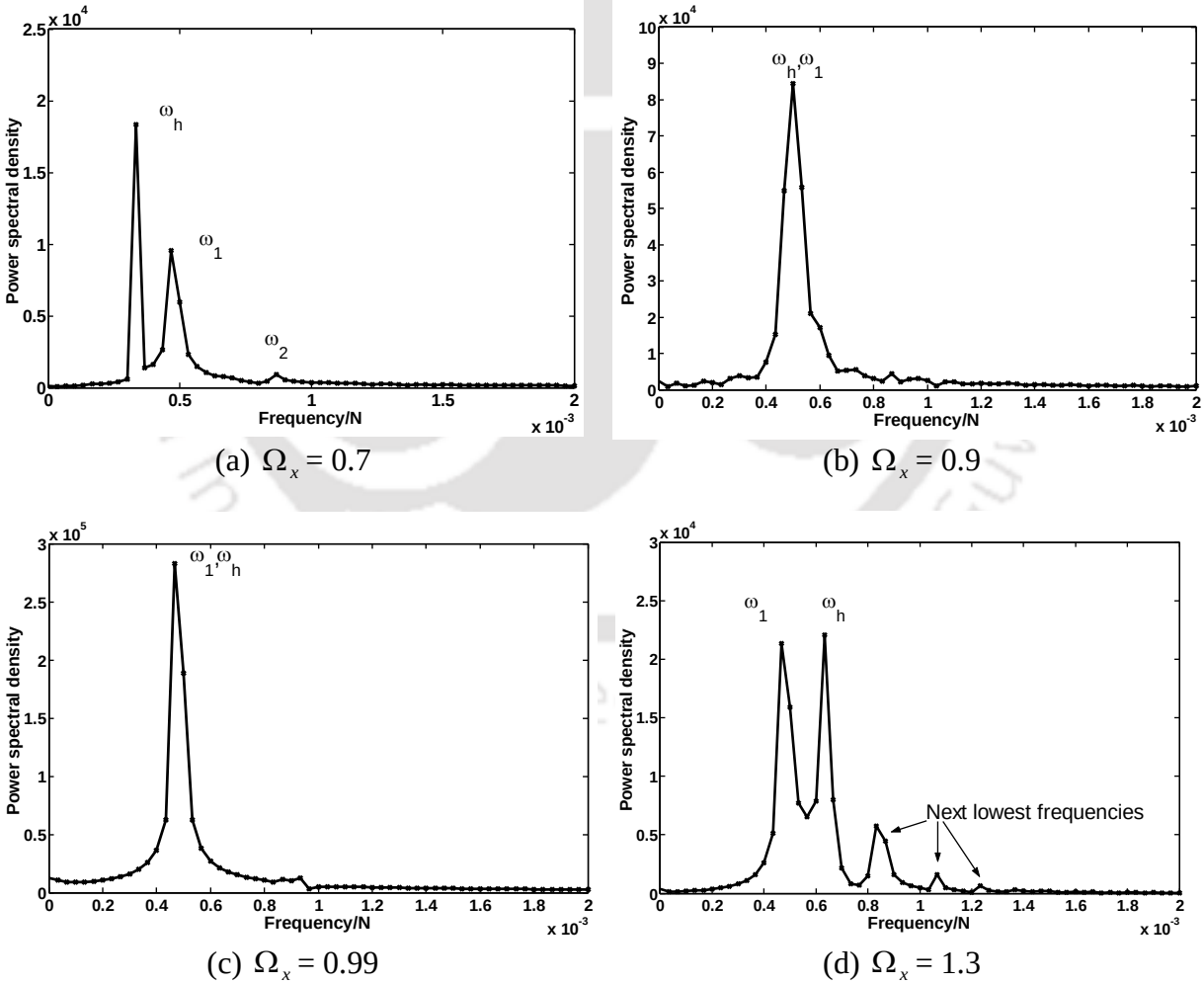

Figure 5.12: Spectrum analysis for horizontal excited tank off and at resonance frequencies for n=1 with grid size 41×61, K_h=0.0034 and $\Delta t = 0.003$ sec.

5.3.5 Vertically Excited Tanks

The initial conditions for a vertically excited tank are same as the sloshing motion simulation of the fixed tank. It is difficult to simulate sloshing only with vertical excitation by experiments. In order to have an initial perturbation in the free surface inside the tank, horizontal motions need to be excited before the vertical excitation. To avoid this situation, the initial standing wave profile is assumed for this work. Initial wave impulse is required for vertically excited condition and it is considered here as $\zeta(x,t)\big|_{\tau=0} = A\cos(K_n x)$. The vertical acceleration of tank is given by $Y_D'' = (-\omega_v A_v \cos(\omega_v t))$, where A_v is the vertical forcing amplitude, t is the time, ω_v is the angular frequency of forced vertical motion. The horizontally excited tank acceleration term X_D'' is switched off from the dynamic boundary condition at top wall for this analysis. The initial velocity potential in the fluid domain is considered as $\varphi(\xi,\eta)\big|_{\tau=0} = 0$.

The waves generated by the vertical excitation are called Faraday waves as explored originally by Faraday (1831) through his experiments. Faraday waves are the resonant waves when the excitation frequency is twice the natural frequency for some initial perturbation in the tank. This resonance condition is called parametric resonance. The study dealing with vertical excitation of liquids in a tank is referred to as parametric sloshing. For the vertically excited tank, the parameter $K_v = A_v\omega_v^{\,2}/g$ is a measure of the importance of the vertical forcing motion and E is the measure of nonlinearity. Frandsen (2004) plotted the instability map between $\Omega_v = \omega_n/\omega_v$ and k_v and discussed results from stability and instability regions. As per Floquet theorem, in order to investigate the stability of a fixed point, one has to linearize the equation of motion around a fixed point. This equation is known as Mathieu equation. If any of the pairs of the parameters lie in the instability region, then the corresponding mode grows exponentially with time. In this section, the profiles are given with stability and instability region. Figures 5.13 (a) and (b) show behavior of the liquid free surface and phase plane diagrams respectively from the stability region (Ω_v = 1.38 and K_v = 0.4). The results of unstable regions from Ω_v = 1 and K_v = 0.4 for elevation and phase plane are plotted in Figures 5.13 (c) and (d).

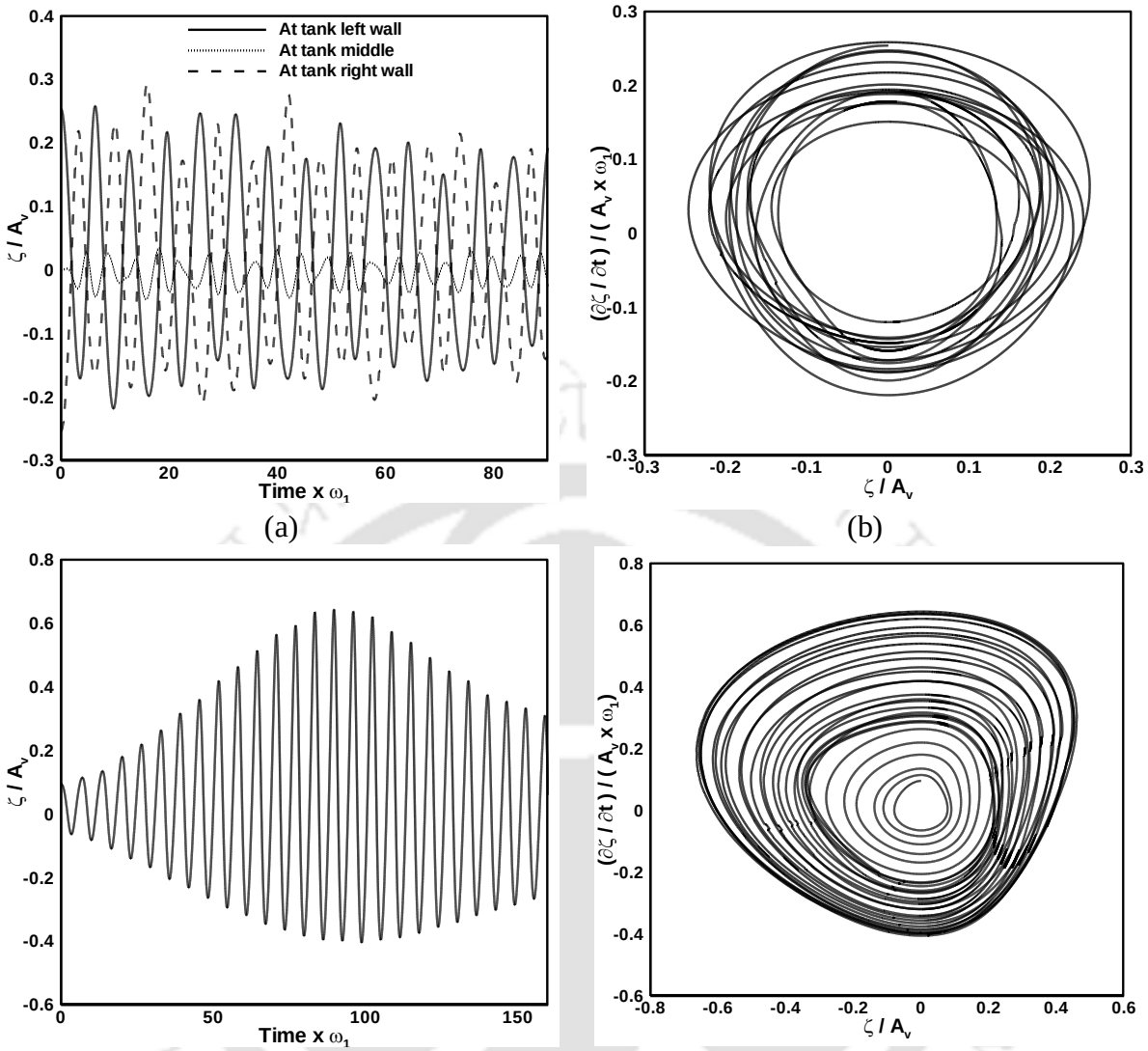

Figure 5.13: Stable and unstable regions from vertically excited tank elevation and phase plane diagram for n=1 with grid size 41×61 and $\Delta t = 0.003$ sec: (a) - (b) Stable solution at $\Omega_v = 1.38$ and $K_v = 0.4$; (c) - (d) Unstable region at $\Omega_v = 1$ and $K_v = 0.4$.

5.3.6 Tanks under Combined Excitation (Sway and Surge Motions)

The combined motion of horizontal and vertical excitation is discussed in this section. The vertical excited tank can be used for an ideal earthquake. The combined motions of horizontal and vertical excitations are two major considerable motions during earthquake. The water waves at resonance may create the impact pressure rise inside the tanks. When the liquid is striking on the wall, the impact pressure which might have been raised near the critical pressure range of the tank material will cause the structural damage in the tanks. The violent sloshing of combined excitation creates localized high impact loads on the tank roof and walls which may damage the tank. During the combined excitation of tank, the flow behavior

becomes tumultuous which creates the intricate free surface shapes during this type of excitation. Due to the vertical excitation being present with this combined motion, the instability regions exist as discussed in section 5.3.5.

The initial wave impulse is required for vertically excited condition and it is considered here as $\zeta(x,t)\big|_{\tau=0} = A\cos(K_n x)$. The vertical acceleration of tank is $Y_D'' = (-\omega_v A_v \cos(\omega_v t))$ and the horizontal excited acceleration is fixed as $X_D'' = (-\omega_h A_h \cos(\omega_h t))$. The initial velocity potential in the fluid domain is considered as $\varphi(\xi,\eta)\big|_{\tau=0} = 0$. The stable and unstable regions from horizontally and vertically excited tank elevation and phase plane diagram are presented Figure 5.14 (a) through (d).

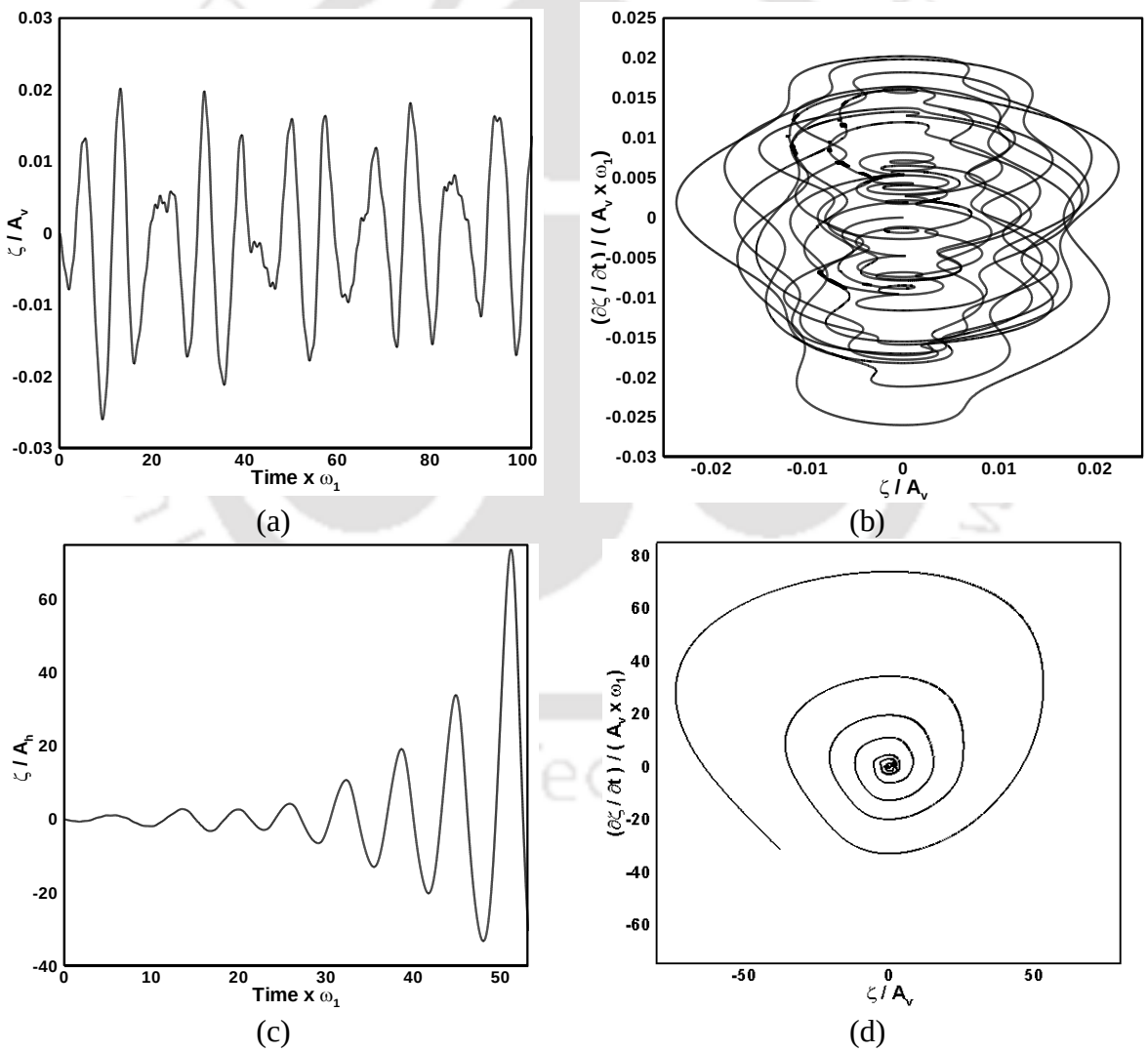

Figure 5.14: Stable and unstable regions from horizontally and vertically excited tank elevation and phase plane diagram for n=1 with grid size 41×61 and $\Delta t = 0.003$ sec: (a) - (b) Stable solution at $\Omega_v = 1.38$, Ω_x =0.7 and $K_v = 0.4$; (c) - (d) Unstable region at $\Omega_v = 0.5$, Ω_x =0.7 and $K_v = 0.4$.

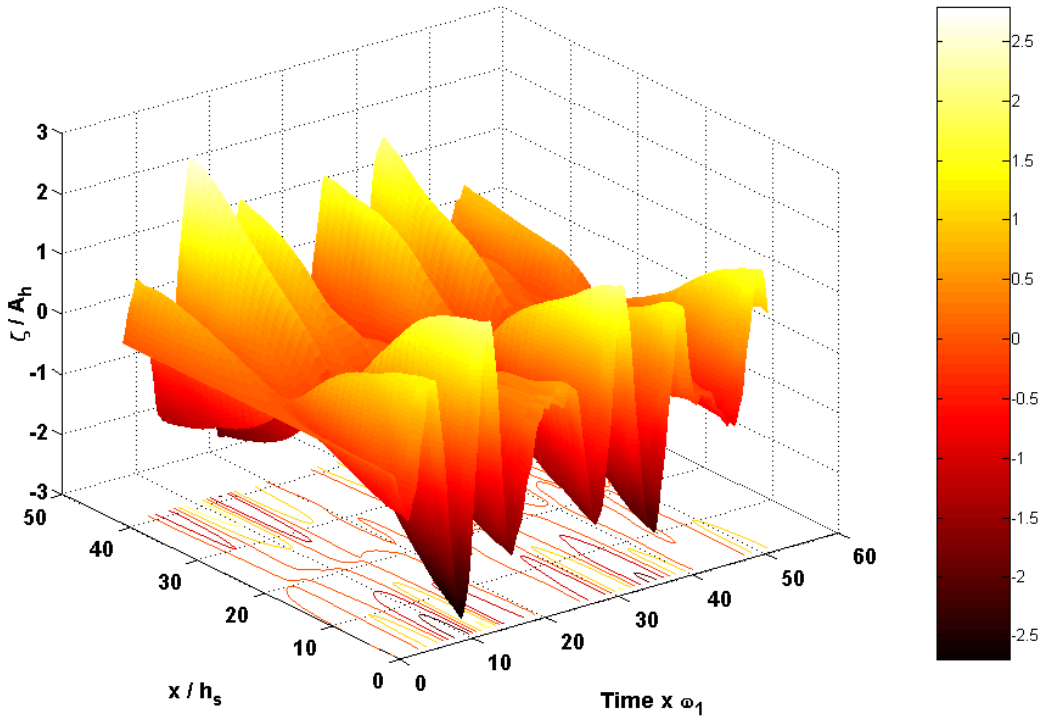

(a)

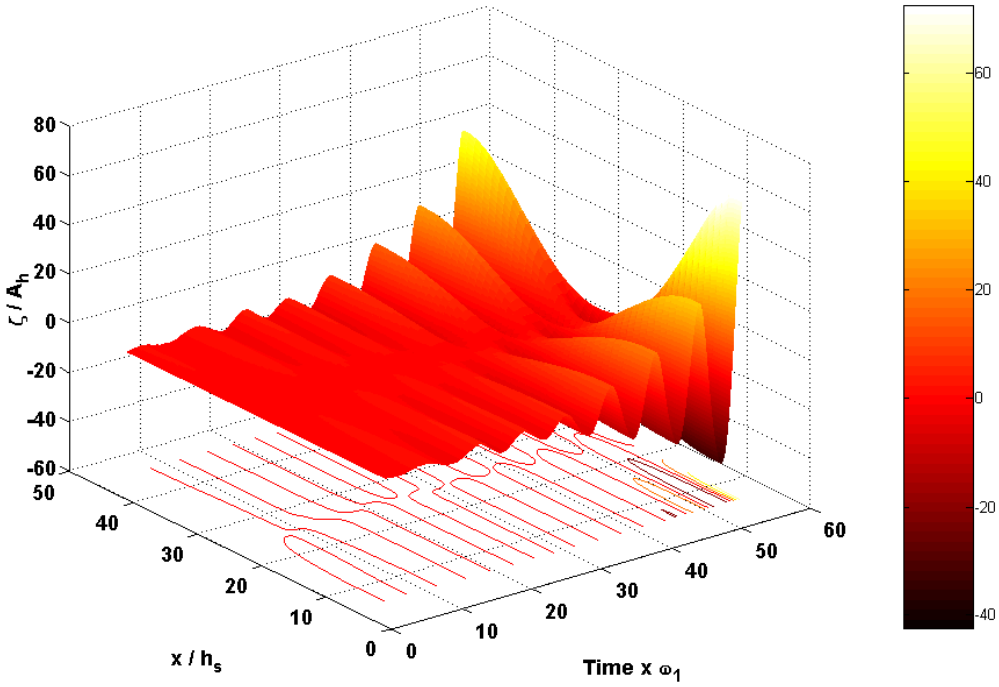

(b)

Figure 5.15: Stable and unstable regions from horizontally and vertically excited tank surface plot for n=1 with grid size 41×61 and $\Delta t = 0.003$ sec at Ω_x =0.7: (a) Stable region Ω_v = 1.38 and K_v = 0.4; (b) Unstable region Ω_v = 0.5 and K_v = 0.4.

Figure 5.14 (a) and (b) are stable solutions from n=1 with grid size 41×61, $\Delta t = 0.003$ sec, Ω_v = 1.38, Ω_x =0.7 and K_v = 0.4 while Figure 5.14 (c) and (d) are from unstable region at n=1 with grid size 41×61, $\Delta t = 0.003$ sec, Ω_v = 0.5, Ω_x =0.7 and K_v = 0.4. As discussed, if any of the pairs of the parameters lie in the instability region, then the corresponding mode grows exponentially with time as shown in Figure 5.14 (c) and (d).

The stable and unstable region surface plots are shown in Figure 5.15 (a) and (b). The surface plot is drawn between time and tank width and free surface elevation which is showed in Figure 5.15 (a) from the stable region (n=1 with grid size 41 × 61, $\Delta t = 0.003$ sec, Ω_v = 1.38, Ω_x =0.7 and K_v = 0.4) and 5.15(b) from unstable region (n=1 with grid size 41 × 61, $\Delta t = 0.003$ sec, Ω_v = 0.5, Ω_x =0.7 and K_v = 0.4). Figure 5.16 shows the free surface elevation from time 2.1 sec to 5.4 sec with the time interval of 0.3 seconds. The free surface elevation along the tank width is illustrated here. It is observed that the waves are moving up and down, and it must not be a uniform wave as observed in a fixed tank. One can easily find the considerable variation due to the combined excitation.

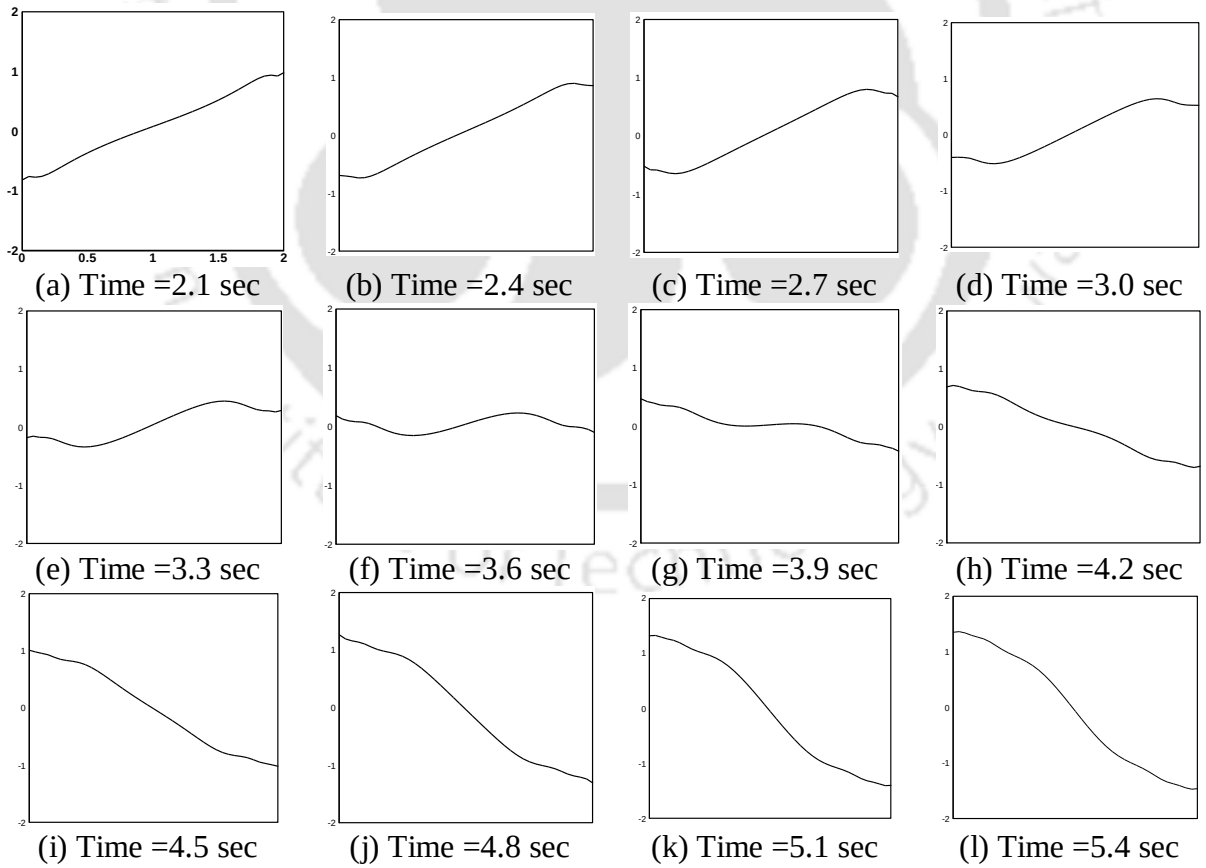

Figure 5.16: Free surface profile diagram for horizontally and vertically excited tank n=1 with grid size 41×61, $\Delta t = 0.003$ sec, Ω_v = 1.38, Ω_x =0.7 and K_v = 0.4.

5.3.6.1 Velocity Vector and Streamline Diagram

Since the viscous effect is neglected in the analysis, the velocity switching is much smoother. However as discussed by Chen and Nokes (2005), the viscous effect creates a clear vortex during the transition period and the vortex does not disappear until the free surface becomes flat. Figure 5.17 and 5.18 show the velocity vector and streamline diagrams at t^* = 38.5 for two different excitation frequencies. Wave peak has a positive gradient for non-dimensional time just before t^* = 38.5 and then exactly at t^*=38.5, the free surface elevation at the right wall reaches its peak with almost zero fluid velocity. After t^* = 38.5 , the direction of the fluid velocity switches from right to left and the magnitudes of these velocities continue to increase until they reach their maximum peak at left wall.

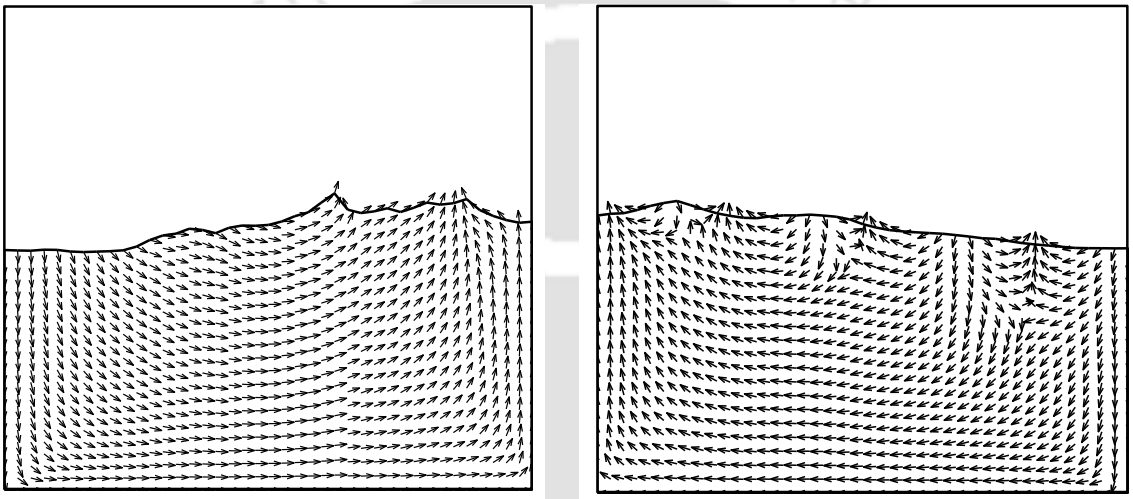

(a) (b)

Figure 5.17: Velocity vector plot for horizontally and vertically excited tank at non-dimensional time =38.5, n=1 with grid size 41×61 and $\Delta t = 0.003$ sec at Ω_v = 1.38 and K_v = 0.4: (a) Ω_x =0.7; (b) Ω_x =1.

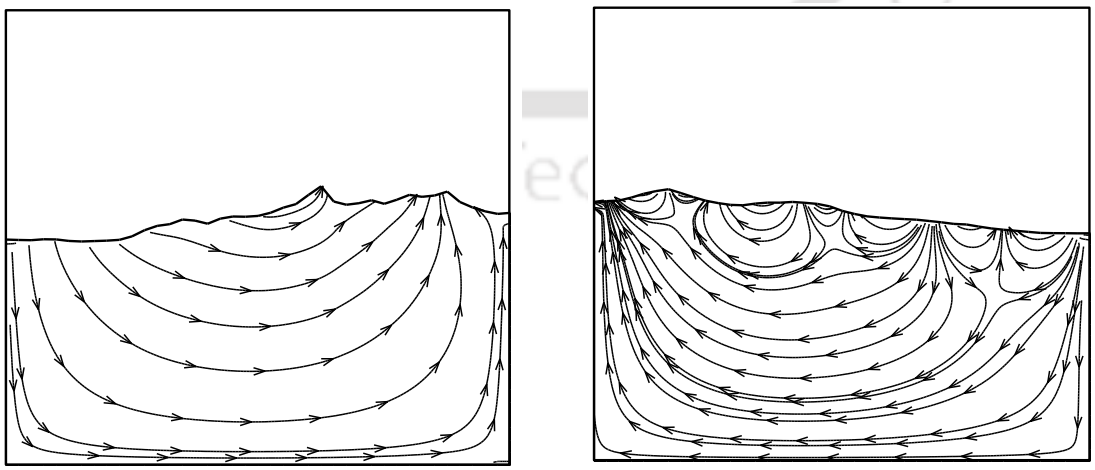

(a) (b)

Figure 5.18: Velocity vector plot for horizontally and vertically excited tank at non-dimensional time =38.5, n=1 with grid size 41×61 and $\Delta t = 0.003$ sec at Ω_v = 1.38 and K_v = 0.4: (a) Ω_x =0.7; (b) Ω_x =1.

5.3.7 Summary of Results for the 2-D Rectangular Tank

The section 5.3 dealt with the non-linear effects of standing wave motion of liquid in a 2-D rectangular tank. Results of liquid sloshing induced by horizontal, vertical and combined (horizontal and vertical) base excitations have been presented for small to steep non breaking waves. Simulations are limited to water fill ratio (h_s/b) of 0.5. A good agreement between our numerical model and previously published result has been obtained for low steeping waves. The numerical wave tank captured steep waves generated by horizontal, vertical and combined forcing amplitudes. The horizontally excited tank free surface elevation and phase plane diagram is discussed with off and at resonance frequencies. Behaviors show the effect of wave excitation while matching with resonance frequency. The spectrum analysis of horizontally excited tank is also presented. The vertical and excitation causes the instability associated with parametric resonance of the combined motion for a certain set of frequencies and amplitude of the vertical motion. The initial condition for the surface elevation is an important parameter as there should be some initial perturbation in the system for the generation of waves due to vertical excitation. These conditions were also applied to combined excitation. Early simulations of the liquid sloshing problem have mostly been performed with waves of small steepness. But the present work reports low and moderate steepness of wave. The present 2-D work is extended to a 3-D tank problem, and the results obtained are discussed below.

5.4 Results and Discussion for the 3-D Rectangular Domain

In 2-D domain case, the initial value of velocity potential (ϕ) is set to zero prescribed as, $\varphi\big|_{t=0} = 0$, over the entire 2-D liquid domain and the initial value of free surface elevation (ζ) is taken as $\zeta\big|_{t=0} = \zeta_0 = A\cos(K_n x)$. For 3-D domain, initial value of free surface

elevation (ζ) is considered in two cases say, initial profile 1 ($\zeta|_{t=0} = \zeta_0 = A\cos(K_n x)$) and initial profile 1 and 2 ($\zeta|_{t=0} = \zeta_0 = A\cos(K_n x) + A_v \cos(K_z z)$). Here, A and A_v are the respective amplitudes of the initial wave profiles on the liquid free surface along the X and Z axes (Figure 4.6), K_n $(= n\pi/b)$, K_z $(= n\pi/w)$ are the respective wave numbers of the initial wave profiles on the liquid free surface along the X and Z axes for n^{th} mode of oscillation (n = 0, 1, 2, …..), and *x and z* are distances along the along the X and Z axes of the fluid tank. The initial wave steepness defined for fixed tank studies is as given below:

$$K_x = A\omega_n^{\,2} / g\,, \tag{5.8}$$

where A is the amplitude of the initial wave profile on the liquid free surface, ω_n is the natural sloshing frequency of oscillations and g is the acceleration due to gravity usually considered as 9.81 m/s^2.

Now the term $\ddot{Y}_t$ in the dynamic boundary condition (Eq. 4.57) is switched off for fixed tank condition. Two quantities are of prime importance in the sloshing studies: the amplitude of the initial wave profile on the liquid free surface and the excitation frequency. Amplitude of the wave is determined from the wave steepness using Eq. (5.8). Here, numerical simulations are conducted for case A, case B, case C, and case D. Case A represents 2-D numerical simulation of regularly excited liquid tank in vertical direction and case B represents 3-D numerical simulation of regularly excited liquid tank in vertical direction with initial profile 1 for liquid free surface. Case C represents 3-D numerical simulation of regularly excited liquid tank in vertical direction with initial profile 1 and 2 for fluid free surface and Case D represents the 3-D numerical simulation of the randomly excited liquid tank in vertical direction.

5.4.1 Grid Independence and Validation Test

Before proceeding with the solution of the governing equations on the computational domain, grid independence study to choose a suitably refined grid for the solution is very important. Grid was successively refined along the three dimensional axes and the free surface plots along the tank length for all the grids at time 7.5 seconds and *Z=0* were compared. As shown in Figure 5.19, initially the grid is refined in the horizontal and axial directions of tank. Since the tank is bounded by fixed vertical walls in the horizontal and axial directions, free surface

plots do not seem to be affected by refining along these directions. But attention is required in the vertical direction, because of the moving free surface on the top. The grid points along the vertical direction were increased from 21 to 41 and then to 61 mesh points and it was found that the free surface plot for the $41\times61\times41$ grid nearly overlaps with the free surface plot for the $41\times41\times41$ grid. Hence, $41\times61\times41$ grid size was found suitable for the present study.

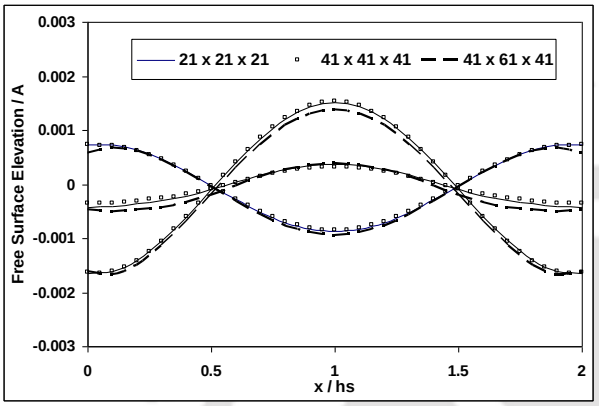

Figure 5.19: Free surface plots along the tank length for four different grids ($21\times21\times21$, $41\times41\times41$ and $41\times61\times41$) for K_x=0.033 at time 7.5 sec and Z=0.

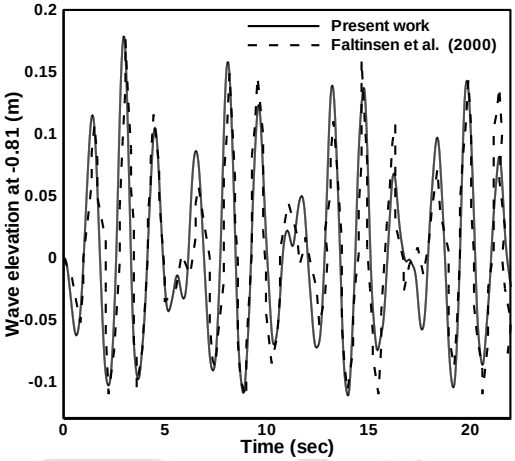

Figure 5.20: Solution of Faltinsen et al. (2000) and the present work showing the free-surface elevation at the left wall in horizontally excited tank; ω_h = 1.283; A_h = 0.029 m and K_h = 0.069.

Faltinsen *et al*. (2000) did a comprehensive analysis of sloshing through theoretical and experimental techniques. Their results are considered as benchmark results for sloshing problems. Figure 5.20 shows the comparison of present numerical work with theoretical result of Faltinsen *et al*. (2000) for the test case: ω_h = 1.283; A_h = 0.029 m and K_h = 0.069. The wave peaks and troughs match well with present work. Therefore, the numerical solution is in reasonable agreement with the work of Faltinsen *et al*. (2000) for this particular test case. The specific test case was previously solved by Hill (2003) and Frandsen (2004). In the present case, similar results have been obtained.

5.4.2 Vertically Excited 3-D Tank: Regular Motion

The initial condition of the liquid free surface used to simulate sloshing in a vertically excited tank is same as for the sloshing motion simulation in a fixed tank. It is difficult to simulate sloshing with a vertical excitation only. In order to have an initial perturbation in the free

surface inside the tank, horizontal motions need to be excited before the vertical excitation. To avoid this situation, the initial standing wave profile is assumed for this work. Initial wave impulse at the fluid free surface is required for vertically excited condition and it is considered in two ways, initial profile 1 and initial profile 1 and 2 (as discussed in chapter 4). The vertical acceleration of tank is given by $\ddot{Y}_t = (-\omega_v A_v \cos(\omega_v t))$, where A_v is the vertical forcing amplitude, t is the time, ω_v is the angular frequency of forced vertical motion. The initial velocity potential in the fluid domain is considered as $\varphi(\xi,\eta)\big|_{\tau=0} = 0$.

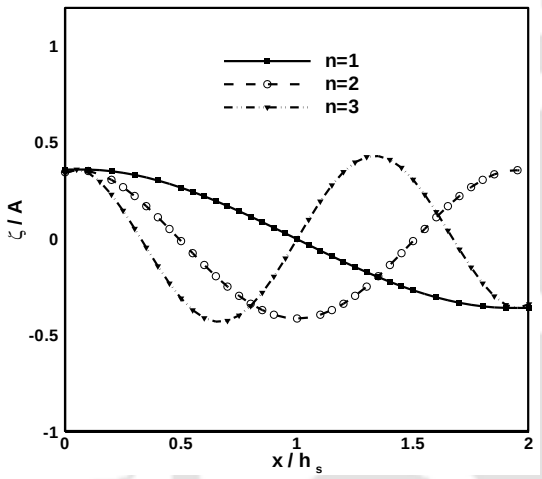

Figure 5.21: Free surface profile diagram along tank length at t=1.5 Sec.

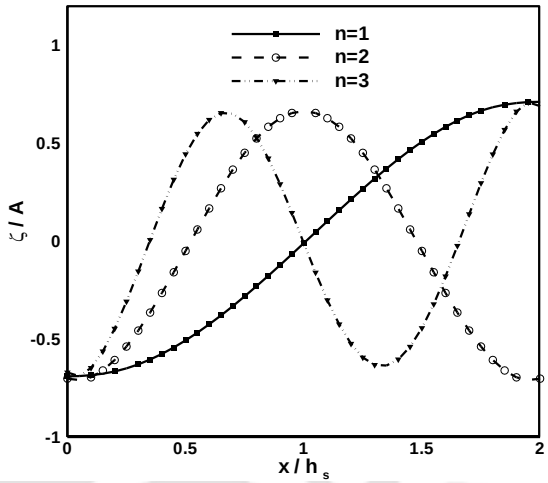

Figure 5.22: Free surface profile diagram along tank length at t=3 Sec.

5.4.3 Effect of Mode Number on Regular Waves Oscillation

For the vertically excited tank, the parameter $K_v = A_v \omega_v^{\,2} / g$ is a measure of the importance of the vertical forcing motion and K_x (the wave steepness) is a measure of nonlinearity. Frandsen (2004) plotted the instability map between $\Omega_v = \omega_n / \omega_v$ and K_v and discussed results from stability and instability regions. If any of the pairs of the parameters lies in the instability region, then the corresponding mode grows exponentially with time. In this section, the profiles are given inside the stability region (Ω_v=1.253 and K_v =0.4). Figures 5.21 and 5.22 show liquid free surface elevation along the tank length for *n=1, 2 and 3* at time 1.5 and 3 seconds, respectively. The mode number defines the shape of the free surface during the numerical simulations. The first few mode natural frequencies of system are dangerous for the structural integrity of the tank during violent motions. Figures 5.23 through

5.25 show the free surface elevations of the liquid near left wall (L_{2D} and LF_{3D}) for *n=1*, Ω_v=1.253; E_b = 0.0033 and K_v =0.4. The case A and case B show almost similar elevation histories. But, case C shows large wave oscillations.

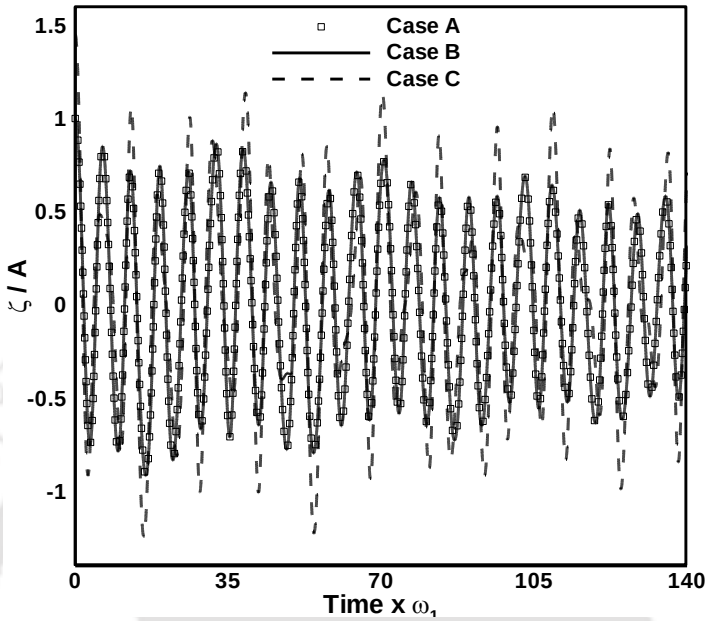

Figure 5.23: Vertically excited tank free surface wave elevation at left wall for *n =1*;

$\Omega_v = \frac{\omega_v}{\omega}$ =1.253; K_v =0.4; E_b = 0.0033 and K_x= 0.015.

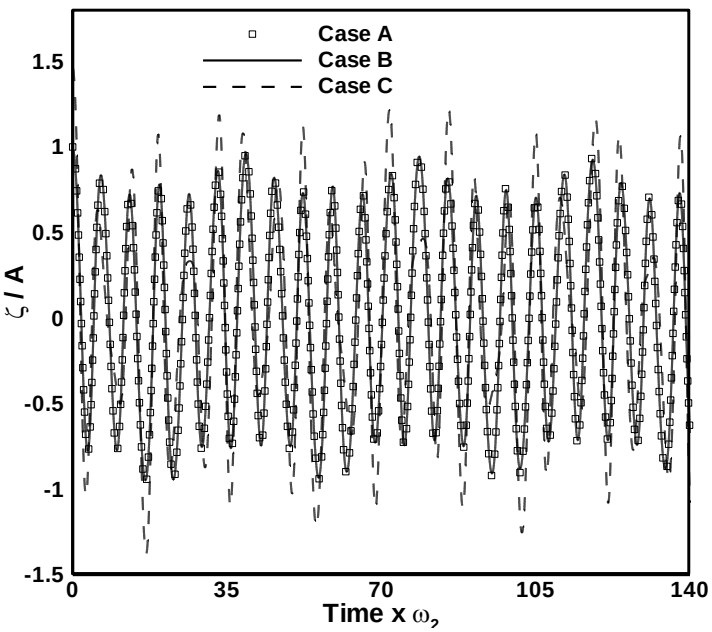

Figure 5.24: Vertically excited tank free surface wave elevation at left wall for *n =2* ;

$\Omega_v = \frac{\omega_v}{\omega}$ =1.253; K_v =0.4; E_b = 0.0024 and K_x =0.015.

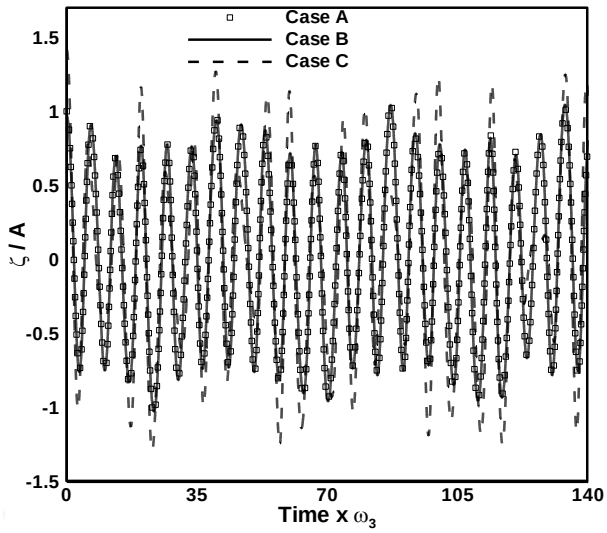

Figure 5.25: Vertically excited tank free surface wave elevation at left wall for $n = 3$; $\Omega_v = \frac{\omega_v}{\omega} = 1.253$; $K_v = 0.4$; $E_b = 0.0016$ and $K_x = 0.015$.

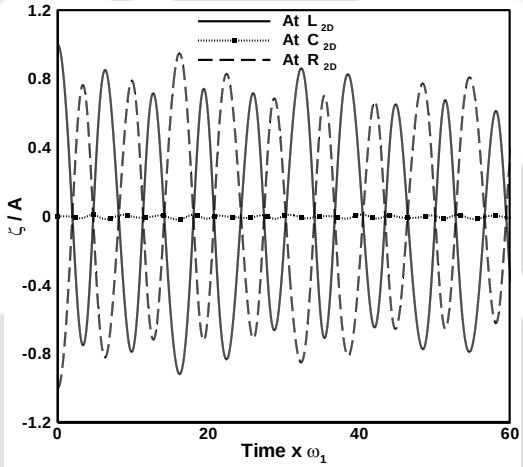

Figure 5.26: Free surface elevation for case A at different locations (left wall (L), center (C) and right wall (R) for $n = 1$; $\Omega_v = \frac{\omega_v}{\omega} = 1.253$; $K_v = 0.4$; $E_b = 0.0033$ and $K_x = 0.015$.

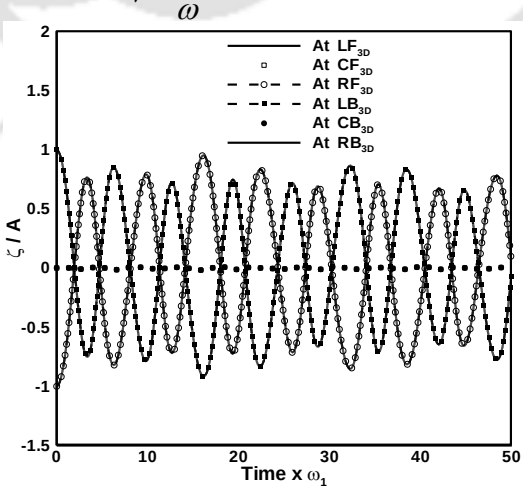

Figure 5.27: Free surface elevation for case B with initial profile 1 at different locations (left front (LF), center front (CF), right front (RF), left back (LB), center back (CB) and right back (RB) for $n = 1$; $\Omega_v = \frac{\omega_v}{\omega} = 1.253$; $K_v = 0.4$; $E_b = 0.0033$ and $K_x = 0.015$.

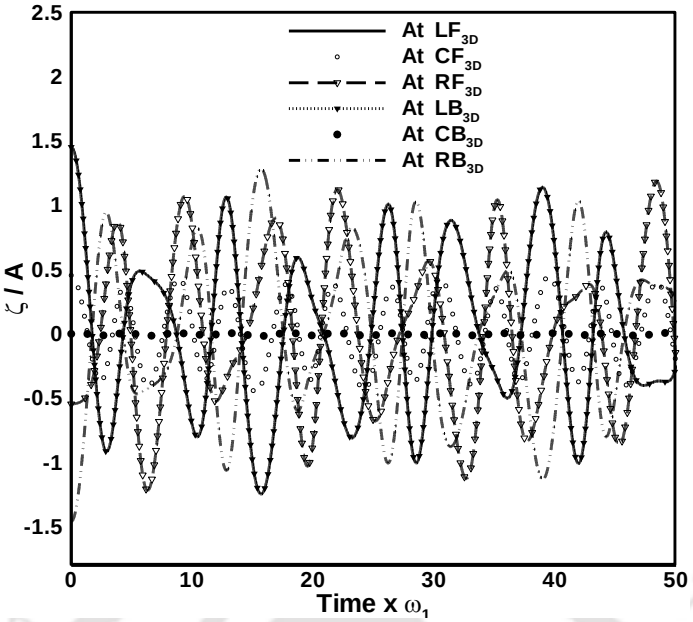

Figure 5.28: Free surface elevation for case C at different locations (left front (LF), center front (CF), right front (RF), left back (LB), center back (CB) and right back (RB) for $n = 1$; $\Omega_v = \frac{\omega_v}{\omega} = 1.253$; $E_b = 0.0033$; $K_v = 0.4$; $K_x = 0.015$.

5.4.4 Free Surface Elevation at Different Locations

Due to the wall effect, one can find the maximum wave amplitude near the wall, while the wave amplitude reduces as we move towards the centre. Here, three points are considered for case A (L_{2D}, C_{2D} and R_{2D}), and six points are considered for the case B and case C (LF_{3D}, CF_{3D}, RF_{3D}, LB_{3D}, CB_{3D} and RB_{3D}). These points are showed in Figures 4.4 and 4.8. Figure 5.26 shows free surface wave elevation time history in the vertically excited 2-D tank for case A at three different locations. The free surface wave elevation time history for case B and case C are shown in Figures 5.27 and 5.28. In all these cases, one can observe that the free surface elevation time histories of case A and case B are similar. Since the assumed initial profiles are same in both cases (refer Figure 4.2 and 4.5), the free surface wave elevation time histories are almost similar. But case C (3-D with initial profile 1 and 2) shows dissimilar behavior and the difference between the crests and troughs also drastically varies from case B due to high nonlinearity. Figures 5.29 (a) and (b) show the phase plane diagram at LT_{3D} for $\Omega_v = 1.253$, $E_b = 0.0033$ and $K_v = 0.4$. In Figure 5.29 (a), the phase plane diagram shows the uniform repeating pattern, but Figure 5.29 (b) shows the non-uniform repeating pattern behavior.

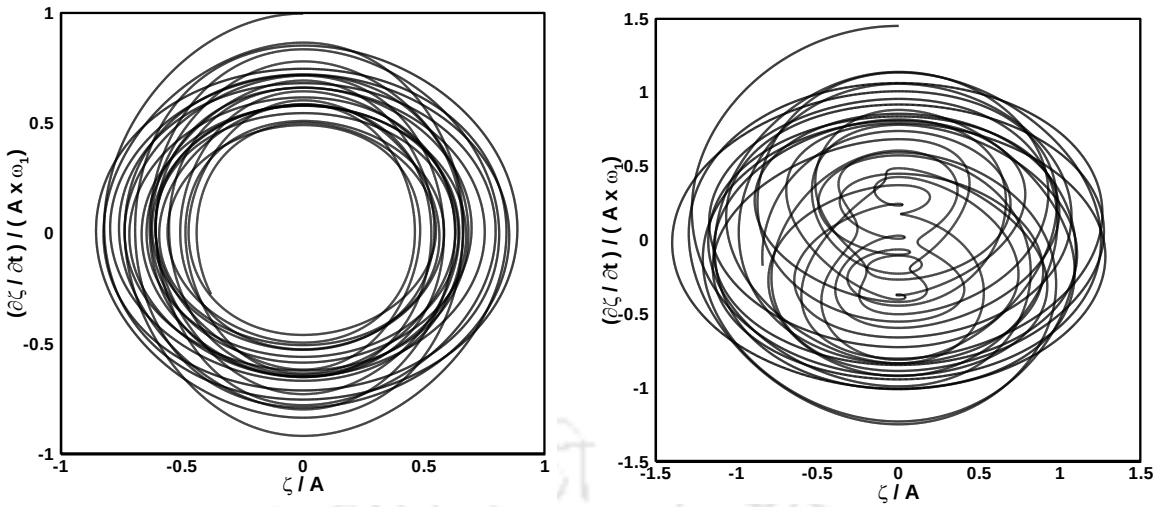

(a) (b)

Figure 5.29: Vertically excited tank Phase-plane diagram at LT_{3D} for *n =1*; $\Omega_v = \frac{\omega_v}{\omega}$ =1.253; E_b = 0.0033; K_v =0.4; and K_x =0.015: (a) Case B; (b) Case C.

5.4.5 Vertically Excited 3-D Tank: Random Motion

In most practical situations, the excitation or the time variation of the system parameters are random in nature (Ibrahim, 2005). The behavior of such systems under deterministic or regular wave parametric excitation is an idealization and an oversimplification of the real behavior. The random excitation originates from many natural and artificial sources. Recently, the 2-D sloshing waves generated by the random excitations have been studied by Wang and Khoo (2005), and Sriram *et al.* (2006). The random vertical oscillation of the tank is considered in this section. As we know, a random input wave can be generated by the linear superposition of a number of monochromatic waves. The total supplied energy to the system is kept constant. Bretschneider spectrum is selected to serve as the input excitation spectrum to generate the random input wave. The relation for the Bretschneider spectrum is as given in Eq. 5.10 and the spectrum and the corresponding displacement time history generated by the spectrum are shown in Figures 5.30 and 5.31.

$$S_\zeta(\omega) = \frac{5H_s^{\,2}}{16\omega_p}\left(\frac{\omega_p}{\omega}\right)^5 \exp\left[-\frac{5}{4}\left(\frac{\omega_p}{\omega}\right)^4\right] \tag{5.9}$$

where H_s is the significant wave height, and ω_p is the modal or peak frequency of the wave. The random input excitation wave is described by,

$$\zeta = \sum_{i=1}^{N_W} A_i \sin\left(\omega^i t + \psi^i\right) \tag{5.10}$$

where t is time, ω_i is the frequency of i^{th} linear wave, and N_w is the number of the linear monochromatic waves. A_i and ψ_i are the wave amplitude and phase of each linear wave, respectively. ω_i and ψ_i are a set of random variables within a pre-selected range.

5.4.5.1 Selection of the linear angular frequencies (ω_i)

N_w denotes the number of linear waves superposed to create the random wave. In the present case, N_w is chosen to be 512 since such a high number ensures that a lot of frequencies within a given range contribute towards the generation of the random wave. The range of the angular frequencies is set as [0, $5\omega_p$] as the frequencies above $5\omega_p$ do not have a significant contribution towards the generation of the random wave. In the present case, ω_p is taken equal to the first natural frequency of the system ω which is 3.759371 *radians/sec*. From Figure 5.30, it is evident that in the energy spectrum, the wave energy (S_ζ) is having the highest values around the modal or peak frequency (ω_p), hence a large no. of angular frequencies are chosen in the narrow band around the value ω_p. Around 150 values of angular frequencies are selected randomly in the range of [2.5, 5.0] which is a very narrow band around the peak frequency marked as *A* in Figure 5.30 and *B* represents the range [0.0, 2.5] and 62 values of angular frequencies are selected randomly in this range. As can be seen from Figure 5.30, the energies in this range are near to zero and hence have negligible contribution in the energy of the final generated random wave. Band *C*, *D* and *E* represent the ranges [5.0, 10.0], [10.0, 15.0] and [15.0, $5\omega_p$] and 100 values of angular frequencies are selected randomly in each of these ranges. The selection of linear angular frequencies within a range is done by using a floating random number generating algorithm that makes use of a fixed seed number and a custom built function '*rand( )*' (that gives the same set of random numbers every time for a fixed seed number). It is to be noted that the energy spectrum for angular frequencies above 10.0 *radians/sec* falls well below 0.01×10^{-6} *Joule*, hence less no. of angular frequencies are selected in this range.

After the selection of angular frequencies, the amplitudes of the linear waves can be calculated by the following equation:-

$$A_i = \sqrt{2S_\zeta(\omega)\Delta\omega} \tag{5.11}$$

where $\Delta\omega$ is nothing but, the difference between adjacent angular frequencies ($\Delta\omega = \omega_{i+1} - \omega_i$).

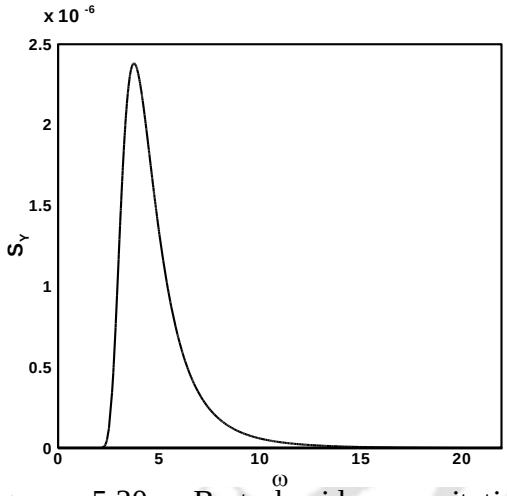

Figure 5.30: Bretschneider excitation spectrum with $H_s = 0.01h_s$ and $\omega_p = \omega_1$.

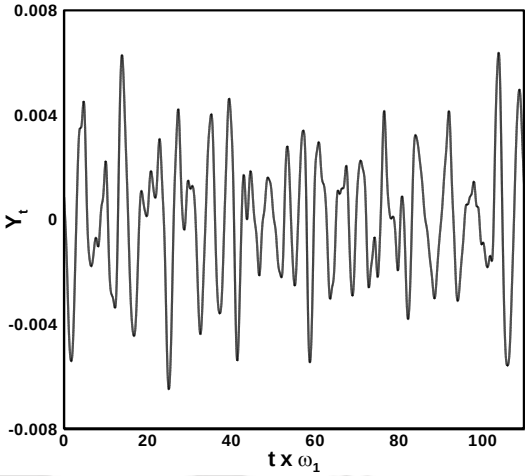

Figure 5.31: Displacement generated from the spectrum.

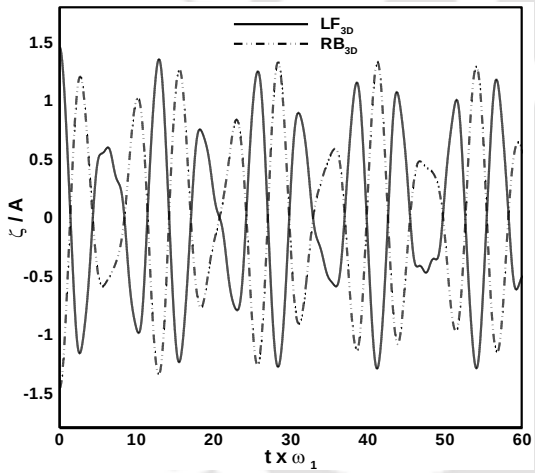

Figure 5.32: Random vertically excited tank free surface oscillation at LF_{3D} and RB_{3D}, for an initial steepness of 0.288; $\omega_p = \omega_1$.

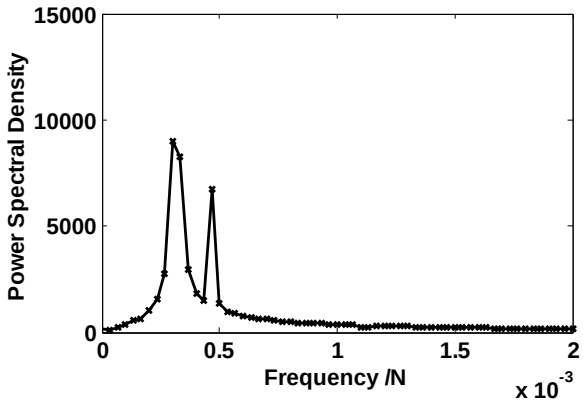

Figure 5.33: Spectra of free surface sloshing waves at LF_{3D} of the wall due to vertical random excitation for an initial steepness of 0.288 and $\omega_p = \omega_1$.

5.4.5.2 Selection of the phase angle (ψ_i)

Using the same algorithm as used for selecting linear angular frequencies, N_w random values of phase angles are selected within the range [0, 2π]. By substitution of the selected random values of angular frequencies (ω_i), amplitudes (A_i) and phase angles (ψ_i) in Eq. 5.11, we can get the resultant random input wave. From Eq. 5.11, the vertically excited tank displacements are obtained from this spectrum as depicted in Figure 5.31. The time history of surface elevation at LF_{3D} and RB_{3D} of the tank due to random vertical excitation is shown in Figure 5.32.

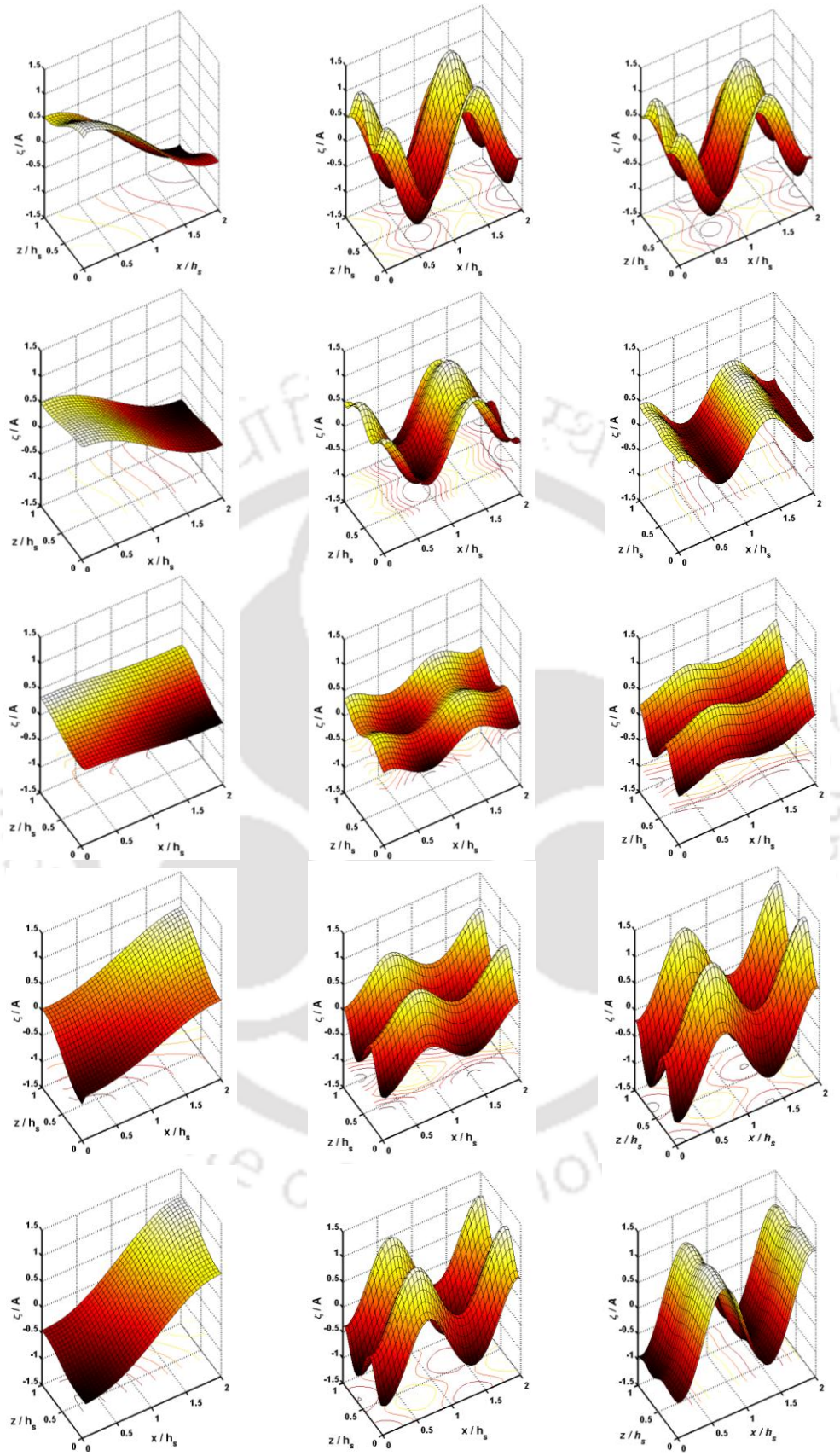

Case **C** and *n=1* | Case **C** and *n=3* | Case **D** and *n=3*

Figure 5.34: Surface plot for different cases from the 32 to 35 non-dimensional time units with Δt = 0.6 time step.

Spectra of free surface sloshing waves at LF_{3D} of the wall due to vertical random excitation for an initial steepness of 0.288 and $\omega_p = \omega_1$. In the case of random excitation in vertical direction, the dominating peak appears only at the first mode (Figure 5.33). The magnitude of the peak is almost the same irrespective of the excitation peak frequency and initial perturbation, contrary to the regular excitation. Sriram *et al.* (2006) found the magnitude is large only if the excitation frequency is equal to twice the first mode (parametric resonance) irrespective of initial perturbation. Figure 5.34 shows the surface plots for three conditions say case C at n=1, n=3 and case D at n = 3 from 32 to 35 non-dimensional time units with non-dimensional time step Δt = 0.6 units. The surface plots show a half cycle of wave's movement. The frames are shown for a wave steepness K_x = 0.04016.

5.4.6 Summary of Results for the 3-D Rectangular Tank

Non-linear effects of standing wave motion of liquid in 2-D and 3-D fixed and forced vertically regularly and randomly excited tanks were studied numerically. The present study was carried out for regularly and randomly excited rectangular tank in vertical direction for four different cases: 2-D tank with regular excitations, the regularly excited 3-D tank with two different initial conditions for liquid free surface and finally, 3-D tank with random excitation in the vertical direction.

Initially, the wave elevation time history have been observed for first few modes of sloshing on the free surface at the left wall for 2-D regular (case A) and 3-D regularly excited tank with two initial profiles (case B and C) in vertical direction. The wave elevation time histories have been plotted at different locations of the free surface. The wave elevation time history at a particular point on the free surface in the domain is then compared for cases A, B and C. Near the tank wall the wave elevations are more due to the wall effect while the center of the tank has low wave elevation profiles. The 2-D and 3-D tank with initial profile 1 had similar wave elevation time history. If nonlinearity in the axial direction is increased by using profile 1 and 2 i.e. a linear superposition of two sinusoidal wave profiles, the 3-D tank showed a different wave elevation time history. The free surface elevation got the intricate shapes for the case C. Sloshing in a randomly excited tank in vertical direction has also been studied. Bretschneider spectrum is selected to serve as the input excitation spectrum to generate the random input wave. In the present study, the ratio of the excitation frequency

and the natural frequency of the system (Ω_v) is kept at 1.253. Hence, the all numerical results are plotted from the stable regions only.

5.5 Results and Discussion for 2-D Cylindrical Domain

As discussed, the σ-transformation have been applied to a partially filled 2-D horizontal cylindrical tank also. The following sections are showing the wave elevation for the 2-D cylindrical tank with horizontal acceleration.

5.5.1 Initial Conditions and Procedures

In this section, the present method is used first to simulate the liquid sloshing in a horizontal circular tank subjected to transverse harmonic motions of small amplitudes. The tank is half-filled. Initially the fluid is assumed to be at rest with some initial perturbation of the free-surface. Thus, the initial conditions are $\zeta(x,t)\big|_{t=0} = A\sin(K_n x)$ and $\varphi(x,t)\big|_{t=0} = 0$, where A is the initial wave amplitude, K_n is the wave number $\left(\frac{n\pi}{b}\right)$ for n^{th} mode number (n = 0, 1, 2, …..) and x is the distance in the horizontal direction. The tank acceleration term (DT'') is set as zero. The volume of error (E_V) can be calculated as follows:

$$E_V = \int \zeta dx \tag{24}$$

The volume correction is adopted in the current scheme for smoothing the free surface, so that the mean water level in the tank remains constant.

To demonstrate that the solution is grid independent, simulations have been performed using different numbers of grid nodes as shown in Figure 5.35. The wave profiles along the tank at two different times for the first sloshing mode (n=1) are plotted. Results for different grid resolutions are shown related to moderate wave amplitude (A=0.002) for time steps of $\Delta t^* = 0.02$. Since the moving boundary is in y direction, increasing grid points in the vertical direction is found to be more effective in improving accuracy. The grid sizes 21 X 41, 41 X 41 and 41 X 61 are chosen for this grid independent study. Increasing the grid points in the vertical direction is found to be more effective in improving accuracy than increasing the grid points in the horizontal direction. In Figure 5.35, there is not much variation in the vertical

direction above the grid size of 41 X 41 for moderate wave steepness, and therefore, the grid size of 41 X 41 is sufficient for this problem.

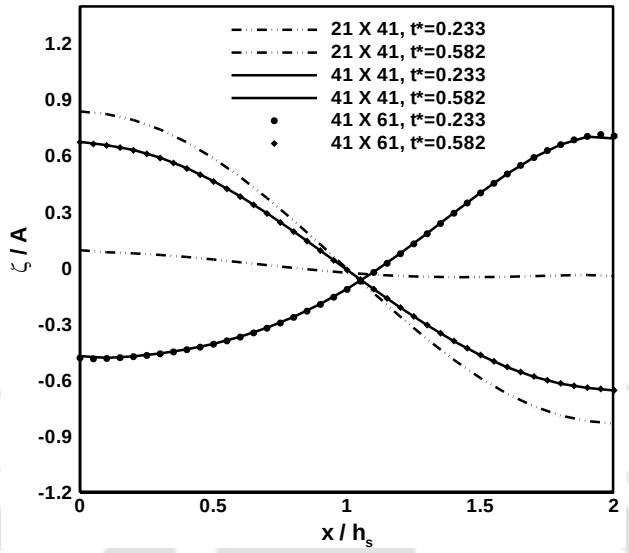

Figure 5.35: Grid independence: Free surface profile for fixed tank.

5.5.2 Behavior of Free Surface on Transverse Excitation

The liquid waves are captured for different excitation values. The acceleration of the tank considered is assumed as the following sine function $DT'' = A_x \omega_x^2 \sin(\omega t)$, where $A_x = 0.002$ is the amplitude of the tank displacement. The initial conditions are now modified as $\zeta(x,t)\big|_{t=0} = 0$ and $\varphi(x,t)\big|_{t=0} = 0$.

Sloshing is a highly nonlinear phenomenon. The sloshing frequencies of a horizontal resting cylindrical tank are difficult to obtain, even for an ideal frictionless liquid (Wiesche, 2008). However, the natural frequency for a half-filled horizontal cylinder can be calculated, which is 1.1644 or 1.169 for the above conditions (Dai and Xu, 2006). Obviously, the stretched grid system exactly matches the time-dependent free-surface wave profile due to the σ-transformation. It can be seen from Figure 5.36 that the liquid heights on the walls are sine waves when the excitation frequency is far from the natural frequency. Figure 5.36 is drawn for horizontal cylindrical tank with $0.2\,\omega_n$, n=1. Since the oscillating frequency is considerably low, the free surface elevation is like sine waves. If the accelerating term is assumed as zero (i.e., $DT''=0$), the free surface elevation becomes a perfect sine waves.

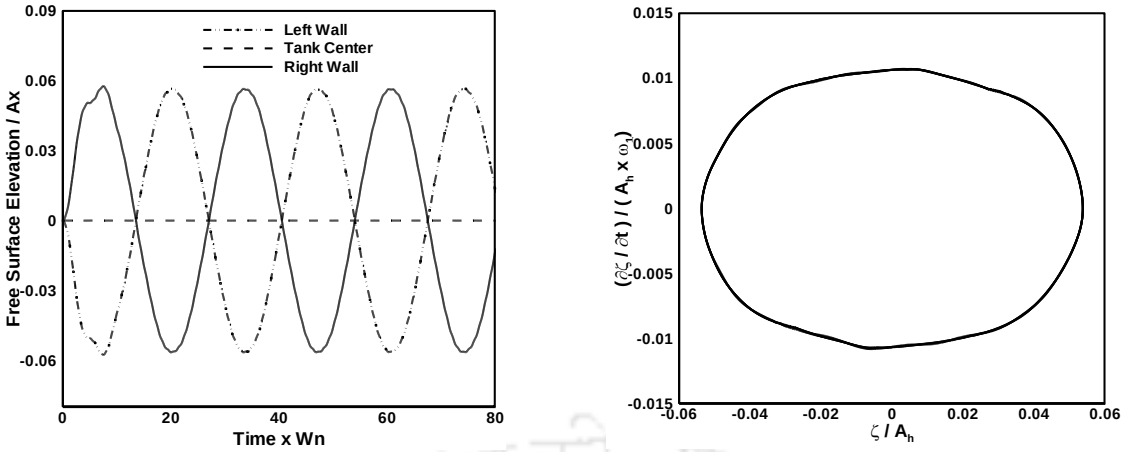

Figure 5.36: Horizontal cylindrical tank in transverse oscillation for frequency 0.2 ω_n , n=1 at tank left wall: (a) Free surface elevation; (b) Wave phase plane diagram at left wall.

The wave phase–plane diagram shows that the free surface wave is a cyclic process of repeatable patterns. The free surface elevation is observed on left middle and right side of the tank. If the excitation frequency increases further to 0.45 ω_n and 0.75 ω_n , the free surface profile changes its shape accordingly as shown in Figures. 5.37 and 5.38. Since *n*=1, the left and right sides profiles are always opposite. In most cases, the oscillation of the liquid height at the tank middle is very small. However, at the tank left and at right sides, liquid elevation drastically varies with different tank excitation. As the tank excitation increases, adjacent crests or the troughs of liquid wave varies with time.

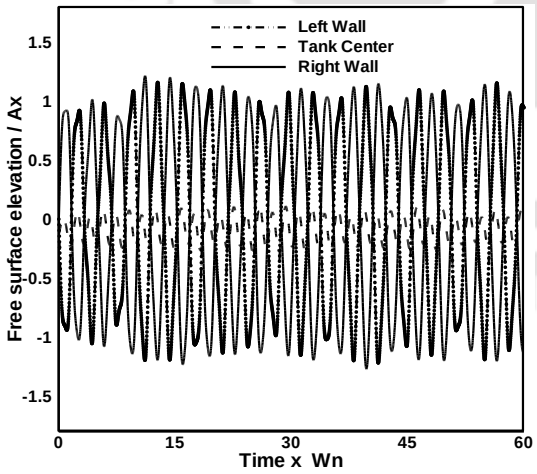

Figure 5.37: Horizontal cylindrical tank free surface elevation at 0.45 ω_n , n=1.

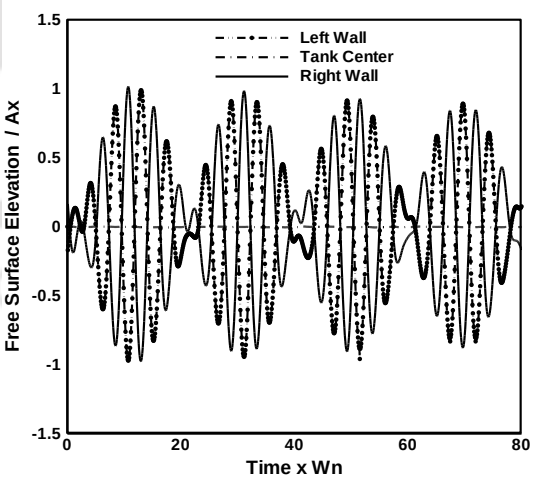

Figure 5.38: Horizontal cylindrical tank free surface elevation at 0.75 ω_n , n=1.

Obviously, a system (i.e., a partially filled liquid tank) has an infinite number of natural frequencies. When the tank excitation frequency is close to one of the natural frequencies of

the tank fluid, large sloshing amplitudes can be expected. If both the frequencies are reasonably close to each other, then resonance will occur. Since the tank excitation frequency is quite close to the first natural frequency of the system as seen in Figure 5.39, the amplitude grows monotonically with time. The wave phase-plane diagram is also drawn for first natural frequency of the system in Figure 5.40.

These types of large amplitude will induce the pressure rise inside a tank which may lead to structural damage of tank, industrial accidents. Different types of sloshing arresting techniques (i.e. large slosh amplitude) have been discussed in open literatures like inserting the baffles like tuned liquid damper (Sayar and Baumgarten, 1982). During earthquake, the random acceleration of ground motion is observed. These motions create high pressure rise inside the tank due to free surface oscillations. It is necessary to find the liquid free surface behavior during earthquake. Even the small oscillations of the liquid free surface are also more sensitive in nuclear reactor tanks. As very limited literatures reported the 2-D horizontal cylindrical tanks under horizontal excitations, a direct comparison of the present results with the published ones could not have been made. It is worth mentioning that when the external horizontal forcing frequency is very near to the natural sloshing frequency of liquid, the resonance will occur. At the condition of resonance, the free surface elevation of liquid grows gradually as shown in Figure 5.40. Moreover, the present results fairly match with the results of horizontal cylindrical tank as obtained by Dai and Xu (2006).

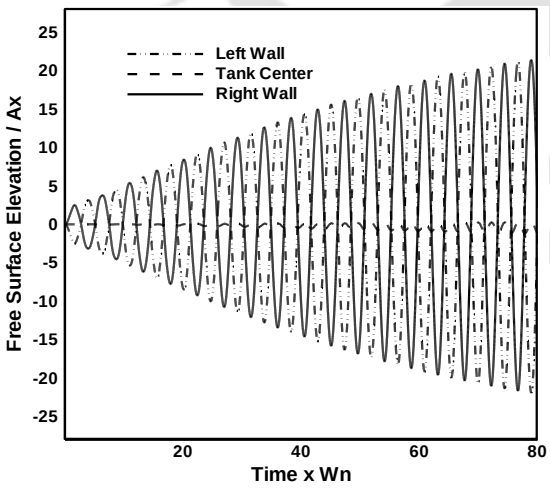

Figure 5.39: Free surface elevation at frequency=1.0 ω_n and n=1 at tank left wall.

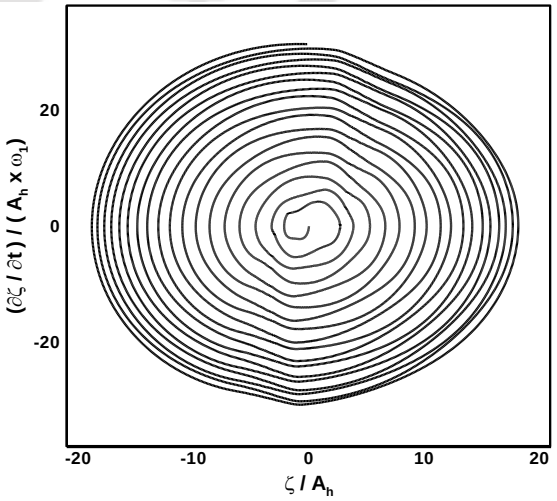

Figure 5.40: Wave phase-plane diagram at frequency=1.0 ω_n and n=1 at tank left wall.

5.5.3 Free Surface Behavior during Earthquake – A Case Study

In this section, the above computational procedure is applied to find the free surface elevation for a real engineering problem. An existing real earthquake acceleration-time history is used to study the sloshing characteristics of liquid in a half filled horizontal cylinder, under the earthquake motion. For this, the acceleration- time history of EW and NS components of the EL-Centro earthquake, California (18th May, 1940) recorded at Imperial Valley Irrigation District is chosen. Initially, the liquid is considered to be at zero elevation. Figures 5.41 and 5.37 show the free surface elevation of liquid in the horizontal cylindrical tank for EW and NS components of El-Centro earthquake. Here, the same half filled tank and the same initial conditions are applied (i.e., $\zeta(x,t)\big|_{t=0} = 0$ and $\varphi(x,t)\big|_{t=0} = 0$). During the earthquake, the irregular acceleration would play over the tank. In that situation, the tank fluid would also behave irregularly inside the cylinder. Due to the random acceleration, the ground motion increases the free surface elevation of liquid from zero level or mean level. The free surface behavior also becomes random, and finally, wave becomes the uniform standing waves as shown in Figures. 5.41 and 5.42.

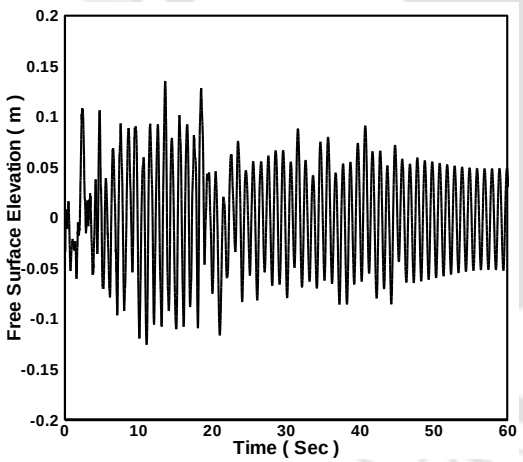

Figure 5.41: Free surface elevation at EW component of EL-Centro earthquake at the tank left wall.

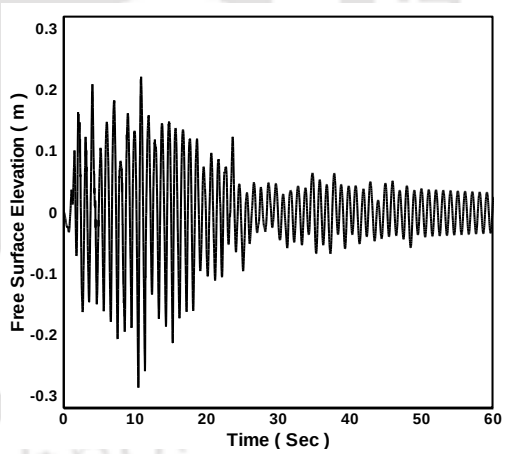

Figure 5.42: Free surface elevation at NS component of EL-Centro earthquake at the tank left wall.

5.5.4 Summary of Results for the 2-D Cylindrical Tank

The nonlinear liquid free surface in the horizontal cylindrical tank is converted into the straight and fixed domain using proper coordinate transformation. The difficulty due to the curved wall was eliminated by this proper mapping technique. This method is a simple way

to simulate non-breaking waves quickly and accurately especially that has a low steepness. Simulations are limited to a half-filled tank. However, this numerical model is valid for any water depth except shallow and deep sloshing. For the shallow sloshing, viscous effects would become important, which we considered as inviscid fluid in our numerical model. The grid independent test was conducted for grid sizes of 21×41, 41×41 and 41×61, and finally, a 41×41 is selected as grid resolution. The liquid free surface elevation and wave phase-plane diagram were plotted for different tank excitation frequency. It has been observed that free surface elevation of the liquid increases with frequency. The amplitude of the standing wave also grows while increasing the excitation frequency of the tank. At the critical frequency of the system, the free surface elevation has more displacement. Finally, the proposed numerical scheme has been applied to a real life problem to find the free surface elevation. For this, acceleration-time history of EW and NS components of the EL-Centro earthquake, California has been studied and analyzed.

5.6 Summary

The present numerical model is easy to implement, computationally accurate and efficient. For the cases presented herein, it eliminates the need for free surface smoothing and remeshing. The model provides a simple way of simulating steep non-breaking waves. The σ - transformation technique can be applied to non-overturning and non-breaking waves. Present results were compared with the benchmark solutions of Faltinsen *et al*. (2000) (third order analytical solutions by multi modal technique). A fully non-linear inviscid numerical model has been developed based on potential flow theory with the mapped governing equations and corresponding boundary conditions solved using finite difference method. Results of liquid sloshing induced by harmonic base excitations are presented for small to steep non-breaking waves. The present numerical model is valid for any water depth except the shallow and deep water sloshing. An error estimation method was used to estimate the error at each iteration to serve as a basis for stopping the iterative solver when the steady state results are reached. The model was validated for different wave lengths and steepnesses. Good agreement has been found between present and previously published theoretical solutions for same test cases. The grid independence test showed that the grid size $41\times61\times41$ is efficient to solve the 3-D sloshing problem in the given liquid tank. Sloshing motion in vertically excited tanks was carried out for the stable region conditions. Sloshing effects in a vertically excited tank in stable regions display similar characteristics as free sloshing motions in a fixed tank when the forcing parameter (K_v) is low. The phase plane diagrams showed the nonlinearity of the free surface waves with respect to time.

Chapter 6

EXPERIMENTAL INVESTIGATION OF LIQUID FREE SURFACE ELEVATION

This chapter pays attention on the image processing technique to find the free surface elevation during liquid sloshing under low excitation frequency. Experiments have been conducted at low frequencies to find the free surface elevation and the results obtained are reported here. Finally, the experimental results for two different frequency ratios are compared with the present numerical results.

CONTENTS

6.1 Introductory Remark

The knowledge of natural frequencies for the liquid free surface is important in the design of liquid tanks subjected to different types of excitation. The dynamic behavior of a free liquid surface depends on the type of excitation and its frequency content. Excitation with frequencies in the vicinity of the lowest natural frequencies of the liquid motion is of primary practical interest. Civil engineers and seismologists have been studying liquid sloshing effects on large dams, oil tanks and elevated water towers under ground motion. Sloshing phenomenon is one of the major concerns in the design of liquid storage tanks undergoing ground excitation (Maleki and Ziyaeifar, 2008). Experimental studies can provide very useful and reliable results for some cases. However, they are generally very expensive. Moreover, there is a lack of high quality experimental data in the area of liquid sloshing (Akyildiz and Unal, 2005).

6.2 Experimental Details

The liquid behavior is captured by means of a video camera and the free surface oscillations of liquid at different excitation frequencies are calculated by image processing technique. Finally, the statistical analysis is performed to show the probability density and power spectral density of signal.

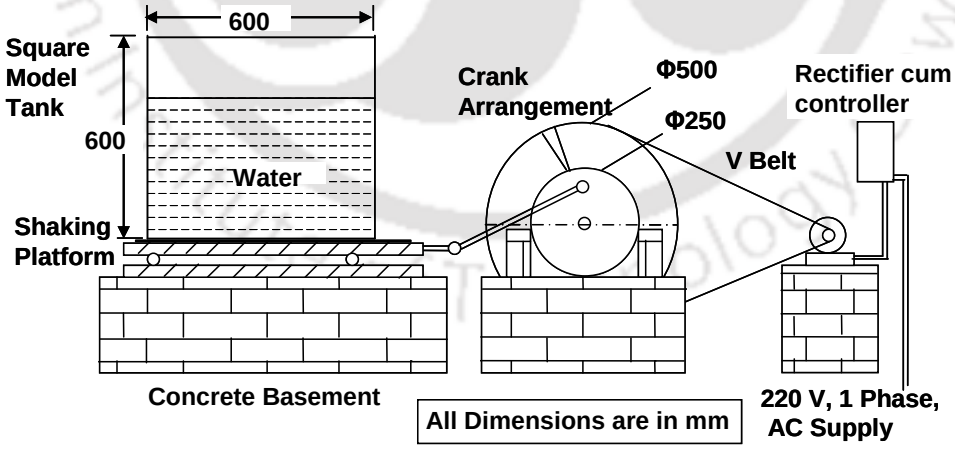

Figure 6.1: Basic experimental set-up.

6.2.1 Experimental Facilities and Procedures

Figure 6.1 shows the schematic diagram of the experimental set-up. The partially filled liquid tank of size 600 mm x 600 mm x 600 mm is attached to a shaking table (915 mm x 930 mm)

which can be moved to and fro by a crank arrangement and is driven by a DC motor (rated 1440 RPM, 220 V, 1 HP). As the frequency of oscillation required is too low, a rectifier-cum-controller is used which gives the desired frequency of oscillation. The controller that converts the alternating current to direct current and feeds it to the DC motor with appropriate regulation is connected with the DC motor. It contains a full wave rectifier, which converts the 220V AC-1ϕ supply to 220V DC. The crank arrangement is used in the set-up to transform the rotary motion to reciprocating motion which connects the DC motor and the platform of the shaking table. The water is used as a working fluid in the experiments.

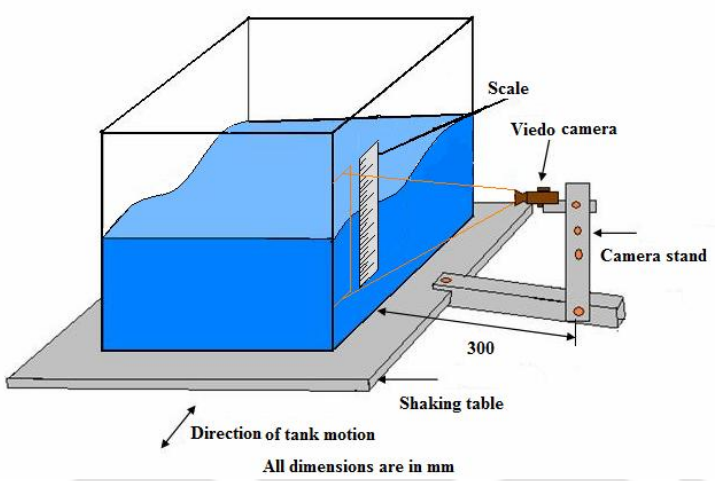

Figure 6.2: Camera arrangement in the set-up for finding the free surface elevation.

A video camera (Sony DCR-SR 300 Handy cam Camcorder) is screwed onto an adjustable beam which is attached to the shaking platform with its lens focusing on the liquid free surface at the left corner of the tank as shown in Figure 6.2. The adjustable beam is moved up or down until a suitable slot is reached so that the camera focuses only on the liquid during its entire motion. The camera was held at a distance of 300 mm away from the liquid free surface and focuses on the water free surface. Initially, the relation between the pixel and millimeter has been found by still images. Now the camera can be used to capture the images of the air-water interface as shown in Figure 6.3.

After adding a coloring agent (navy blue) in the liquid, an excellent contrast between the liquid and the white marker particles is obtained that gives a superior image quality with lesser noise. Experiments have been conducted under natural light by covering the sides of tank with black cloth to improve further the contrast between the liquid and the seed particles. The horizontal excitation is imparted to the tank using the motor and the cam arrangement.

The motor is allowed to rotate whose speed can be varied using a speed controller. The speed of the motor is kept sufficiently low so that the sloshing occurs without much turbulence. The tank can be filled to any desired level and a scale attached to the side wall of the tank gives the height. The experiments have been conducted by varying the frequencies and the h_s/L ratio of the tank for different case studies.

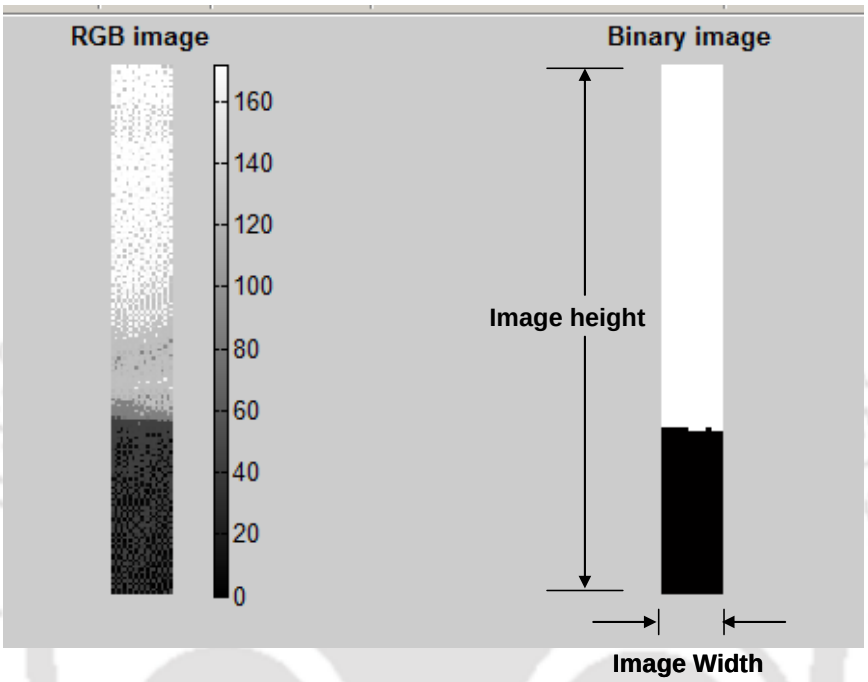

Figure 6.3: Conversion of RGB image into binary image

6.2.2 Interface Location Technique to Capture the Free Surface Elevation

The videos captured by the video camera are then transferred to the computer, and further image analysis is carried out. A MATLAB code is written to compute the free surface displacement of liquid. As the RGB image carries the unnecessary noises (as shown in Figure 6.4) due to natural and surrounding light source, the RGB scale images are converted to the binary images (Figure 6.3) which has the intensity value of 0 or 1. Here the binary image indicates 1 as intensity for air region and at a certain point, it drops to 0 intensity value along the vertical line. This represents the interface edge region (Figure 6.5). The intensity gradient at each point is calculated. The location of maximum gradient is considered as interface as described by Law *et al.* (1999). The luminance contrast between the liquid and the air which indicates the location of the interface is determined by maximum intensity gradient method. In other words, the liquid height is observed by the intensity variation of the interface between the air and liquid. The intensity gradient at each point has been calculated. The location of maximum gradient has been considered as interface. The movement of interface

can be analyzed by cross-correlation between these matrices. The free surface oscillations are plotted for different excitation frequencies. Figures 6.4 and 6.5 show the typical pixel intensity variation along a vertical line cutting across the interface region. The movement of the interface can be tracked by analyzing its displacement between two successive images. This vertical location with image width is plotted in Figure 6.6.

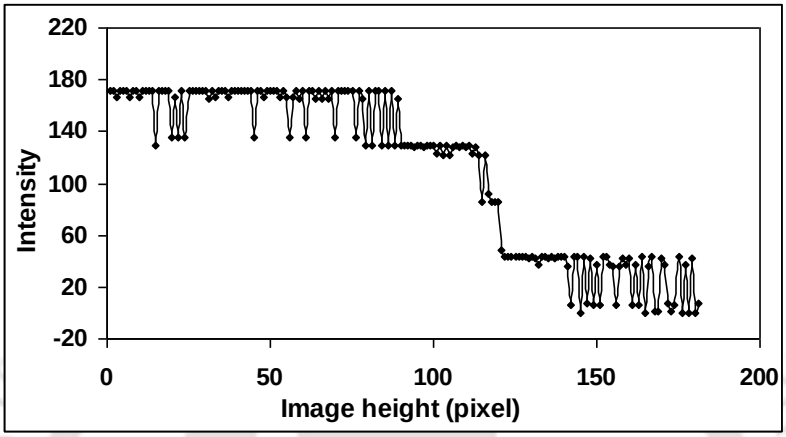

Figure 6.4: Intensity values for RGB image.

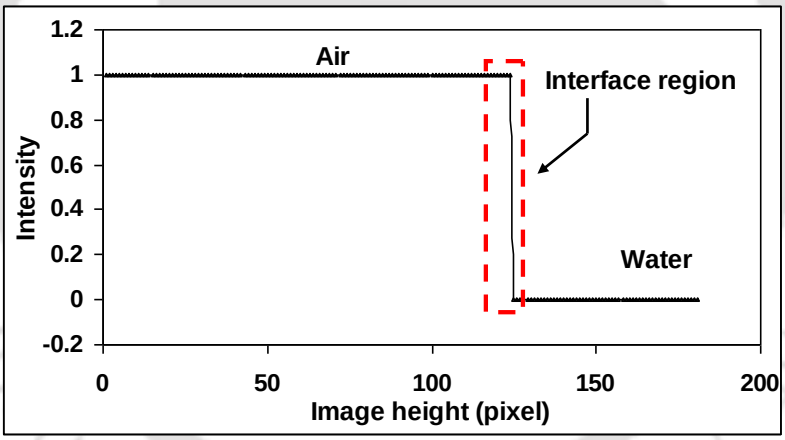

Figure 6.5: Intensity values for binary image.

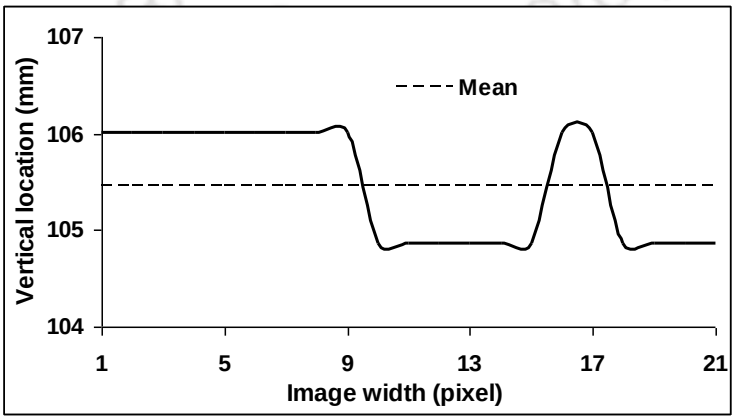

Figure 6.6: Free surface fluctuation along image width.

All images are then available in the form of a vertical location matrix. The movement of interface can be analyzed by cross-correlation between these matrices. The standard deviation of extracted vertical locations denotes the interface fluctuation with time and the mean value gives the mean fluctuation for the corresponding excitation frequency and h_s/L ratio.

6.3 Tests to Ensure the Accuracy of Experimental Results

Depending upon the type of liquid, nature of external disturbances on the tank, tank shape and h_s/L ratio, the free liquid surface can experience different motions like simple planar, non-planar, rotational, irregular beating, symmetric, asymmetric, quasi-periodic and chaotic (Ibrahim, 2005). The amplitude of slosh, in general, depends upon the nature, amplitude and frequency of the tank motion, liquid-fill depth, liquid properties and tank geometry (Pal *et al*., 2002, Akyildiz and Unal, 2006). As the rectangular tank oscillates, different sloshing waves are created depending on the liquid depth and frequency of oscillations. In this study, the problem was restricted to liquid sloshing in a rectangular tank under surge (movement of tank only in horizontal direction) oscillations.

The dynamic tank velocity (V_t) can be determined from the following equation,

$$V_t = -\mathrm{A}_t \omega \cos(\omega t), \tag{6.1}$$

where A_t is the tank excitation amplitude and ω is the oscillation frequency. The amplitude of the tank excitation is 100 mm. For a given rectangular prismatic tank, the natural frequencies of the fluid depending on the fill depth are given by,

$$\omega_n^{\,2} = g\frac{n\pi}{L}\tanh\left(\frac{n\pi}{L}d\right) \tag{6.2}$$

where L and d are the tank width and water depth respectively and n is the mode number (Akyildiz and Unal, 2005). In Table-6.1, different combination of liquid h_s/L ratio, excitation frequency and excitation amplitude are shown for a total of thirty six cases. It is to be noted that at higher frequency, the turbulence level becomes higher. If the frequency of the tank motion is close to the natural frequency of the liquid, large sloshing amplitude occurs. Since the liquid elevation is calculated through image processing, the more turbulence of liquid should be avoided which will induce noises while processing. Thus, all the experiments have been conducted at low frequencies only.

Table 6.1: Experimental parameter for measuring free surface elevation.

Set No.	**Case**	**Excitation Amplitude (EA)**	**Fill level (FL)**		**Excitation Frequency (ω_h)**		**First mode natural Frequency (ω_1)**	**FR** $\left(\frac{\omega_h}{\omega_1}\right)\times 100$
		mm	**mm**	***h_s/L* ratio**	**cycle/sec**	**rad/sec**	**rad/sec**	%
Set 1	1	30	120	0.2	0.3	1.885	5.34835	35.245
	2				0.4	2.513		46.986
	3				0.5	3.142		58.747
	4	40			0.3	1.885		35.245
	5				0.4	2.513		46.986
	6				0.5	3.142		58.747
	7	60			0.3	1.885		35.245
	8				0.4	2.513		46.986
	9				0.5	3.142		58.747
Set 2	10	30	210	0.35	0.3	1.885	6.41167	29.4
	11				0.4	2.513		39.194
	12				0.5	3.142		49
	13	40			0.3	1.885		29.4
	14				0.4	2.513		39.194
	15				0.5	3.142		49
	16	60			0.3	1.885		29.4
	17				0.4	2.513		39.194
	18				0.5	3.142		49

Set 3	19	30	300	0.5	0.3	1.885	6.86364	27.464
	20				0.4	2.513		36.613
	21				0.5	3.142		45.777
	22	40			0.3	1.885		27.464
	23				0.4	2.513		36.613
	24				0.5	3.142		45.777
	25	60			0.3	1.885		27.464
	26				0.4	2.513		36.613
	27				0.5	3.142		45.777
Set 4	28	100	210	0.35	0.3	1.885	6.41167	29.399
	29				0.35	2.199		34.297
	30				0.4	2.513		39.194
	31				0.5	3.142		49.004
	32		120	0.2	0.3	1.885	5.34835	35.212
	33				04	2.513		47.261
	34		180	0.3	0.3	1.885	6.15000	30.591
	35				0.4	2.513		40.817
	36		240	0.4	0.3	1.885	6.60861	28.523
Repeatability test								
Set 5	37	30	300	0.5	0.8	5.0265	6.86364	73.234
	38							
	39							
	40							
	41							

(*H = Height of the test tank; h_S = Fill water level; L= Length of the tank*).

6.3.1 Uncertainty Analysis

Uncertainty is a quantification of the doubt about the measured result. The maximum possible uncertainty is estimated from the minimum value of quantity measured and accuracy of the measuring system. The maximum error calculated while measuring the excitation frequency is 0.014 cycle/sec. The experiments were repeated and found consistent. (The detailed error analysis is discussed in Appendix A-2).

6.3.2 Repeatability of Experiments

In the experimental plan as mentioned in Table 6.1, the set 5 was used for the check repeatability of experiments. The repeatability of the slosh phenomenon was investigated by running the same experiment several times. The test is conducted by plotting the height versus time for case numbers from 37 to 41 which is sketched in Figure 6.7. It is seen that the measurements are very close to each other. To get a measure of how close the experiments are, the standard deviation is calculated for each time instant. The calculation of the standard deviation $\sigma(t)$ is given by

$$\sigma(t) = \sqrt{\frac{1}{4}\sum_{i=1}^{5}(\zeta(t) - m(t))^2} \tag{6.3}$$

$$m(t) = \frac{1}{5}\sum_{i=1}^{5}\zeta_i(t) \tag{6.4}$$

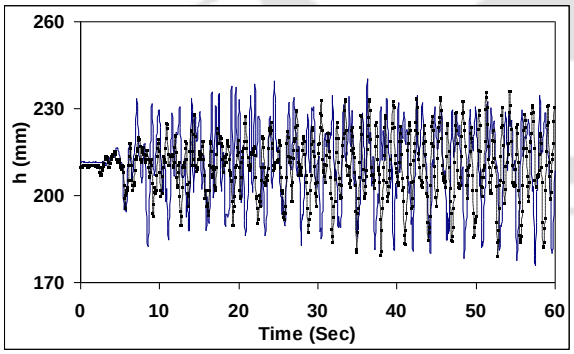

Figure 6.7: Repeatability test (case-37 to 41).

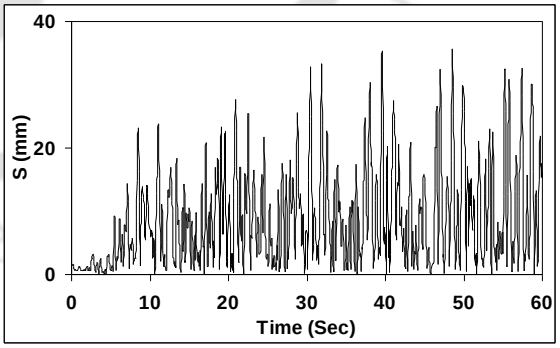

Figure 6.8: Standard deviation of experiments (case-37 to 41).

where ζ_i is the measured surface elevation of experiment i = *1,2 . . . ,5* and $m(t)$ is the average of all experiments. The standard deviation $\sigma(t)$ is shown in Figure 6.8. The standard

deviation is found smaller as compared to the measured value, thus showing the repeatability of the tests.

6.4 Results and Discussion of Free Surface Elevation

6.4.1 Effect of Excitation Amplitude

As the rectangular tank oscillates, different sloshing waves are created depending on the liquid depth and frequency of oscillations. These waves are asymmetric and at large amplitude, the tank excitations may be combined with the travelling waves. Liquid height for different frequency ratios under low excitation amplitude (EA=30 mm) for cases 11 and 12 as per Table 6.1 is shown in Figures 6.9 and 6.10 respectively. For the case of low amplitude excitation, the liquid height reaches the steady level quickly. It is observed that the slosh amplitude follows a sinusoidal pattern which means slosh amplitude increases initially with the increase in applied frequency and thereafter it decreases and again with the increase in external frequency the slosh amplitude increases. This is because of the sinusoidal nature of applied external excitation.

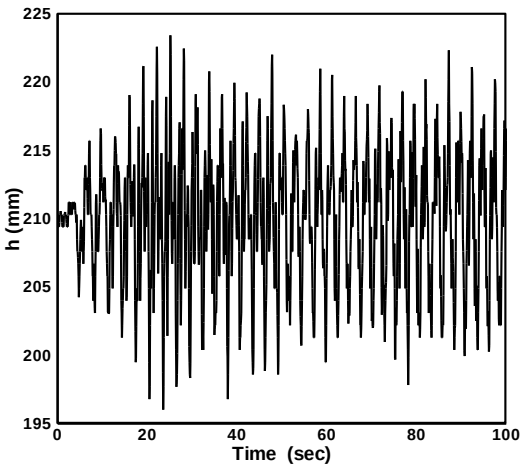

Figure 6.9: Free surface elevation for case-11 (FR=39 %; h_s/L =0.35; EA=30 mm).

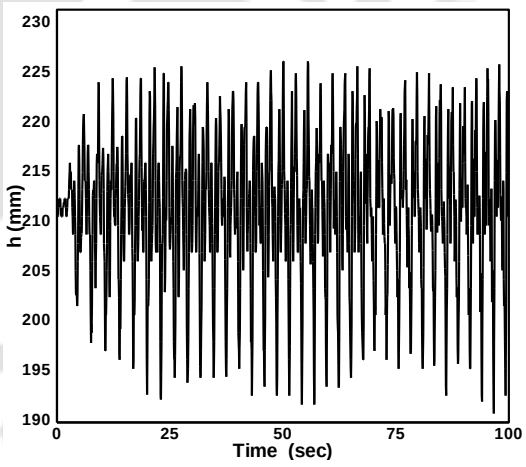

Figure 6.10: Free surface elevation for case-12 (FR=49 %; h_s/L =0.35; EA=30 mm).

As the amplitude of excitation is increased (EA=100 mm), the liquid responds violently related to the fluid motion that occurs due to the occurrence of turbulence, hydraulic jump, wave breaking and 3-D effects. Figure 6.11 shows the liquid height for different frequencies at 100 mm excitation amplitude. It has been observed that the wave amplitude grows initially

with the time up to a certain time period. After reaching this period, the wave amplitude remains constant and enters the fully developed region. In other words, in the first phase, the wave amplitude rises slowly from mean level up to certain period whereas in the second phase, a uniform oscillation can be observed. Similar trend is noticed for rest of the cases (case-28 to case-36) in set 4 experiments of Table-6.1. Free surface oscillation or the instantaneous wave height (h) for first phase (i.e., 0 to 20 seconds) and for second phase (i.e., 100 to 120 seconds) at tank left wall for case-28 is shown in Figures 6.12 (a) and (b) respectively and their corresponding wave phase plane diagrams are depicted in Figure 6.13 (a) and (b). In each case, the instantaneous wave height is plotted for first phase and second phase time periods.

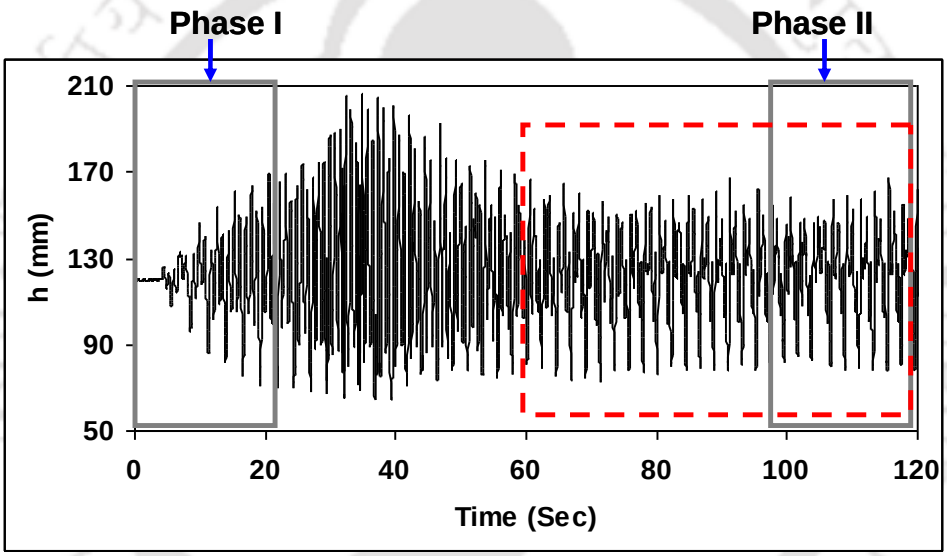

Figure 6.11: Free surface elevation for case-28 (FR=29 %; h_s/L =0.35; EA=100 mm).

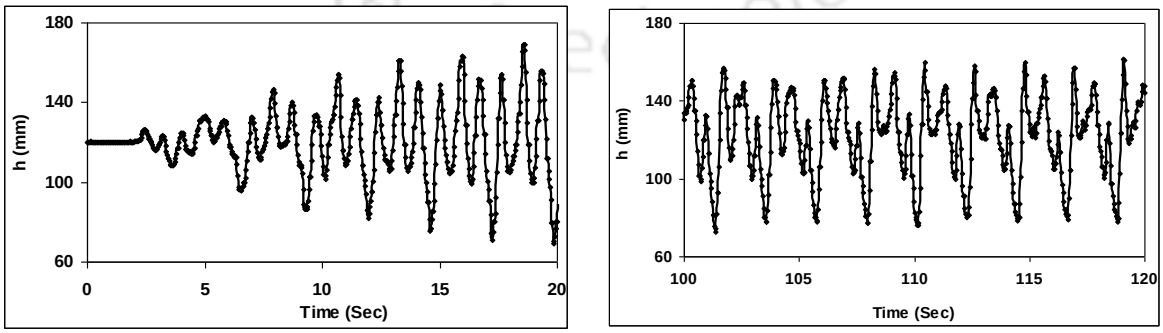

(a) (b)

Figure 6.12: Free surface elevation for case-28 (a) phase I; (b) phase II.

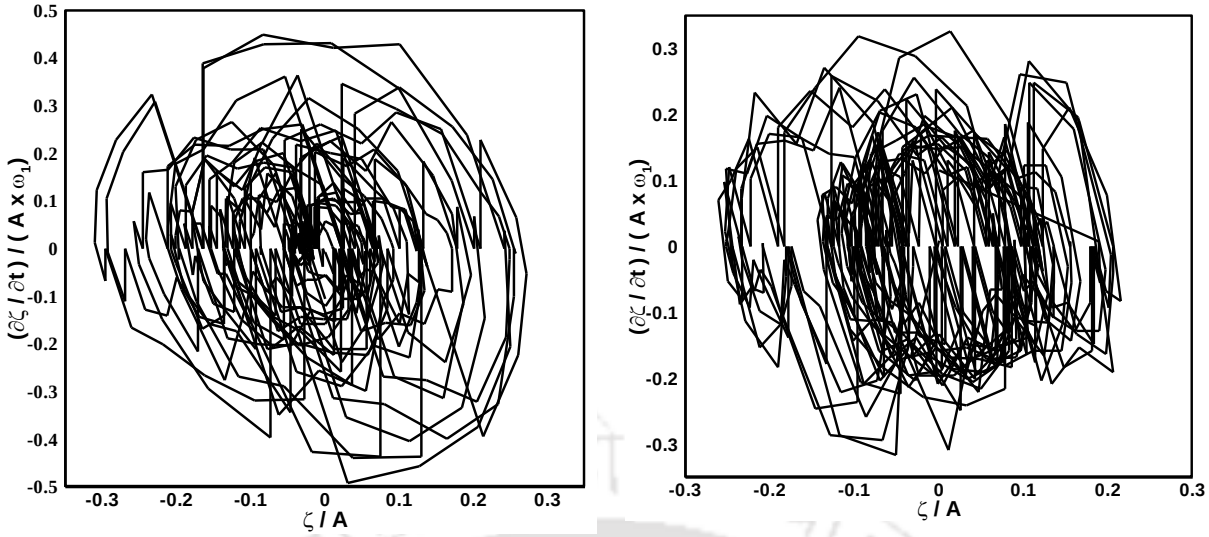

(a) (b)

Figure 6.13: Phase plane diagram for case-28: (a) Phase I; (b) Phase II.

6.4.2 Effect of Excitation Frequency and Fill Level

As the tank moves, it supplies energy to sustain the liquid motion. The four possible types of waves are standing wave, traveling wave, hydraulic jump and a combination of these. Figures 6.14 and 6.15 show the effect of excitation frequency and effect of fill level. As the frequency increases, the standing wave transforms into a train of traveling waves of very short length, and the hydraulic jump occurs near first mode natural frequency. Further, with increase of frequency, the standing wave transforms into a train of traveling waves of very short length. Hydraulic jump, usually, takes place due to a small disturbance and appear over a range of frequencies near the resonant frequency (Akyildiz and Unal, 2005). With further increase in frequency, the jump will pass into a solitary wave. For deeper liquid, sloshing near the resonance is characterized by the formation of large amplitude standing waves. These waves are asymmetric in nature, and at a large amplitude, tank excitations may be combined with the traveling waves.

Figure 6.16 shows the bar chart representation of maximum and minimum wave heights for case 1 through 4. The maximum and minimum wave height for first phase and second phase is represented as Imax, Imin and Smax, Smin respectively. It shows that the maximum wave height increases and minimum wave height decreases while increasing the frequency.

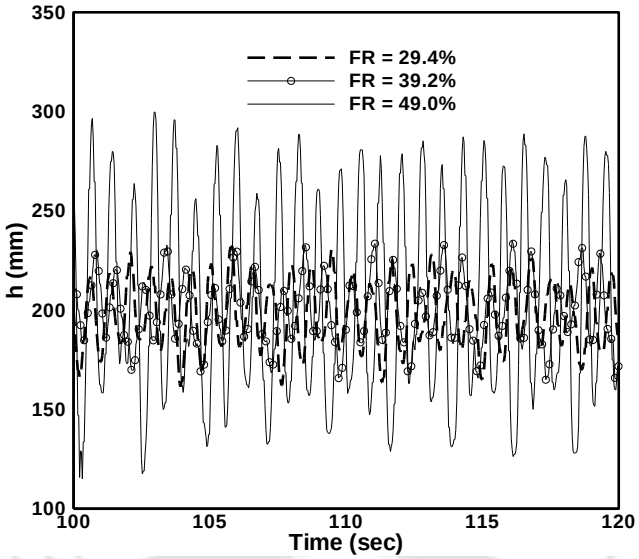

Figure 6.14: Effect of frequency for cases – 13, 14 and 15 (h_s/L =0.35; EA=40 mm).

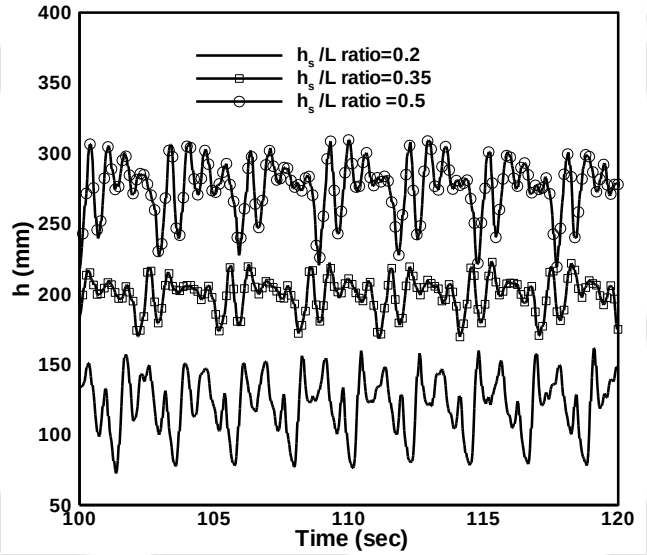

Figure 6.15: Effect of fill levels for cases-8, 17 and 27 (FR ≈ 49; h_s/L =0.35; EA=30 mm).

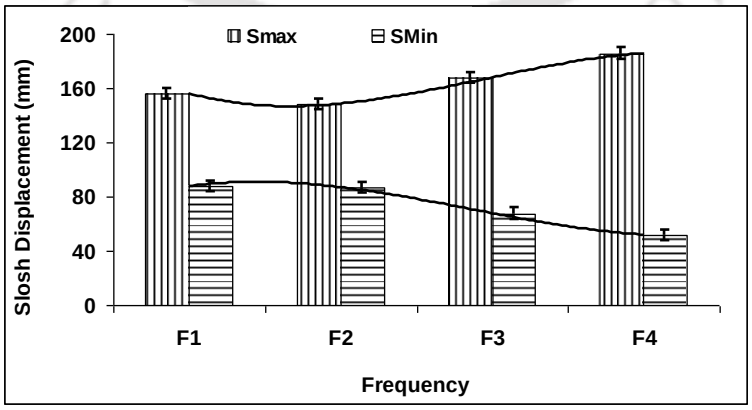

Figure 6.16: Bar chart representation of maximum and minimum slosh displacement with frequency for cases-28 to 31(h_s/L =0.35; EA=100 mm). (F1 – 1.885 rad/sec, F2 – 2.199 rad/sec, F3 – 2.513 rad/sec, F4 – 3.142 rad/sec).

6.4.3 Spectra of Wave Elevation

The spectra of a wave elevation are computed by the Fast Fourier Transform (FFT) as shown in Figure 6.17, where *S* is the wave elevation spectrum. Figure 6.17 shows the spectra of wave elevations at the tank left corner. It causes peaks in the power spectra and more peaks appear at different frequencies. The sloshing waves have been analyzed with the probability density and energy spectrum.

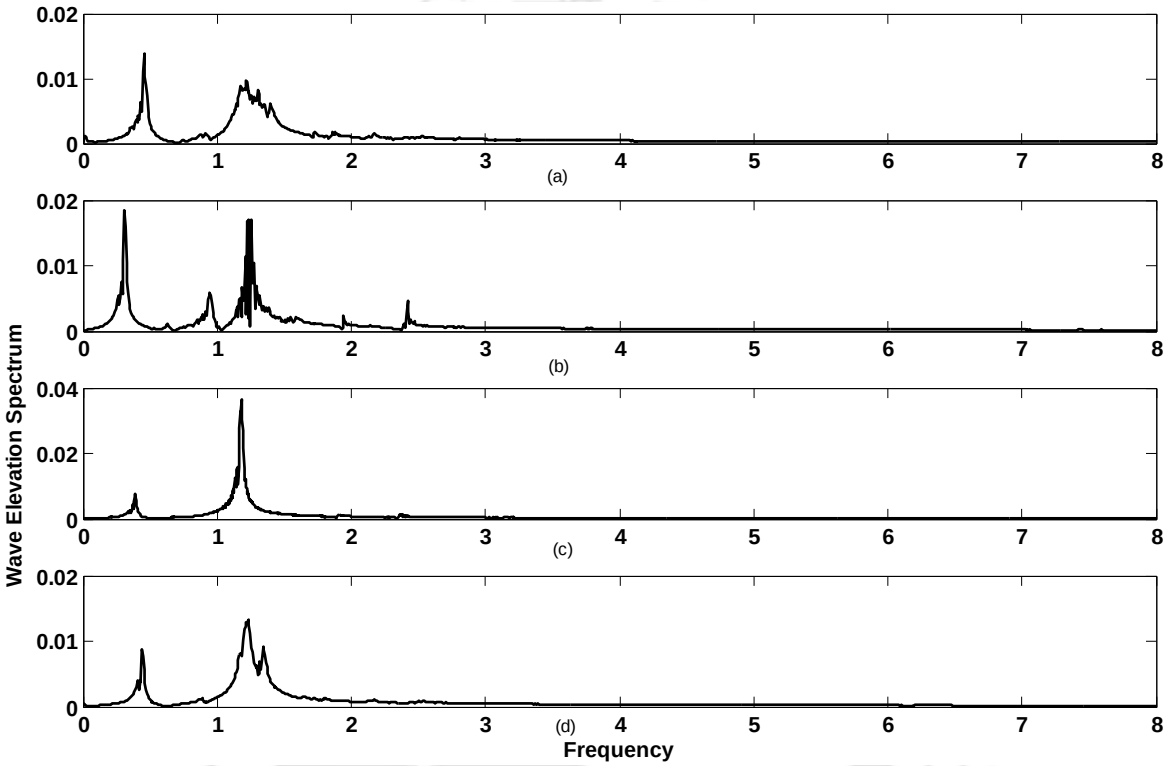

Figure 6.17: Power spectra of wave elevation at the tank left corner: (a) case-28; (b) case-29; (c) case-30; (d) case-31.

6.5 Comparison of Experimental and Numerical Results

In this subsection, the experimental results for two different frequency ratios are compared with the data of numerical simulation and are shown in Figure 6.18 and 6.19. A minor discrepancy has been observed in free surface elevation between simulated and experimental results during the motion of tank. Two cases are considered for such a validation by choosing two different frequency ratios. In both the cases, the excitation amplitude and the fill ratio (h_s/L=0.5) remains constant. The EA value has been chosen as 30 mm since better results can

be expected with low excitation amplitude for the present experimental and numerical works. When the results are closely examined, one can observe that the numerical results clearly over scoop the experimental results for the case of high frequency ratio (Figure 6.19). But when the frequency ratio is low, the crest and trough points in both results are matched well.

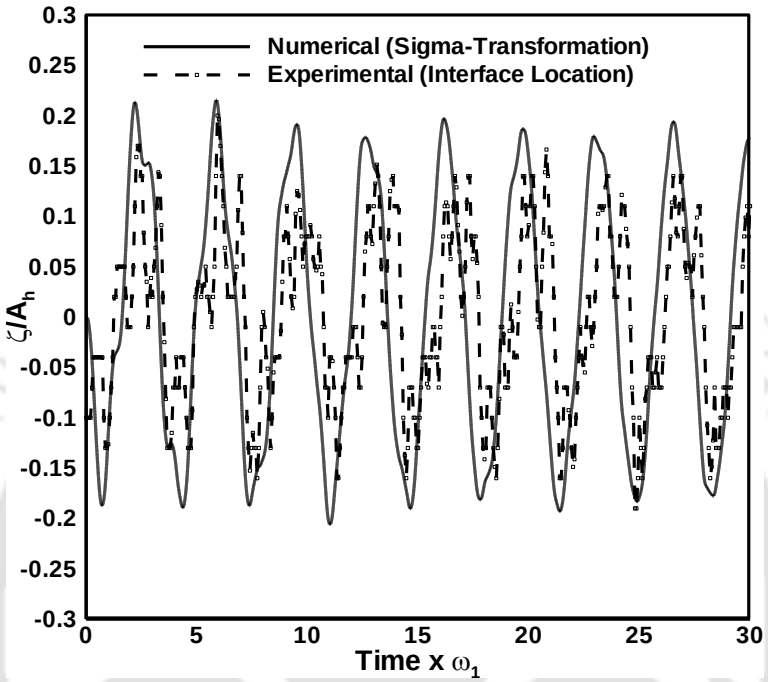

Figure 6.18: Free surface elevation for case-19 (FR=27.4 %; h_s/L =0.5; EA=30 mm).

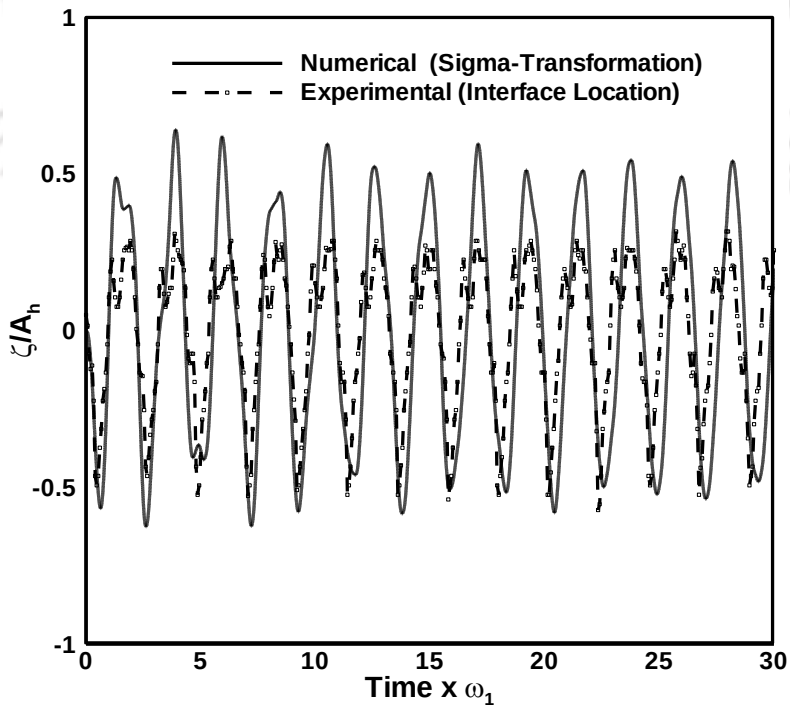

Figure 6.19: Free surface elevation for case-20 (FR=36.6 %; h_s/L =0.5; EA=30 mm).

6.6 Summary

This chapter is devoted to present the experimental procedure for finding the free surface elevation in a moving rectangular tank. The liquid free surface behavior at low frequency oscillation has been elaborately studied from experiments. Initially, the history of wave or long term behavior of free surface oscillation (0 to 120 seconds) is observed. Thereafter, to study in detail, two time phase periods are focused and instantaneous wave heights are plotted for each case. It has been observed that the wave amplitude grows initially with the time upto a certain time period. After reaching this period, the wave amplitude remains constant and enters the fully developed region. It is found that the maximum wave height increases with an increase a frequency, while the minimum wave height decreases with increasing frequency. It also causes the peaks in the power spectra to become larger and encourages more peaks to appear at different frequencies. The sloshing waves have been analyzed with the energy spectrum. It is clear that the trend of deviation of wave height increases with an increase in frequency. This suggests that a stronger nonlinearity give rise to the increase of the deviation. It is interesting to note that such an increase seems to indicate a fairly linear trend with frequency. Finally, the experimental data was compared with the results obtained from numerical simulation.

Chapter 7

EXPERIMENTAL INVESTIGATION OF LIQUID FREE SURFACE VELOCITY

In this chapter, the unsteady free surface velocities during the surge motion of a liquid tank determined through experiments have been discussed. A new experimental approach has been discussed for capturing the liquid free surface velocity during the tank excitation. The velocities are measured for various liquid fill levels and excitation frequencies. The average line velocity at the tank wall (V_W) and tank center (V_C) with respect to time are estimated and compared with the tank velocity.

CONTENTS

7.1 Introductory Remark

In order to avoid the violent motion, the tank is excited with low frequency (upto 47% of first mode frequency) which leads to the low steeping waves in the tank. When a tank oscillates at low excitation frequency, the wave amplitude (*A*) is usually small. Since the wave steepness (*E*) is directly proportional to the wave amplitude, the wave steepness is also small during the motion. The planar 2-D Particle Image Velocimetry (PIV) technique is used to calculate the *U* and *V* velocity of the free surface, while the interface location technique is used for finding the vertical velocity of the interface (*W*).

7.2 PIV Technique

The basic theory for particle image velocimetry was first presented nearly 25 years ago and the technique has undergone tremendous developments in the last fifteen years (Adrian, 2004). PIV is a non-intrusive measurement technique for studying the velocity profiles. It uses images of marker particles in a fluid flow to measure instantaneous velocity fields. It is a technique which enables instantaneous measurement of the flow velocity at several positions in a plane. Two images of each particle in the sheet are recorded in a short time interval. This technique relies on the imaging of tracer particles embedded within a flow at two distinct times, t_1 and t_2 to estimate the velocity of the fluid. The distance separating the two images gives a local velocity vector. The images are generally recorded onto either a film (photographic or holographic) or a charge coupled device (i.e CCD) array. The correlation analysis is used to extract the particle displacements, Δx and the first-order velocity estimate,

$$u = \frac{\Delta x}{\Delta t}, \tag{1}$$

where Δx is the average displacement of particles in the fluid over the time interval $\Delta t = t_1 - t_2$ (Hu *et al.*, 1999). The t_1 and t_2 images can either be made on the same frame or on separate frames (referred to as one-frame and two-frame PIV respectively).

Sloshing can be broadly classified into two types, namely self-induced sloshing and externally induced sloshing, based on how sloshing is generated inside the tank. The main difference is that, in self-induced sloshing, the tank is immobile whereas in externally induced sloshing, the tank will move owing to external disturbances. In the case of externally induced sloshing, external forces such as an earthquake or a sudden brake on a moving tank

vehicle act as the excitation source for sloshing. This type of sloshing can be found in real-time applications such as liquid-oil carrier vehicles, space vehicles, and LNG vessels in cargo ships. The fluid dynamic mechanism of the externally or self-induced sloshing phenomenon should be understood clearly in order to attain an optimum safety design of the reactor vessels to prevent the occurrence of sloshing (Saga *et al*., 2000a). For example, in a liquid metal fast-breeder reactor, the self-induced or externally induced sloshing of the high-temperature sodium coolant may occur in reactor vessels. This kind of sloshing will result in very high thermal stresses on the vessel walls, which may cause severe damage to the vessel structure (Okamoto and Madarame, 1998).

In the case of self-induced sloshing, the tank is stationary so that the images can be easily taken for particle image velocimetry (PIV) analysis. However, if the tank moves, the camera probably cannot focus on the liquid portion alone. This means that it is possible that the tank can slide away from the camera's focus area. For the above reason, image processing cannot be performed easily for this type of distorted image with accuracy. Hu *et al.* (1999) investigated the self-induced sloshing phenomenon using the PIV technique experimentally and found three different flow patterns in the test tank for the same system parameter settings. They are the reverse vortex flow pattern, the first-sloshing-mode flow pattern, and the second-sloshing-mode flow pattern. As reported by Hu *et al.* (1999), self-induced sloshing in a rectangular tank was first systemically studied by Okamoto *et al.* (1991). PIV and also Laser Doppler Velocimetry (LDV) measurements on self induced sloshing flow in a rectangular tank were conducted by Saga *et al.* (2000a) and the PIV measurements were compared with the LDV measurements quantitatively in order to evaluate the accuracy level of the PIV measurements. Singh *et al*. (2006) measured the magnitude of fluid velocity fluctuations from PIV analysis for a concentrated suspension in free-surface flow in a channel. A comprehensive experimental programme was conducted by Nasar *et al.* (2009) to find the liquid sloshing pressure in a rectangular tank inside a barge and the barge responses. Several investigations on self-induced sloshing in a rectangular tank with circulating flow have been conducted experimentally and numerically in the past 20 years (Takizawa *et al*., 1992; Okamoto *et al*., 1993; Fukaya *et al*., 1996). Most of the studies on sloshing were limited to self-induced excitations. However, works in the area of flow visualization techniques on externally induced sloshing with surge motion of the tank is scarce.

The present work deals with the study of the liquid free-surface velocity in a moving tank experimentally. The primary objective is to find the *U*, *V* and *W* velocity components of the free surface of the liquid for low-steepness waves. When a tank oscillates at a low excitation frequency, the wave amplitude *A* is usually small. It is the amplitude that decides the wave steepness. The wave steepness is defined as $E = A\omega_n^2 / g$ (Frandsen, and Borthwick, 2003), where *A*, ω_n and *g* are the wave amplitude, natural frequency and the acceleration due to gravity respectively. At low excitation frequencies, the images of the free surface of a liquid with low-steepness waves are captured by a video camera. These images are then transferred to the computer and cross-correlations of images are performed using the PIV Sleuth software which offers efficient interrogation for image analysis (Christensen *et al*., 2000).

7.3 Investigation Procedure for Free Surface *U* and *V* Velocity

The liquid free-surface *U* and *V* velocities were calculated using the planar two-dimensional (2-D) PIV technique. The following sections describe the experimental arrangements and techniques for processing images.

7.3.1 Experimental Set-up for *U* and *V* Velocity

A steel stand made from two vertical thin slotted steel sheets is kept at the side of the tank and another similar slotted steel sheet was connected horizontally between the two vertical steel rods with the help of nuts and bolts, as shown in the Figure 7.1. The steel stand is placed at a suitable position across the tank. The video camera (Sony DCR-SR 300 Handycam Camcorder) is screwed on to the middle horizontal beam with its lens focusing down on the liquid. The middle horizontal steel beam is moved up or down until a suitable slot is reached so that the camera focuses only on the liquid during its entire motion. The camera is held at a distance of 1m away from the free surface of the liquid and focuses on the free surface of the water. Figure 7.2 shows the top view of the test tank. Acrylic-paint-coated thermocol balls with an average diameter of 6 mm are used as a tracer or marker particles. After adding a colouring agent (navy blue) in the tank liquid, an excellent contrast between the liquid and the white marker particles is obtained that gives a superior image quality with less noise. Experiments have been conducted under natural light by covering the sides of the tank with black cloth to improve the contrast further between the liquid and the seed particles. A horizontal excitation is imparted to the tank using an arrangement consisting of a motor and a

cam. The motor is allowed to rotate and its speed is varied using a speed controller. The speed of the motor is kept sufficiently low so that sloshing occurs without much turbulence. The tank can be filled to any desired height. In order to achieve this, a scale attached to the side wall of the tank is used. The experiments were conducted by varying h_s/L ratio of the tank for different case studies. The images captured by the video camera are then transferred to the computer and further image analysis is carried out using the PIV Sleuth software which offers efficient interrogation for image analysis.

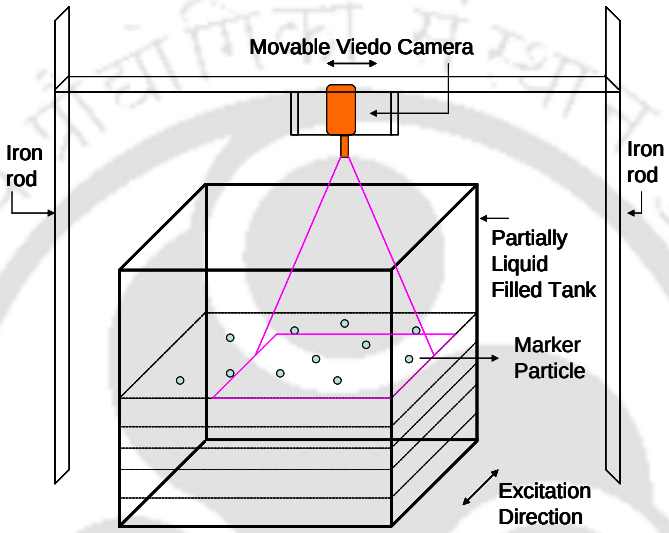

Figure 7.1: Camera arrangement in the setup for measuring the *U* and *V* velocities.

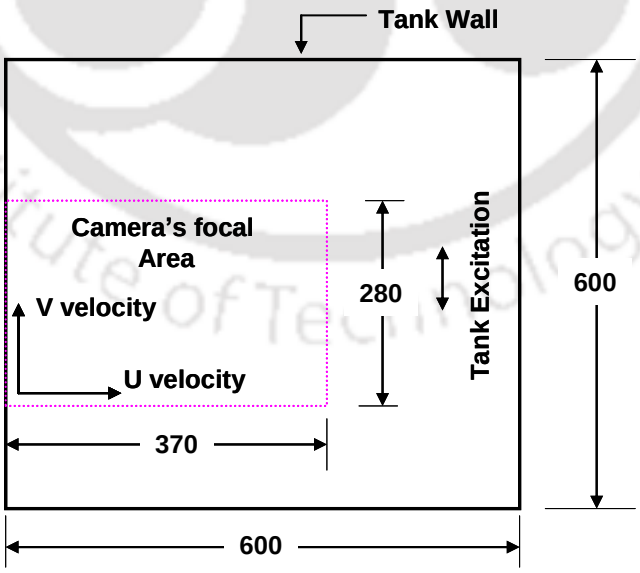

Figure 7.2: Top view of the test tank.

Normally, the tracer particle sizes are smaller for the cases in which the tracer particles have the same density as the fluid. However, in the present investigation, the objective is to measure the surface velocities, and hence, floater particles have been used. Since the tank area is quite large in comparison with the particle size, the 6 mm floaters are not expected to disturb the flow. Moreover, the use of a slightly larger floater particle helps not only to keep track of the movement of the particles but also to capture good quality images. It has been observed that at low excitation frequencies of the tank, the floater particles do follow the real flow of the liquid. Some trial experiments have been conducted at various excitation frequencies with different sizes of marker particles and different numbers of marker particles so as to arrive at a final selection. Furthermore, sufficient care has been taken to ensure that the marker particles do not cluster during the motion. The markers should float on the liquid surface and be clearly visible through the camera.

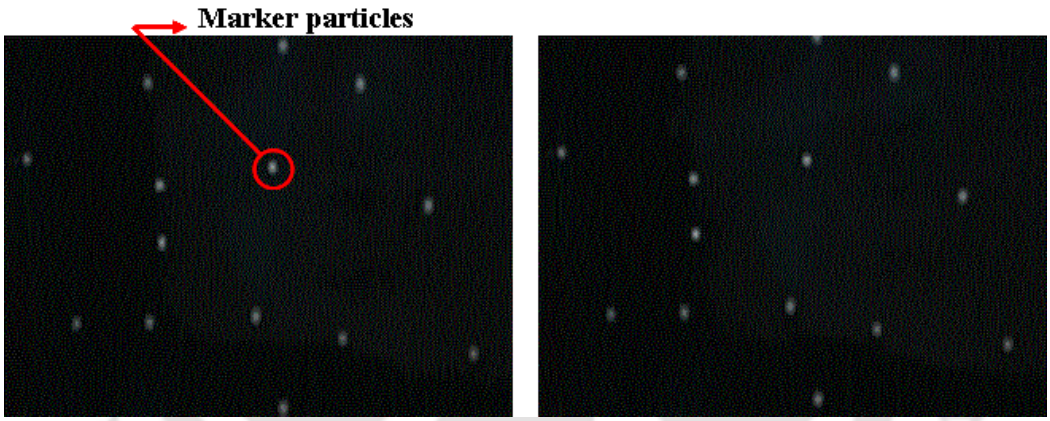

Figure 7.3: Two sample image frames.

7.3.2 Interrogation of PIV images

The video of marker particles on the free surface captured from the video camera is transferred to the computer. The first 20 seconds of video are then analyzed because the waves in the tank moved the marker particles slowly away from the focused area. Two sample frames of images of size 320 × 240 pixels can be seen in Figure 7.3. Once the spatially displaced images are stored in two separate frames, each velocity vector is extracted by performing mathematical correlation analysis on a cluster of particles within each interrogation region between the two frames (eliminating the problem of directional ambiguity). The PIV interrogation process is repeated until all the required velocity information is extracted from the captured record. Figure 7.4 shows the step-wise

interrogation process in detail. Typically, the image field is divided into small sub-domains referred to as interrogation spots. Each of these sub-domains is then analyzed separately to obtain the velocity field over the entire image. It should be noted that the velocity of a particular interrogation spot is a function of the average displacement of the particles in the spot (Christensen *et al*., 2000).

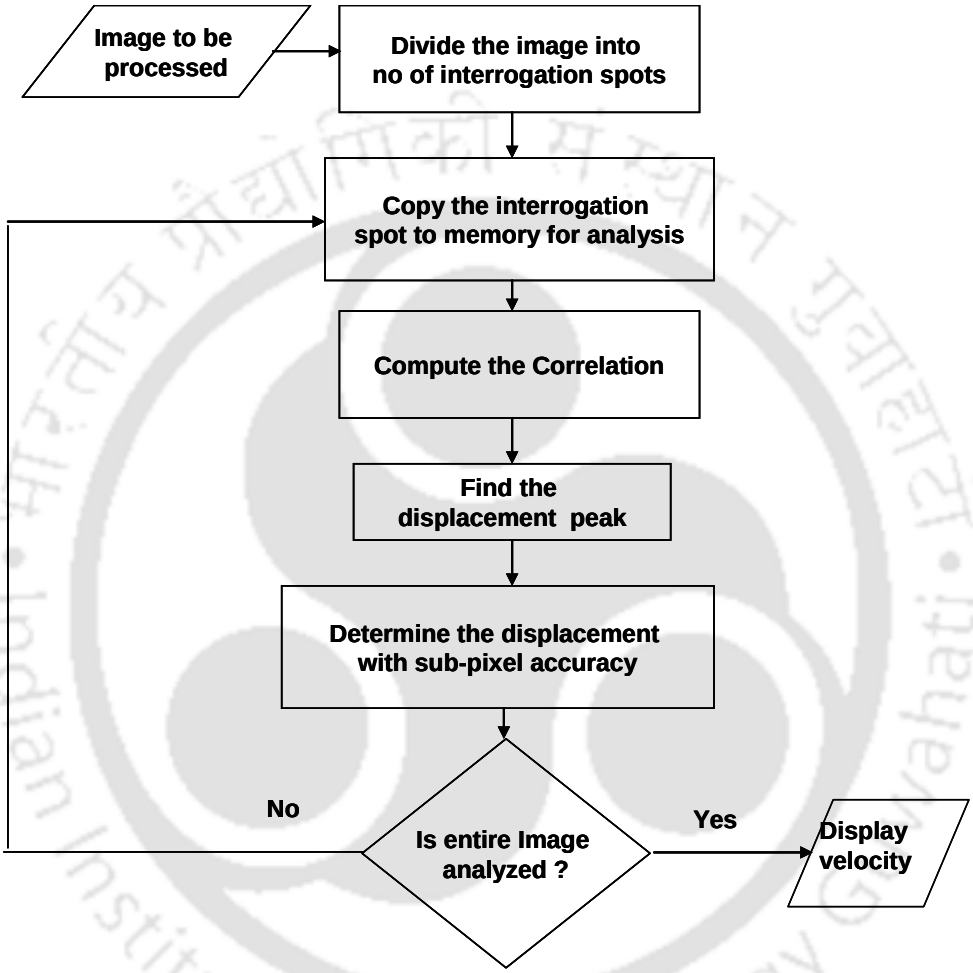

Figure 7.4: Interrogation flow chart.

7.3.3 Cross Correlation of Image

Correlating the first interrogation spot with a second spot that is offset in the mean flow direction is known as cross-correlation analysis. The aim of the cross-correlation is to find the distance that the particle pattern has moved during the interimage time and to translate this into a velocity measure. The direct method to compute the cross correlation quickly becomes very heavy to apply when larger data sets are to be analyzed. A more efficient way to estimate cross-correlation functions is to use FFTs (Bendat and Piersol, 1986). This is

classified into one-frame and two-frame cross-correlation. The second-order correlation technique is applied here to increase the effective spatial resolution without loss of accuracy. This technique is developed by Hart (1998). The basic principle is that correlation planes of adjacent interrogation spots are compared in an effort to reduce the measurement noise and to enhance the displacement peak (Christensen *et al.*, 2000). Since only a single displacement peak is obtained, two-frame cross-correlation analysis is ideal for flows that have reversals, since no extra image shifting is necessary to resolve directional ambiguities. Also, two-frame cross-correlation is a highly accurate method and is used in this analysis. As the noise in the correlation should be random, there should be no correlation of the noise between the adjacent interrogation spots. This technique increases the signal-to-noise ratio.

As discussed above, the images were analyzed using the two-frame cross-correlation method. In this method, the pair of images was converted on to separate frames. Interrogation windows with an FFT size of 128 × 128 pixels were chosen and the second frame was offset from the first by 10 pixels in the stream-wise direction. Erroneous vectors were removed from the vector field. The video of tank motion containing water and marker particles taken from the video camera was first converted to frames which were then analyzed using the PIV Sleuth software. A MATLAB code was written to generate the velocity profiles and to compute the average velocities in both the *x* direction (namely *U*) and the y direction (namely *V*) over an entire second. This was because, for each second, 30 data files were created similar to the number of frames in a second.

7.4 Experimental Procedure for determination of Vertical Velocity

It is difficult to find experimentally the liquid free surface vertical velocity at all the points in a moving tank. The liquid free-surface velocity can be found at a particular location using a traditional wave height gauge such as a capacitance wave height gauge (Pal and Bhattacharyya, 2010). The wave height gauge gives the free surface elevation at a particular point. The velocity can be found from the variation in the elevation with respect to time at a particular location. This work pays attention to the image-processing technique to find the vertical velocity during liquid sloshing under a low excitation frequency. If the camera moves together with the tank, it can be focused at a particular location continuously. In the present investigation, the effect of the low excitation frequency of the tank on the liquid free-surface elevation is studied near the left end of the tank.

7.4.1 Experimental set-up

The experimental arrangements are the same as discussed in Chapter-6. The video camera is screwed on to an adjustable beam which is attached to the shaking platform with its lens focusing on the free surface of the liquid at the left corner of the tank, as shown in Figure 6.2. The adjustable beam is moved up or down until a suitable slot is reached so that the camera focuses only on the liquid during its entire motion. The camera was held at a distance of 300 mm away from the free surface of the liquid and focuses on the free surface of the water. Initially, the relation between the pixel and the millimetre has been found by still images. The interface location technique is used to capture the free surface elevation versus time and the free surface velocity is calculated from the elevation.

7.4.1.1 Location of the interface and determination of the vertical velocity

The procedure for interface location technique was discussed in Chapter-6 in detail. However, in brief, the videos captured by the video camera are transferred to the computer and further image analysis is carried out. A MATLAB code was written to compute the free-surface displacement of the liquid. The intensity gradient at each point is calculated. The location of the maximum gradient was considered as the interface, as described by Law *et al. (*1999). The luminance contrast between the liquid and the air, which indicates the location of the interface, is determined by the maximum intensity- gradient method. In other words, the liquid height is observed using the variation in the intensity of the interface between the air and the liquid.

7.5 Results and Discussion of Free Surface Velocities

Depending upon the type of the liquid, the nature of external disturbances on the tank and tank shape, and the h_s/L ratio, the free liquid surface can experience different motions such as simple planar, non-planar, rotational, irregular beating, symmetric, asymmetric, quasi-periodic and chaotic (Ibrahim, 2005). The amplitude of the slosh wave, in general, depends upon the nature, amplitude and frequency of the tank motion, the liquid-fill depth, the liquid properties and the tank geometry (Pal *et al*., 2002, Akyildiz and Unal, 2005, Akyildiz and Unal, 2006). As the rectangular tank oscillates, different slosh waves will be created depending on the liquid depth and the frequency of oscillations. In this study, the problem

was restricted to liquid sloshing in a rectangular tank under surge (movement of the tank only in the horizontal direction) oscillations. The dynamic tank velocity V_t can be determined from the following equation

$$V_t = -A_t \omega \cos(\omega t), \tag{7.1}$$

where A_t is the tank excitation amplitude and ω is the oscillation frequency. The amplitude of the tank excitation is 100mm. Figure 7.5 shows the theoretical dynamic tank velocity for 0.3 cycle/s and 0.4 cycle/s which are computed using equation (1). These motions are undoubtedly symmetric. For a given rectangular prismatic tank, the natural frequencies of the fluid depending on the fill depth are given by

$$\omega_n^2 = g \frac{n\pi}{L} \tanh\left(\frac{n\pi}{L} d\right) \tag{7.2}$$

where L is the tank width, d is the water depth and n is the mode number (Akyildiz and Unal, 2005). In Table-6.1, the liquid h_s/L ratios at corresponding frequencies for different cases are shown.

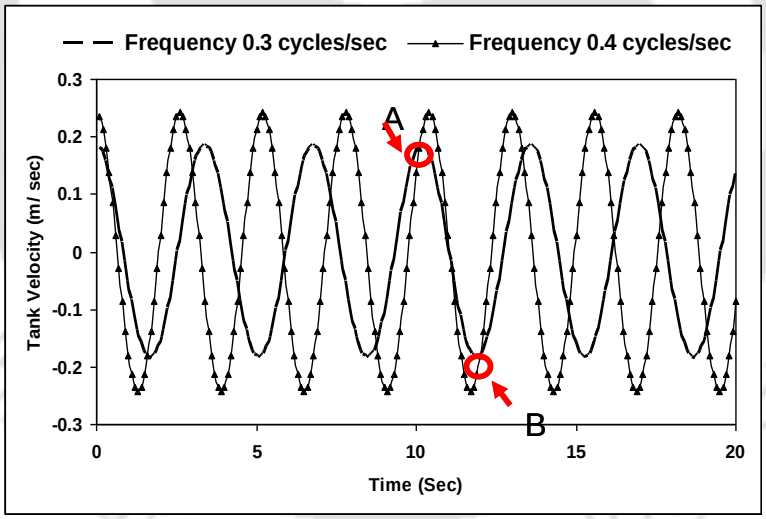

Figure 7.5: Dynamic tank velocity profile with respect to time.

The analysis is carried out at two different frequencies and at three different h_s/L ratios, as indicated in Table 6.1. The repeatability of the sloshing phenomenon was examined by running the same experiment several times. The maximum error is calculated while the excitation frequency is 0.014 cycle/s. The experiments were repeated and found to produce consistent results. It should be noted that, at higher frequencies, the turbulence level becomes higher. This requires the use of sophisticated instruments such as a laser sheet, a mirror arrangement, a high-quality camera and glittering particles. Usually, the laser sheet is passed

through mirrors to the tank liquid which has the glittering tracer particles and a high-quality video camera captures the movement of the tracer particles. However, the present work deals with low excitation frequencies (or low-steepness waves) and hence the image-processing technique is used. Figure 7.6 shows the velocity components and the corresponding notation used in this study. As shown in the figure, the liquid free-surface velocity V_f was classified as the average line velocity V_w near the wall and the average line velocity V_c near the tank centre. The average line velocity V_w near the wall will have two components, namely U_{vel} and V_{vel} (i.e. the velocity U and the velocity V respectively). Similarly, the average line velocity V_c near the tank centre will have the same two components. U_{vel} is perpendicular to the tank excitation direction and V_{vel} is parallel to the tank excitation direction. This section addresses the experimental set-up arrangement and procedure to find these velocities. The procedure and arrangement corresponding to the vertical velocity W have been reported in section 7.4.

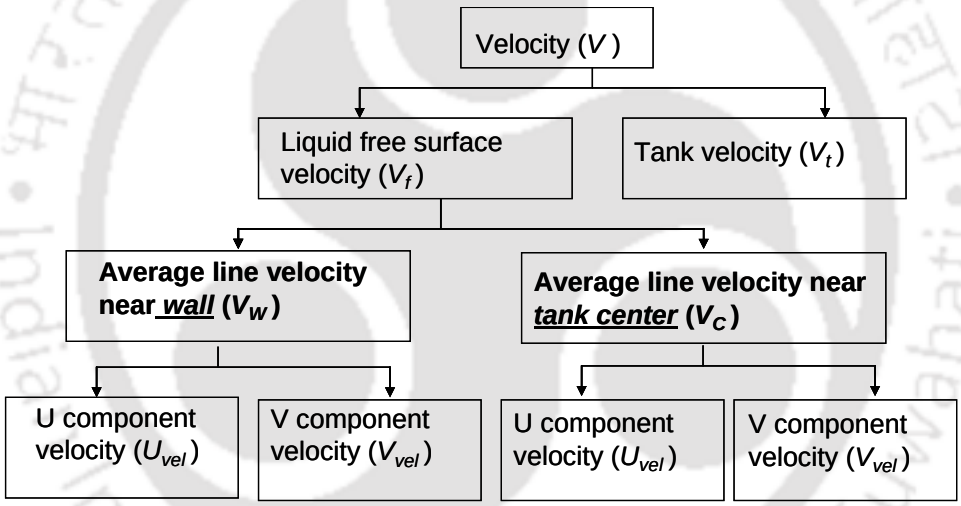

Figure 7.6: Associated velocity terms and notations used in PIV study.

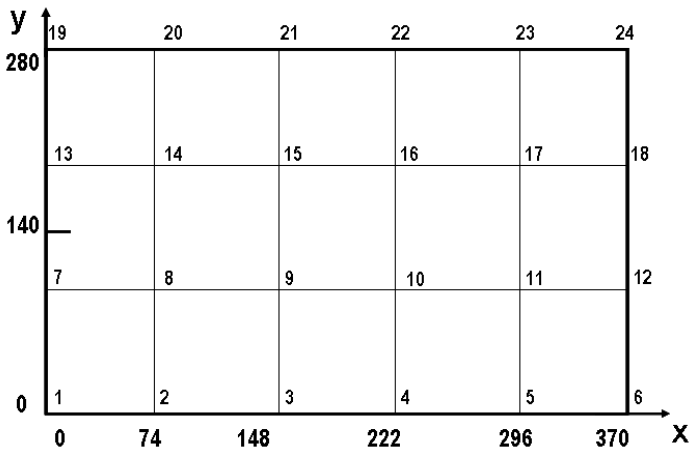

Figure 7.7: Velocity locations of camera's focal area in fluid domain for FFT size 128 × 128 pixels, where the x and y scales are in millimeters.

7.5.1 Average Line Velocity near Wall and Tank Center

In order to study the velocity variation and free surface profile through the PIV technique, a series of experiments in the above set-up was carried out. The cross-correlations of images were performed for an FFT size of 128 × 128 pixels. For analysis with an FFT size of 128 × 128 pixels, the image field is divided into small sub-domains referred to as interrogation spots of size 128 pixels in both directions. Figure 7.7 shows the schematic diagram of interrogation windows used in the cross-correlation analysis for an FFT size of 128 × 128 pixels. This analysis gives instantaneous velocities at 24 locations in the camera's focal area on the fluid domain. In Figure 7.7, the grid points 1, 7, 13 and 19 are closest to the tank wall. Averaging the velocity vectors at these locations gave the measurement of the wall velocity. Similarly, the tank average centre-line velocity was obtained by averaging over the grid points 5, 11, 17 and 23, which approaches 300 mm approximately. In other words, as the width of the tank is 600 mm and the camera focal length is 370 mm (Figure 7.2), the focal area is divided into five (Figure 7.7). Thus, the fourth vertical line (grid points 5, 11, 17 and 23) shows the tank centre-line. The ultimate aim is to find the average line velocity near the wall and near the tank centre.

When an external force is applied to the tank, the liquid will oscillate together with the tank initially. However, the momentum of the liquid will provide some additional energy to the liquid. This applied excitation force and the additional energy created owing to momentum is divided into three component velocities U_{vel}, V_{vel}, and W_{vel} of the fluid. Since the liquid behavior is analyzed from the top of the tank, only the U_{vel} and V_{vel} values of the liquid are plotted here. V_w and V_c are compared with the tank velocity V_t in Figures 7.8 (a) to (c) for Case -32 (the h_s/L ratio of the tank 0.2 and the excitation frequency of tank motion 0.3 cycle/s). The surface velocities are measured for 6–7 cycles of tank excitation. During this interval the velocity vectors have been obtained at every 0.033 *seconds*. The approximate maximum velocities V_{vel} of fluid for V_c and V_w are 0.15 *m/s* and 0.1 *m/s* respectively. However, the maximum value for V_t is 0.2 *m/s* (Figure 7.5). Since the present experiments have been conducted at very low excitation frequencies, steady state is reached much more quickly. Furthermore, to calculate the *U* and *V* velocities using the PIV technique, the results are shown for the first 20 *seconds*. This period is sufficient to demonstrate the initial propagation of the wave for low frequency oscillations. For almost all the cases, the waves have developed completely within the first two or three oscillations.

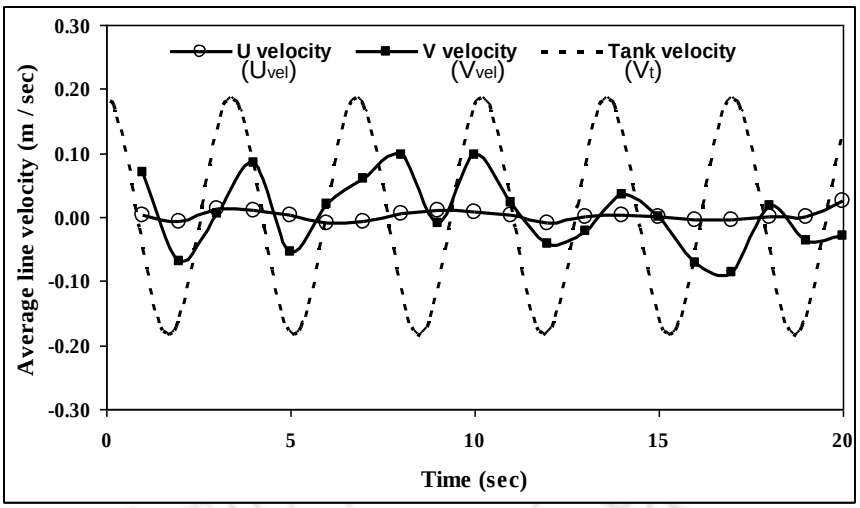

(a)

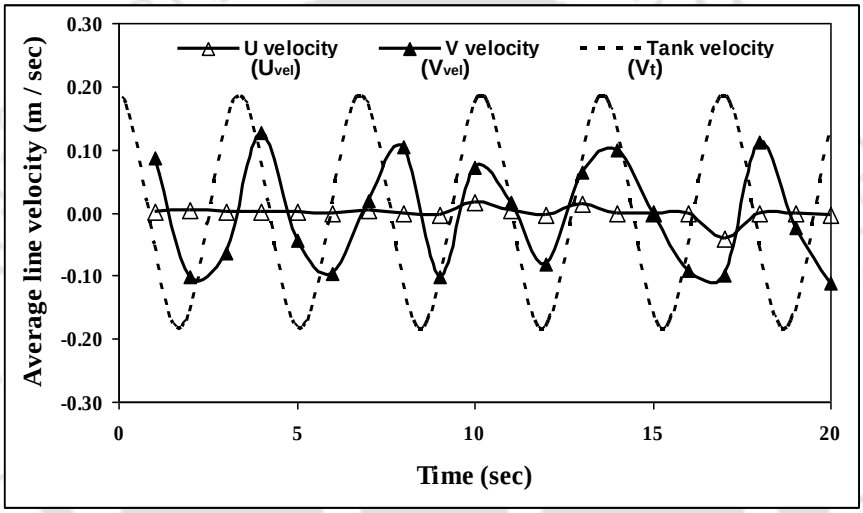

(b)

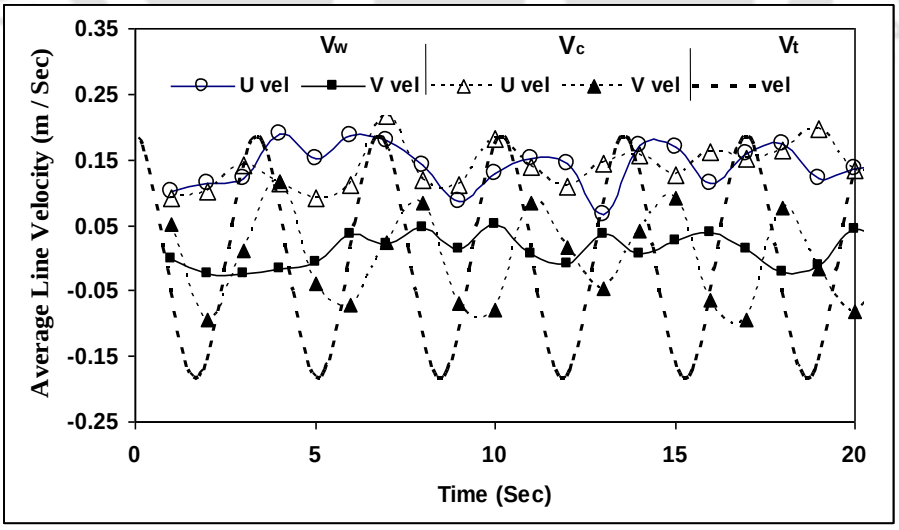

(c)

Figure 7.8: Comparison of the average line velocity profiles for Case -32, where V_w is the average line velocity at the tank wall, V_c is the average line velocity at tank centre, and V_t is the theoretical dynamic tank velocity: (a) average line velocity V_w near the tank wall for an FFT size of 128 × 128 pixels; (b) average line velocity V_c at the tank centre for an FFT size of 128 × 128 pixels; (c) average line velocity for an FFT size of 64 × 64 pixels.

Figures 7.8 (a) and (b) show the plots for Case -32 with an FFT size of 128 × 128 pixels. As expected, the U_{vel} values of the fluid near the tank wall and tank centre are very low and very near to zero for an FFT size of 128 × 128 pixels. Similarly, the case when the FFT size is 64 × 64 pixels is also tested which has 180 instantaneous velocity vector locations on the camera's focal area in the fluid domain and is shown in Figure 7.8 (c). However, an FFT size of 64 × 64 pixels produced a non-zero U_{vel} value for all the cases. This indicates that analysis with 64 × 64 pixels does not yield the correct correlation peaks, resulting in the wrong velocity vectors. This occurs because the interrogation spots are very small in the case of 64 × 64 pixels. Some interrogation spots, therefore may be empty (i.e. a spot which has no tracer particles) which lead to the wrong vectors. For this reason, an FFT size of 128 × 128 pixels was utilized. Moreover, in Figure 7.8 (a), the curve of V_{vel} near the tank centre versus time has almost five complete wave cycles. Among those wave cycles, the last four gives the frequency of the V_c versus time wave as 0.29 (= 4/14) *cycles/s*, which is almost exactly equal to the frequency of 0.3 *cycle/s*. The first cycle can be ignored because the motor takes some time to reach its desired frequency of 0.3 *cycle/s* from the position of rest. Also, because of the low initial frequency, the first peak of V_{vel} is smaller than the rest of the peaks. Even though Figure 7.8 (c) shows velocities for Case -32 with an FFT size of 64 × 64 pixels, it fails to meet the expectations. The average U velocity V_w of the fluid near the tank wall is 0.13 m/s, which is false.

7.5.2 Free Surface Velocity for Various h_s/L Ratios and Frequencies

Thus, it is observed that only the FFT size of 128 × 128 pixels results in correct velocity vectors. Hence, further results are presented only for an FFT size of 128 × 128 pixels. The average of all the instantaneous velocities along the line near the tank wall tank centre are plotted in Figure 7.9 for the Case -33, Case -34 and Case -35 conditions (refer Table 6.1 for details of the cases). Figures 7.9 (a) and (b) are plotted for Case -33 (h_s/L = 0.2; excitation frequency, 0.4 cycle/s) and Case -34 (h_s/L =0.3; excitation frequency, 0.3 cycle/s) respectively. As the tank moves in the x direction (which is parallel to the camera's y direction), the V velocity is greater than the U velocity in the plots. In other words, the U velocity is much less than the V velocity, which can be easily understood from the fact that the main fluid motion is in the y direction of the camera. The V velocity versus time graph shows a periodic wave with almost equal heights of peaks and valleys. From Figures 7.9 (a)

to (d), it is evident that, when the h_s/L ratio level is 0.2 in the tank, the fluid will oscillate together with the tank. This behaviour diminishes slowly as the ratio increases further. In the case of h_s/L = 0.4 ratio, the fluid oscillation lags slightly initially i.e. up to about 8–10 *s*. Later, fluid oscillations try to match the tank velocity. The amplitude of the standing wave also becomes larger as the excitation frequency of the tank is increased.

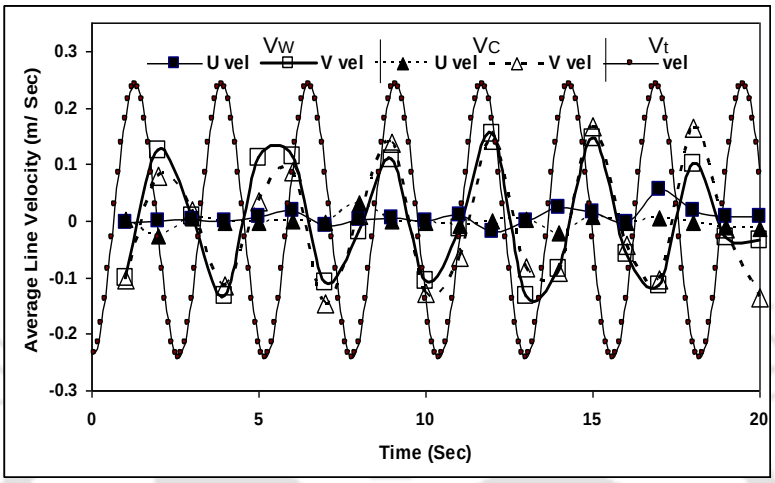

(a)

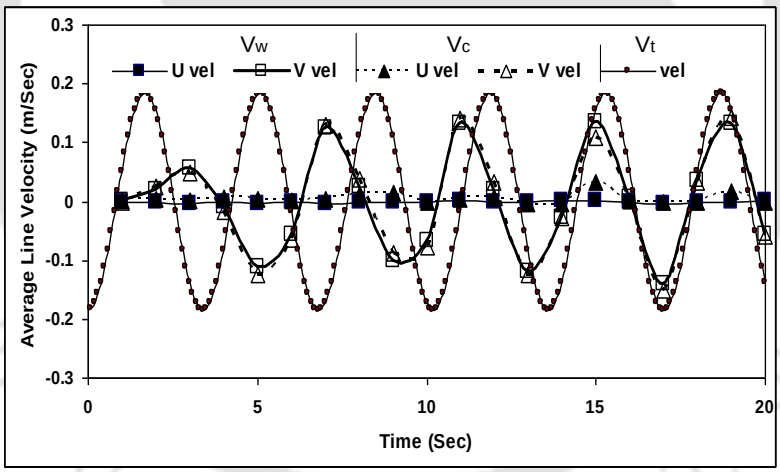

(b)

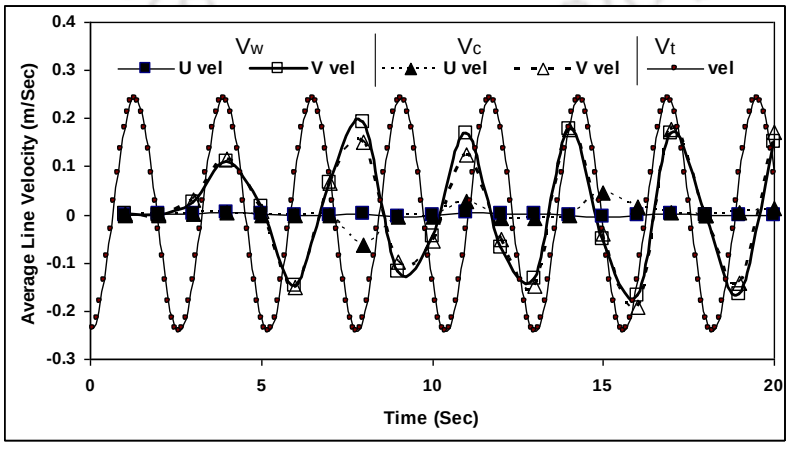

(c)

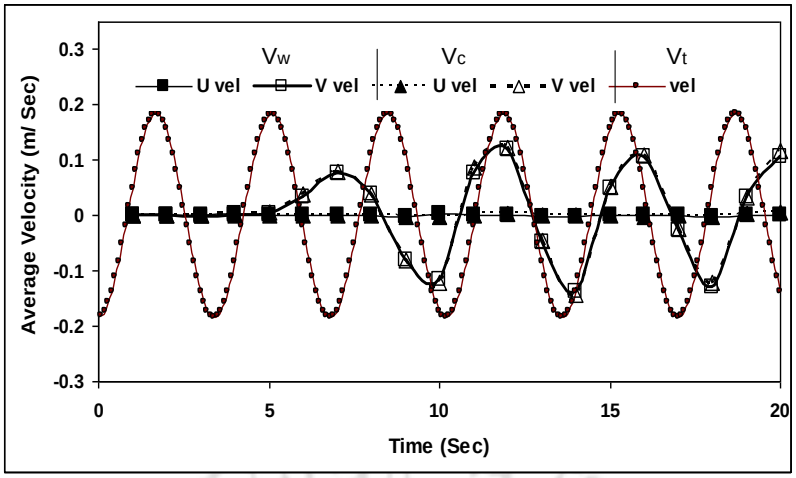

(d)

Figure 7.9 Average line velocity profiles for (a) Case -33; (b) Case -34; (c) Case -35 and (d) Case -36 with respect to time.

7.5.3 Streamlines and Velocity Contour

Figures 7.10 (a) and (b) are the streamline plots at a particular instant of time in the Case -32 conditions. In Figures 7.10 (a) and (b), the alternate upward and downward flow directions of streamlines are observed owing to the surge motion of the tank. These alternate upward and downward flow directions of the streamlines are obtained for the entire time period in all the cases except for a few. The vector map in Figure 7.11 clearly shows the complex nature of the flow. Because of the surge motion of the tank, a series of single directional regular waves are formed initially. Further, the wall effect also caused irregular waves especially near the wall. Evidence for the irregular waves is shown in Figures 7.11 (a) to (d). Samples of different flow patterns are observed in Figures 7.11 (a) to (d). They occur owing to the merging of complex waves as occurs in overturning breaking waves and in a hydraulic jump with standing waves. These are interesting phenomena in the sloshing studies. As the wave merges, the smooth free surface becomes irregular.

The present results show that the velocity contour undergoes drastic changes even between adjacent frames. This may occur as a result of the surge motion of the tank. During this motion, the water waves will strike the walls of the tank and a sudden rise in the waves will occur. The amount of the rise depends on the velocity of the wave. This rise and fall disturbs other succeeding waves. For this reason, a sudden change can be expected from frame to frame. These occurrences happen because the tank fluid is surrounded by the structural parts (i.e. tank walls) and also because of the random rise and fall of overturning breaking waves

and hydraulic jump. If excitation of the tank increases, the irregular motion of the free surface of the liquid seems to have splashing, breaking waves, etc. These complex wave patterns which are observed in the experiments are difficult to simulate numerically. These wave patterns are taken from Case -35 conditions. This type of wave pattern can be expected in other cases also but at lower frequencies of the tank, smooth waves are observed in most situations, as seen in Figures 7.10 (a) and (b).

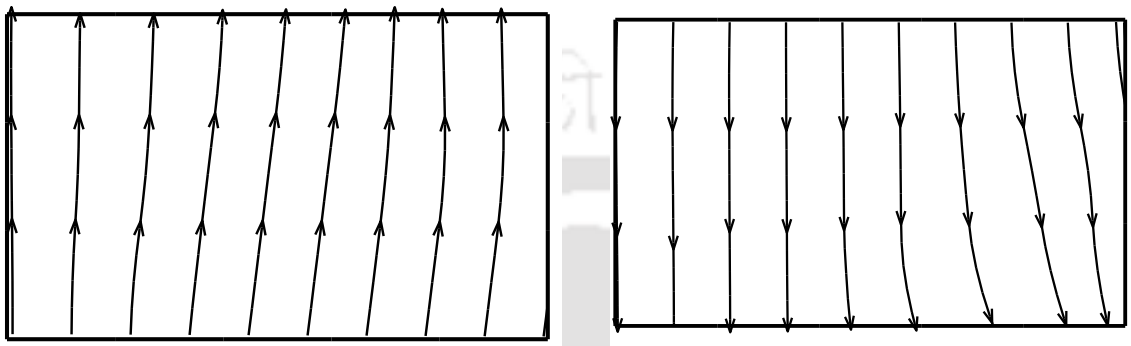

(a) (b)

Figure 7.10 Streamline profiles at L = 30 per cent and F = 0.3 cycles/s for an FFT size of 128 × 128 pixels (Case -32): (a) *t* = 1 s, eleventh frame; (b) *t* = 2 s, eighth frame

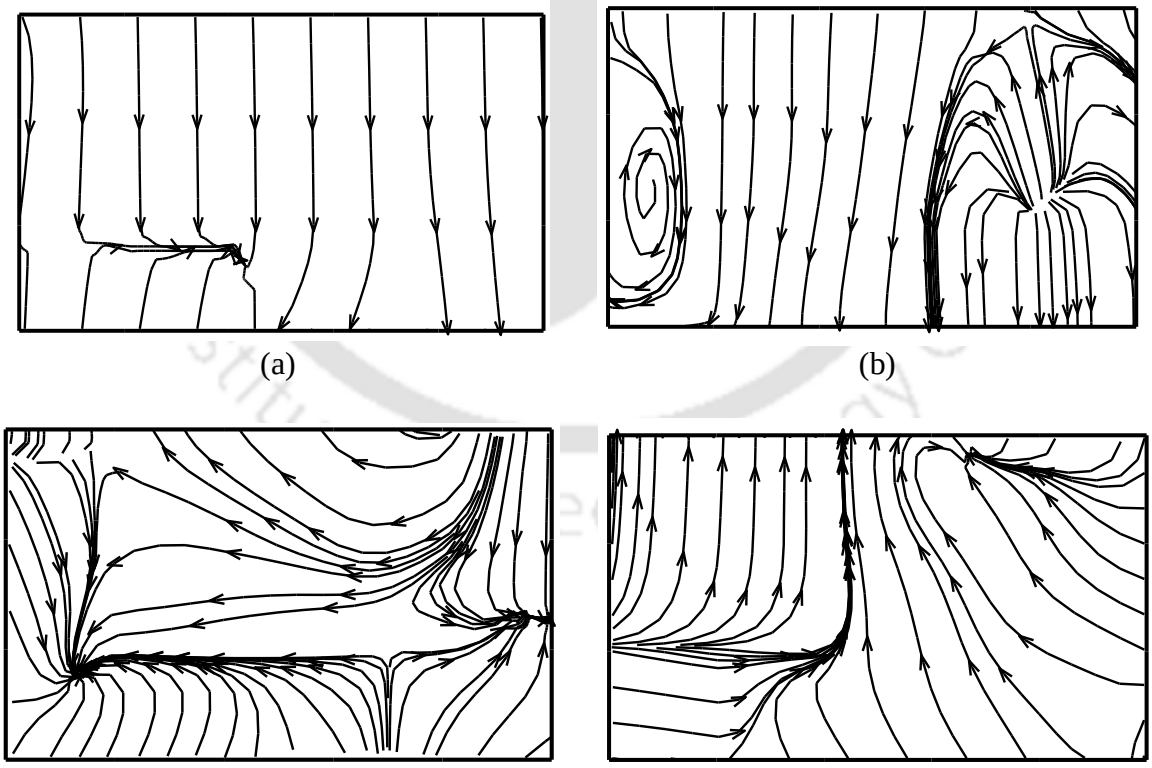

(a) (b)

(c) (d)

Figure 7.11: Samples of different flow patterns of the streamline profile (Case -35): (a) *t* = 5 s, eleventh frame; (b) *t* = 10 s, eleventh frame; (c) *t* = 15 s, eleventh frame; (d) *t* = 20 s, eleventh frame.

It should be noted that the direction of V_{vel} is the direction of tank excitation. Figures 7.12 (a) to (d) show the instantaneous velocity contours at the tenth and twelfth seconds for Case -32. This is because, at these two instants, the tank velocity V_t show peak values for Case -32 as indicated by points A and B in Figure 7.5. Figures 7.12 (a) and (b) are adjacent frames of Case -32 at the tenth second. At this moment, the tank velocity shows a positive peak and therefore, positive values of V_{vel} can be expected near the tank wall and near the tank centre. The same velocity contour is shown in two adjacent frames at the twelfth second, where the tank velocity shows a negative peak.

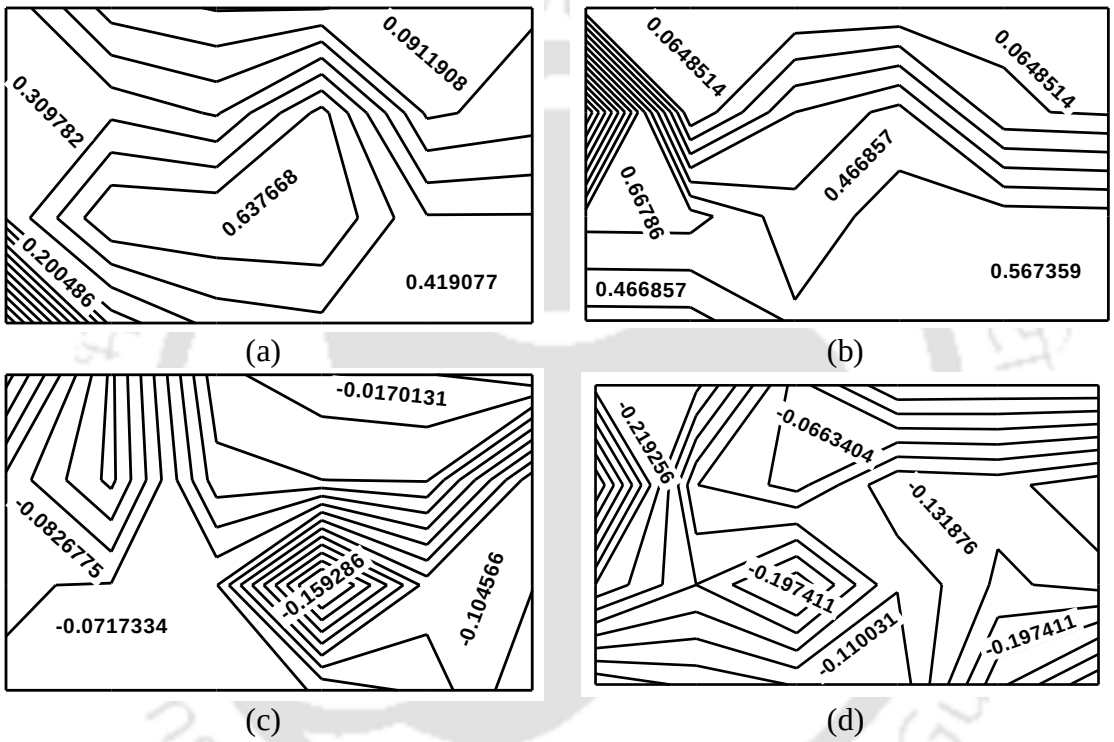

Figure 7.12 Instantaneous V velocity contour diagrams for Case -32, where points A and B are shown in Figure 7.5: (a) at point A, t = 10 s, seventh frame; (b) at point A, t = 10 s, eighth frame; (c) at point B, t = 12 s, seventh frame; (d) at point B, t = 12 s, eighth frame.

7.5.4 Vertical Velocity W_{vel} at the Left Wall

This section explains the effects of the h_s/L ratio and excitation frequency on the vertical velocity near the left wall of the tank, where the camera is focused. Figures 7.13 (a) to (c) demonstrate the variation in the vertical velocity with respect to time for h_s/L ratios of 0.2, 0.3 and 0.4. The effect of the excitation frequency is shown in Figure 7.14. The maximum and minimum velocity points are taken and plotted separately. This is to show the effects of the h_s/L ratio and excitation frequency on the vertical velocity of the liquid, as shown in Figure

15. When the h_s/L ratio is very low (less than 0.1) or very high (greater than 1.0), the type of motions are called shallow sloshing and deep sloshing respectively (Faltinsen and Timokha, 2009). It is seen that, at the same excitation frequency, the maximum vertical velocity for the h_s/L = 0.2 ratio (Case -32) is higher than for the h_s/L = 0.3 ratio. However, when the h_s/L ratio is increased to 0.4, the maximum vertical velocity is also increased. On the other hand, on increasing the excitation frequency, the vertical velocity also starts to increase.

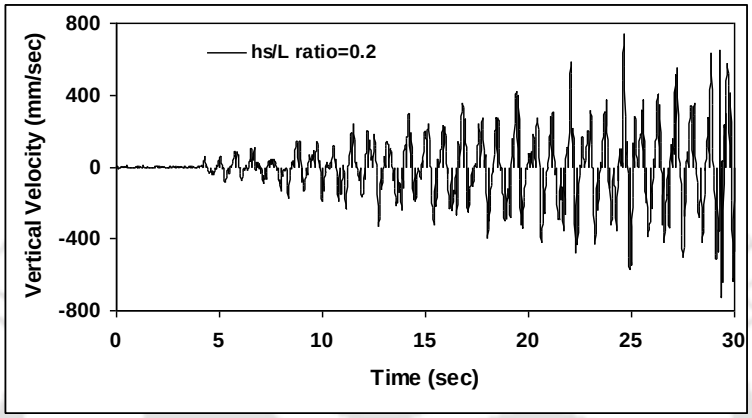

(a)

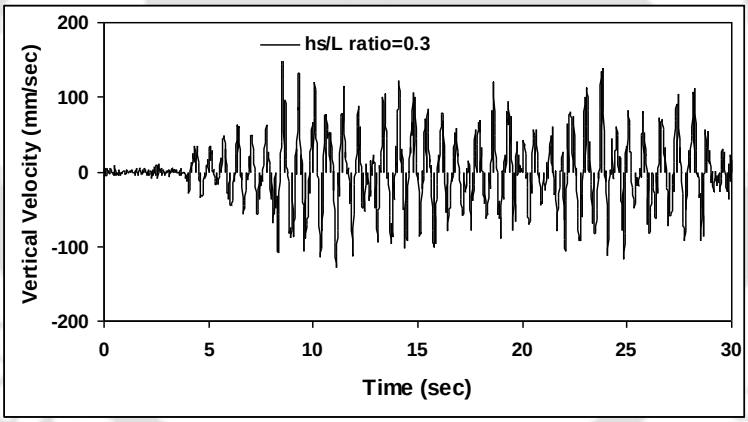

(b)

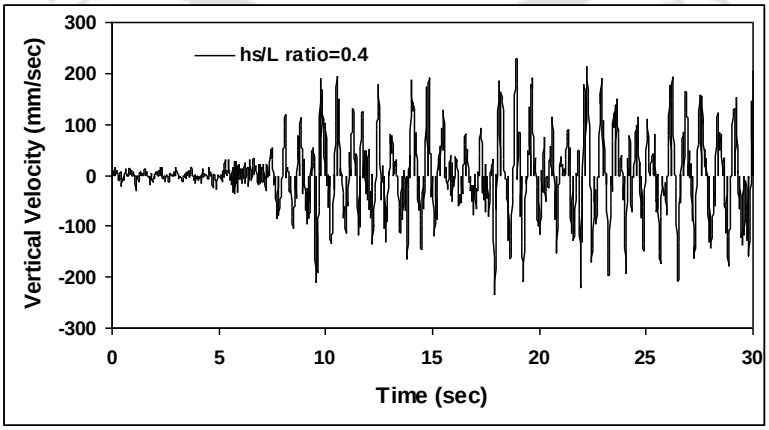

(c)

Figure 7.13 Effect of the h_s/L ratio on the vertical velocity W_{vel} near the left wall of the tank: (a) h_s/L = 0.2 (Case -32); (b) h_s/L = 0.3 (Case -34); (c) h_s/L = 0.4 (Case -36).

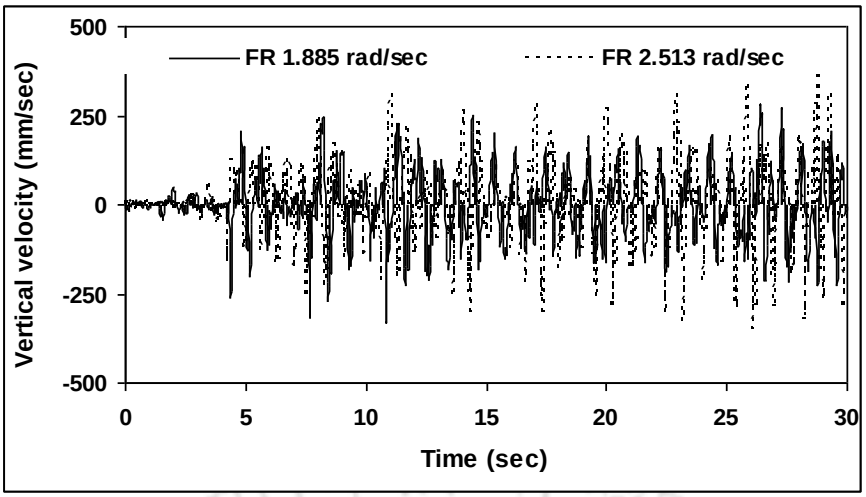

Figure 7.14 Effect of the frequency on the vertical velocity W_{vel} near the left wall of the tank.

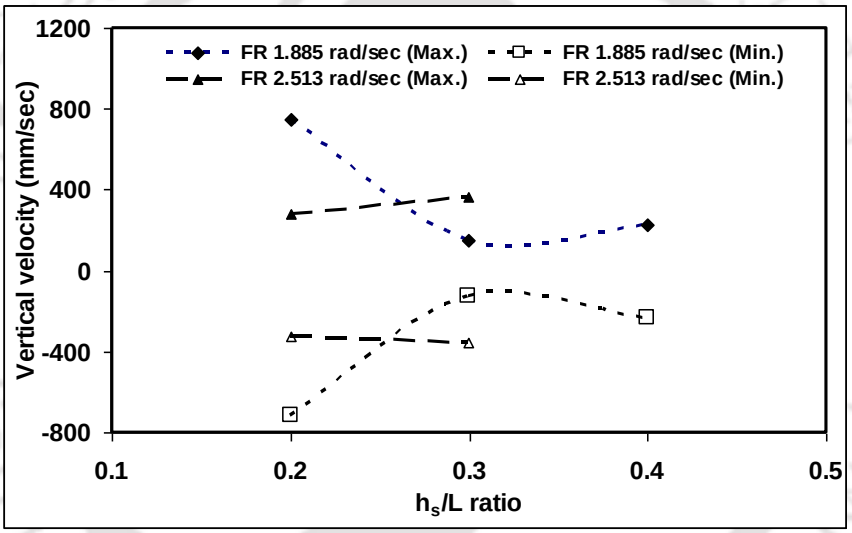

Figure 7.15: Maximum and minimum vertical velocities W_{vel} near left wall of the tank.

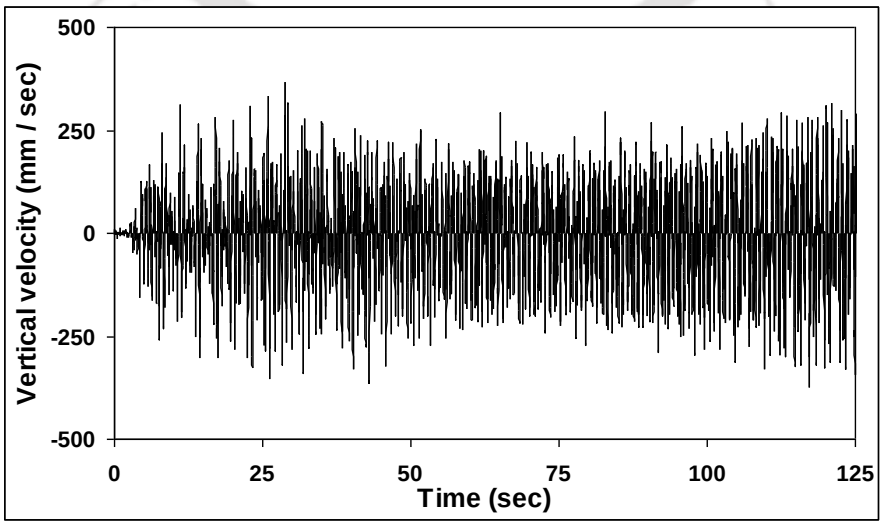

Figure 7.16: Vertical velocity near the left wall for Case -35 (fully developed).

As the excitation frequency increases, the standing wave transforms into a train of traveling waves of very short length. As it is evident from the literature (Ibrahim, 2005), it can be understood that this vertical velocity will increase with respect to the excitation frequency up to the first-mode natural frequency and then it will start to decrease. Whenever the vertical velocity meets any of the system's natural frequencies, the oscillation becomes higher. Figure 7.16 illustrates the fully developed profile for the vertical velocity near the left wall of the tank.

7.6 Summary

In this work, the planar 2-D PIV technique is used to calculate the *U* and *V* velocities of the free surface and the interface location technique is used to obtain the vertical velocity *W* of the interface in a sloshing tank. The surface of the water in the tank was sprinkled with marker particles which float on it and the motion was captured with a video camera. The cross-correlations of images were performed with an interrogation window of FFT size 128 × 128 pixels. Using this technique, the average line velocity near the tank wall and centre-line are determined. The vertical velocity of the free surface of the liquid was found using the interface location technique with a moving-camera arrangement. The noteworthy findings of the present investigation are listed below.

a) The present PIV method allowed two components (along the tank wall and near the tank centre) of the velocity at the surface to be determined. The interrogation window chosen for averaging was much smaller than the wave amplitude. A comparison of the *U* and *V* components of the fluid velocity with the tank velocity shows that the results are in qualitative agreement. The present PIV method gave us two components (along the tank wall and near tank center) of the velocity at the surface. The comparison of *U* and *V* components of fluid velocity with tank velocity shows that the results are in qualitative agreement.

b) It was found that, when the h_s/L ratio was increased gradually from 0.2 to 0.4, the fluid oscillation lags slightly at initial times of up to a few seconds. Later, fluid oscillations try to match the tank velocity. The amplitudes of the *U* and *V* velocities depend on the excitation frequency and the excitation amplitude. Also, the amplitude of the standing wave becomes larger as the excitation ratio of the tank increases. If excitation of the tank

increases, irregular motion of the free surface of the liquid is observed. This complex motion of the liquid is obtained owing to breaking waves, jumping waves, etc. during the motion.

c) Alternate upward and downward flow directions of streamlines were observed owing to the surge motion of the tank. This result was obtained for the entire time period in all cases except a few. The velocity contour diagrams were plotted for a maximum peak and a minimum peak of the tank velocity (points A and B respectively). Because of the surge motion of the tank, a series of single directional regular waves are formed initially. Further, the wall effect also caused irregular waves especially near the wall. The results indicate that the complex nature of the flow in the 2-D planar components is indeed from the nature of flow.

d) The interface location technique was applied to find the liquid vertical velocity at the free surface in a tank by measuring the intensity variation of the images. During sloshing, due to the low excitation frequency, the vertical velocity oscillations will increase from zero up to a certain time and then will reach the fully developed state, which gives constant oscillations. The vertical velocity component of the free surface is calculated directly from the images of the liquid. Hence the accuracy attained in this study to find the free-surface velocity profile under low-steepness waves is better than those obtained with conventional instruments.

The PIV technique has already been applied several times to study self-induced sloshing. However, this investigation focuses on an externally induced tank. The above flow visualization method is a simple technique to find the free-surface velocity during externally induced sloshing at low frequencies.

Chapter

INVESTIGATIONS OF LIQUID PRESSURE IN A MOVING TANK

8

The objective of this chapter is to present numerical and experimental investigations of the liquid pressure distribution near the tank walls. The liquid pressure is calculated with and without baffles. Thus, the slosh arresting power of baffles in the moving tank is also studied. For the numerical analysis, the structural part is also considered to show the effect of fluid structure interaction on free surface elevation. The response of the coupled system is obtained by using the well-known software Automatic Dynamic Incremental Nonlinear Analysis (ADINA). The pressure sensor used to measure the liquid pressure experimentally at various fill levels. A direct comparison of numerical simulation with the experimental data is shown for the moving tank with and without baffles.

CONTENTS

8.1 Introductory Remark

A fluid–structure interaction phenomenon is an important consideration in several engineering fields. This is manifestly the case in design of automotive and aerospace structure as well as modeling the response of offshore structures, long span bridges and high rise buildings. Fluid–structure interaction also plays an important role in the safety assessment of power generation plants and many other industrial purposes. The general topics of fluid–structure interaction is indeed a particularly broad subject in that it simultaneously brings together all the aspects associated with both structural mechanics and fluid mechanics. Each of these two areas is complex by themselves, and when considered together, the situation becomes even more complex. In fact, interaction (or coupling) between the fluid and solid response can be viewed as a feed back loop as illustrated in Figure 8.1.

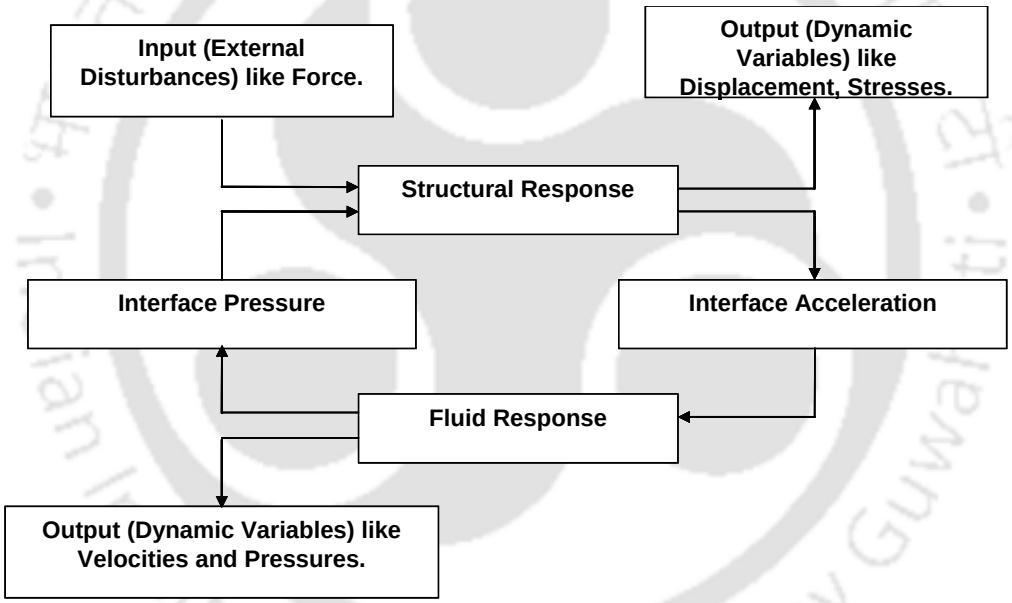

Figure 8.1: Feedback loop in fluid–structure interaction.

Over years, the sloshing problem has been studied by a host of researchers by using variational principle (Lawrence *et al.*, 1958; Siekmann and Chang, 1970; Liu and Uras, 1988; Rocca *et al.*, 2000; Yuanjun *et al.*, 2007). Experimental investigations on effect of tank sizes, flexibility of tank bottom wall and effect of frequencies in system were analyzed (Stofan and Sumner, 1963; Chiba, 1992; Akyildiz and Unal, 2005) to find the liquid sloshing effect. Pal *et al*. (1999) presented a numerical model using finite element technique to study the dynamics of inviscid, incompressible liquid cylindrical tanks under small displacements in a coupled manner. Celebi and Akyildiz (2002) presented the liquid sloshing in the 2-D tanks based on

the finite difference method. Kim (2001) simulated the slosh flows in 2-D and 3-D liquid tanks based on finite difference method (FDM) formulation and the results obtained were found to have a favorable agreement with experimental data. Researchers have reported comparative surveys of the computational fluid dynamics (CFD) methods, which are applicable to nonlinear sloshing problems (Frandsen, 2004; Craig and Kingsley, 2007; Yang and Löhner, 2005). A coupled particle and finite element method for the analysis of fluid-structure interaction problems involving large deformations was carried out by Lee *et al*. (2007). Rocca *et al*. (2005) gave fair comparison between experimental and numerical results for free and forced oscillations in a square-section plexi-glass tank. Akyildiz and Unal (2006) developed a numerical model by using the FDM approximation and validated the results with their own experimental data. Cho *et al*. (2005) carried out a parametric study to find the effect of baffles for damping the liquid oscillations. Arafa (2007) developed the finite element formulation for partially filled externally excited rigid rectangular tank and investigated the effect with and without baffle arrangements in tank.

8.2 Numerical Procedures

Several methods have been used to approximate the free surface. A simple yet powerful method is the volume of fluid (VOF) (Hirt and Nichols, 1981). This method seems to be more flexible and efficient than other methods for treating complicated free surface. It was designed for two or more immiscible fluids where the position of the interface between the fluids is of interest. The VOF method has been used for many years in sloshing applications including free surface flows, marine tank, etc. The main advantage of the VOF method is their ability to capture the complex surface geometries with overturning or breaking waves and splashing (Nielsen, 2003). This method tracks the volume fraction of each phase in each computational cell. The fields for all variables and properties are shared by the fluids present in each cell and represent the volume-averaged values. The tracking of the interfaces between the phases can also be computed when the VOF model is used. In this study, the fluid and solid are modeled in ADINA. ADINA-FSI has good features of FSI solution schemes for couple structural finite element models (Bathe, 1996; Rugonyi and Bathe, 2001; Bathe and Zhang, 2004). Bathe and Ledezma (2007) studied benchmark problems for incompressible fluid flows with structural interactions using ADINA-FSI.

8.2.1 Mathematical Formulation

8.2.1.1 Structural equations

The Lagrangian equations of motion of the structure can be written as

$$\rho \frac{\partial^2 \underrightarrow{u}}{\partial t^2} = \underrightarrow{\nabla} \cdot \tau + \underrightarrow{f_B} \tag{8.1}$$

where ρ is the density, $\underrightarrow{u}$ is the vector of structural displacements, t is the time, τ is the Cauchy stress tensor, $\underrightarrow{f_B}$ is the vector of body forces, and $\left(\underrightarrow{\nabla} \cdot\right)$ represents the divergence operator (in the deformed configuration). Equation 8.1 can be linear or nonlinear depending on the constitutive relations used for the material in consideration and also the displacements which may be small or large (Bathe, 1966).

The boundary conditions needed to solve Equation 8.1 are,

$$u = u_s \text{ on } S_u \text{ and } \tau \cdot n = f^s \text{ on } S_f \tag{8.2}$$

where S_u and S_f represent the parts of the boundary with prescribed displacements, u_s, and tractions, f^s, respectively; and n is a unit outward normal vector to the boundary.

8.2.1.1 Fluid flow equations

The effects of a few parameters of the system, such as the liquid filling level, presence of passive sloshing damper at various frequencies have been examined. The numerical model solves the complete Navier–Stokes equations in primitive variables by using the finite element method.

In a general fluid domain,

$$\frac{\partial \rho}{\partial t} + \underrightarrow{\nabla} \cdot (\rho \underrightarrow{q}) = 0 \tag{8.3}$$

$$\rho \frac{\partial \underrightarrow{q}}{\partial t} + \underrightarrow{\nabla}.(\rho \underrightarrow{q}\underrightarrow{q}) = -\underrightarrow{\nabla} P + \underrightarrow{\nabla}.\underline{\underline{\tau}} + \underrightarrow{f_b} \tag{8.4}$$

where $\underrightarrow{q}$ is the velocity vector and $\rho, p, \underline{\underline{\tau}}$ and f_b are liquid density, pressure, stress tensor and force acting on the body respectively. Fluid is considered to be irrotational, incompressible, inviscid and Newtonian in a three-dimensional tank. These momentum and continuity equations are solved simultaneously with necessary boundary conditions. One of the most important body forces included in f_b is gravitational force (g).

$$f_b = \rho \underset{\rightarrow}{g} \tag{8.5}$$

For incompressible, inviscid fluid,

$$\underset{\rightarrow}{\nabla} \cdot \underset{=}{\tau} = 0 .$$

The fluid domain assumed here is a rectangular shape as shown in Figure 8.2. The fixed coordinate system is denoted by *OXYZ*. In the figure, Z direction is acting against gravity. Fluid model is analyzed based on the Arbitrary-Lagrangian–Eulerian (ALE) coordinate system since the fluid–structure interface is deformable. Obviously, the NS equations need to be rewritten in the ALE system. Let us consider a transformation such that the new coordinate is the sum of the initial coordinate and its displacement.

$$R = r + d(r,\tau) = R(r,\tau) \tag{8.6}$$

$$t = \tau$$

where the moving coordinate system (R,t) has been transformed into a new coordinate system (r,τ). The vector $d(r,\tau)$ is used to deal with the arbitrarily moving coordinates. Using $w\left(=\frac{\partial R}{\partial \tau}=\frac{\partial d}{\partial \tau}\right)$ to represent the moving coordinate velocity, the time derivative of an arbitrary, $f(R,t) = f\left[r + d(r,\tau),\tau\right]$ is

$$\frac{\partial f}{\partial t} = \frac{\partial f}{\partial \tau} - \left(\frac{\partial R}{\partial \tau} \times \frac{\partial f}{\partial R}\right) = \frac{\partial f}{\partial \tau} - w \cdot \nabla f. \tag{8.7}$$

When this equation is applied to time derivatives in the NS equations that are expressed in a purely Eulerian coordinate system, the differential form of ALE equations is obtained.

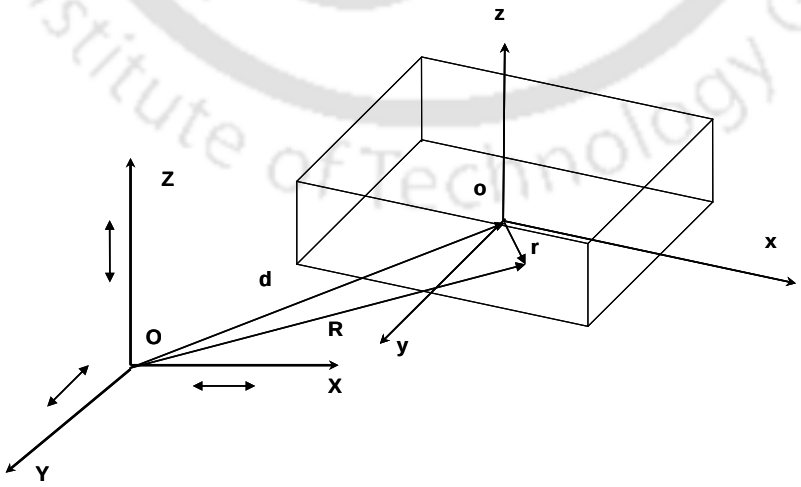

Figure 8.2: Moving coordinate system of domain.

For example, in the ALE system, the conservative continuity equation becomes,

$$\frac{\partial \rho}{\partial t} + \underset{\rightarrow}{\nabla} \cdot \left(\rho \left(\underset{\rightarrow}{q} - \underset{\rightarrow}{w} \right) \right) = 0 . \tag{8.8}$$

The compact form of the continuity equation can be rewritten in the following integral form in an arbitrary moving system as

$$\frac{\partial}{\partial \tau} \int_V \rho dV + \oint_s \left(- w\rho + \rho \left(\underset{\rightarrow}{q} - \underset{\rightarrow}{w} \right) \right) \cdot d\underset{\rightarrow}{S} = 0 \quad , \tag{8.9}$$

where *V(t)* is an arbitrary material volume enclosed by its surface *S(t)* and *S* is the surface vector of *S(t)* in the outward direction.

8.2.2 Numerical Modeling of Fluid and Solid Domains

The present study focuses on the computer modeling to simulate response of liquid storage tank without and with baffles. The dynamic response of baffled liquid storage tank has been studied to know the influence of baffle parameters such as, the installation location and baffle shapes under sinusoidal excitation. In view of this, a thin wall rectangular tank with flat type baffle fixed normal to the tank is considered in the present analysis. Here the tank wall and baffles are made of an elastic and isotropic material. The liquid in the tank is considered in the present case as water. The elastic solid tank walls, baffles and fluid domains are modeled in ADINA. The thickness of the tank wall and baffles are modeled as 0.4 mm, while the length and the breadth of the baffle is taken as $300\,\text{mm} \times 120\,\text{mm}$. Fluid model is simulated as an incompressible and inviscid fluid using 3-D fluid elements. The elastic solid tank wall and baffles have been discretized with two-dimensional 9 node shell elements, whereas the fluid has been discretized with three-dimensional 27 node fluid elements as shown in Figure 8.3 to 8.6. Hydrodynamic pressure generated in the fluid–structure interface and the free surface displacement of the liquid is evaluated. The tank is subjected to the following forced sinusoidal horizontal acceleration.

$$\ddot{a} = -A\omega^2 \sin(\omega t) \quad \text{for } t \geq 0 , \tag{8.10}$$

where *A* is the amplitude of motion (maximum displacement from reference line) and ω is frequency in rad/sec ($\omega = 2\pi/t$, *t* being the period of oscillation).

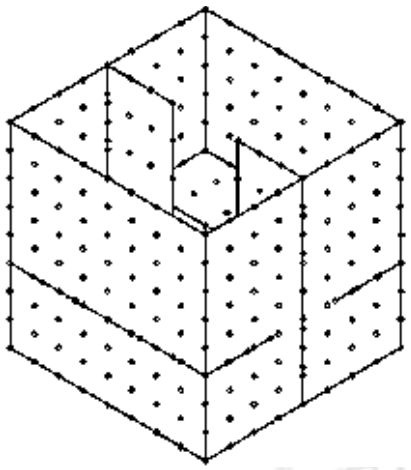

Figure 8.3: Discretized empty baffled tank.

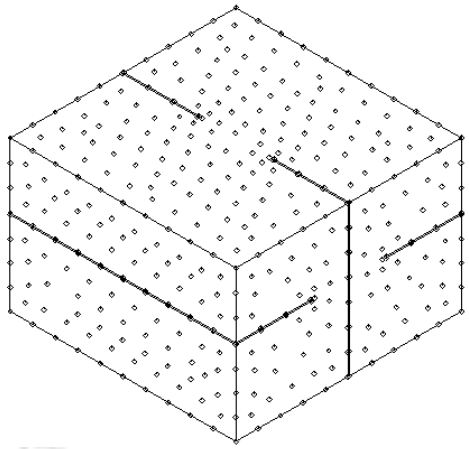

Figure 8.4: Discretized fluid domain.

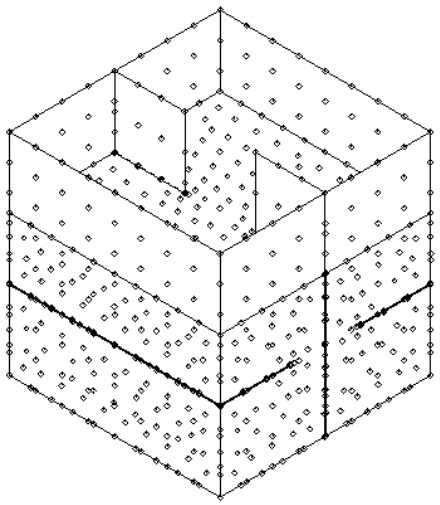

Figure 8.5: Discretized fluid-solid coupled model.

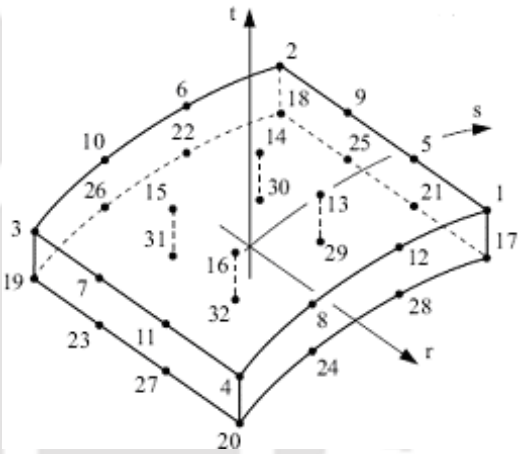

Figure 8.6: Nine node shell element with top and bottom nodes.

In this study, the VOF method is used to capture the free surface of the liquid. Since the method is designed for two or more immiscible fluids, a portion of air with a height of 150 mm is chosen and introduced above the liquid level for all cases. The air portion is also modeled and discretized using the 3-D fluid element. For each cell, the volume fraction (V_F) is determined by

$$V_{F_i} = \frac{V_L}{V_T}, \tag{8.11}$$

where V_L and V_T are the *i*-th species of volume of the liquid in the cell and total volume of the cell respectively (Nielsen, 2003). A cell with a V_F value (scalar quantity) of 0 is void and a value of 1 represents a full cell. The cell contains a free surface if the V_F value is between 0 and 1. Initially, in this numerical analysis, liquid portion is denoted as VOF- Species1 and a V_F value of 1 is assigned for each cell. This field is also integrated in time by solving a

transport Equation 8.12. At each time step, a transport equation is solved to find the distribution of the fluid. Fluids share the momentum equations and each of the fluids is convicted through the domain.

$$\frac{\partial(V_{F_i})}{\partial t} + \underset{\rightarrow}{q} \cdot \underset{\rightarrow}{\nabla}(V_{F_i}) = 0 . \qquad (8.12)$$

Table 8.1- Experiments conducted to measure hydrodynamic pressure and displacement.

Fill level	Frequency (Cycle/sec)	CASE - A (Without Baffle)		CASE - B (Horizontal –cum-Vertical Baffle)		CASE - C (Ring Baffle)	
		Test No	Measured Variables	Test No	Measured Variables	Test No	Measured Variables
H/6	0.25	1	D, P(1, 4)	22	D, P(1)	--	--
	0.33	2	D	23	D	--	--
	0.42	3	D	24	D	--	--
3H/12	0.25	4	D	25	D	--	--
	0.33	5	D	26	D	--	--
	0.42	6	D	27	D	--	--
H/3	0.25	7	D, P(1,4)	28	D, P(1)	--	--
	0.33	8	D	29	D	--	--
	0.42	9	D	30	D	--	--
5H/12	0.25	10	D	31	D	43	D
	0.33	11	D	32	D	44	D
	0.42	12	D	33	D	45	D
H/2	0.25	13	D, P(1, 4)	34	D	46	D
	0.33	14	D	35	D	47	D
	0.42	15	D	36	D	48	D
7H/12	0.25	16	D	37	D	49	D
	0.33	17	D	38	D	50	D
	0.42	18	D	39	D	51	D
2H/3	0.25	19	D, P(1, 2, 3)	40	D, P(3)	52	D, P(3)
	0.33	20	D	41	D	53	D
	0.42	21	D	42	D	54	D

D = Displacement , P(#) = Pressure (Pressure Gauge Position)

8.3 Experimental Procedure

The basic experimental set-up was discussed in Chapter-6 and Chapter-7 in detail. The tank attached to a shaking table can be moved to and fro by a cam arrangement driven by a DC

motor (Figure 6.1). A total of six different pressure gauges, designated as PG1 to PG6, were placed at different heights of water levels on the walls of the tank (Figure 8.7). Excitation voltage of 15 V is applied to the pressure gauges. The output of the pressure gauges was fed to the channels of the data acquisition system that was coupled to a PC. The data were decrypted using software named 'Dasylab' that displayed the output in millivolts. The calibration was done by converting the voltage to pressure using an appropriate factor calculated by taking the static pressures and the corresponding voltage.

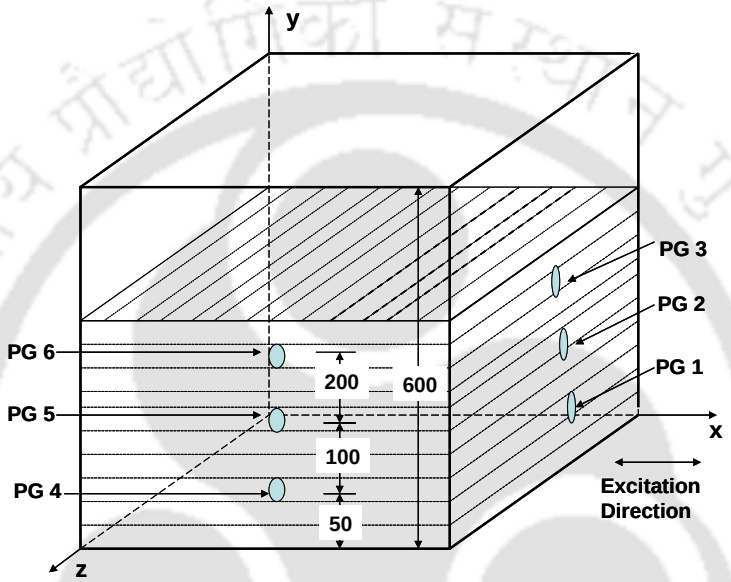

Figure 8.7: Location of pressure gauges (PG) in tank.

When a tank is subjected to linear instability, a series of waves are formed in the liquid and so the liquid gets displaced and hence exerts a pressure on the walls of the tank. This pressure varies with time. Pressure studies were carried out by changing the excitation frequency of the shaking table and the fill level in the tank. Two different types of baffles viz., horizontal-cum-vertical and ring type have been used. The frequency level was maintained as 0.25 cycles/s, while the fill level was changed from *H/6* to *2H/3* from the base of the tank. The effect of baffles has been studied to find the displacement level of the free surface above and below the mean position. Displacement studies have been carried out by changing the excitation frequency of the shaking table and the fill level in the tank. The frequency level was varied from 0.25 to 0.42 cycles/s. In each case, the maximum and minimum displacement was found.

Table 8.1 shows the total number of tests conducted to study the pressure and free surface displacement variations. In the above table, case-A represents the tests without baffles; while

case-B indicates the conditions with horizontal-cum-vertical baffles; and case-C to that of ring baffles. A total of 54 tests were conducted covering various fill levels, different frequencies and use of baffles. As for example, test no. 13 represents the case without baffle with corresponding fill levels of *H/2* and frequency of 0.25 cycles/s. Further, D, P (1, 4) denotes the free surface displacement value and hydrodynamic pressure at PG1, PG4 (Pressure gauge position in tank) values. Similarly, the Test no. 34 shows the use of horizontal-cum-vertical baffles with the displacement data. The numerical work presented in this chapter is an attempt to simulate the experimental data (as indicated in Table 8.1).

The ultimate aim is to find the pressure variations along with influence of baffles in tank with various types and positions of the baffles. The study was made so as to validate the experimental data as discussed earlier. It is a well-known fact that ADINA-FSI is equipped with ADINA F and ADINA (Structure). ADINA F was used to model the fluid part and ADINA to that of the structural part, and later they have been merged to a single program. This facilitates to solve a fluid and structural system as one for highly nonlinear problems.

8.4 Effects of Baffles on Pressure

Initially, experiments were conducted without any baffle and then the same experiments were repeated by incorporating two vertical and two horizontal baffles, and a ring baffle. The sloshing severity depends on various factors like depth of liquid, tank geometry, the amplitude and nature of the tank motions. Moreover, the frequency of excitation over a range close to natural frequencies also affects the severity rate of sloshing to a greater extent. Figures 8.8 and 8.9 show a direct comparison of numerical simulation with the experimental data for the case without baffles, while Figures 8.10–8.15 show the influence of baffles only at various fill-levels. As stated, Figure 8.8 shows the comparison of numerical and experimental results of hydrodynamic pressure variation with time at various fill levels and without baffle. The numerical results obtained show the significance of fill level with respect to sloshing pressure.

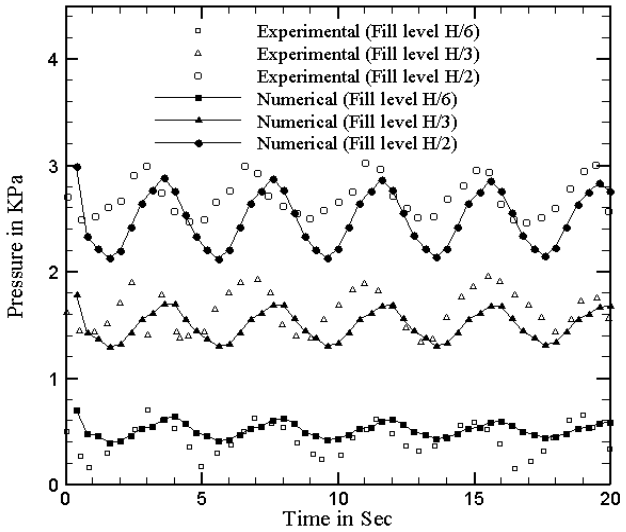

Figure 8.8: Pressure values at PG 1 under frequency of 0.25 Cycles/Sec for without baffles.

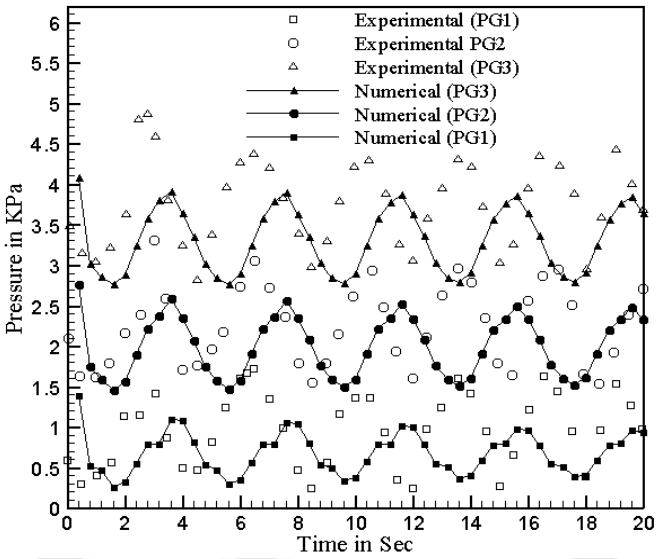

Figure 8.9: Pressure values for fill level 2H/3 with 0.25 Cycles/Sec for without baffle.

It can be stated that as the fill level increases (from H/6 to H/2), the numerical results also show a similar trend of wave profile to that of experimental data with allowable accuracy. When the fill level is increased, the variation in the maxima and minima of pressure changes are varying with respect to tank geometry. Figure 8.9 shows the pressure variation with time for maximum fill level (2H/3) at various positions of pressure gauges. The difference of maxima and minima of pressure waves is more near the free surface and slowly gets reduced as the depth of liquid increases (i.e., at H/2). Next, the slosh responses of the liquid with baffles (horizontal-cum-vertical) have been studied numerically and the results are compared with the one without baffles (Figure 8.10). These numerical results have further been

compared with experimental data (Figure 8.11). In both the cases, the hydrodynamic pressure variation with time is shown at PG1 and with fill level H/6. However, the numerical results show a slight deviation from the experimental data. Similarly, Figures 8.12 and 8.13 show the comparative assessment at PG2 location. The effect of adding ring baffles has been studied numerically at PG3 location and the results are shown in Figure 8.14. The corresponding experimental data are shown in Figure 8.15. The observation shows that the ring baffles are the best choice as they reduce the pressure to the maximum extent. This happens because the ring baffle not only suppresses the velocity of impact of the fluid at the walls, but also retards the vertical motion of the liquid near the other two adjacent walls, thereby suppressing the wave amplitude. The turbulence is created due to its sharp edges at all the walls and thereby dissipating the violent energy to all the walls. This reduces the stress on the impact walls.

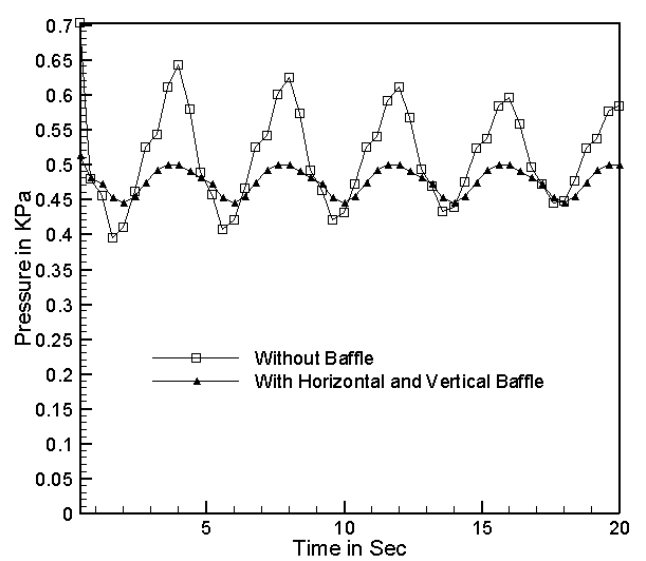

Figure 8.10: Numerical variation of pressure at PG1 for fill level H/6.

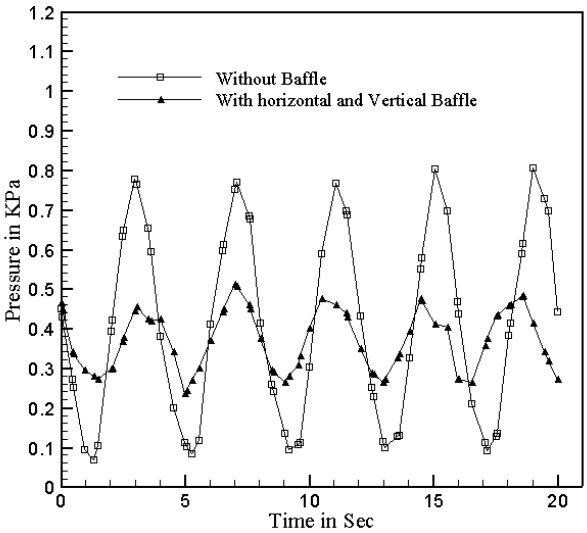

Figure 8.11: Experimental variation of pressure at PG1 for fill level H/6.

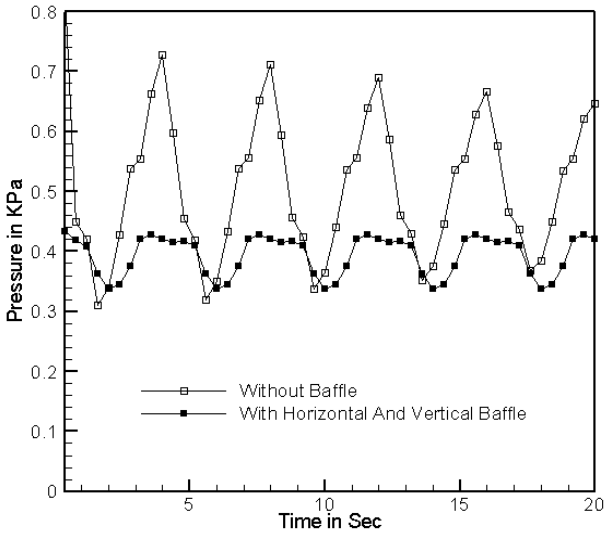

Figure 8.12: Numerical variation of pressure at PG2 for fill level H/3.

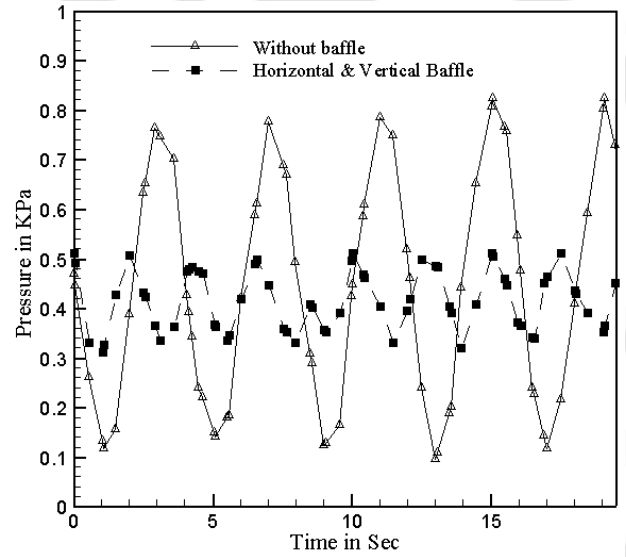

Figure 8.13: Experimental variation of pressure at PG2 for fill level H/3.

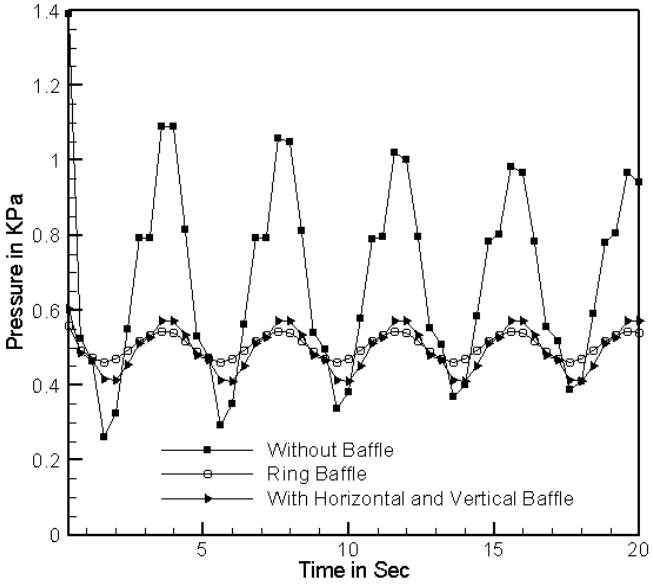

Figure 8.14: Numerical variation of pressure at PG3 for fill level 2H/3.

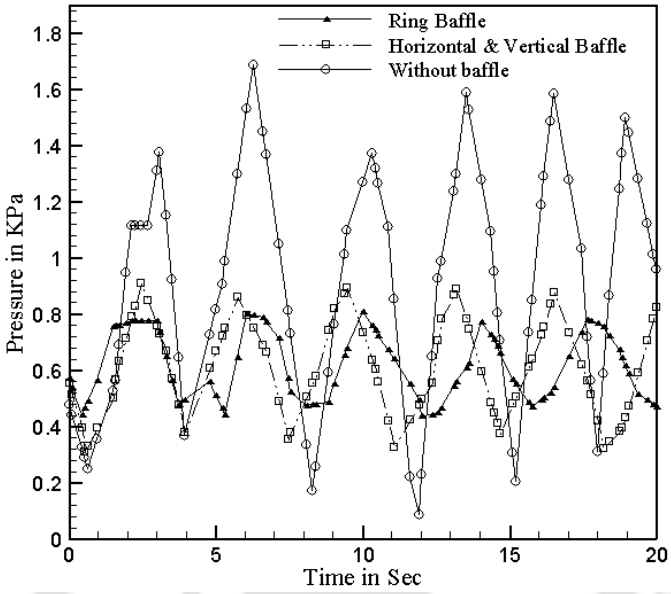

Figure 8.15: Experimental variation of pressure at PG3 for fill level 2H/3.

8.5 Effect of Baffles on Surface Displacement

Figures 8.16 and 8.17 show numerical and experimental results of free surface displacement of liquid in the tank at excitation frequency of 0.25 cycles/s, respectively. Similarly, Figures 8.18 and 8.19 show numerical and experimental results of free surface displacement at excitation frequency of 0.33 cycles/s, respectively, while Figures 8.20 and 8.21 show the same at 0.42 cycles/s, respectively.

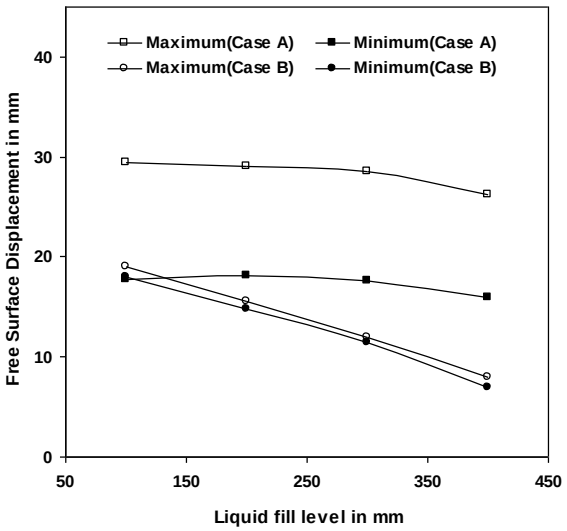

Figure 8.16: Surface displacement at excitation 0.25 cycles/sec for numerical work.

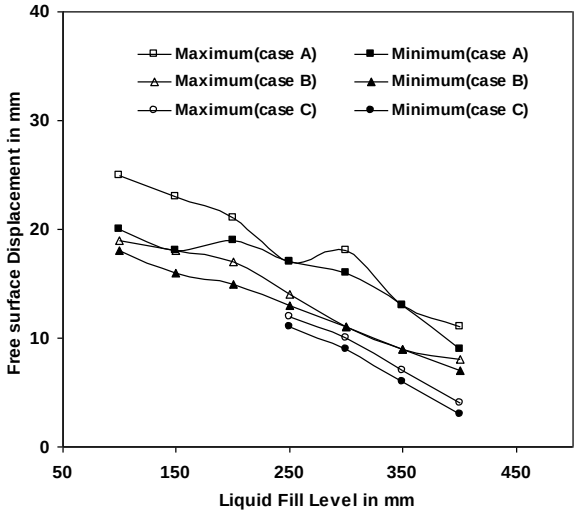

Figure 8.17: Surface displacement at excitation 0.25 cycles/sec for experimental work.

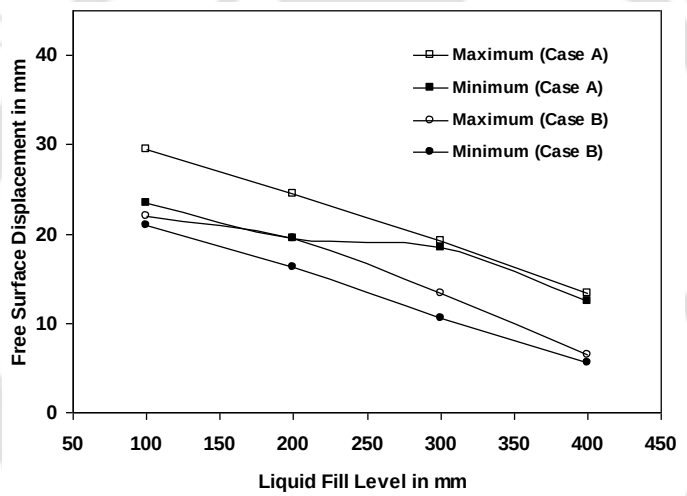

Figure 8.18: Surface displacement at excitation 0.33 cycles/sec for numerical work.

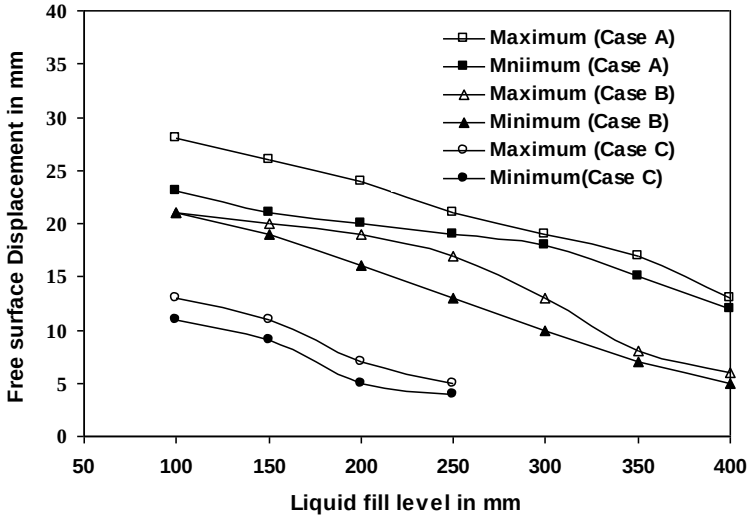

Figure 8.19: Surface displacement at excitation 0.33 cycles/sec for experimental work.

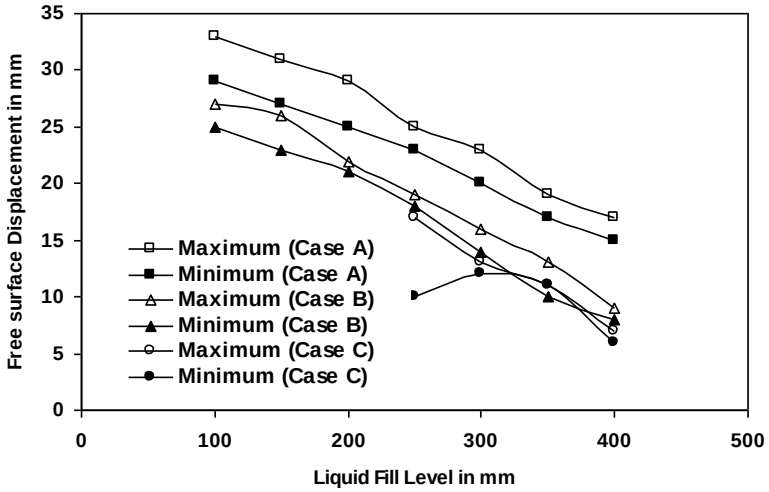

Figure 8.20: Surface displacement at excitation 0.42 cycles/sec for experimental work.

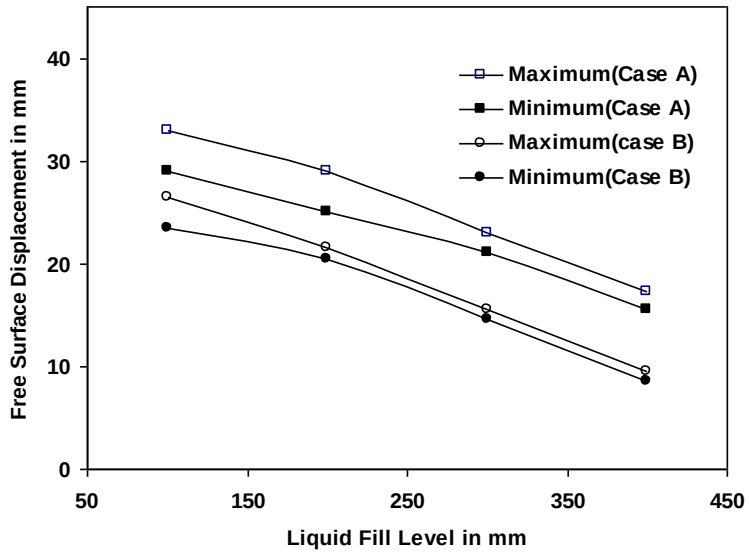

Figure 8.21: Surface displacement at excitation 0.42 cycles/sec for numerical work.

Variation of the free surface displacement with respect to the changing fill depths in the baffled and the un-baffled tanks graphs shows that the curves drop from left to right, i.e., have a negative slope, which signifies that an increase of fill depth in the tank, the oscillation of the unrestrained surface of the liquid decreases. This is because when liquid mass in the tank is increased, the sudden disturbances in the tank are absorbed to an extent by the liquid and thus reduces its sloshing effect. The graphs also depicts that the sloshing decreases more with the use of ring baffles and becomes least without baffles.

Further, it is seen that the plot for the ring baffle starts from fill depth of 250 mm. This is because the ring baffle is fixed at 225 mm above the base and therefore, its effect is experienced only above this height. The free surface displacement also sharply decreases

after 250 mm when the vertical as well as horizontal baffles are used. This is because the horizontal baffles are fixed at a height of 225 mm and above this height the combined effect of both the types eventually reduces sloshing. The vertical baffle suppress the horizontal component of the liquid velocity while the horizontal and ring baffle decrease the vertical component of the liquid velocity.

8.6 Summary

The objective of this chapter is to present the effect of baffles on liquid sloshing for a partially filled tank. Numerical simulations were carried out based on volume of fluid techniques with ALE formulation. The response of the coupled system is obtained by using the well-known software ADINA. The numerical results obtained (hydrodynamic pressure vs. time, free surface displacement vs. time) have been compared with the available experimental data and were found to be in good agreement. In practice, for complex geometries, analytical solutions are tedious. The present method of fluid–structure interaction is very simple and can be simulated with allowable accuracy. The present work also can be extended to examine the effect of sloshing with different inclination of the tank bottom and different types of liquid. Moreover, the model can be employed to handle vertical excitation in addition to further baffle configurations, such as multiple baffles and its shapes. The inclusion of the liquid viscosity and surface tension effects in the model would also be worthwhile.

Chapter 9

CONCLUSIONS AND FUTURE SCOPE

This chapter is devoted to sum up the major achievements of the present investigation. The dynamic behaviors of liquid like free surface elevation, free surface velocity and liquid pressure are captured by the numerical and experimental investigations during liquid sloshing. The important issues and the outcome of work while capturing those properties are discussed and highlighted in this chapter.

CONTENTS

9.1 Contribution of Present Work

The liquid sloshing problem has made a substantial progress since early nineteen seventies till date, especially in the computation of capturing or tracking the free surface flows. In this thesis, flow field properties of the liquid, such as the free surface elevation, surface velocity and liquid pressure in a partially filled tank is studied numerically and experimentally. In summary, the following specific goals have been addressed.

The work lives true to its original aim as (i) the 2-D and 3-D numerical simulations are performed based on σ-transformed finite difference solver to capture the free surface elevation in partially filled liquid moving tank, (ii) the free surface elevation is captured during the motion of the tank experimentally by using interface location method**,** (iii) sloshing flow properties like liquid velocity at free surface and the liquid pressure is found at various locations of the tank. The velocities are measured at various liquid fill levels and excitation frequencies, and (iv) the liquid pressure at the tank walls is calculated by using piezo-resistive transducer and to compare with the fluid-structure coupled numerical analysis. Experiments and analysis have been made without and with baffled tanks.

9.1.1 Capture of Liquid Free Surface Elevation

Primarily, the free surface vertical displacement or free surface elevation is captured numerically as well as experimentally. From this investigation, the following conclusions could be drawn.

- The potential flow equations are good enough to study the free surface characteristics where the gravity force is predominant than other forces. In this investigation, a fully nonlinear inviscid numerical model is developed based on the potential flow theory with mapped governing equations and the corresponding boundary conditions are solved using finite difference method.
- A good agreement between the present numerical model and the previously published results is obtained for low steeping waves. The horizontally excited tank free surface elevation and phase plane diagram are discussed with off and at resonant frequencies. The behaviors show the effect of wave excitation while matching with resonant frequency.

- The vertical excitation causes the instability associated with parametric resonance of the combined motion for a certain set of frequencies and amplitude of the vertical motion. The Bretschneider spectrum is selected to serve as the input excitation spectrum to generate the random input wave. The present numerical model is easier to implement, computationally accurate and efficient. The model provides a simple way of simulating steep non-breaking waves.
- It is observed that the wave amplitude grows initially with the time up to a certain time period. After reaching this period, the wave amplitude remains constant and enters the fully developed region.
- It is found that the maximum wave height increases and the minimum wave height decreases with an increase in the frequency. It also causes the peaks in the power spectra to become larger and more peaks to appear at different frequencies.
- The sloshing waves are analyzed with the probability density and energy spectrum. It is evident from the analysis that the trend of deviation of wave height increases with an increase in frequency. This suggests that a stronger nonlinearity gives rise to the increase of the deviation. It is interesting to note that such an increase seems to indicate a fairly linear trend with frequency.
- The free surface elevations for both simulated and experimental results are compared during the motion of tank and a minor discrepancy has been observed. Experimental results agree well with the simulation results.

9.1.2 Capture of Liquid Free Surface Velocity

Another flow property, the free surface velocity is studied in detail. Using 2-D planar PIV, the average line velocity near the tank wall and near the centre-line are determined. The vertical velocity of the free surface of the liquid is found using the interface location technique with a moving camera arrangement. The interface location technique is applied to find the liquid vertical velocity at the free surface in a tank by measuring the intensity variation of the images. The key findings from this could be summarized below:

- During sloshing, at low excitation frequency, the vertical velocity oscillations increases from zero up to a certain time and then reaches the fully developed state, thereby giving constant oscillations.

- It is found that, the amplitudes of the *U* and *V* velocities depend on the excitation frequency and the excitation amplitude. Also, the amplitude of the standing wave also becomes larger as the excitation ratio of the tank increases. With an increase in tank excitation, an irregular motion of the free surface of the liquid is observed. This complex motion of the liquid is obtained owing to breaking waves, jumping waves, etc., during the motion.
- Alternate upward and downward flow directions of streamlines are observed owing to the surge motion of the tank. This result is obtained for the entire time period in all cases except a few. The velocity contour diagrams are shown for a maximum peak and a minimum peak of the tank velocity. Further, the wall effect also causes irregular waves especially near the wall. The results indicated that the complex nature of the flow in the 2-D planar components is indeed from the nature of flow.

9.1.3 Capture of Liquid Pressure to Control Slosh

Finally, the liquid pressure which is an important flow field property is studied extensively. For this, the response of the coupled system is obtained by using the well-known software ADINA where the simulations are carried out without baffle and with vertical, horizontal and ring baffles. Further, in order to compare the results, the experiments have also been conducted without and with baffles. The following are the important points from this study:

- It is found that as the fill level increases, the numerical results show a similar trend of wave profile when compared with the experimental data. When the fill level increases, the variation in the maxima and minima of pressure changes varies with respect to the tank geometry. The difference of maxima and minima of pressure waves is more near the free surface, and slowly reduces with an increase in depth.
- The observation shows that the ring baffles are the best choice as they reduce the pressure to the maximum extent. This happens because the ring baffle not only suppresses the velocity of impact of the fluid at the walls, but also retards the vertical motion of the liquid near the other two adjacent walls, thereby suppressing the wave amplitude.
- The variation of the free surface displacement with respect to the changing fill depths in the baffled and the un-baffled tank shows that the curves drop from left to right, i.e., it has got a negative slope. This indicates that with an increase of fill-depth, the oscillation of the unrestrained surface of the liquid decreases. This is because when

liquid mass in the tank increases, the sudden disturbances in the tank are absorbed to an extent by the liquid and thus reduce its sloshing effect.

- The results also indicated that the sloshing decreases more with the use of ring baffles, and becomes least without baffles. The vertical baffle suppresses the horizontal component of liquid velocity while the horizontal and ring baffle decreases the vertical component of the liquid velocity.

9.2 Novelty of Present Work

- Most of the numerical works are focused on 2-D tanks. However, in the present work, the 2-D tank problem is extended to 3-D tank and the problem is solved with finite difference based σ-transformation algorithm. To show the feasibility of present transformation technique, the 2-D cylindrical tank is also solved.
- This thesis reports more accurate results from both numerical as well as experimental investigations.
- The flow visualization study is performed to investigate the behavior of free surface during the liquid motion. Most of the flow visualization studies on sloshing were limited to self-induced excitations. And works in the area of flow visualization techniques on externally induced sloshing with surge motion of the tank is scarce. The present work deals with the study of the liquid free-surface velocity in a moving tank experimentally.

9.3 Scope for Future Work

In the present investigation, an attempt has been made to develop and expand the field of liquid sloshing for incompressible inviscid flows; but the potential still remains to explore many more areas and break new grounds. The following are some of the probable areas that may be taken up in future.

- The tank sloshing can be investigated with detailed numerical and experimental analysis for flow in the simple geometry with flow resisting device or object like baffles, semi-circular domain. Asymmetric geometries and complicated geometries like LNG tank, elliptical cylinder can also be solved for sloshing flows.

- The recent emerging area of computational fluid dynamics is Lattice Boltzmann Method (LBM) which can be used to find the liquid sloshing problem. In contrast to the Navier–Stokes solvers, the LBM solvers do not make use of the nonlinear convective term, because the convection becomes a simple advection term. Thus, the computations with LBM can produce better results.

- Most of the numerical models are used to solve two-dimensional problems. Only in certain cases, numerical models have been made to solve real three-dimensional problems. Therefore, there is a huge possibility to develop and implement numerical models to solve three-dimensional complex geometries.

- In this thesis, the computations of 2-D and 3-D σ-transformation for rectangular domain are carried out to obtain free surface elevation for gravity waves using potential flow theory. A similar study with σ-transformation method for compressible flows in micro gravity regions can be an interesting and important area of research.

- Liquid sloshing is controlled by magnetic and electric fields using magnetorheological and electrorheological fluids, respectively are still an emerging area with some unanswered questions. For example, the swirling effects for unstable and stable regions are still not clear. Resolving this problem may be another goal for research.

- Recent flow visualization techniques like steamball can be applied for flow visualization of liquid free surface during liquid sloshing.

References

Abramson HN, (1966), The dynamics of liquids in moving containers, Report SP 106, NASA.

Abramson HN, **Bass RL, Faltinsen O**, and **Olsen HA**, (1974), Liquid sloshing LNG carriers, The 10th Symposium on Naval Hydrodynamics, Cambridge, Massachusetts, ACR-204, 1974, pp. 371–388.

ADINA R&D Inc. (2003), ADINA-F theory and modeling guide, Report No. ARD-03-9.

Adrian RJ, (1991), Particle-imaging techniques for experimental fluid mechanics. *Annual Reviews in Fluid Mechanics*, Vol. 23, pp. 261-304.

Adrian RJ, (2004), Twenty years of particle image velocimetry, Proceedings of the 12th International Symposium on Applications of Laser Techniques to Fluid Mechanics, Lisbon, July 12-15.

Akyildiz H, and **Unal E**, (2005), Experimental investigation of pressure distribution on rectangular tank due to sloshing, *Ocean Engineering*, Vol. 32, pp. 1503-1516.

Akyildiz H, and **Unal N**, (2006), Sloshing in a three-dimensional rectangular container: numerical simulation and experimental validation, *Ocean Engineering*, Vol. 33, pp. 2135–2149.

Arafa M, (2006), Finite element analysis of sloshing in liquid-filled containers, Production Engineering and Design for Development, PEDD7, Cairo, February 7 – 9.

Arafa, M, (2007), Finite element analysis of sloshing in rectangular liquid-filled containers," *Journal of Vibration Control*, Vol. 13(7), pp. 883–903.

Babu SS, and **Bhattacharyya SK,** (1996), Finite element analysis of fluid-structure interaction effect on liquid retaining Structures due to sloshing, *Computers & Structures*, Vol. 59 (6), pp. 1165-l I71.

Baeten A, (2009), Optimization of LNG tank shape in terms of sloshing impact pressure", Proceedings of the Nineteenth International Offshore and Polar Engineering Conference (ISOPE), Osaka, Japan, June 21-26.

Bathe KJ, and **Ledezma GA,** (2007), Benchmark problems for incompressible fluid flows with structural interactions, *Computers & Structures*, Vol. 85, pp. 628–44.

Bathe KJ, and **Zhang H**, (2004), Finite element developments for general fluid flows with structural interactions, *International Journal of Numerical Methods in Engineering*, Vol. 60, pp. 213–32.

Bathe KJ, (1996), Finite element procedures, Prentice Hall, Englewood-Cliffs.

Behr M, and **Abraham F**, (2002), Free-surface flow simulations in the presence of inclined walls, *Computer Methods in Applied Mechanics and Engineering*, Vol. 191(47-48), pp. 5467-5483.

Bendat JS, and **Piersol AG**, (1986), Random data, analysis and measurement procedures, 2nd edition, Wiley–Interscience, New York.

Bingham HB and **Zhang H**, (2007), On the accuracy of finite-difference solutions for nonlinear water waves, *Journal of Engineering Mathematics,* Vol.58, pp. 211-228.

Biswal KC, (2003), Dynamic response of liquid filled composite containers with baffles considering liquid– structure interaction, PhD thesis, IIT Kharagpur.

Blazek J, Computational fluid dynamics: Principles and applications, Elsevier Science (2001).

Blumberg AF, and **Mellor GL, (1980),** A coastal ocean numerical model, *Mathematical modeling of estuarine physics*. pp. 203-219.

Bo L, and **Jia-xiang T**, (1994), Vibration studies of base-isolated liquid storage tanks, *Computers & Structures*, Vol. 52(5). pp. 1051-1059.

Bucchignani E, **Stella F** and **Paglia F**, (2004), A partition method for the solution of a coupled liquid-structure interaction problem, *Applied Numerical Mathematics*, Vol. 51, pp. 463-475.

Bugg F, (1970), Determination of liquid oscillation frequency in an inclined right circular cylinder, NASA TM X-64540.

Celebi MS, and **Akyildiz H,** (2002), Nonlinear modeling of liquid sloshing in a moving rectangular tank, *Ocean Engineering*, Vol. 29, pp. 1527–53.

Chen BF, (1999), Viscous free surface effect on coastal embankment hydrodynamics, Ocean Engineering, Vol. 26, pp. 47-65.

Chen BF, and **Nokes R**, (2005), Time-independent finite difference analysis of fully non-linear and viscous fluid sloshing in a rectangular container, *Journal of Computational Physics*, Vol. 209, pp. 47-81.

Chern MJ, **Borthwick AGL**, and **Taylor RE**, (1999), A Pseudospectral σ -Transformation Model of 2-D Nonlinear Waves, *Journal of Fluids and Structures*, Vol. 13, pp. 607- 630.

Chiba M, (1992), Nonlinear hydroelastic vibration of a cylindrical tank with elastic bottom containing liquid. Part I Experiment, *Journal of Fluids and Structures*, Vol. 6, pp. 181-206.

Cho JR and **Lee HW**, (2004), Numerical study on liquid sloshing in baffled tank by nonlinear finite element method, *Computer Methods in Applied Mechanics and Engineering*, 193 (2004) 2581–2598.

Cho JR, **Lee HW**, and **Ha SY**, (2005), Finite element analysis of resonant sloshing response in 2D baffled container, *Journal of Sound Vibration*, Vol. 288, pp. 829–845.

Christensen KT, **Soloff SM**, and **Adrian RJ**, (2000), PIV-sleuth: integrated particle-image velocimetry (PIV) interrogation/validation software. Technical report 943, Department of Theoretical and Applied Mechanics, University of Illinois at Urbana-Champaign.

Colagrossi A, **Palladino F**, **Greco M**, **Lugni C**, and **Faltinsen OM**, (2004), Experimental and numerical investigation of 2D sloshing: scenarios near the critical filling depth, Proceedings of 19th International Workshop on Water Waves and Floating Body, Cortona, Italy.

Cole HA, (1966), Baffle thickness effects in fuel sloshing experiments NASA TN D-3716.

Courant R, (1943), Variational methods for the solution of problems of equilibrium and vibrations, *Bulletin of the American Mathematical Society*, Vol. 49, pp. 1-23.

Craig KJ, and **Kingsley TC**, (2007), Design optimization of containers for sloshing and impact, *Structural* and *Multidisciplinary Optimization*, Vol. 33, pp. 71–87.

Dai L, and **Xu L**, (2006), A numerical scheme for dynamic liquid sloshing in horizontal cylindrical containers, Proceedings of the Institution of Mechanical Engineers, Part -D, *Journal of Automobile Engineering*, Vol. 20, pp. 901-918.

Decoene A and **Gerbeau JF**, (2009), Sigma transformation and ALE formulation for three-dimensional free surface flows, *International Journal for Numerical Methods in Fluids***,** Vol. 59 (4), Pp. 357–386.

Djavareshkian MH and **Khalili M**, (2006), Simulation of sloshing with the volume of fluid method, FDMP, *Tech. science Press*, Vol.2(4), pp. 229-307.

Dodge F, (1966), Experimental and theoretical studies of liquid sloshing at simulated low gravities, Technical Report No. 2, Contract No. NAS8-20290, National Aeronautics and Space Administration, Alabama.

Drosos GC, **Dimas AA**, and **Karabalis DL**, (2008), Discrete models for seismic analysis of liquid storage tanks of arbitrary shape and fill height *Journal of Pressure Vessel Technology*, Vol. 130, pp. 041801-1-12.

Faltinsen, OM, (1974), A nonlinear theory of sloshing in rectangular tanks. *Journal of Ship Research*, Vol. 18 (4), pp. 224 241.

Faltinsen OM, **Rognebakke OF**, **Lukovsky IA**, and **Timokha AN**, (2000), Multidimensional modal analysis of nonlinear sloshing in a rectangular container with finite water depth, *Journal of Fluid Mechanics*, 407, pp. 201–234.

Faltinsen OM, and **Timokha AN**, (2009), Sloshing, First print, Cambridge University Press, New York.

Faraday M, (1831), On a peculiar class of acoustical figures, and on certain forms assumed by groups of particles upon vibrating elastic surfaces, Philosophical Transactions of the *Royal* Society**,** Vol. 121, pp. 299–340.

Feng GC, (1973), Dynamic loads due to moving liquid, AIAA Paper No: 73, 409.

Ferziger JH, and **Peric M**, (2002), Computational Methods for Fluid Dynamics, 3rd rev. edition, Springer-Verlag Berlin Heidelberg, New York.

Frandsen JB, and **Borthwick AGL**, (2003), Simulation of sloshing motions in fixed and vertically excited containers using a 2-D inviscid σ -transformed finite difference solver, *Journal of Fluids and Structures*, Vol. 18, pp. 197-214.

Frandsen JB, (2004), Sloshing in Excited Containers, *Journal of Computational Physics*, Vol. 196, pp. 53-87.

Fujino Y, **Sun L**, and **Pacheco BM**, (1992), Tuned liquid damper (TLD) for suppressing horizontal motion of structures, *Journal of Engineering Mechanics*, Vol. 118(10), pp. 2017-2030.

Fukaya M, **Madarame H**, and **Okamoto K**, (1996), Growth mechanism of self-induced sloshing caused by jet in rectangular tank (2nd Report, Multimode Sloshing Caused by Horizontal Rectangular Jet), *Transactions of Japan Society of Mechanical Engineers*, Vol. 62(599), pp. 64-71.

Godderidge B, **Turnock S**, **Earl C**, **Tan M**, (2009), The effect of fluid compressibility on the simulation of sloshing impacts, *Ocean Engineering*, Vol. 36, pp.578–587.

Graham EW, and **Rodriquez AM**, (1952), The characteristics of fuel motion which affect airplane dynamics, *Journal of Applied Mechanics*, Vol. 19(3), pp. 381–388.

Grundelius M, and **Bernhardsson B**, (1999), Control of liquid slosh in an industrial packaging machine, Proceedings of IEEE International Conference on Control Applications, pp. 1654-1659.

Guillot MJ, (2006), Application of a discontinuous Galerkin finite element method to liquid sloshing, ASME *Journal of Offshore Mechanics and Arctic Engineering*, Vol. 128, pp. 1-10.

Gupta RK, (1995), Sloshing in shallow cylindrical tanks, *Journal of Sound and Vibration*, Vol. 180(3), pp.397-415.

Guzel UB, **Gradinscak M**, **Semercigil SE** and **Turan OF**, (2004), Control of liquid sloshing in flexible containers part 1. Added mass, 15th Australasian Fluid Mechanics Conference, University of Sydney, Australia.

Haney RL, 1991, On the pressure gradient force over steep topography in sigma-coordinate ocean models, *Journal of Physical Oceanography*, Vol. 21, pp. 610-619.

Haroun MA, (1980), Dynamic analysis of liquid storage tanks, Report EERL, No. 80-4, California Institute of Technology, Pasadena, California.

Haroun MA, (1983), Vibration studies and tests of liquid storage tanks, *Earthquake Engineering & Structural Dynamics*, Vol. 11, pp. 179–206.

Hart DP, (1998), The elimination of correlation errors in PIV processing, In Proceedings of Ninth International Symposium on Applications of Laser Techniques to Fluid Mechanics, Vol. 1, pp. 13.3.1–13.3.8.

Hashimoto H, and **Sudo S**, (1988), Violent liquid sloshing in vertically excited cylindrical containers, *Experimental Thermal and Fluid Science*, Vol. 1, pp. 159-169.

Hatayama K, **Zama S**, **Nishi H**, **Yamada M**, **Hirokawa M**, and **Inoue R**, (2005), The damages of oil storage tanks during the 2003 tokachi-oki earthquake and the long period ground motions, Proceedings of the JSCE-AIJ Joint Symposium on Huge Subduction Earthquakes—Wide Area Strong Ground Motion Prediction, pp. 7–18.

Hill DF, (2003), Transient and steady-state amplitudes of forced waves in rectangular basins, *Physics of Fluids*, Vol. 15(6), pp. 1576–1587.

Hirt CW, and **Nichols BD**, (1981), Volume of fluid (VOF) method for the dynamics of free boundaries, *Journal Computational Physics*, Vol. 39, pp. 201–205.

Housner GW, (1957), Dynamic pressures on accelerated fluid containers, *Bulletin of the Seismological Society of America*, Vol. 47(1), pp. 15-35.

Housner GW, (*1963)*, The dynamic behavior of water tanks, *Bulletin of the Seismological Society of America*, Vol. 53(2), pp. 381-387.

Hu H, **Kobayashi T**, **Saga T**, **Segawa S**, and **Uemura T**, (1999), A PIV study on the self-induced sloshing phenomena in a rectangular tank. Proceeding of Korea-Japan Joint Seminar on Particle Image Velocimetry, pp. 132-139.

Hwang Y, **Jung J**, **Kim D**, and **Ryu M**, (2008), An experimental study and numerical simulation on sloshing impact pressures with two identically shaped rectangular 2-dimensional model tanks with different sizes, Proceedings of the Eighteenth International Offshore and Polar Engineering Conference, Canada, pp. 184-190.

Ibrahim RA, (2005), Liquid sloshing dynamics: Theory and applications, first edition, Cambridge University Press, New York.

Jacobsen LS, and **Ayre RS**, (1951), Hydrodynamic experiments with rigid cylindrical tanks subjected to transient motions, *Bulletin of the Seismological Society of America*, Vol. 41(4), pp. 313-346.

Khezzar L, **Seibi A**, and **Goharzadeh A**, (2009), Water sloshing in rectangular tanks – an experimental investigation & numerical simulation, *International Journal of Engineering*, Vol. 3 (2), pp. 174-184.

Kim KH, (2002), Simulation of surface ship dynamics using unsteady RANS codes, RTO AVT Symposium, April 22-25, France.

Kim Y, (2001), Numerical simulation of sloshing flows with impact load, *Applied Ocean Research*, Vol. 23, pp. 53–62.

Kline SJ, and **McClintock FA,** (1953), Describing uncertainties in single-sample experiments, *Mechanical Engineering*, Vol. 75, pp. 3–8.

Kwon YW, (2008), Coupling of Lattice Boltzmann and finite element methods for fluid-structure interaction application, *ASME Journal of Pressure Vessel Technology*, Vol.130, pp. 011302-1-6.

Lamb H, (1932), Hydrodynamics, sixth edition, Cambridge University Press, Cambridge.

Law CNS, **Khoo BC**, and **Chew TC**, (1999). Turbulence structure in the immediate vicinity of the shear-free air-water interface induced by a deeply submerged jet, *Experiments in Fluids*, Vol. 27, pp. 321-331.

Lawrence HR, **Wang CJ**, and **Reddy RB**, (1958),Variational solution of fuel sloshing modes. TRW Space Technology Labs, Los Angeles, California, Defense Technical Information Center.

Lee CJK, **Noguchi H**, and **Koshizuka S**, (2007), Fluid–shell structure interaction analysis by coupled particle and finite element method. *Computers & Structures*, Vol. 85, pp. 688–97.

Liu D, and **Lin P**, (2008), A numerical study of three-dimensional liquid sloshing in tanks, *Journal of Computational Physics*, Vol. 227, pp. 3921–3939.

Liu WK, and **Uras RA**, (1988), Variational approach to fluid–structure interaction with sloshing. *Nuclear Engineers Design*, Vol. 106, pp. 69–85.

Maleki A, and **Ziyaeifar M**, (2008), Sloshing damping in cylindrical liquid storage tanks with baffles, *Journal of Sound and Vibration*, Vol. 311, pp. 372–385.

Matsui T, (2007), Sloshing in a cylindrical liquid storage tank with a floating roof under seismic excitation, *ASME Journal of Pressure Vessel Technology*, Vol. 129, pp. 557-566.

Matsui T, (2009), Sloshing in a cylindrical liquid storage tank with a single-deck type floating roof under seismic excitation, *ASME Journal of Pressure Vessel Technology*, Vol. 131, pp. 021303-1-10.

Mellor GL, and **Blumberg AF,** (1985), Modeling vertical and horizontal diffusivities with the sigma coordinate system. *Monthly Weather Review*, Vol. 113, pp. 1379-1383.

Moaleji R, and **Greig AR**, (2007), On the development of ship anti-roll tanks, *Ocean Engineering*, Vol. 34, pp. 103–121.

Modi VJ, and **Munshi SR**, (1998), An efficient liquid sloshing damper for vibration control, *Journal of Fluids and Structures*, Vol. 12, pp. 1055-1071.

Modi VJ and **Seto ML**, (1997) Suppression of flow-induced oscillations using sloshing liquid dampers: analysis and experiments. *Journal of Wind Engineering & Industrial Aerodynamics*, 67-68 1-3, pp. 611–625.

Nasar T, **Sannasiraj SA**, and **Sundar V**, (2008), Experimental study of liquid sloshing dynamics in a barge carrying tank, *Fluid Dynamics Research*, Vol. 40, pp. 427–458.

Nasar T, **Sannasiraj SA**, and **Sundar V**, (2009), Wave-induced sloshing pressure in a liquid tank under irregular waves, Proceedings of the Institution of Mechanical Engineers, Part M: *Journal of Engineering for the Maritime Environment*, Vol. 223(2), pp. 145-161.

Nielsen KB, (2003), Numerical prediction of green water loads on ships, *PhD thesis*, Maritime Engineering, Department of Mechanical Engineering, Technical University of Denmark.

Okamoto K, **Madrarame H**, and **Hagiwara T**, (1991), Self-induced oscillation of free surface in a tank with circulating flow, Proceedings of Institution of Mechanical Engineers, *Flow Induced Vibrations*, Vol. 1991-6, pp.539-545.

Okamoto K, **Fukaya M**, and **Madarame H**, (1993), Self-induced sloshing caused by flow in a tank, *ASME Journal of Pressure Vessels and Piping*, Vol. 258, pp. 105-111.

Okamoto K, and **Madarame H**, (1998), Fluid Dynamics of Free Surface in Liquid Metal Fast Breeder Reactor, *Progress in Nuclear Energy*, Vol. 32, No.1/2, pp. 159-207.

Pal NC, **Sinha PK**, and **Bhattacharyya SK**, (1999), Finite element coupled slosh analysis of rectangular liquid filled laminated composite tanks, *Journal of Reinforced Plastics and Composites*, Vol. 18, pp. 1375.

Pal NC, **Bhattacharyya SK**, and **Sinha RK**, (2001), Experimental investigation of slosh dynamics of liquid-filled containers, *Experimental Mechanics*, Vol. 41(1), pp. 63-69.

Pal NC, **Bhattacharyya SK**, and **Sinha PK**, (2002), Non-Linear coupled slosh dynamics of liquid-filled laminated composite containers: A two dimensional finite element approach, *Journal of Sound and Vibration*, Vol. 261(1), pp 729-49.

Pal P, (2008), Characterization of liquid filled composite containers using meshless local Petrov-Galerkin method considering fluid-structure interaction, *PhD thesis*, Department of Civil Engineering, IIT Kharagpur.

Pal P, and **Bhattacharyya SK**, (2010), Sloshing in partially filled liquid containers - Numerical and experimental study for 2-D problems, *Journal of Sound and Vibration*, Vol. 329(21), pp. 4466-4485.

Panigrahy PK, (2006), Development of a test setup to study the sloshing behavior of liquids in baffled tanks. *MTech thesis*, Department of Mechanical Engineering, IIT Guwahati, India.

Panigrahy PK, **Saha UK**, **Maity D**, and **Sharma S,** (2006), Wall pressures on a square tank due to liquid sloshing, Proceedings of 3rd international (& 33rd national) conference on fluid mechanics and fluid power, December 7–9, IIT-Bombay, India.

Panigrahy PK, **Saha UK**, and **Maity D**, (2009), Experimental studies on sloshing behavior due to horizontal movement of liquids in baffled tanks, *Ocean Engineering*, Vol. 36, pp. 213–222.

Papell SS, (1965), Low viscosity magnetic fluid obtained by the colloidal suspension of magnetic particles, U. S. Patent 3215,572.

Partom LS, (1987), Application of the VOF method to the sloshing of a fluid in a partially filled cylindrical container, *International Journal for Numerical Methods in Fluids*, Vol. 7(6), pp. 535-550.

Phillips NA, (1957), A coordinate system having some special advantages for numerical forecasting. *Journal of Atmospheric Sciences*, Vol. 14, pp.184–185.

Popov G, **Sankar S, Sankar TS**, and **Vatistas GH**, (1993), Dynamics of liquid sloshing in horizontal cylindrical road containers, Proceedings of The Institution of Mechanical Engineers, Part C: *Journal of Mechanical Engineering Science*, Vol. 207- C6, pp. 399-406.

Rhee SH, (2005), Unstructured grid-based Reynolds-averaged Navier–Stokes method for liquid tank sloshing, *Journal of Fluids Engineering*, Vol. 127(3), pp. 572–582.

Rocca ML, **Sciortino G**, **Adduce C**, and **Boniforti MA**, (2005), Experimental and theoretical investigation on the sloshing of a two-liquid system with free surface, *Physics of Fluids*, Vol. 17(16), pp. 062101-17.

Rocca ML, **Sciortino G**, and **Boniforti MA**, (2000), A fully nonlinear model for sloshing in a rotating container. *Fluid Dynamics Research*, Vol. 27, pp. 23–52.

Romero JA, **Ramırez O**, **Fortanell JM**, **Martinez M**, and **Lozano A**. (2005), Analysis of lateral sloshing forces within road containers with high fill levels, Proceedings Institution of Mechanical Engineers, Part D: *Journal of Automobile Engineering*, Vol. 220, pp. 303-312.

Rugonyi S, and **Bathe KJ** (2001), On the finite element analysis of fluid flows fully coupled with structural interactions. *Computer Modeling in Engineering and Sciences*, Vol. 2, pp. 195–212.

Saga T, **Hu H**, **Kobayashi T**, **Murata S**, **Taniguchi S**, **Okamoto K**, and **Nagoshi M**, (2000a), A comparative study of the PIV and LDV measurements on a self-induced sloshing flow. *Journal of Visualization*, Vol. 3(2), pp. 145-156.

Saga T, **Hu H**, **Kobayashi T**, **Segawa S**, and **Taniguchi N**, (2000b), Research on the self-induced sloshing phenomena in a rectangular tank. Proceedings of the 9th international symposium on flow visualization, Edinburgh.

Sakamoto D, **Oshima N**, and **Fukuda T**, (2001), Tuned sloshing damper using electro-rheological fluid, *Smart Materials and Structures*, Vol. 10, pp. 963–969.

Sawada T, **Ohira Y**, and **Houda H**, (2002), Sloshing motion of the magnetic fluid in a cylindrical container due to the horizontal oscillation, *Energy Conservation and Management*, Vol. 43, pp. 299-308.

Sayar BA, and **Baumgarten JR**, (1982), Linear and nonlinear analysis of fluid slosh dampers, *American Institute of Aeronautics and Astronautics*, Vol. 20(11), pp.1534.

Siekmann J, and **Chang S**, (1970), Note on liquid sloshing in a container of arbitrary shape, *Journal of Applied Mathematics and Physics*, Vol. 21, pp. 830.

Singh A, **Nir A**, and **Semiat R**, (2006), Free-surface flow of concentrated suspensions, *International Journal of Multiphase Flow*, Vol. 32 (7), pp. 775-790.

Siva Prasad BG, (2006), Analysis of lubricant sloshing in a rail compressor application, International Compressor Engineering Conference, Purdue, C113, pp. 1-7.

Sriram V, **Sannasiraj SA**, and **Sundar V**, (2006), Numerical simulation of 2D sloshing waves due to horizontal and vertical random excitation, *Applied Ocean Research*, Vol. 28, pp. 19–32.

Stofan AJ, and **Sumner IE**, (1963), Experimental investigation of the slosh-damping effectiveness of positive-expulsion bags and diaphragms in spherical tanks, *Lowis Research Center*, Ohio.

Sudo S, **Hashimoto H**, **Ikeda A**, and **Katagiri K**, (1987), Some studies on magnetic liquid sloshing, *Journal of Magnetism and Magnetic Materials*, Vol. 65, pp. 219-222.

Sweedan AMJ, (2009), Equivalent mechanical model for seismic forces in combined tanks subjected to vertical earthquake excitation, *Thin-Walled Structures*, Vol. 47 (8-9), pp. 942-952.

Takizawa A, **Koshizuka S**, and **Kondo S**, (1992), Generalization of physical components boundary fitted coordinate (PCBFC) method for the analysis of free surface flow, *International Journal for Numerical Method in Fluids*, Vol. 15, pp.1213-1237.

Taniguchi T, (2004), Rocking behavior of unanchored flat-bottom cylindrical shell tanks under action of horizontal base excitation, *Engineering Structures*, Vol. 26, pp. 415–426.

Terashima K, and **Yano K**, (2001), Sloshing analysis and suppression control of tilting-type automatic pouring machine, IFAC *Journal of Control Engineering Practice*, 9 (6), 607–620.

Topliss ME, **Cooker MJ**, **Peregrine DH**, (1992), Pressure oscillations during wave impact on vertical walls, Proceedings of the Twenty third International Conference on Coastal Engineering, ASCE.

Turnbull MS, **Borthwick AGL**, and **Taylor RE**, (2003), Numerical wave container based on a σ-transformed finite element inviscid flow solver, *International Journal for Numerical Methods in Fluids*, Vol. 42, pp. 641–663.

Turner MJ, **Clough RW**, **Martin HC** and **Topp LJ**, (1956), Stiffness and deflection analysis of complex structures, *Journal* of *Aeronautical Sciences*, Vol. 23, pp. 805-823.

Ueda T, **Nakagaki R,** and **Koshida K**, (1992), Suppression of wind-induced vibration by dynamic dampers in tower-like structures, *Journal of Wind Engineering and Industrial Aerodynamics*, Vol. 41-44, pp. 1907–1918.

Uras RA and **Tang Y**, (1994), Sloshing analysis of tanks containing multiple fluid layers, U.S. National Conference on Earthquake Engineering, Chicago, United States, ANL/RE/CP-80865; CONF-940752-3.

Valentine DT, (2005), Numerical investigation of 2D sloshing: Nonlinear internal waves, *ASME Journal of Offshore Mechanics and Arctic Engineering*, Vol. 127, pp. 300-305.

Vandiver JK, and **Mitome S,** (1982), Effect of liquid storage tanks on the dynamic response of offshore platforms, Dynamic Analysis of Offshore Structures: Recent Developments, Progress in Engineering Sciences 1, CML Publications, Southampton, 25–32.

Versteeg HK and **Malalasekera W**, (1995), An introduction to computational fluid mechanics – The finite volume method, Addison Wesley Longman Group Ltd., England

Wang CZ, and **Khoo BC**, (2005), Finite element analysis of two-dimensional nonlinear sloshing problems in random excitations, *Ocean Engineering*, Vol. 32, pp. 107–133.

Warnitchai P, and **Pinkaew T**, (1998), Modeling of the liquid sloshing in rectangular tanks with flow damping device, *Engineering Structures*, Vol. 20(2), pp. 593-600.

Wiesche S, (2003), Computational slosh dynamics: Theory and industrial application, computational Mechanics, Vol. 30, pp.374-387.

Wiesche S, (2008), Sloshing dynamics of a viscous liquid in a spinning horizontal cylindrical tank, *Aerospace Science and Technology*, Vol. 12(6), pp. 448-456.

Winslow WM, (1949), Induced vibrations of suspensions, *Journal of Applied Physics*, Vol. 20, pp. 1137-1140.

Wu GX, **Ma QW**, and **Taylor ER**, (1998), Numerical simulation of sloshing waves in a 3D tank based on a finite element method, *Applied Ocean Research*, Vol. 20, pp. 337–355.

Yang C, and **Löhner R**, (2005), Computation of 3D flows with violent free surface motion, Proceedings of International Society of Offshore Polar Eng (ISOPE) Conference, Korea (No: JSC-284).

Yano K, and **Terashima K**, (2005), Sloshing suppression control of liquid transfer systems considering a 3-D transfer path, *IEEE/ASME Transactions on Mechatronics*, Vol. 10(1), pp. 8-16.

Yuanjun H, **Xingrui M**, **Pingping W**, and **Benli W**, (2007), Low-gravity liquid nonlinear sloshing analysis in a tank under pitching excitation, *Journal of Sound Vibration*, Vol. 299, pp. 164–77.

Zhu G, **Borthwick AGL** and **Taylor RE**, (2001), A finite element model of interaction between viscous free surface waves and submerged cylinders, *Ocean Engineering*, Vol. 28, pp. 989-1008.

Appendix A

Pseudocode for 3-D Rectangular Tank

1. Specify the initial conditions (mode of oscillation, defining the time step, final time, etc.).
2. Calculate all geometric coefficients, parameters, and physical and computational grid.
3. Define an initial profile and initial conditions on the grid.
4. Calculate $\zeta_{i,j}$ for all the grid points at top surface using initial conditions (as depicted in section 5.4).
5. Apply the kinematic boundary (Eq. 4.62) and dynamic boundary (Eq. 4.63) conditions on the top surface of the grid. (Switch off the acceleration terms for fixed tank case).
5. Updating $\zeta_{i,j}$ value at all points.
6. Apply the right, left, front, back and bottom surface conditions (Eqs. 4.59 to 4.61) and then calculate the $\phi_{i,j}$ values at boundary nodes.
7. Calculate the $\phi_{i,j}$ values in all the node points of computational domain using Eq. 4.57.
8. Calculate the residual error and if it satisfies the error norm, go to step 9.
9. Update all the variables.
10. Increment the time until it reaches the predefined final time.

Appendix B

Error Analysis

Kline and McClintock (1953) proposed a procedure for estimating the uncertainty of any measured quantity in experimental studies. If an estimated quantity R depends on independent variables like $x_1, x_2, x_3, \ldots x_n$ then,

$$R = R\,(x1, x2, x3, \ldots xn) \tag{B.1}$$

Then the maximum value of uncertainty is given by:

$$w_R = \sqrt{\left[\left(\frac{\partial x_1}{x_1}\right)^2 + \left(\frac{\partial x_2}{x_2}\right)^2 + \left(\frac{\partial x_3}{x_3}\right)^2 + \ldots \left(\frac{\partial x_n}{x_n}\right)^2\right]} \tag{B.2}$$

where $w_R = \frac{\partial R}{R}$ and $\frac{\partial x_1}{x_1}$, $\frac{\partial x_2}{x_2}$, etc., are the errors in the independent variables.

The important quantities measured/ estimated during the experiments for liquid sloshing is time, pressure, liquid height and frequency.

B.1 Measured Quantities

In this experimental investigation the parameters time, pressure and liquid height are measured quantities. Stop watch is used to measure time and piezo-resistive sensor is used for pressure analysis. During motion of the tank, the liquid height is measured by interface location technique and traditional wave height gauge.

Table B.1: Maximum possible uncertainty for measured quantities.

Sl. No.	Measurement	Device	Accuracy	Minimum Quantity	Maximum Uncertainty
1	Time	Stop Watch	± 0.5 s	120 s	± 0.5 %
2	Pressure	Piezo- resistive type transducer	± 0.01bar	5 bar	± 0.2 %
3	Wave height	Capacitance wave gauge	± 0.2 mm	0.05m	± 0.4%

B.2 Estimated Quantities

The frequency parameter is estimated from the number of cycles completed per second. Here the uncertainty is calculated as $\frac{\Delta F}{F} = 0.42\%$.

B.3 Validation with Wave Height Gauge

Wave elevation can also be measured using wave height gauge. As shown in Figure B.1, three distinct marks viz., upper, lower and midpoint are made on the probe wire for convenience. Initially, the lower mark is set to immerse in the tank liquid and the liquid level is adjusted to coincide with the middle mark. The difference in permittivity between water and air is used to measure the surface elevation in a moving tank. Then the gauge results are compared with the results obtained from interface location technique as shown in Figure B.3. When the surface is oscillating, a thin layer of liquid is formed on the package wall. This thin layer of liquid moves down much slower than the surface of the liquid. However, the result matches well with allowable accuracy.

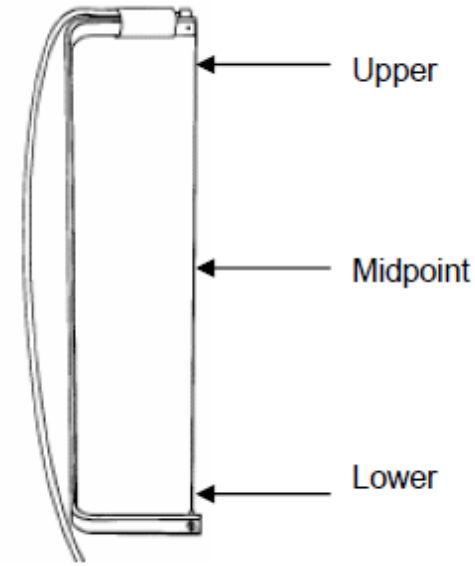

Figure B.1: Wave probe.

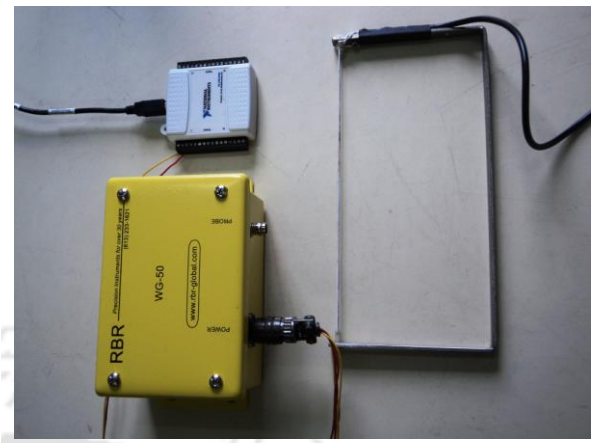

Figure B.2: Perspective view of wave probe and analog to digital converter.

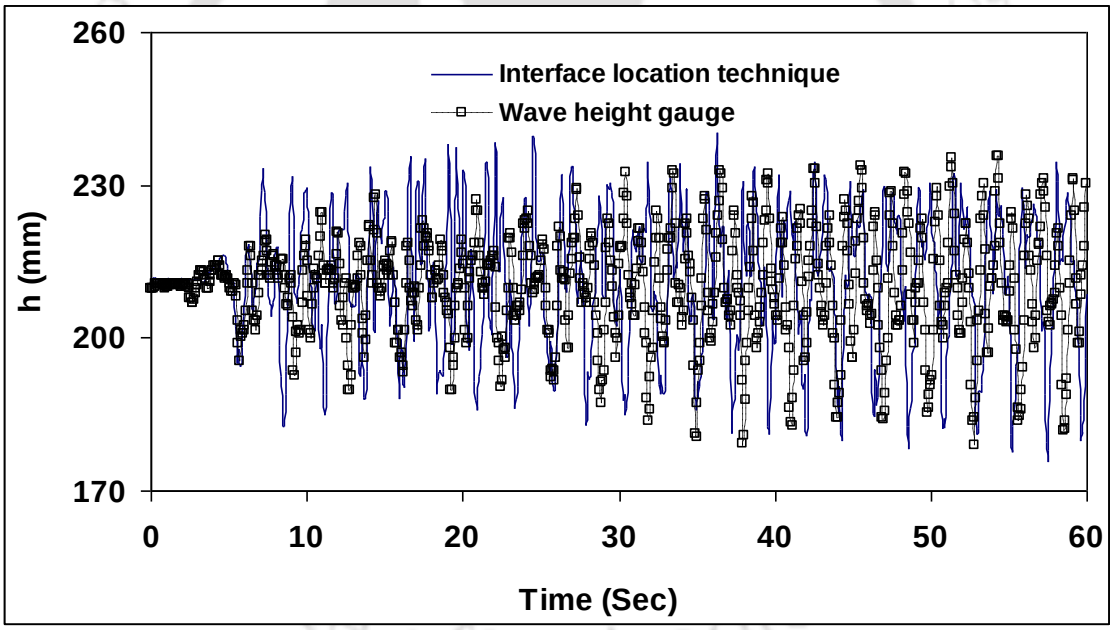

Figure B.3: Tank 600 x 600 x 600 mm, FL=200 mm, FR=0.6, Excitation amplitude=60 mm.

Appendix C

Specifications of Instruments

Table C.1: Specifications of instruments used.

Equipment/Instrument	Specifications	
Motor	HP:	1HP
	RPM:	1440
	Voltage:	220V
	Phase:	Single
	Current:	1 A
	Frequency:	50Hz
Wave Height Gauge	Model:	WG-50
	Make:	RRB Ltd, Canada
	Probe length	100 mm to 2m
	Accuracy	±0.4%
Pressure Gauges	Make:	Druck and Co., Germany
	Transducer Type:	PMP 1400
	Range:	100m bar g to 25 bar g
	Output Voltage:	0-5V
	Non-linearity and Hysteresis:	±0.25% BSL Max.
	Temperature Errors:	±2% max
	Total Error Band:	over 20^0C to +80 C

Rectifier cum Controller	Input Supply:	220 V (AC), ±10% 50 Hz
	Output Field Voltage :	210V (DC) Fixed
	Output Armature Voltage:	0-200V (DC) Variable
	Operating Temperature:	0-45º C
	Speed Ratio:	1/10
	Feedback:	Armature
	Max. Speed Resistance:	50-100% of rated speed
	Min. Speed Resistance:	50-10% of rated speed
	Power:	1HP
Data Acquisition System	Make:	VPL Infotech and Consultants, India.
	Input Channel:	8 differential
	Analog Input Type:	mV,V
	Sampling Rate:	10 Samples/sec
	Bandwidth:	15.7 Hz
	Accuracy:	± 0.1%
	Zero Drift:	20 µV/ ^{0}C
	Power Supply:	: +10 to +30 V DC
Computer System	Make:	HCL India
	Processor:	Pentium IV, 2.4 GHz
	RAM:	512 MB

Figure C.1: Photograph of the experimental setup

Figure C.2: DC motor arrangement with channel framework

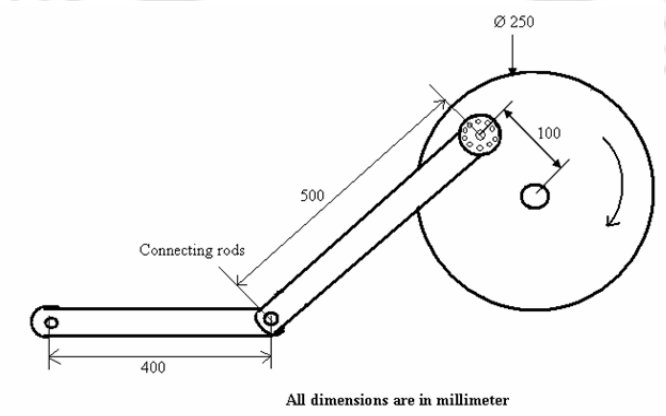

Figure C.3: Crank Arrangement with link

LIST OF PUBLICATIONS

International Journals:

Published

1. Eswaran M, Saha UK and Maity D, (2009), Effect of baffles on partially filled cubic tank: Numerical simulation and experimental validation, ***Computers & Structures***, Vol. 87(3-4), Pp 198-205.

2. Eswaran M, Singh A and Saha UK, (2010), Experimental investigation of liquid velocity at free surface in an excited tank, Proceedings of the Institution of Mechanical Engineers, Part M: ***Journal of Engineering for the Maritime Environment***, Vol. 225, pp. 133–148.

3. Eswaran M and Saha UK, (2011), Sloshing of liquids in partially filled tanks – A review of experimental investigations, ***Ocean Systems Engineering***, Vol. 1, Issue 2, pp. 131–155.

Under Review

4. Eswaran M and Saha UK, (2011), Finite difference based coordinate transformation approach for liquid sloshing in a rectangular tank under regular wave excitation, ***Engineering Applications of Computational Fluid Mechanics***.

5. Eswaran M, Virk AS and Saha UK, (2011), Numerical simulation of 3-D sloshing waves in a regularly and randomly excited container in vertical direction, ***ASME Journal of Offshore Mechanics and Arctic Engineering***.

6. Eswaran M and Saha UK, (2011), Experimental investigation of free surface elevation through image processing, ***International Journal of Emerging Multidisciplinary Fluid Sciences.***

International Conferences:

7. Eswaran M, and Saha UK, (2009), Low steeping waves simulation in a vertical excited container using σ-transformation, Paper No. OMAE2009–80248, ***ASME 28th International Conference on Ocean, Offshore and Arctic Engineering***, May 31–June 5, 2009, Honolulu, Hawaii, USA.

8. Eswaran M, and Saha UK (2009), Numerical simulation of low steeping waves in a horizontally excited container using σ-transformation, Paper No. M27, ***3rd International Congress on Computational Mechanics and Simulation*** (ICCMS-09), December 1 – 5, IIT Bombay, India.

9. Eswaran M, and Saha UK, (2010), Waves simulation in an excited cylindrical tank using σ-transformation, Paper No. IMECE2010–39752, ***ASME International Mechanical Engineering Congress and Exposition***, November 12–18, Vancouver, Canada.

10. Eswaran M, and Saha UK, (2010), Effect of excitation frequency of air-water interface dynamics in a rectangular tank, ***7th International Conference on Flow Dynamics***, November 1–3, Sendai, Japan.

11. Eswaran M, and Saha UK, (2010), Dynamics of air-water interface in an excited tank – an experimental study, ***4th International (& 37th National) Conference on Fluid Mechanics and Fluid Power***, December 16-18, IIT Madras, India.

12. Eswaran M, and Saha UK, (2011), A numerical scheme for dynamic liquid sloshing in a rectangular container under random oscillation, ***International Conference on Mathematical Modelling and Applications to Industrial Problems***, MMIP 2011, March 28 – 31, NIT Calicut, India.